Katrine Sjaastad Hanssen

Dissecting the complexities of Alzheimer's disease

Engineering selectively vulnerable neural networks *in vitro*

Doctoral thesis

NTNU
Norwegian University of Science and Technology
Thesis for the Degree of
Philosophiae Doctor
Faculty of Medicine and Health Sciences
Kavli Institute for Systems Neuroscience
Department for Neuromedicine and
Movement Science

NTNU
Norwegian University of
Science and Technology

Katrine Sjaastad Hanssen

Dissecting the complexities of Alzheimer's disease

Engineering selectively vulnerable neural networks *in vitro*

Thesis for the Degree of Philosophiae Doctor

Trondheim, November 2023

Norwegian University of Science and Technology
Faculty of Medicine and Health Sciences
Kavli Institute for Systems Neuroscience
Department for Neuromedicine and Movement Science

NTNU
Norwegian University of
Science and Technology

NORGES TEKNISK-NATURVITENSKAPELIGE UNIVERSITET

FAKULTET FOR MEDISIN OG HELSEVITENSKAP

Populærvitenskapelig sammendrag

«Nye metoder for å studere nevrale nettverk i tidlige faser av Alzheimers sykdom»

Alzheimer sykdom er en nevrodegenerativ sykdom som forårsaker gradvis svekkelse av hukommelse og til slutt fører til kognitiv svikt. Mange år før pasienter opplever symptomer som å glemme veien hjem eller hvem de var sammen med forrige uke, starter proteinopphopninger av beta-amyloid og tau å akkumulere i hjernen. Disse proteinopphopningene er en tidlig indikator på sykdomsutviklingen. Spesielt i de tidligste stadiene av sykdommen har forskning vist at spesifikke nevroner i lag II av en liten hjerneregion kalt den entorhinale cortex (EC) blir syke og dør. Disse nevronene har en tett forbindelse til et annet hjerneområde kalt hippocampus, et område som videre er påvirket av proteinopphopninger og celledød ettersom sykdommen gradvis utvikler seg. For å finne en effektiv kur og bremse sykdomsutviklingen er det avgjørende for forskningsfeltet å bedre forstå de underliggende sykdomsmekanismene. Grunnforskning har i mange år jobbet mot dette målet, og det er fortsatt behov for utvikling av nye metoder for å forske på spesifikke sykdomsmekanismer.

I mitt doktorgradsarbeid har jeg gjennom tre artikler jobbet med utvikling av nye metoder for modellering av Alzheimer sykdom ved bruk av cellekulturer. I den første artikkelen presenterer jeg en metode for å dissekere ut EC lag II nevroner fra forskningsdyr som bærer et transgen for Alzheimers, og gro disse videre i cellekulturer. Resultatene viser at nevronene vokser sammen til et nettverk og uttrykker elektrofysiologisk aktivitet opp til to måneder. I den andre artikkelen etablerer vi cellekulturer i små mikrofluidikk-kamre som består av fire separate brønner, videre koblet sammen via små mikrotunneler hvor aksonene (armene til nevronene) kan gro gjennom. Her viser vi hvordan nettverkene kobler seg sammen og utvikler kompleks nettverksaktivitet over tid. For å vise hvordan denne metoden kan brukes til å modellere Alzheimers sykdom, inkluderte vi i tillegg til EC lag II nevroner, spesifikke nevroner fra tre ulike deler av hippocampus fra voksne rotter og mus (transgen for Alzheimers). I den tredje artikkelen undersøker vi hvordan indusert tau patologi i nevrale nettverk påvirker strukturelle og funksjonelle aspekter ved nettverksdynamikken over tid. Strukturelt, viser resultatene at tau patologi fører til tilbaketrekning av aksoner, og dermed induserer en restrukturering av nettverket. Funksjonelt ser vi redusert nettverksaktivitet, hvor den gjenværende aktiviteten er mer synkron sammenlignet med friske kontroller.

Sammenlagt viser resulter fra mitt doktorgradsarbeid hvordan vi kan bruke ny mikrofluidikkteknologi til å skape mer anatomiske relevante nettverk for å studere Alzheimers sykdom i tidlige sykdomsstadier. Jeg håper at mitt arbeid fra denne avhandlingen skal kunne bidra til forskningsfeltet hvor vi ved bruk av utbedrede metoder lettere kan studere nettverksforandringer over tid, raskere teste nye medisiner og komme frem til en løsning på hvordan vi kan stoppe sykdomsprosessen.

Navn kandidat: Katrine Sjaastad Hanssen
Institutt: Kavli instituttet for nevrovitenskap og Institutt for Nevromedisin og Bevegelsesvitenskap
Veiledere: Dr. Asgeir Kobro-Flatmoen, Prof. Ioanna Sandvig og Prof. Menno P. Witter
Finansieringskilder: NTNU Bioteknologi, Olav Thon Stiftelsen, Civitan Forskerfond for Alzheimer sykdom og Samarbeidsorganet Helse Midt-Norge

Summary: Dissecting the complexities of Alzheimer's disease

Alzheimer's disease (AD) is a progressive, neurodegenerative disease where accumulation of neuropathology can start up to two decades before symptom onset. With no cure for the disease, relevant models of AD are needed to better understand initial disease cascades. Transgenic AD animal models and cell culture models have been crucial in the study of AD, and have contributed to a better understanding of neuropathology, disease progression and altered network activity. Applying basic research strategies is crucial before testing new therapeutics to translate the efficacy of potential treatments to the clinic. *In vitro* modelling of AD introduces a reductionist approach for investigating the disease at the cellular and molecular level. Such models can be particularly useful for studying the early stages of AD, as they allow for the analysis of neural network dynamics. The harvest and *in vitro* culturing of adult primary neurons from AD animal models is an elegant way to model early phases of AD as the neurons retain their epigenetic profile and age-effects as in the living animal.

In this thesis, the overarching aim has been to develop new methods for modelling of AD by the use of cell cultures. In the first paper we present a method to dissect and longitudinally culture adult layer specific lateral entorhinal cortex layer II (LECLII) neurons from AD transgenic APP/PS1 model mice. Furthermore, in addition to LEC LII, we dissected hippocampal subregional DG, CA3 and CA1 neurons from adult AD transgenic mice and rats and cultured these on four-nodal microfluidic devices (Paper II). We show that adult neurons dissected from rodent AD models re-form structural connections and display sustained electrophysiological activity. By use of commercially available cortical-hippocampal neurons we show the utility of microfluidic devices ensuring feedforward connectivity with emergence of complex structure-function dynamics in our networks (Paper II). In the third paper we used two-nodal microfluidic devices to study changes in structure-function neural network dynamics on networks perturbed with viral vector delivery of mutated tau protein (Paper III).

Altogether, work in this thesis presents an *in vitro* modelling system relevant for preclinical disease modelling. We provide novel results through the establishment of layer and subregion specific entorhinal and hippocampal neuron cultures dissected from adult transgenic AD model animals. As technology advances, these models will become increasingly sophisticated and realistic, allowing for more accurate and comprehensive investigations into the complex pathology of AD.

"Progression of Alzheimer's disease through crocheting"

Photo credit: Sara Wuillermin. Published with approval.

Acknowledgements

I am deeply grateful to Ioanna, Axel and Menno for giving me this opportunity and welcoming me into the Witter lab and the Sandvig lab. To my main supervisor Asgeir, thank you for all careful scientific advice, support, and guidance. I appreciate your encouragement for me to expand my scientific network and communication skills and supporting all my extracurricular activities. To Yanna, thank you for your endless support, scientific advice, guidance, and feedback. I am excited to continue pursuing science in the Sandvig lab. To Menno, thank you for being such a great mentor. Your guidance and support has been invaluable. I further would like to thank all co-authors of the papers, especially Nicolai and Janelle. I could not have asked for better collaboration partners; it has been great teamwork from the beginning. Not least Salome, the second paper would not have been possible without your contributions. To all my wonderful colleagues at INB and the Kavli, the scientific and social environment has been inspiring, and I have been privileged to get to know so many wonderful people. Bente, thank you for always being there for me, your advice, and our friendship. Grethe, without your support, technical help, and guidance I would have been lost. Janelle, Christiana, Karoline, and Flo, thank you all for being such a huge support throughout these years. You have all helped me grow as a researcher and person. To all my current office mates, Ingvild, Kristian and Rej, I have enjoyed sharing an office with you all and I appreciate our friendship. I would like to give a special thanks to all animal technicians, Hanne Mali Møllegård and Grethe Mari Olsen for the breeding, genotyping, and taking care of the mice and rats.

To my friends and family, thank you for always cheering on me, for sharing my frustrations, and for keeping me sane. Anna and Lisa, thank you for all concerts, roof-top beers, and pep-talks. Julie, for the endless numbers of dinners. Gøril, Cathrine, Ingvild, Ida, Lene, Anniken, Astrid, Marit, Anne Mette, Nina, and all other friends in Norway and Denmark, thank you for always being there for me and cheering on me always. Especially Jens, thank you for your endless love and support, for always being there, and for being my reason for coming home.

List of papers

Paper I

Dissection and culturing of adult lateral entorhinal cortex layer II neurons from APP/PS1 Alzheimer's model mice

Katrine Sjaastad Hanssen, Menno P. Witter, Axel Sandvig, Ioanna Sandvig and Asgeir Kobro-Flatmoen

Published in Journal of Neuroscience Methods, March 2023, doi.org/10.1016/j.jneumeth.2023.109840

Paper II

Reverse engineering of feedforward cortical-hippocampal neural networks relevant for preclinical disease modelling

Katrine Sjaastad Hanssen*, Nicolai Winter-Hjelm*, Salome Nora Niethammer, Asgeir Kobro-Flatmoen, Menno P. Witter, Axel Sandvig and Ioanna Sandvig

Preprint in bioRxiv, June 2023, doi.org/10.1101/2023.06.26.546556
* Shared first author

Paper III

Altered structural organization and functional connectivity in feedforward neural networks after induced perturbation

Janelle Shari Weir*, **Katrine Sjaastad Hanssen***, Nicolai Winter-Hjelm, Axel Sandvig and Ioanna Sandvig

Preprint in bioRxiv, September 2023, doi: https://doi.org/10.1101/2023.09.12.557339
* Shared first author

x

Abbreviations

Anatomical regions

CA1	Cornu ammonis 1
CA2	Cornu ammonis 2
CA3	Cornu ammonis 3
DG	Dentate gyrus
EC	Entorhinal cortex
HPC	Hippocampus
LEC	Lateral entorhinal cortex
lLEC	Lateralmost lateral entorhinal cortex
MEC	Medial entorhinal cortex
Sub	Subiculum

Terminology

AAV	Adeno Associated Virus
Aβ	Amyloid-β
AD	Alzheimer's disease
APP	Amyloid precursor protein
ApoE	Apolipoprotein E
CaMKII	Ca2+/calmodulin-dependent protein kinase IIα
DIV	Days *in vitro*
MCI	Mild cognitive impairment
pTau	Phosphorylated tau
PS1/PS1	Presenilin 1/2

Supplements and equipment

BDNF	Brain Derived Neurotrophic Factor
DAPI	4',6-diamidino-2-phenylindole
DMEM	Dulbecco's modified Eagle medium
FBS	Fetal Bovine Serum
FGF2	Human FGF-2/bFGF Recombinant Protein
GFP	Green fluorescent protein
HBSS	Hanks Balanced Salt Solution
MAP2	Microtubule associated protein 2
MEAs	Microelectrode arrays
PS	Penicillin-Streptomycin
NPM	Neurobasal Plus Medium
PBS	Phosphate buffered saline
PFA	Paraformaldehyde
PLO	Poly-L-Ornithine
RI	Rock inhibitor (Y-27632 (Dihydrochloride) RHO/ROCK pathway inhibitor

1

Table of Contents

List of Figures

Introduction

A brief introduction to Alzheimer's disease

In 1907, the neuropathologist Alois Alzheimer described 'peculiar changes' in the brain of his patient Auguste Deter (Alzheimer et al., 1995), now known as the two major pathological hallmarks of Alzheimer's disease (AD), namely amyloid-β (Aβ) and neurofibrillary tangles (NFTs). AD is a fatal neurodegenerative disease, associated with increased amounts of Aβ and pathological hyperphosphorylation of the protein tau, both which accumulate over time in the brain. Through complex processes, these pathological events lead to disturbances of synaptic contacts, destabilizes neurons, and eventually lead to neurodegeneration, memory loss and cognitive failure (Braak et al., 1991; Gomez-Isla et al., 1996; Thal et al., 2002). In clinical terms, the disease continuum can be divided into five stages, starting with a symptom free preclinical stage followed by mild cognitive impairment (MCI), mild-, moderate-, and severe AD (**Fig. 1;** ("2023 Alzheimer's disease facts and figures," 2023)). Today, AD is the most prevalent form of dementia accounting for 60-80% (WHO, A Blueprint for Dementia, 2022) of all cases and is one of the foremost reasons for disability worldwide, affecting more than 51 million people ("2023 Alzheimer's disease facts and figures," 2023). In fact, *every three seconds*, someone is diagnosed with dementia (**Fig. 1**; Alzheimer's Disease International: Dementia statistics). The disease burden is expected to triple within 2050 amounting to 60 billion, including caregiving, production loss and disease burden (Menon Report, 63/2020). Since Alzheimers' discovery of the disease over a century ago, intense research has been conducted and we now know more about the pathological impacts and disease progression. However, despite immense technological developments in basic research, diagnostic tools and >2700 AD clinical trials, only seven drugs have been approved by the US Food and Drug Administration, although none of them stops the underlying disease progression (C. K. Kim et al., 2022). Due to the fact that AD is a highly complex disease, a major issue still present in the research field are that procedures that work in transgenic AD model animals have failed to translate to human patients (C. K. Kim et al., 2022).

Thus, refined methods to study anatomically relevant neural networks affected in the early disease stages of AD are strongly needed. By introducing more advanced cellular models through neuroengineering and network-specific models, we gain a reductionist approach to study ongoing alterations of structural and functional network dynamics at both the subcellular and network level (Slanzi et al., 2020). In the three papers presented in this thesis, my work has overall aimed to establish such *in vitro* methods for modelling of AD-relevant neural networks. This included methods for the

extraction and long-term culturing of layer specific entorhinal and hippocampal neurons, that are known to be vulnerable in the early stages of AD, from adult AD transgenic mice and rats. Furthermore, the work included implementation of engineered neural networks on multinodal microfluidic devices relevant for the study of structure-function network dynamics in healthy and diseased networks. Before introducing *in vitro* neural networks and how these can be used for modelling AD, I will introduce central aspects of AD pathology, neurodegeneration, risk factors and the anatomical relevance of the entorhinal cortex and the hippocampal region.
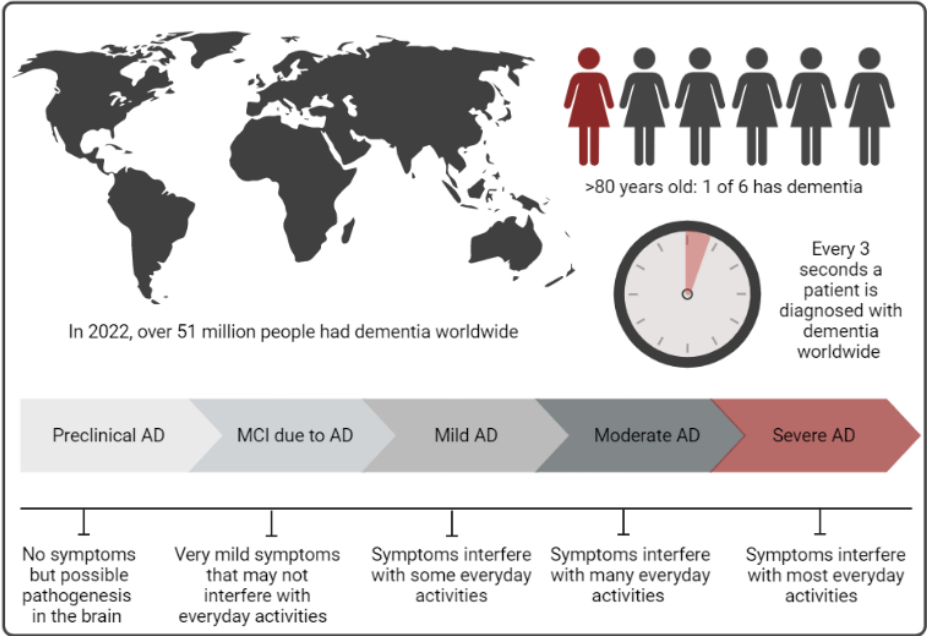
Figure 1. Global impact of Alzheimer's disease (AD) and disease continuum. MCI; Mild cognitive impairment. AD disease continuum timeline modified from ("2023 Alzheimer's disease facts and figures," 2023). Figure created in BioRender.com.

Alzheimer's pathology

One of the major pathological hallmarks of AD is formation of neurofibrillary tangles (NFTs), caused by hyperphosphorylation of the microtubule associated protein (MAP) tau (Braak et al., 1991), which is then referred to as p-tau. Under physiological conditions, tau proteins are generally assumed to stabilize microtubules and hence the neuronal cytoskeleton by interacting with tubulin, enabling cargo

transportation along neurites (González-Billault et al., 2002). But more recent work has challenged this notion, suggesting that tau actually enables labile domains on the axons in response to activity demands (Baas et al., 2019; Qiang et al., 2018). This has called into question the notion that pathological hyperphosphorylation of tau destabilize the stabile domains of microtubules (Medeiros et al., 2011). Clearly, more work is needed to establish the interactions between tau and microtubules, and how AD affects this. Tau contains phosphate groups and is phosphorylated at different serine (Ser) and threonine (Thr) sites (Medeiros et al., 2011), and the dynamic regulation of tau kinases is important for normal phosphorylation of tau (Buée et al., 2000). Abnormal hyperphosphorylation of tau at different sites, like Ser262, Ser235 and Thr231 (as reviewed in (Gong et al., 2008)) have been found to be 3-4 times higher in AD brains compared to controls (Kenessey et al., 1993).

Spread of tau pathology in AD (i.e. p-tau and NFTs) can be divided into Braak-stages I-VI, with entorhinal cortex layer II (EC LII) neurons being affected first (Braak et al., 1991). Subsequently, it spreads to hippocampal regions at stage III-IV and neocortical areas at stage V-VI. In the latter stages, p-tau and NFTs also start appearing in subcortical structures. Notably, the locus coeruleus has been shown to develop early p-tau (Braak et al., 2011), however, this appears to be of a form that is less pathological than that seen in for example the entorhinal cortex (Kaufman et al., 2018). By using functional magnetic resonance imaging (fMRI) to measure functional connectivity (FC) of brain regions in relation to deposition of tau and Aβ, Adams et al., showed that regions with strong entorhinal connectivity have more tau, and this FC-tau relationships correlated with levels of Aβ (Adams et al., 2019). Furthermore, by positron emission tomography (PET) imaging on patients with MCI and AD, tau pathology has been found to correlate well with brain atrophy (Bejanin et al., 2017), and cognitive impairment (Malpetti et al., 2020) expressed by impaired clinical rating scale (CDR) scores (Bierer et al., 1995; Hyman, 1997). Recent advances using blood biomarkers have enabled researchers to detect elevated levels of p-tau markers up to 20 years prior to symptom onset (Palmqvist et al., 2020). Taken together, these findings point to a central role for the entorhinal cortex in the onset of typical AD.

Another major pathological hallmark of AD is the accumulation of Aβ-plaques. In physiological conditions, Aβ is involved in controlling synaptic activity (Palop et al., 2010) and has been proposed to have a protective role before it fails and becomes neurotoxic (Rischel et al., 2022). Aβ-plaques are caused by the accumulation of insoluble Aβ fragments that are the result of cleavage of the amyloid precursor protein (APP) (Palop et al., 2010). APP is a transmembrane protein required for neuronal development and activity in the adult brain, and can be cleaved either through an *amyloidogenic* or a *non-amyloidogenic* pathway (**Fig. 2;** (Zheng et al., 2006)).
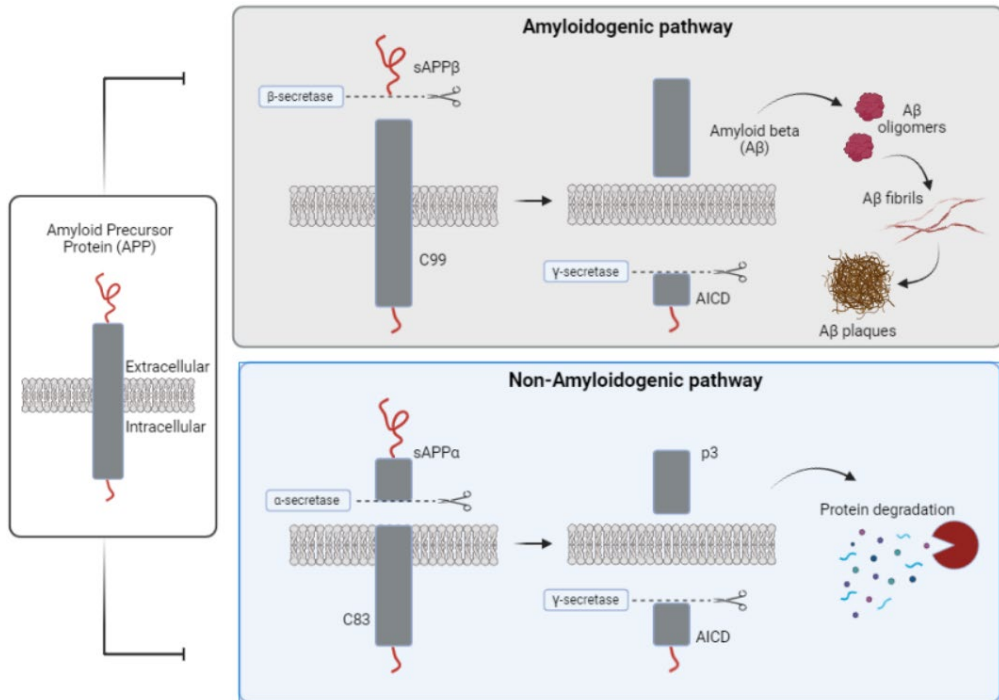
Figure 2. Processing of the APP protein. In the amyloidogenic pathway, APP is first cleaved by β-secretase, which leaves a soluble APPβ fragment (sAPPβ) and an intracellular C-terminal fragment (99 amino acid chain) (C99). The remaining C99 is further cleaved by γ-secretase into the APP intracellular domain (AICD) and the Aβ-peptide. Insoluble oligomeric Aβ will over time form Aβ fibrils and subsequently accumulate into Aβ plaques. In the non-amyloidogenic pathway, APP is first cleaved by α-secretase, within the Aβ sequence, releasing a sAPPα and a remaining C-terminal fragment (C83). Subsequently, cleavage by γ-secretase releases a small peptide called p3 along with an AICD.

In the non-amyloidogenic pathway, APP is first cleaved by α-secretase to release a secreted fragment (sAPPα) and a remaining C-terminal fragment (C83). Because α-secretase cleaves within the Aβ sequence, formation of Aβ is prevented. Subsequently, cleavage of γ-secretase releases a small peptide called p3 along with an APP intracellular domain (AICD). Cleavage by the non-amyloidogenic pathway leads to soluble fragments, which are further degraded (**Fig. 2**). In the amyloidogenic pathway, the extracellular APP-N-terminal is first cleaved by β-secretase (BACE-1), releasing a secreted APP ectodomain (sAPPβ). The remaining C-terminal fragment (99 amino acid chain) is further cleaved by γ-secretase into an AICD and the Aβ-peptide. Aβ peptides can vary in length from 38-43 amino residues, where Aβ42 constitutes the most toxic form being more prone to aggregation (Yan et al., 2006). Over time, these Aβ peptides clump into oligomers, subsequently forming fibrils and sticky Aβ-plaques (El-Agnaf et al., 2000). Unlike Aβ plaques, oligomeric Aβ is found to be highly correlated with cognitive decline (Lublin et al., 2010; Viola et al., 2015).

The spatiotemporal progression of Aβ-plaques throughout the brain can be divided into five phases. Phase 1 includes formation of Aβ-plaques in parts of the neocortex. In phase 2, Aβ-plaques start to appear in the allocortex, including the entorhinal cortex and hippocampal subregions. By phase 3, diencephalic nuclei, the striatum, and cholinergic nuclei of the basal forebrain are also affected. Phases 4-5 represent a further increase in all these regions, while brainstem nuclei and the cerebellum also start to form Aβ-plaques (Thal et al., 2002). While NFTs increase throughout the disease continuum, Aβ-plaques seem to peak at symptom onset of the disease (Serrano-Pozo et al., 2011).

Prior to the onset of Aβ plaques, accumulation of intracellular Aβ (iAβ) is anticipated to lead to synaptic and neuronal dysfunction (Bayer et al., 2010) (**Fig. 3**). Increased levels of iAβ was suggested to be present early in entorhinal and hippocampal areas, regions known to be vulnerable at early AD stages (Gouras et al., 2000). Since then, accumulation of iAβ has been demonstrated in both post-mortem brain tissue (D'Andrea et al., 2001; Gouras et al., 2000; Kobro-Flatmoen et al., 2016) and AD transgenic animal models (Heggland et al., 2015; Takahashi et al., 2002). Thus, there is convincing evidence in favor of the notion that increased levels of iAβ represent an early pathological hallmark in AD. By injection of iAβ in the hippocampus of a mouse model, Roos et al., showed that iAβ seem to play an important role in the prion-like spread of Aβ throughout the brain, with neuronal damage and dystrophic neurites in anatomically connected brain regions (Roos et al., 2021). Furthermore, by the time Aβ plaques accumulate, levels of iAβ have been shown to decrease in the brain, both in post-mortem brain tissue (Gouras et al., 2000; Mori et al., 2002) and neuronal cultures from AD transgenic mice (Oddo et al., 2006). This indicates iAβ involvement as an early hallmark in the disease progression, which likely contributes to increased Aβ plaque load.
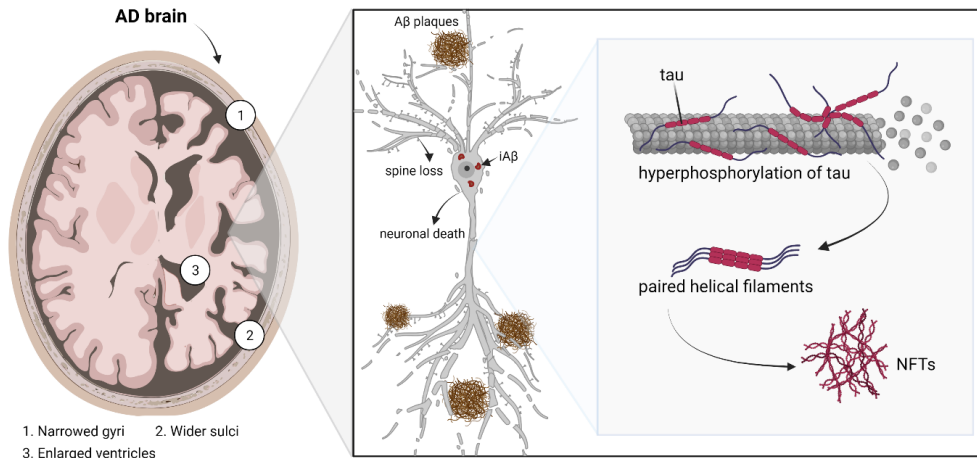
Figure 3. Pathogenesis in the AD brain. Left side: Schematic of a human cranium containing a normal healthy brain (left hemisphere) vs an AD brain (right hemisphere). In the AD brain, brain atrophy is evidenced by narrowed gyri (1), wider sulci (2), and enlarged ventricles (3) (Apostolova et al., 2012). Right side (boxed): Schematic illustrating an AD neuron suffering spine loss (Dorostkar et al., 2015), surrounded by Aβ plaques (Alzheimer et al., 1995; Thal et al., 2002). Zoom-in of the axon illustrates how hyperphosphorylation of tau in the neuron cytoskeleton clumps into paired helical filaments, ultimately forming NFTs (neurofibrillary tangles) (Braak et al., 1991).

Forms of AD and risk factors

Age is by far *the* main risk factor for AD. It is estimated that by the age of 80 years, 1 of 6 people will have dementia (**Fig. 1**; (Prince et al., 2013)). Overall, AD can be subdivided into a sporadic form and a familial form.

Sporadic AD (sAD) account for >95% of all cases and the disease onset is typically after 65 years of age (Chakrabarti et al., 2015), with more women than men being affected (Scheyer et al., 2018). Most sAD cases (60%) are carriers of the ε4 allele of the Apolipoprotein E (ApoE)-*gene* on chromosome 19 (Bekris et al., 2010). ApoE is expressed via three major alleles, ε2, ε3 or ε4, with ApoE- ε3 being the most common form. Relative to APoe3, a combination of ε3 + ε4 leads to a 2-3-fold risk of developing AD, whereas a combination of ε4 + ε4 leads to a 10-12-fold increase for AD (Roses, 1996). However, being a carrier of an ε4 allele does not guarantee that one will develop the disease. On the other hand, the ε2 allele is protective (Z. Li et al., 2020) and is associated with a reduced amount of Aβ depositions compared to the most common form ApoE-ε3 (Nagy et al., 1995). This protective role of ApoE-ε2 seems to be specific for AD (Goldberg et al., 2020), and in a two year follow up study from the AD Neuroimaging Initiative (ADNI), carriers of ApoE-ε2 exhibited a slower rate of hippocampal atrophy compared to ApoE-ε3 carriers, providing strong evidence for the protective role of ApoE-ε2 (H. Kim et al., 2022). Further, environmental factors like smoking, early-life hearing loss, sleeping disorders, poor

diet, traumatic brain injuries, diabetes and a low level of physical activity are known to increase the risk of developing AD (as reviewed in (Scarmeas et al., 2009)).

Familial AD (fAD) is a far rarer form accounting for <5% of all cases, and is caused by having one of several possible mutations on either of three genes, namely the *amyloid precursor protein gene (APP-gene),* the *presenilin 1 gene* (*PSEN1-*gene) or *the presenilin 2 gene* (*PSEN2-gene*) (Takada et al., 2022) (Reitz et al., 2014). AD-related mutations in these genes lead to increased cleavage and accumulation of Aβ 40-42, or a greater Aβ42/40 ratio, through altered synthesis or processing of APP (Bekris et al., 2010; Wu et al., 2012). Specifically, mutations on the *APP-gene* tend to cause increased cleavage by β-secretase (BACE1), resulting in an overall increase in Aβ production (N. M. Li et al., 2019), whereas mutations of the *PSEN1-gene* or *PSEN2-gene* lead to increased cleavage by γ-secretase (Iwatsubo et al., 1994), causing an increased Aβ42/40 ratio (De Strooper, 2007). Mutations of the *APP-gene*, *PSEN1-gene*, and *PSEN2-gene* accounts for 10-15%, 18-50% and <2% of all fAD cases, respectively (Bekris et al., 2010; L. Dong et al., 2022).

The anatomy of memory

The role of the hippocampus and the entorhinal cortex in memory

The entorhinal cortex (EC) and the hippocampus are located in the medial temporal lobe (**Fig. 4**), also called *the memory center of the brain*, and are important for processing, storage, and retrieval of memories. Important historical experimental evidence comes from the case of H.M., who had parts of his medial temporal lobe resected, including most of the hippocampus, to contain his severe epileptic seizures (Scoville et al., 1957). Following this procedure, H.M was no longer able to process and store new memories, and this finding proved essential for advancing the understanding of the role of the hippocampus in declarative memory, spawning a wealth of studies in the decades that followed (Knierim, 2015; Squire, 1992). The discovery of place cells in the hippocampus (O'Keefe & Dostrovsky., 1971), head direction cells in the presubiculum, as well as grid cells, border cells and time cells in the entorhinal cortex (Fyhn et al., 2008; Tsao et al., 2018), have established the entorhinal-hippocampal circuit as important for spatial navigation and perception of time. The fact that these structures are highly vulnerable in the earliest stages of AD is in line with the first symptoms of the disease, which frequently includes problems with navigating in space and keeping track of events related to when they occurred (Allison et al., 2016).
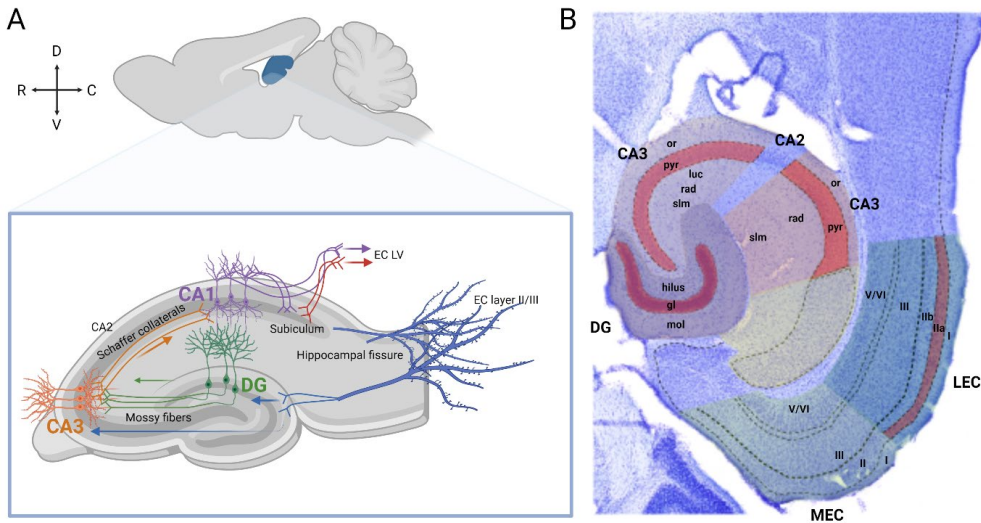
Figure 4. Entorhinal cortex and hippocampus in the rodent brain. (A) Cartoon of a rodent brain with the hippocampus highlighted (blue). Below (boxed) is a transverse section of the hippocampus showing the basic organization of the entorhinal connections with the hippocampus, along with the intra-hippocampal connectivity. D = dorsal, C = caudal, V = ventral, R = rostral (adapted from (Bjorkli, 2022)). **(B)** Nissl-stained horizontal section from a mouse brain. Hippocampal and parahippocampal regions delineated. Figure modified from (van Strien et al., 2009). DG = dentate gyrus, CA3/CA1 = Cornu ammonis region 3 and 1, Sub = Subiculum, LEC = lateral entorhinal cortex, MEC = medial entorhinal cortex, or = oriens, pyr = pyramidale, luc = lucidum, rad = radialis, slm = stratum lacunosum moleculare.

Neuroanatomy of the hippocampus

The hippocampus consists of the dentate gyrus (DG) and Cornu Ammonis regions 1, 2 and 3 (CA1, CA2 and CA3) (Figure 4). When including the subiculum, the term hippocampal formation is typically used (Scoville et al., 1957) (van Strien et al., 2009). Neuronal projections arising from layer II and III of the EC is the major input source to the hippocampal formation (Hyman et al., 1986; Witter et al., 1989) and give rise to the major projection sites to all subfields of the hippocampus, making up the perforant pathway and the temporo-ammonic pathway (**Fig. 4A**). EC LII sends the majority of its projections to the DG and CA3, whereas EC LIII projects to the CA1 and subiculum (Sub). Within the hippocampus, DG sends projections to CA3 via mossy fibers. CA3 in turn projects to CA1 through the Schaffer collaterals, with distal and proximal CA3 projecting to proximal and distal CA1, respectively (**Fig. 4A**; (Witter et al., 1989)). Similarly, projections from the proximal and distal CA1 projects to the distal and proximal subiculum, respectively (Amaral et al., 1991; Naber et al., 2001). Several back-projections are also present in the hippocampus, which have been extensively reviewed (van Strien et al., 2009).

The DG contains a densely packed granular layer consisting of principal granular neurons, enclosed by a superficial molecular layer and a deeper polymorphic layer, also called the hilus (**Fig. 4B**). The CA-

regions (CA1-3) contain a prominent pyramidal cell layer, followed by a deeper cell-free layer, also called stratum oriens (van Strien et al., 2009). The pyramidal layer widens out prominently in the subiculum making it cytoarchitectonically distinguishable from CA1 (**Fig. 4B**). Superficial to the pyramidal layer we find the molecular layer, which in CA3 is divided into a deeper layer called stratum lucidum, a middle part called the stratum radiatum, and the outermost layer stratum lacunosum moleculare. We find the same organization in the CA1-CA2 with exception of the stratum lucidum, which does not extend to these fields. In the subiculum the molecular layer is homogenous (Cappaert et al., 2015).

Neuroanatomy of the entorhinal cortex

EC is part of the periallocortex, although six cell layers can be recognized, as first described by Ramon y Cajal over 100 years ago (**Fig. 4B**, (Cajal, 1902)). EC is an anatomical hub, receiving strong convergent projections from the perirhinal and postrhinal cortex, sending projections into the hippocampus, and receive information from the hippocampus to the deeper layers V/VI and further sending projections back out to cortical areas (Doan et al., 2019; Insausti et al., 1997; Witter et al., 1989). Additionally, EC receive projections from several olfactory nuclei, multimodal sensory cortical domains, and higher order- and subcortical structures (Insausti et al., 1997). In rodents, the EC can be subdivided into two defined areas, namely the lateral entorhinal cortex (LEC) and the medial entorhinal cortex (MEC) (Burwell et al., 1998; Kerr et al., 2007). This subdivision of LEC and MEC is based on morphological, functional, and molecular differences (Canto et al., 2012a, 2012b). For an extensive review of all cell types present in the EC, see (Kobro-Flatmoen et al., 2019). Superficially, both MEC and LEC consist of a relatively cell free layer (layer I). Layer II (LII) consists of reelin- (Re+) and calbindin positive (Cb+) principal neurons. These LII neurons in EC are strikingly bigger compared to LII neurons in surrounding cortical areas making them cytoarchitectonically distinguishable (**Fig. 5**; (Kobro-Flatmoen et al., 2019)). In mice, Cb+ neurons in MEC LII tend to occupy the superficial part of the layer, while Re+ neurons tend to occupy the deep part of the layer. This is in contrast to what is found regarding MEC in other small mammals, as for example rats, where the Re+ neurons occupy the superficial part of layer II and Cb+ neurons occupy the deep part. In LEC LII, the distribution of Cb+ and Re+ neurons is similar for mice and rats. Thus, in LEC LII the outermost part is populated almost exclusively by Re+ neurons, whereas the inner part of LII is populated mainly by Cb+ neurons. Since this part of LEC LII is separated by a cell free zone, two sublayers are sometimes denoted, then referred to as LIIa and LIIb, respectively. Layer III (LIII) contains a mix of large and medium sized pyramidal neurons in both MEC and LEC. Layer IV (lamina dissecans) is a cell-free layer that is more prominent in MEC compared to LEC. Layer V can be subdivided into layer Va vs. Vb, containing larger pyramidal neurons vs. smaller and more densely

packed pyramidal neurons, respectively (Insausti et al., 1997). Notably, in MEC, layer V takes on a prominent radial organization, such that columns of LV pyramidal can be seen to radiate out superficially from the border with LVI. This feature is not present in LV of LEC (**Fig. 5**), which is one of the defining criteria I used to separate MEC from LEC during dissections in Paper I and II. Layer VI is similar in both regions and is homogenous in cell size and shape, exhibiting a columnar distribution at caudal levels and a decreasing cell density towards the white matter (Insausti et al., 1997). In humans, the EC can also be subdivided into two distinct regions, referred to as the anterolateral EC (homologue to LEC in rodents) and posterior-medial EC (homologue to MEC in rodents) (Maass et al., 2015; Navarro Schröder et al., 2015; Olsen et al., 2017; Syversen et al., 2021).

Figure 5. Cytoarchitectonic landmarks to identify lateral entorhinal cortex layer II. (A) A Nissl-stained mouse horizontal brain section. **(B)** Layer II neurons are much larger and seem to extend into layer I in LEC (marked by arrow heads) compared to the anteriorly bordering perirhinal cortex (PRh). **(C)** Layer V neurons form radial patterns in MEC (marked by arrows), a feature not present in LEC (C). **(D-F)**. The same features as seen when using the neuronal marker NeuN (D, E, F corresponds to A, B, C, respectively). DG = dentate gyrus, CA1-CA3 = Cornu ammonis 1-3, LEC = lateral entorhinal cortex, MEC = medial entorhinal cortex, PRh = perirhinal cortex.

Neurodegeneration of entorhinal and hippocampal regions in AD

Neurodegeneration by synapse loss and neuronal loss is a key feature of AD. EC LII neurons are not only affected initially by accumulation of iAβ and tau pathology, but also suffer major neuronal loss at early stages of the disease (Gomez-Isla et al., 1996), likely even before symptoms onset (Kordower et al., 2001). A recent study found that in subjects without cognitive impairment as assessed using standard tests, atrophy of anterolateral EC correlated with decreased performance on a cognitive assessment task (Olsen et al., 2017). This is in line with prior work using fMRI and finding that by the stage of mild AD, 50% of the LEC LII volume and 29% of the CA1 volume is already lost (Price et al., 2001). DG and CA3, two of the major projection sites of LEC LII neurons, has been shown to display a synaptic loss in

DG in humans (Scheff et al., 2006) and a reduction of presynaptic terminals in CA3 of AD transgenic mice (Hsia et al., 1999). DG and CA3 further send projections to CA1, where a structural decrease of presynaptic terminals and functional impairment of synaptic transmission between CA3 to CA1 is prominent in transgenic mice expressing human APP, but not in healthy controls (Hsia et al., 1999). Furthermore, CA1 are affected early in AD by a prominent synaptic and neuronal loss (Scheff et al., 2006; West et al., 2004). By the late stage of AD, severe neuronal loss of ECLII is evident, reaching a loss of up to 90% of the neurons (Gomez-Isla et al., 1996). This neuronal loss appears to greatly exceed the amount of NFTs, suggesting factors aside from p-tau and NFTs are also involved in causing neuronal loss (Gómez-Isla et al., 1997).

The reelin protein and its involvement in AD

During the past decade several researchers investigated the involvement of the glycoprotein reelin, its molecular mechanisms, and its downstream signaling pathways in relation to AD pathophysiology (Botella-López et al., 2010; Chin et al., 2007; Kobro-Flatmoen et al., 2016; Krstic et al., 2013; Sáez-Valero et al., 2003; Seripa et al., 2008; Yu et al., 2016). Reelin signaling requires the presence of at least one of two receptors, ApoE receptor 2 (ApoER2) or the very low-density lipoprotein receptor (VLDLR) (Tissir et al., 2002). Signal transduction of reelin involves binding to either of the two receptors, leading to the activation of Dab1 (**Fig. 6**; (D'Arcangelo et al., 1999)). This in turn activates cytosolic kinase pathways involving Scr-family kinases (SFKs) leading to the phosphorylation of NMDAr subunit NR2 on the postsynaptic membrane and the concomitant potentiation of NMDAr-mediated Ca2+ influx (**Fig. 6**). Additionally, activation of Dab1 leads to the recruitment and activation of additional non-receptor tyrosine kinases allowing the activation of cytosolic kinase cascades, involving PI3K and Akt/PKB. Activation of these non-receptor tyrosine kinases results in the inhibition of glycogen synthase kinase 3 β (GSK3β), as well as CDK5, two of the main kinases that phosphorylates tau protein (as reviewed in (Tissir et al., 2003). A downregulated activity of GSK3β has been shown to lead to alterations in downstream kinase activity causing abnormal phosphorylation of tau, subsequently altering axonal transport, and leading to formation of NFTs (as reviewed in (Deutsch et al., 2006) and (Yu et al., 2016)).
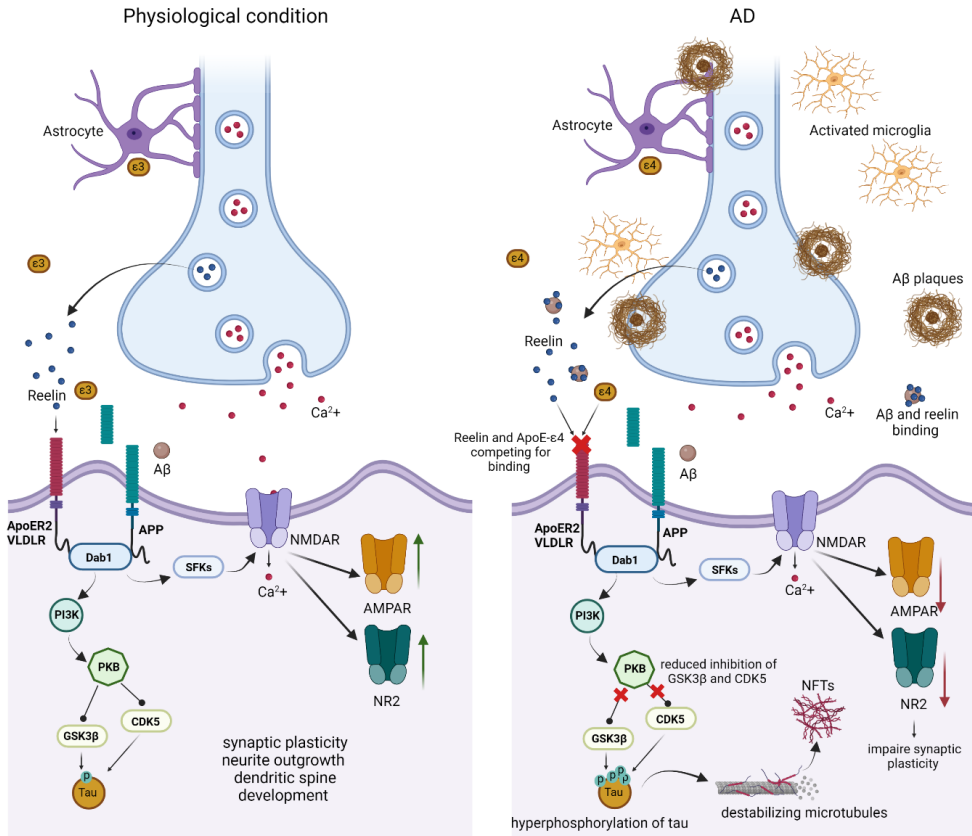
Figure 6. Proposed involvement of the reelin signaling cascade in AD. *Physiological condition*: reelin binds to either of the two receptors, ApoER2 or VLDLR, leading to activation of Dab1. This in turn activates cytosolic kinase pathways involving SFKs leading to the phosphorylation of NMDAR subunit NR2 on the postsynaptic membrane and the concomitant potentiation of NMDAr-mediated Ca^{2+} influx (Chen et al., 2005). Dab1 also activates cytosolic kinase pathways involving PIK3 and PKB/Akt. This leads to inhibition of GS3β and CDK5, two of the main kinases that phosphorylates tau protein (Beffert et al., 2002) Reelin signaling is known to be important for synaptic plasticity, neurite outgrowth and dendritic spine development (Tissir et al., 2002). *AD*: In pathological conditions, ApoE4 suppress reelin binding, leading to a downregulation of GSK3β, ultimately modifying reelin's ability to inhibit tau phosphorylation (Deutsch et al., 2006). These alterations of downstream kinase activity can lead to changes in NMDAR induced Ca^{2+} signaling abnormal phosphorylation of tau, destabilized microtubule and axonal transport and widespread formation of NFTs (Yu et al., 2016). NMDARs, N-metyl-D-aspartate receptor; SFKs, Scr-family kinases; Dab1, Disabled-1; AMPAR, α-amino-3-hydroxy-5-methyl-4-isoxazolepropionic acid receptor; ApoER2, Apolipoprotein 2 receptor; PI3K, Phosphoinositide 3-kinase; PKB, Protein kinase B; CDK5, cyclin dependent kinase 5; GSK3β, glycogen synthase kinase 3 beta; NFTs, neurofibrillary tangles. Figure modified from (Doehner et al., 2010) and (Kobro-Flatmoen et al., 2021). Figure made in BioRender.com.

Reelin has been found to interact with Aβ in human brain tissue (Botella-López et al., 2010; Cuchillo-Ibañez et al., 2016), with accumulated extracellular deposits in aged individuals (Doehner et al., 2010). In AD transgenic (human APP) mice and post-mortem human brains, Chin et al., observed a significant reduction of reelin immunoreactive principal neurons in layer II of the entorhinal cortex (EC LII), but not in interneurons (Chin et al., 2007), suggesting a vulnerability of reelin expressing (Re+) principal

neurons. In the same transgenic mice, hippocampal regions DG and CA1 had decreased levels of full-length and 180 kDa reelin fragments, suggesting that hAPP/Aβ-induced reductions of reelin expression in EC LII neurons may reduce the amount of reelin released onto subregions of the hippocampus (Chin et al., 2007). A study from our group has shown that reelin expressing EC LII neurons align along a gradient where those located successively closer to the rhinal fissure express increasingly higher amounts of reelin, in both humans and AD transgenic rats (Kobro-Flatmoen et al., 2016). Intriguingly, these neurons selectively accumulate iAβ and this accumulation aligns along the same gradient (Kobro-Flatmoen et al., 2016). Furthermore, a recent follow-up study showed that lowering reelin expression in EC LII neurons led to a concomitant decreased accumulation of iAβ (Kobro-Flatmoen et al., 2023). Interestingly, initial spread of tau pathology align on the same gradient as reelin neurons are expressed along the olfactory and limbic pathways in the developing brain (extensively reviewed in (Krstic et al., 2013)).

Genetic variants of reelin have been shown to play a considerable role in AD pathogenesis, in particular for females, with a specific genotype (8/8) significantly overrepresented in AD cases vs. controls (Seripa et al., 2008) (Kramer et al., 2011). Moreover, in a recent paper the authors reported on a remarkable case with fAD due to having the PSEN1-E280A mutation, in which the subject exhibited extreme resilience to dementia. Aside from the fAD-related mutation, this subject was shown to be heterozygous for a rare mutation in the reelin gene (H3447R) and appears to have a largely intact EC LII despite having inherited the normally fully penetrant fAD mutation (Lopera et al., 2023).

Overall, alterations of reeling signaling seems to play a key role in initial AD stages, and Re+ EC LII pose to be selectively vulnerable by impaired reelin signaling, affected by early iAβ accumulation (Kobro-Flatmoen et al., 2023); (Kobro-Flatmoen et al., 2016), and downstream signaling alterations, impaired inhibition of GSK3β (Beffert et al., 2002), ultimately leading to hyperphosphorylation of tau and build-up of NFTs (Deutsch et al., 2006; Yu et al., 2016).

Network activity affected by pathogenesis and degeneration in AD

So how will these alterations of the structural networks by accumulation of pathology, synapse loss, and neurodegeneration affect the functional network dynamics? Accompanied by accumulating pathology, neuronal circuits in AD transgenic mice are known to be vulnerable for hyperactivity in the very early stages of AD (Busche et al., 2015; Minkeviciene et al., 2009; Palop et al., 2009; Vossel et al., 2013). Using two-photon Ca2+ imaging in an AD mouse model (APP23xPS45) a decrease in neuronal activity was seen in 29% of layer 2/3 cortical neurons, however, 21% of neurons displayed an increase in the frequency of spontaneous Ca2+ transients (Busche et al., 2008). Not only did hyperactive neurons

fire more frequently, but they also did this in a correlated manner, thus increasing the risk for seizure-like activity. A subset of neurons in the DG of hAPP transgenic mice are also shown to be affected by hyperactivity displayed by non-conclusive seizure activity (Palop et al., 2007). Interestingly, by Ca^{2+} imaging in APP/PS1 model mice, Busche et al., showed that neurons in CA1 express severely altered neuronal activity with a mix of hyperactive and silent neurons (Busche et al., 2012).

A factor that can lead to hyperactivity in neural networks is dysfunction of interneurons, where decreased levels of the interneuron specific and parvalbumin cell-predominant voltage-gated channel subunit Nav1.1 has been implicated (Verret et al., 2012). Another finding suggests that Aβ-dependent hyperactivity could be caused by suppression of glutamate uptake in CA1 pyramidal neurons (Zott et al., 2019). Impaired calcium homeostasis with calcium overload in neurites of transgenic APP model mice has also been described as a contributor the hyperactive state related to Aβ pathology, leading to distortion of neuritic morphology and disruption in neural network activity (Kuchibhotla et al., 2008). In early disease stages it has been shown that soluble oligomeric Aβ alters the function of neuronal circuits and large-scale networks by disrupting the balance of synaptic excitation-inhibition (as reviewed in (Busche et al., 2016)).

Altered structural organization may also have implications on network activity. For example, in a mouse model of AD, dendritic structural degeneration was functionally linked to cellular hyperexcitability (Šišková et al., 2014). Studies have also found that increased levels of Aβ42 oligomers or APP can result in an increase in surface expression of sodium channels in AD models, both *in vitro* (Wang et al., 2016) and *in vivo* (Liu et al., 2015). In one transgenic AD mouse model (Tg2576), an early alteration in firing properties of LEC LII, but not MEC LII neurons was observed (Marcantoni et al., 2014). In the same mouse model, recordings by acute and anesthetized single-unit electrophysiology found that LEC LII neurons exhibit early hyperactivity and linked this to iAβ precursor protein C-terminal fragments from projecting cortical regions and soluble Aβ (Xu et al., 2015). However, no difference was observed in odor discrimination and memory in transgenic vs. control animals.

Epileptiform activity and seizures are also observed in human patients, where genetic forms of AD marked by abnormal processing and deposition of Aβ is suggested to be particularly likely to be associated with seizures (as reviewed in (Friedman et al., 2012)). The risk of epileptic seizures is particularly high in AD patients during early disease stages, reaching an 87-fold increase in seizure incidence compared with an age-matched reference population (Amatniek et al., 2006). Treatment with the anti-epileptic drug, Levetiracetam, showed a reversal of hyperactive seizure activity in neuronal networks and reversing synaptic and cognitive deficits (Sanchez et al., 2012).

AD animal models

Transgenic animals are the most widely used model in AD research, and have provided important insights into disease pathogenesis, spread, and attempts at drug development (as reviewed in (Benedikz et al., 2009; Esquerda-Canals et al., 2017). Since the first transgenic AD mouse line was developed in 1995 (Games et al., 1995), a large number of models have been generated, and today 197 different AD model mice and 17 AD model rats exist as according to Alzforum.com. Animal models will not develop the full pathological disease cascade as it occurs in humans, but specific pathological features are recapitulated. By carrying a human APP transgene, the animal models typically overexpress increased levels of Aβ (Leon et al., 2010; Radde et al., 2006) (Leon et al., 2010). Additionally, knock in of human MAPT can lead to pathological tau load (Jawhar et al., 2012; Oddo et al., 2003). The high failure rate in clinical trials can be related to genetic, anatomical, and physiological variations between rodents and humans (Drummond et al., 2017).

For the work in this thesis, two transgenic AD models were used, the APP/PS1 mouse model (Paper I and II) and the McGill-R-Thy1-APP rat model (Paper II). The APP/PS1 mouse model is based on a C57BL/6J genetic background and carries one human transgene for APP that contains the APP K670_M671delinsNL (Swedish mutation) (Mullan et al., 1992) and the PSEN1 L166P mutation (Moehlmann et al., 2002), under the control of the Thy1 promoter (Radde et al., 2006). The expression of the human APP transgene is approximately 3-fold higher than endogenous murine APP. This leads to deposition of amyloid plaques starting already at 6 weeks in the neocortex, before appearing in the hippocampus at 3-4 months (Radde et al., 2006). Significant memory deficits have been reported by 5 months (Zhu et al., 2017). The McGill-R-Thy1-APP rat model is based on a Wistar (HsdBrl:WH) genetic background and carries a human APP_{751} transgene cassette, containing the APP K670_M671delinsNL (Swedish mutation) and the APP V717F (Indiana mutation), under control of the Thy1 promoter (Leon et al., 2010).

Cellular models of AD

Primary cortical and hippocampal neuronal cultures

Since the establishment of a primary cell culture of frog nerve fibers by R.G. Harrison in 1907 (Ambrose, 2019), primary hippocampal and cortical neurons have been the object of intense research. Such neurons are usually derived from early postnatal or embryonic animals, as the networks are still not fully developed and fully innervated, and harbors extensive neurite outgrowth (Sciarretta et al., 2010).

Compared to adult neurons, embryonic or postnatal neurons tend to survive better in culture and are easier to maintain over longer time periods. Moreover, embryonic, or postnatal neurons are widely accessible as they can be frozen in stock and are commercially available. Neuron cultures are thus well in line with thee 3R (Reduction, Refinement, Replacement) in the use of laboratory animals and also reducing the need for animal facilities and tissue preparation (Koganezawa et al., 2023). However, as AD affects the adult brain, primary neurons derived from adult animal models confer significant advantages in terms of preclinical modelling of AD. Several studies have demonstrated that cultured adult cortical and hippocampal neurons from both mice and rats retain both electrophysiological (Evans et al., 1998; Varghese et al., 2009) and morphological characteristics (Eide et al., 2005; Varghese et al., 2009) as seen in the brain.

In AD research, it has been argued that cell cultures established from transgenic AD model animals offer several advantages compared to *in vivo* experiments and tissue slices for the study of efficacy and compounds in drug applications (Trinchese et al., 2004). This includes the possibility of maintaining cells long-term under a controlled environment, accessibility for selective perturbations (Fiskum et al., 2021; Valderhaug et al., 2021; Weir et al., 2023), direct monitoring of molecular- or chemogenetic responses (Y. Dong, Sameni, et al., 2019; Westhaus et al., 2020), and the ability to monitor neuronal and synaptic responses (Bauer et al., 2022). Compared to cultured adult hippocampal neurons from non-transgenic animals, hippocampal neurons from the 3xTg AD model mice have been reported to exhibit global metabolic alterations with increased inflammatory responses and decreased glutamate and GABA metabolites (Y. Dong, Digman, et al., 2019). Furthermore, cultures from embryonic AD transgenic animals display elevated levels of human $A\beta40$ and $A\beta42$, p-tau and alterations of calcium homeostasis already by 11-12 days in vitro (DIV) (Trinchese et al., 2004). Thus, moving such neurons into the culture enables the study of pathological network activity responses in a reductionist approach within a short time frame, '*providing an exceptional tool to investigate pharmacological approaches*' (Vale et al., 2010).

In vitro electrophysiology using microelectrode arrays

Microelectrode arrays (MEAs) was first described in 1972 (Thomas et al., 1972) and has since been the most used implementation for measurement of *in vitro* electrophysiological activity (**Fig. 7**). MEAs are interfaces where neurons are plated on a coating substrate above a set of electrodes, such that the electrodes are able to capture neural network activity in the form of spontaneous *or* evoked neural spiking activity (Frega et al., 2012) or local field potentials (Gold et al., 2006) (Gonzalez-Sulser et al., 2012). Extracellular electrodes measure fluctuations in the electrical field potential surrounding the

electrode. These fluctuations are caused by local movements of ions in response to ion channels opening and closing as action potential propagate down the axons of neurons. MEAs can capture ongoing network activity summed from thousands of neurons and have been implemented in cultures derived from several species, like mice (Zhang et al., 2021), rats (Napoli et al., 2016), monkeys (Zhang et al., 2021) and humans (Zhang et al., 2021) (Napoli et al., 2016). Measuring such network activity can enable one to capture subtle dynamics over time, and differences between healthy and diseased *or* perturbed conditions (Djemil et al., 2020) (Frega et al., 2012).

Figure 7. Microelectrode arrays. Schematic of a microelectrode array with an inset of a cell culture showing neurons widespread around the electrodes (black circles). The electrodes will capture spontaneously evoked extracellular network activity from the neurons which can be captured as network bursts (top) and single spikes (bottom). Figure created in BioRender.com.

Engineered neural network approaches to model Alzheimer's disease

In recent years, microfluidic technologies have provided a means for creating more physiologically relevant neural networks by providing multinodal compartments connected by microchannels that are only permissible for axons (Taylor et al., 2005; Taylor et al., 2003). As compared to single-node culturing platforms, microfluidic devices have as such opened an avenue to establish more complex network configurations, including the ability to capture network dynamics across several nodes. When coupled to MEAs, complex network dynamics within different nodes can be monitored as intranodal connectivity, i.e., within one node, or internodal connectivity, i.e., across nodes (Pan et al., 2015) (Vakilna et al., 2021; Winter-Hjelm N, 2023). The continuous advancement in engineered microfluidic devices presents the possibility to capture complex network dynamics at both the network and subcellular level (DeMarse et al., 2016; Poli et al., 2018; Vakilna et al., 2021). The most common design used in the field has been two-nodal microfluidic devices interfaced with microelectrode arrays, also referred to as 'microelectromechanical systems (MEMS)' (DeMarse et al., 2016; Pan et al., 2015). It has been shown that culturing cortical neurons in one node followed by the culturing of a second set of

neurons in a second note, done with a delay of a few days, allows for growth of axonal projections through the microchannels, promoting unidirectional connectivity between nodes (DeMarse et al., 2016; Dworak et al., 2009). This has been evidenced by both spontaneously evoked network activity and stimulation of networks initiating a response in a feedforward manner (DeMarse et al., 2016; Pan et al., 2015). However, a major drawback with plating neurons at various time points is that one introduces neurons with different maturation stages, which may affect the physiological behaviour of the networks relative to neurons plated at the same time. A recent study by the Sandvig lab has shown that such feedforward activity can also be promoted by implementing a Tesla valve design of the microtunnels, which includes spine structures on the postsynaptic side to misguide the axons from entering the presynaptic side (Winter-Hjelm N, 2023). This design builds upon previous studies which have proven that such geometrical constraints do control the directionality of axonal outgrowths in multinodal devices (Forró et al., 2018; Mahoney et al., 2005; Peyrin et al., 2011). Complimentary to the use of different culturing time points and geometrical constraints initiating feedforward connectivity of networks, is the possibility to add chemical cues (Kundu et al., 2013) and growth factors (Habibey et al., 2022) to initiate feedforward connectivity of the networks.

The utility of microfluidic technologies has further enabled the study of more anatomically relevant neural networks *in vitro*, with the possibility to include various subregional cell types in each node, which are interconnected by microtunnels. A few studies have provided reconstruction of primary hippocampal (Brewer et al., 2013) and entorhinal-hippocampal (Poli et al., 2018; Vakilna et al., 2021) neural networks on microfluidic devices derived from rats at P4. By quantitative polymerase chain reaction (qPCR), they showed that their putative hippocampal DG, CA3 and CA1 networks were in fact enriched in certain neuronal types (Brewer et al., 2013). Because AD progresses over time, with accumulation of pathology and network activity dysfunction, it is of high interest to enable studies allowing one to follow the pathogenesis and alteration of network dynamics in real time. Our work in this thesis, i.e., modelling EC-hippocampal networks, builds upon and expands on previous work by others (Brewer et al., 2013; Poli et al., 2018; Vakilna et al., 2021).

Thesis aims and objectives

The overarching aim of this thesis was to establish methods for extraction and long-term culturing of layer-specific neurons from adult AD-model mice and rats on MEAs and microfluidic devices. Furthermore, by using engineered multinodal microfluidic devices, we aimed to establish anatomically relevant neural networks to study long-term neural network dynamics associated with the healthy vs diseased state, and to capture alterations in structural organization and functional connectivity.

From this overarching aim, I have worked to reach three specific objectives:

i) Establish a method for dissection and culturing of adult lateralmost lateral entorhinal cortex layer II (lLEC-LII) neurons from AD-model APP/PS1 mice (Paper I), in addition to DG granular layer (gl), CA3- and CA1- pyramidal neurons (pyr) neurons from adult AD model rats and mice (Paper II), to enable the study of specifically vulnerable neurons in the early stages of AD.

ii) Recapitulate AD-relevant neural networks on a four-nodal microfluidic device with unidirectional microtunnels to enable the study of structure-function network dynamics (Paper II).

iii) Investigate how perturbation of mature healthy neural networks with human mutated tau affects structure-functional network dynamics over time (Paper III).

Synopsis of methods

Paper I – Dissection and culturing of adult lateral entorhinal cortex layer II neurons from the APP/PS1 Alzheimer's mouse model

For the first paper, 48 APP/PS1 AD model mice and littermate controls were used for development of the protocol. Of these, nine mice were included for the results in the paper. Brains were extracted fresh and sectioned horizontally (at 300 μm) on a vibratome (frequency of 5.3 Hz with a speed of 8 mm/ s.) **(Fig. 8)**. I then viewed each section under a stereoscope using cross polarized lights and dissected out lLEC. Subsequently, the tissue was dissociated into a single cell solution by enzymatic dissociation (papain) and manual trituration (pipetting) and then plated onto culture vessels (MEAs or 24-well plates) pre-coated with Poly-L-Ornithine and laminin with a monolayer of astrocytes. Electrophysiological recordings were done using Multichannel a MEA2100 recording system (Multichannel systems, MCS, Reutlingen, Germany). Evoked spontaneous activity was recorded for 10 minutes, collected at a rate of 10 kHz/channel, starting at 15 DIV and every three days onwards until 69 DIV. All data was converted to .h5 hierarchical data format files before further analysis was done in MatLAB2020a. Immunocytochemistry was conducted at 61 DIV by staining for neuronal marker (NeuN), reelin and intracellular amyloid beta (A11). Furthermore, to quantify neurons co-expressing Re+, NeuN and A11, we took images of each relevant channel from five different regions in a culture and applied a threshold to identify neuronal somata using Fiji (version 1.53i).
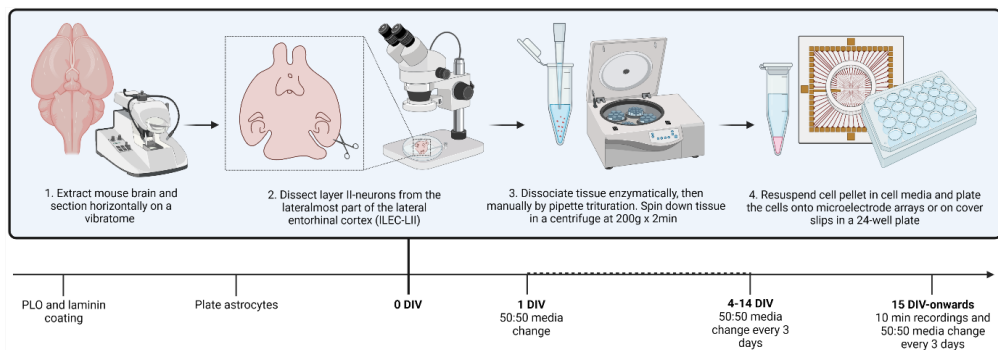
Figure 8. Overview of experimental setup: Paper I. Before plating of the lateralmost lateral entorhinal cortex layer II (lLEC-LII-neurons), we coated the culture wells with Poly-L-Ornithine (PLO) and laminin. 48 hours prior to plating of neurons we added a monolayer of rat cortical astrocytes. On day 0, we extracted and horizontally sectioned APP/PS1 mouse brains, and then dissected strips of lLEC-LII-neurons under a stereoscope. The strips were dissociated enzymatically and then manually triturated with a 100 μL pipette, and then spun down in a centrifuge at 200g x 2min. The cell pellet was re-suspended in 100 μL cell media before plating. At 1 DIV half the media was changed; this was subsequently repeated every 3 days. From 15 DIV we started recording spontaneous activity. DIV; days in vitro. Created with BioRender.com.

Paper II – Reverse engineering of feedforward cortical-hippocampal neural networks relevant for preclinical disease modelling

For the second paper, 42 adult McGill-Thy1-APP AD-model rats and 2 adult APP/PS1 AD-model mice, in addition to commercially available cortical and hippocampal primary neurons were plated on customized four-nodal microfluidic devices at a concentration of 750 cells/mm2 i.e., 15 000 *or* 1000 cells/mm^2, i.e., 2000 per node, for adult and commercial neurons, respectively. Before plating of the neurons, all devices were coated with Poly-L-Ornithine (PLO) and Laminin before commercially available Rat Primary Cortical Astrocytes were plated at a concentration of 100 cells/mm^2, i.e., 2000 per microchamber **(Fig. 9)**. Microfluidic devises on microelectrode arrays (mMEAs) were used for electrophysiological recordings and microfluidic devised on glass slides was used for immunocytochemistry. A MEA2100 workstation (Multichannel Systems) was utilized for all recordings with a sampling rate of 25 000 Hz and all cultures were allowed to equilibrate for 5 min before recording of spontaneous and electrically evoked electrophysiological activity. mMEAs with adult and embryonic neurons were recorded for 10 and 15 minutes, respectively. All data pre-processing and analyses were conducted in Matlab R2020b. Before spike detection, a 4th order Butterworth bandpass filter was used to remove noise <300 Hz and >3000 Hz in addition to a notch filter to remove noise at 50 Hz from the power supply mains. Immunocytochemistry included staining for neuronal marker NeuN and neurofilament marker NFH for adult neurons, in addition to reelin for LEC LII neurons. The commercial primary cortical and hippocampal neurons were stained for MAP2, β3-tubulin, GFAP, NeuN, NFH and GAP43.
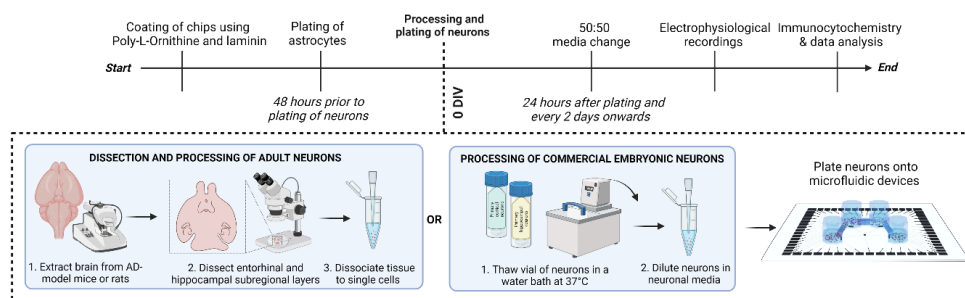
Figure 9. Overview of experimental setup: Paper II. Before plating of the primary neurons, we coated the culture wells with Poly-L-Ornithine (PLO) and laminin and plated rat cortical astrocytes. On day 0, we extracted and horizontally sectioned APP/PS1 mouse brains, and then dissected strips of lLEC-LII-neurons under a stereoscope. The strips were dissociated enzymatically and then manually triturated with a 100 µL pipette, and then spun down in a centrifuge at 200g x 2min. The cell pellet was re-suspended in 100 µL cell media before plating. At 1 DIV half the media was changed; this was subsequently repeated every 3 days. From 15 DIV we started recording spontaneous activity. DIV = days in vitro. Created with BioRender.com.

Paper III – Altered structural organization and functional connectivity in feedforward neural networks after perturbation

For the third paper, commercially available rat primary cortical neurons were plated on in-house developed two-nodal microfluidic devices (n=7) (Winter-Hjelm N, 2023) **(Fig. 10)** or on 8-well chambered Ibidi chips (n=2). All culture wells were pre-coated with PLO and laminin solution and a monolayer of rat cortical astrocytes (plated 48 h prior to neurons). Networks were maintained in an incubator (37°C, 20% H_2O and 5% CO_2) consistently except during media changes, imaging, and recording. Networks were supplemented by 50% fresh media every two days and electrophysiological recordings commenced using a MEA2100 recording systems (Multichannel Systems). Evoked spontaneous network activity was recorded for 15 minutes from 16 DIV and every four days onwards. Additional electrical stimulations were conducted from 26 DIV, consisting of a spike train of 60 spikes at ± 800 mV of 200 μs duration with an interspike interval of 5s. Immunocytochemistry was performed on parallel cultures on Ibidi chips at 21 DIV to assess network maturity (CamKII, MAP2, GAD65), intranodal connectivity (MAP2) and phosphorylated tau (AT8 and Phospho-tau (Thr217)). At 28 DIV, four neural networks were transduced using a viral construct (AAV8-GFP-2A-P301L) carrying a human tau mutation (P301L) diluted in cell media. The viral load was introduced to the presynaptic node of the networks, while control networks (n=3) received fresh media only. A titration of $3x10^2$ viral units per neuron were used after extensive testing of various loads. Viral expression was confirmed after 48 hours based on GFP expression in the transduced networks. All data analysis was done using Matlab2020a.
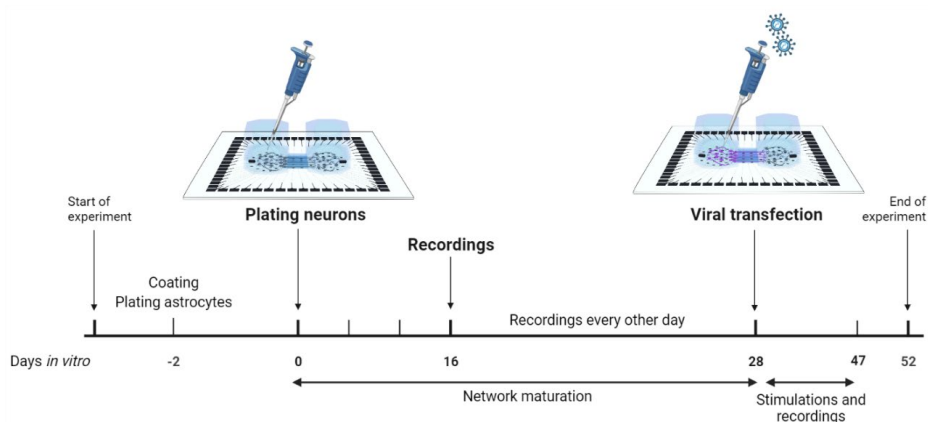

Figure 10. Overview of experimental setup. Schematic of *in vitro* methods for establishing networks, transduction, and electrophysiological recordings. Created with BioRender.com.

Synopsis of results

Paper I – Dissection and culturing of adult lateral entorhinal cortex layer II neurons from the APP/PS1 Alzheimer's mouse model

In the first paper we show a method for the dissection and long-term culturing of lateralmost lateral entorhinal cortex layer II (lLEC-LII) neurons from APP/PS1 Alzheimer's model mice. lLEC-LII neurons extruded neurites already 2 hours after cellular attachment to the culture vessels (**Fig. 11A**) and we observed a pronounced neurite outgrowth over time, and by 51 DIV highly branched neurites were still present (**Fig. 11B**). Characterization by immunocytochemistry (ICC) at 61 DIV, where we stained for neuronal marker NeuN in combination with reelin, showed that we had acquired and cultured the neurons of interest, i.e., reelin-expressing lLEC-LII neurons. By further staining against oligomeric amyloid-β (Aβ) using A11 we showed that the lLEC LII-neurons retain the ability to express Aβ *in vitro* (**Fig. 11C**). By quantification of ICC from five different regions in one culture we found that 84/88 neurons co-expressed NeuN, reelin and A11. This is in line with the known strong intracellular expression of iAβ in such neurons seen in vivo in the APP/PS1 mice, and also known to be strongly present in ECLII in human brains during preclinical stages of AD. Functional activity was measured by electrophysiological recordings using 60-electrode MEAs (Multichannel Systems, Reutlingen, Germany). lLEC-LII-networks were spontaneously active, showing spikes by 15 DIV and remaining active beyond two months, albeit with a low firing rate (**Fig. 11D**). Overall, our method to dissect and culture lLEC LII neurons from adult AD model animals offers a neuron and network-specific *in vitro* system and may represent a valuable tool to study early pathogenesis in AD-relevant neural networks over time.
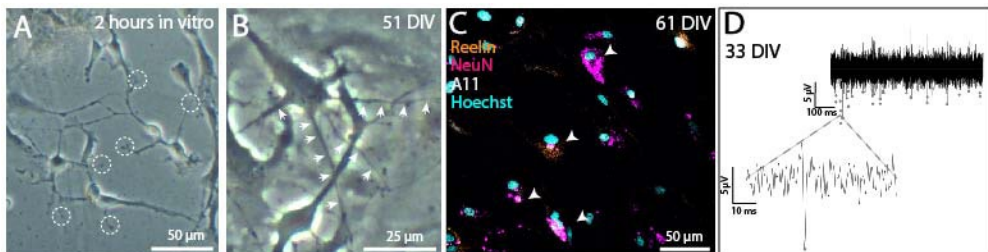
Figure 11. Overview of results: Paper I. Adult lLEC LII neuron cultures reform structural connections and display network activity. **(A)** Dissected and cultured adult lLEC-LII neurons start to reorganize structural connections after 2 hours in vitro. **(B)** Structural connections in the same cultures as in (A) remain at 51 DIV. **(C)** The neurons co-express neuronal marker NeuN, reelin and oligomeric Aβ (A11) at 61 DIV **(D)** The networks display functional neural activity in form of spiking activity. DIV = days *in vitro*.

Paper II – Reverse engineering of feedforward cortical-hippocampal neural networks relevant for preclinical disease modelling

In the second paper, we show the utility of reverse-engineered multinodal cortical-hippocampal networks with controllable feedforward network organization using custom-designed microfluidic devices with microelectrode arrays. Both spontaneously evoked (**Fig. 12A**) and stimulation induced network activity show that the multinodal microfluidic device promote establishment of feedforward network activity, displayed by network bursts propagating across the four nodes. At 28 DIV, as much as 24.2% of the network bursts propagated through all four nodes, compared to less than 2% at 12 DIV. Increased complexity of the network dynamics was evidenced by increased correlation of intranodal (within nodes) and internodal (between nodes) activities over time. By 20 DIV integration of all neighbouring nodes was established, with an increased correlation by non-neighbouring nodes at 28 DIV, indicating a higher network-wide synchronization. To advocate the broader applicability of this model system, we provide proof of concept for the long-term culturing of adult layer- and subregion specific LEC LII and hippocampal DG-gl, CA3-pyr and CA1-pyr neurons derived from transgenic AD model mice and rats. Such adult networks reform structural connections in the culture (**Fig. 12B**) and exhibit electrophysiological activity from 15 DIV until 47 DIV, at which point the cultures were terminated. Together, our results highlight the suitability and potential of our approach for reverse engineering of biologically and anatomically relevant neural networks, supporting the study of dynamic structure-function relationship in both healthy and pathological conditions.
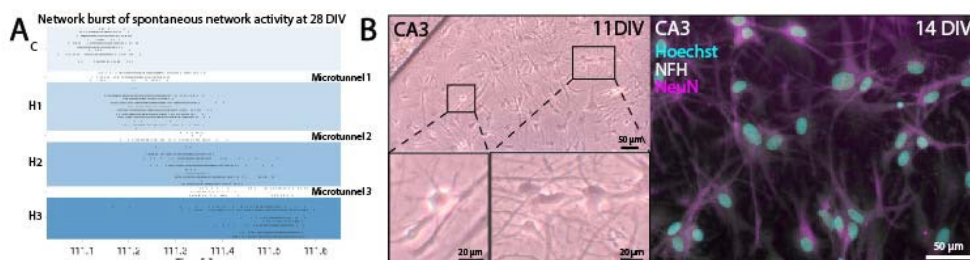
Figure 12. Overview of results: Paper II. Structural connection and functional connectivity. **(A)** Cortical and hippocampal (commercially available) neural networks on the four-nodal microfluidic devise display bursting behaviour with network bursts initiated in the first node (cortical) and gradually spreading through the microtunnels in a feedforward manner. DIV, days in vitro; C, cortical node; H1-3, Hippocampal node 1-3. **(B)** Adult hippocampal DG neurons derived from McGill-R-Thy1-APP rats reform structural connections in culture and express neuronal marker NeuN and neurite marker neurofilament heavy (NFH).

Paper III – Altered structural organization and functional connectivity in feedforward neural networks after induced perturbation

In the third paper, we investigated ongoing structural and functional network dynamics in engineered feedforward neural networks following perturbation by viral transduction of human mutated tau. The networks were perturbed in the presynaptic node at 28 DIV, and we observed a stronger fluorescent signal of antibodies AT8 and Phospho-tau (Thr217) in the perturbed networks compared to controls. Already four days after addition of the mutated tau (at 32 DIV) we could observe ongoing axonal retraction in the presynaptic node (**Fig. 13A**). By 52 DIV, this retraction had progressed and was evident also in the postsynaptic node. This was not observed in the control networks at any stage throughout the culturing period (**Fig. 13A**). We showed that such prominent structural changes happened in concert with aberrant functional changes over time (**13. B**). Compared to the control networks, this manifested as disrupted electrical activity by a decrease in firing rate and mean burst rate of the perturbed networks, with a concomitant increase in network synchrony. To assess the internodal connectivity between the two nodes from time of perturbation and onwards, we induced electrical stimulations of one electrode in the presynaptic node. While we observed a small spiking response in the postsynaptic node following stimulations at 45 and 47 DIV in the control networks, this was not evident in the perturbed networks. Together, our results show the utility for elucidating ongoing structural and functional neural network changes in the initiation, development and progression of network disruptions induced by human mutated tau.
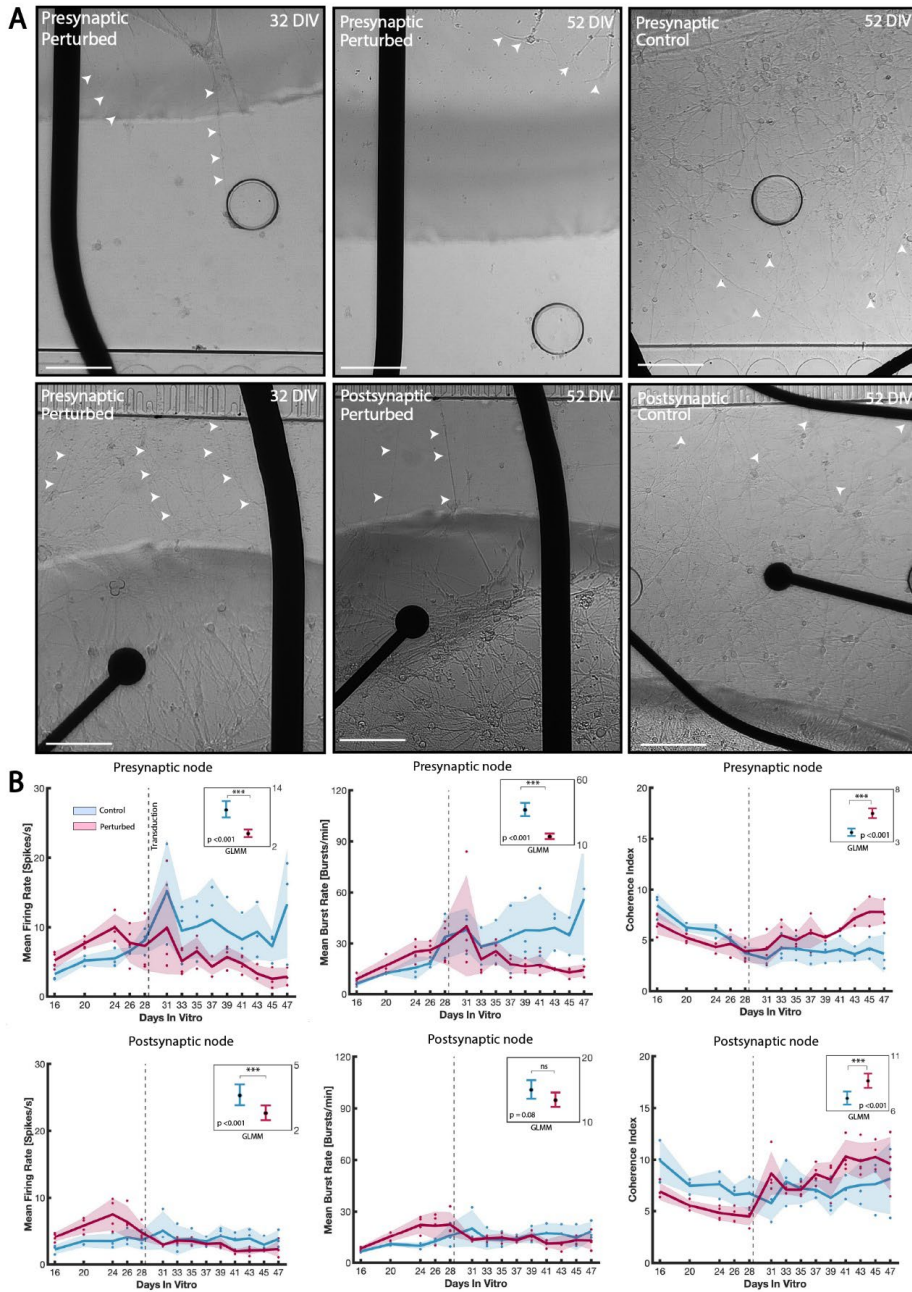
Figure 13. Overview of results: Paper III. Altered structural organization and functional connectivity in perturbed networks. **(A)** Structural reorganization by axonal retraction was observed in the presynaptic node already at 32 DIV, four days after transduction by mutated tau (perturbation). This axonal retraction had progressed drastically by 52 DIV in the presynaptic node and was also evident in the postsynaptic node. In comparison, the control networks did not show the same axonal retraction, in either the pre- or postsynaptic node. **(B)** After transduction at 28 DIV, the presynaptic node in the perturbed networks displayed a decrease in firing rate ($p < 0.001$), mean burst rate ($p < 0.001$) with a concomitant increase in network synchrony ($p < 0.001$) measured by coherence index. GLMM, generalized linear mixed models. DIV = days *in vitro*. GLMM = general linear mixed models.

Methodological considerations

Dissection and processing of adult entorhinal and hippocampal neurons

All brain sections were sectioned horizontally along a ventral to dorsal axis using a vibratome (**Supplementary fig. 1**), before I dissected out lateralmost LEC LII (lLEC LII). Recognition of cytoarchitectonic features and dissection of specific cell layers from fresh tissue is feasible when viewed under a stereoscope and illuminated by cross polarized light **(Fig. 14)**. Thus, for Paper I, regarding the dissection of LEC LII, I used the following criteria: In the ventral-to-dorsal axis, layer V neurons in MEC, contain a columnar shaped, which can be distinguished from the more densely spread organization of layer V in LEC **(Fig. 14D-E)**. Anteriorly, LEC may be separated from piriform and perirhinal cortex contain by the fact that LEC has larger LII-neurons, some of which are ectopic, meaning that they appear to situate in deep parts of layer I **(Fig. 5)**.

For Paper II, I dissected the DG granular layer (DG-gl), the CA3- and CA1 pyramidal layers (CA3-pyr and CA1-pyr), and LEC LII, from both adult AD transgenic APP/PS1 mice and McGill-R-Thy1-APP rats. We used two APP/PS1 mice and a total of 47 McGill-R-Thy1-APP rats (**Supplementary table 1**). LEC LII was dissected in the same way as for Paper I. For dissection of the hippocampal subregions, I relied on the following anatomical traits. The DG-gl can is a densely packed layer of granular neurons that follow a v-U-V shape when going from the ventralmost-to-dorsalmost sections in both the mouse and rat brain and is easily separated from the superficial molecular layer and deeper hilus (**Fig. 5; Supplementary fig.1**). The CA3-pyr contain a prominent compact layer of pyramidal neurons starting at the proximal end, bordering the hilus of DG (**Fig. 5**). Moving in the distal direction, approaching CA2, the pyramidal layer widens as the neurons here are more loosely organized. This feature, which also characterizes CA2 itself, abruptly changes as one moves into CA1, where the pyramidal layer is densely packed. Continuing further in the distal direction, the CA1 pyramidal layer becomes noticeably wider when approaching the border with the subiculum. Dissected tissue was immediately transferred to 15 mL falcon tubes held on ice consisting of Hibernate-A media (Gibco™, A1247501) supplemented with 2% B27 Plus Supplement (Gibco™, A3582801₁), 1% Penicillin-Streptomycin (Gibco™, Cat# 15070063) and 2.5 mL/L Glutamax supplement (Gibco™, 35050061).

After dissection, all tissue was dissociated into a single cell solution by enzymatical dissociation (Papain) and manual trituration (Pipetting). Enzymatic dissociation using Papain was used as it has been shown to result in higher neuronal viability compared to other components, like Trypsin (Brewer, 1997).

Notably, our method for dissociation of the dissected tissue is simpler than the gradient purification method described by Brewer et al., (Brewer et al., 2007).
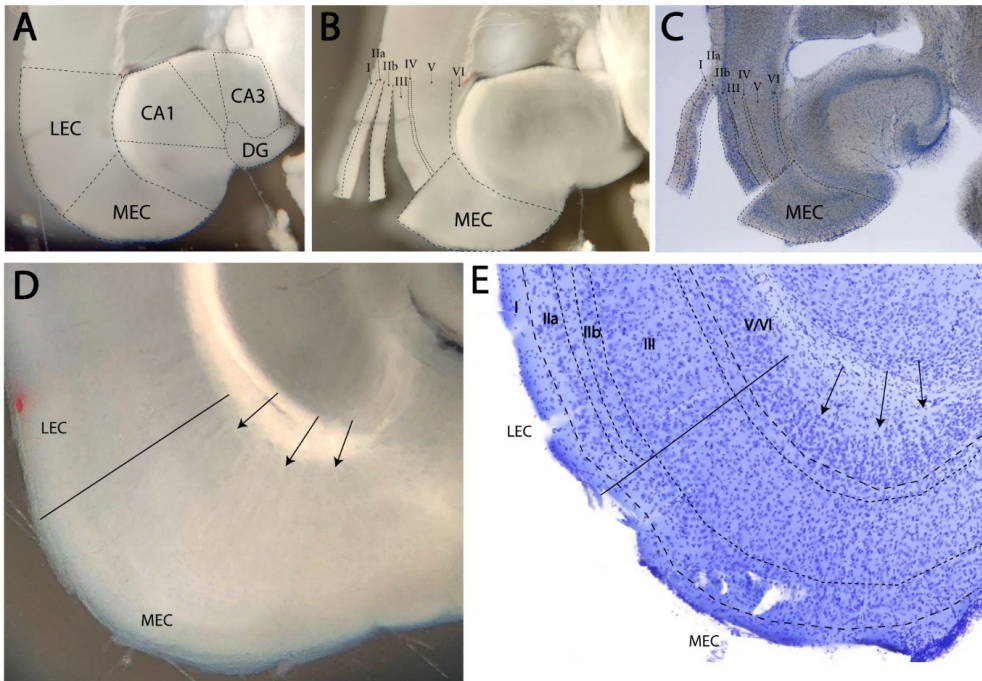

Figure 14. Cytoarchitectonic features of LEC vs. MEC. (A) A horizontal brain section viewed under a stereoscope with cross-polarized light using two fiber optic lamps. Entorhinal and hippocampal subregions were delineated based on salient neuroanatomical features. (B) Same section as in (A) with layers in LEC delineated (dashed lines) with superficial LIIa and LIIb cut and spread out. (C) Same section as in (A-B) stained with Cresyl Violet; note that LIIb has been pushed against LIII under the coverslip, such that only LIIa points out leftward. (D) Example of a freshly cut section seen under the stereoscope, with the border between LEC and MEC indicated by the black line. Arrows indicate the columnar shape of LV neurons in MEC, which can be seen even on a conventional photography. (E) Section of EC from the same level as that in (D), stained with Cresyl Violet. Arrows indicating columnar shape of LV in MEC.

Primary neural networks *in vitro* – establishment and maintenance

Established primary neural networks can be maintained for weeks if handled and maintained correctly. Before plating of neurons, coating of the culture vessel is important for attachment of cell bodies and neurite outgrowth, and various coating approaches is used for various cell types (Davis et al., 2019). For all three papers in this thesis, a combination of Poly-L-Ornithine (PLO) and 0.02 µg/mL laminin was used as coating agents, both having been shown important for neuronal attachment and neurite outgrowth (Haile et al., 2008; Liang et al., 1992; Manthorpe et al., 1983). Following coating procedures, an isogenic layer of astrocytes was plated, adding structural support and physiological relevance (Boehler et al., 2007; Fellin, 2009). To establish a monolayer of astrocytes 24-48 hours prior to plating of the neurons

was found to be crucial for neuronal attachment and viability of our adult neuronal cultures. For the work in this thesis, we used freshly dissected entorhinal and hippocampal neurons from adult AD transgenic mice and rats (Paper I and II) and commercially available primary cortical and hippocampal neurons (Paper II and III). To provide neuronal attachment and long-term viability of such adult neurons, extensive testing and refinement of protocols was conducted. Neurons were plated at a density of 700-850 cells/mm^2 i.e., a total of 140 000-170 000 cells (Paper I). For Paper II and III, adult neurons were plated at a total density of 750 cells/mm^2, i.e., a total of 15 000 cells, while embryonic neurons were plated at a total density of 1000 cells/mm^2, i.e., a total of 20 000 cells. The plating density of neurons in culture vessels have been shown to affect morphological and electrophysiological parameters of neural networks, with sparse plating (<500 cells/mm^2) yielding a higher synapse-to-neuron ration compared to medium or high plating-density (500-4500 cells/mm^2) after 21 DIV (Cullen et al., 2010). By visual inspection, using a brightfield microscope, we observed higher levels of debris in the adult neuronal cultures plated at higher densities in the microfluidic devices. Such debris consists of dead cells and will thus tend to increase apoptotic factors and increase the likelihood of excitotoxicity. Therefore, adult neurons were plated at a slightly lower plating density compared to embryonic neurons on the microfluidic devices (Paper II).

Table 1. Media supplements for all three papers

Supplement	Concentration	Purpose	Supplier, catalogue nr	Cell type it was included for
Y-27632 (Dihydrochloride) RHO/ROCK pathway inhibitor (RI)	0.1 µL/mL	Prevent apoptotic factors	STEMCELL™ Technologies, #72302	APP/PS1 McGill-R-Thy1-APP Commercially available neurons
Brain Derived Neurotrophic Factor	0.1 µL/mL	Support neuronal proliferation and survival	Neurotrophins, #450-02	APP/PS1
Fetal Bovine Serum	100 µL/mL	Maintain cell viability, facilitate metabolism and growth	Sigma-Aldrich, #12106C	APP/PS1 McGill-R-Thy1-APP
FGF2 (Human FGF-2/bFGF) Recombinant Protein)	10 ng/mL	Promote neuronal survival	Gibco™, #13256-029	McGill-R-Thy1-APP
Penicillin-Streptomycin	1 µL/mL	Prevent bacterial contamination	Gibco™, #15070063	APP/PS1 McGill-R-Thy1-APP Commercially available neurons

Successful maintenance of cultured networks involves correct storage in incubators (at 37°C, 5% CO_2 and 20% O_2), regular supply of nutrients through cell media changes, efficient handling of cultures outside of the incubators and prevention of bacterial contaminations (Stacey, 2011). For all three papers, the Neurobasal Plus Medium culture system (Gibco™, A3582901) supplemented with B27 Plus Supplement (Gibco™, A3582801) and 2.5 mL/L GlutaMAX™ Supplement (Gibco™, 35050061) was used. This neuronal media composition has been shown to increase viability of primary neuron cultures by up to 60 % compared to traditional Dulbecco's Modified Eagle's Medium (DMEM) (Brewer et al., 1993). Additionally, various supplements were added to the cell media composition, with some small variances for the adult and embryonic cultures; all supplements included are listed in **Table 1**, including information regarding the purpose for inclusion and the suppliers. In paper II, we tested a total of six different media composition protocols for culturing of adult entorhinal and hippocampal neurons derived from rats. This was done as previous literature has shown a difference in addition of growth factors BDNF and FGF2 for adult neurons derived from mouse and rats, respectively (Brewer et al., 2007).

To provide a favorable microenvironment to the neurons, regular media changes were conducted. For paper I, extensive testing for recurrence of media changes of the adult neural cultures was carried out, where we found 50:50 (of 1 mL total) media changes every three days to yield the highest viability of the cultures in the long-term. As the total volume was much lower (100 µL for each well) in the microfluidic devices, media changes were conducted every two days (Paper II and III).

Immunocytochemistry

All primary and secondary antibodies used for Paper I-III can be found in (**Supplementary Table. 2**). In paper I, we used neuronal marker NeuN to establish the presence of mature neurons (Mullen et al., 1992) derived from adult APP/PS1 model mice. Further characterization in the form of reelin co-expression with NeuN validated the presence of Re+ lLEC LII neurons in our cultures. This was also evident for adult LEC LII neurons derived from the AD transgenic rats (Paper II). For all hippocampal neurons we stained for NeuN and neurofilament marker NFH. To characterize the presence of various cell types in the culture, future work should aim to include markers for various types of glial cells and interneurons. However, for the purpose of the studies included for this thesis, the fact that our cultures were rich in hippocampal neurons and Re+ LEC LII as measured >1 month in culture was considered sufficient.

In paper III, we found staining for AT8 and Phospho-tau (Thr217) to be present in both perturbed and control conditions. However, by quantification of fluorescent intensity we observed a difference in

antibody expression in perturbed networks displaying increased levels of AT8 and pTau in cytosolic compartments, compared to control unperturbed networks.

Imaging by phase contrast- and fluorescent microscopy

For visual inspection of neuronal attachment, neurite outgrowth, and re-organization of structural connections in culture, phase contrast imaging using a Zeiss Axio Vert V.1 microscope was obtained throughout the culturing period. For Paper II, further quantification of neurite length in relation to neuronal media composition was done at 4-5 DIV using Neurolucida (Hanssen & Winter-Hjelm et al., 2023; Supplementary Fig. 3C). For all three papers, imaging of cultures used for ICC was done using an EVOS M5000 microscope (Thermo Fischer Scientific, AMF5000) connected to a light source and using an Olympus 20x/0.75 NA objective (N1480500), with the following filter sets/channels: DAPI (AMEP4650), CY5 (AMEP4656), GFP (AMEP4651) and TxRed (AMEP4655).

Quantification for co-localization of oligomeric Aβ with Re+ neurons (Paper I)

Quantification of five representative micrographs of a neuronal culture stained by ICC was done to count Re+ lLEC-LII neurons co-labelling oligomeric iAβ using ImageJ/Fiji ((Hanssen et al., 2023)). Owing to the astrocytic monolayer below the neuronal layer, the neurons will reside at slightly different depths. Thus, it is not possible to image all neurons on a given sample simultaneously.

Quantification for neurite length of adult neurons in relation to cell media composition (Paper II)

Quantification of neurite length in relation to testing of different cell media compositions (**Table 1**) was done in Neurolucida 360 where I counted a total of 285 neurites at 4-5 DIV (Fig. S2. in Paper II).

Quantification of fluorescent signal of AT8 and Phospho-Tau (Thr217) in perturbed and unperturbed cultures (Paper III)

Quantification of fluorescent intensity profile was done from a total of six cell body clusters and five axonal bundles from perturbed and unperturbed networks stained at 22 DIV using Fiji/ImageJ2.Assessment was done for total fluorescent signal (mean intensity/pixel) measured by mean grayscale.

Microelectrode arrays (MEAs) and microfluidic devices

For all three papers, we used MEAs to capture electrophysiological network activity. For Paper I, we used commercially available 60ecoMEAs containing 60 gold electrodes, in which one was serving as internal reference electrode (Multichannel Systems, Reutlingen, Germany). The electrodes were 100 µm diameter with an electrode spacing of 700 µm. For Paper II and III we used in-house developed

MEAs (Nanolab, NTNU), containing 60 nanoporous platinum black electrodes (50 μm diameter with an electrode spacing of 100 μm), of which one served as an internal reference electrode. Recordings of network activity were conducted using a Multichannel MEA2100 recording setup (Multichannel Systems) at a sampling rate of 25 000 Hz. A temperature controller was used to maintain temperature at 37°C throughout the recording session.

Initial design and production of the microfluidic devises was done by PhD student Nicolai Winter-Hjelm (at Nanolab, NTNU) and a detailed description of all fabrication steps can be found in a published preprint (Winter-Hjelm N, 2023). The microfluidic devices consist of several nodes interconnected by microtunnels. For Paper II and Paper III, we used four-nodal and two-nodal microfluidic devices, respectively **(Fig. 15)**. The microchannels were inspired by the Tesla valve design, containing spine structures on the postsynaptic side to return the axons to their chamber of origin. This was done to initiate a controllable feedforward network connectivity from the presynaptic node to the postsynaptic node.

Two-nodal microfluidic device
Paper III

Four-nodal microfluidic device
Paper II
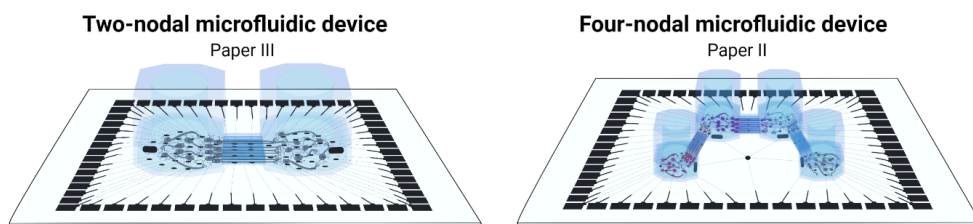
Figure 15. **Two-nodal and four-nodal microfluidic devices**. Schematic of the two- and four-nodal microfluidic devices. Schematics made by Nicolai Winter-Hjelm.

Electrical stimulations and perturbation of neural networks

Electrical stimulations

To estimate functional connectivity between different nodes of the microfluidic devices, electrical stimulations were performed for experiments in Paper II and III. For both papers, stimulations and activity responses were obtained directly after the recordings of spontaneous electrophysiological activity. During the recording session, we noted the most active electrode measured in spikes per second, and this electrode was chosen for electrical stimulations. This was done to assure that the chosen electrode had sufficient coupling within the network(s) to induce activity (Brewer et al., 2009; Pasquale et al., 2010; Winter-Hjelm N, 2023). Electrical stimulations were done using a train of 60 spikes at ± 800 mV (positive phase first) of 200 μs duration with an inter-spike interval of 5 s, based on previous

studies (Pan et al., 2015). As stated previously, for the experiments of papers II and III, the stimulations were initiated from 28 DIV onwards.

Viral transduction of MAPT$_{P301L}$ in vitro

The viral tool (AAV-CBA-GFP-2A-P301L, from herein referred to as AAV-tau) used for Paper III in this thesis was kindly gifted by Dr. Christiana Bjørkli (previously used for transduction *in vivo* in transgenic AD model mice) and was originally developed in the Hyman lab (Wegmann et al., 2019). The neural networks were transduced at 28 DIV (n=4), by first removing 80% of the cell media before adding a dilution of $3x10^2$ viral units per neuron in cell media and leaving them to incubate at 37°C, 5% CO_2 and 20% O_2 for 4 hours. Subsequently, cultures were topped up with fresh media and left to incubate for 24 hours followed by a 50:50 media change. The titre of the viral particles per neuron was chosen after extensive testing of various concentrations, and viability was observed by visual inspection 24-48 hours after transduction. We subjected the control networks (n=3) to the same protocol, excepting the viral vector.

Initially, we included a GFP (AAV-CMV-GFP) viral vector as a vector control for our control networks (n=3), produced by Dr. Rajeevkumar (Kavli Institute for Systems Neuroscience). However, control cultures transfected with the same vector control titre as in perturbed conditions ($3x10^2$ viral units per neuron) died within 7 DIV. One explanation for the reduced viability after AAV-GFP transfection is the lack of promoter specificity (i.e., the cytomegalovirus (CMV) promoter in AAV-GFP), since the Chicken β-actin (CBA) promoter of the AAV-tau transfers mainly excitatory neurons and did not affect cell viability (Wegmann et al., 2019). The CMV promoter may also have adverse effects and be cytotoxic on developing neuronal networks (van den Pol et al., 2007), however, due to time constraints further testing was not feasible and the results from these control cultures were excluded.

Data analysis

All raw data files were converted to .h5-files using the Multichannel data manager software and further analysed in Matlab R2021b. Further, the data was filtered through a 4th order Butterworth bandpass filter (Butterworth, 1930) to remove frequencies <300 Hz and >3000 Hz. Additionally, a notch filter was applied to remove noise at 50 Hz from the power supply mains. Such noise be caused by unshielded electronics either in or around the recording setup that is picking up magnetic fields from the main electrical power. This can be caused by the power supply or heater of the recording system or other electronic devices in the vicinity of the recording setup. Other filtering methods can be used, as extensively reviewed in a recent publication (de Cheveigné et al., 2019). For spike detection we used the cited Precise Time Spike Detection (PTSD) algorithm (Maccione et al., 2009), which iterates through

the data and looks for the relative maximum/minimum of spikes where the peak-to-peak amplitude is above the defined threshold. All recordings were filtered at a standard deviation of 7.5 for adult neurons, and a standard deviation of 8.5 for embryonic neurons. For papers II and III, scripts for neuronal burst detection and network burst detection developed by (Pasquale et al., 2010) were used. Additional data analysis and scripts included for data analysis can be found in the methods section of each paper.

Discussion

Summary of key findings

In this thesis, I demonstrate how to extract and carry out long-term culturing of lLEC-LII neurons from adult AD-model mice and rats. I show that specifically the Re+ lLEC-LII neurons can be targeted for this purpose, which is of high relevance given the fact that this specific subpopulation of EC neurons constitutes the population that is typically first to degenerate in the course of AD. I furthermore show the utility of engineered multinodal microfluidic devices for the purpose of establishing anatomically AD-relevant entorhinal and hippocampal networks, and that such networks can be studied in long-term experiments to help discern neural network dynamics associated with the healthy vs diseased state. By way of cortical-hippocampal neural networks I also show that the networks develop complex dynamics suggestive of a capacity for both segregated and integrated activity. Lastly, following perturbations by viral transduction of human mutated tau (P301-L) in the presynaptic node of two-nodal feedforward cortical networks, we show longitudinal structural and functional alterations of the perturbed networks compared to unperturbed controls. These alterations further resulted in impaired spontaneous and evoked internodal signal propagation in the perturbed networks.

In vitro models as complimentary to in *vivo models*

By establishing a novel method for culturing adult LEC LII neurons on MEAs over an extended period, the work in Paper I introduces a valuable modelling tool to investigate neurons that are particularly vulnerable in preclinical AD. Due to the highly intricate cascades of structural and functional network alterations in AD, the ability to move such neurons to culture offers a useful reductionist approach to study ongoing network dynamics in an isolated environment. A key advantage of neuronal cultures is the precise control they offer over the extracellular environment. By manipulating the culture conditions one can explore the impact of specific processes without external confounding factors that are always at play in living animals, such as the impact of illness, stress, food, and water intake. Additionally, the continuous visual access provided by microscopy allows for real-time monitoring of the neuronal networks, enabling the observation of dynamic changes over extended periods. In living animals, such monitoring of ongoing structural parameters is limited due to the restricted access to the brain before termination of the animals.

Importantly, the use of cultured neurons also contributes to the refinement and reduction of animal experimentation, aligning with the 3Rs: replacement, refinement and reduction of research animals (Lewis, 2019). By utilizing refined methods for moving neurons into culture, researchers can reduce the

number of animals needed for experiments. This reduction not only addresses ethical considerations but also enhances the efficiency and cost-effectiveness of many research endeavors.

When moving neurons from the brain into culture, an important question arises: *Can we capture pathological features in culture that resemble those observed in the brain?* In the case of our lLEC LII neuron cultures, we show that these cultures are rich in Re+ neurons that co-express iAβ, aligning with the strong intracellular expression of Aβ in AD transgenic rats and post-mortem brains (Kobro-Flatmoen et al., 2016). It was previously shown that already by 11 DIV, neuronal cultures derived from the 3xTg AD mouse model exhibit differences in the expression of human APP/Aβ and tau pathology compared to control cultures (Vale et al., 2010). Similarly, another study reported increased levels of Aβ40 and Aβ42 in hippocampal neuron cultures derived from APP/PS1 model mice already after 12 DIV (Trinchese et al., 2004). These findings suggest that not only do neurons from AD transgenic animals capture pathological features in culture but may offer a more efficient approach for testing of pharmacological agents, since pathology seems to arise much earlier than what is the case for these neurons in their *in vivo* setting.

In vitro modelling also allows for extraction, culturing, and monitoring of neurons and networks from different brain regions simultaneously, which is difficult to do at high resolution in the brain. Work by others has shown the ability to model early postnatal EC-hippocampal cultures on both two-nodal (Brewer et al., 2013) (Poli et al., 2018) and four nodal microfluidic devices (Vakilna et al., 2021). In our work from Paper II, we show the utility of establishing hippocampal DG-gl, CA3-pyr and CA1-pyr neurons, in addition to LEC LII neurons on a multinodal microfluidic device. Our work thus provides novelty by long-term culturing of layer and subregional specific EC and hippocampal neurons dissected from adult AD transgenic animals. Furthermore, such reverse engineering of neural networks on microfluidic devices offers a unique opportunity to create mixed networks consisting of both healthy and diseased neurons in separate nodes. For example, in our four-nodal mMEA, LEC neurons from AD transgenic mice could be plated in the first node with hippocampal neurons from healthy littermate controls in the following nodes (**Fig. 16**). As such, this presents a method for monitoring proposed spread of accumulated Aβ and tau pathology from a diseased network to healthy networks and investigating how such pathology would affect the structural and functional connectivity over time.

The prion-like propagation hypothesis (Walker, 2018) has suggested aggregations of misfolded proteins spreading by cell-to-cell transmission. Such prion-like spread of intracellular Aβ has been suggested to occur through synaptic spread from the soma to neuronal processes (Roos et al., 2021). These state-of-the-art approaches thus open up an avenue for studying progression of pathogenesis and network dynamics both within and across an isolated subset of nodes over time. By characterizing such changes,

it becomes possible to gain a deeper understanding of the mechanisms underlying the progression of AD pathology and its impact on both the local and global network properties.
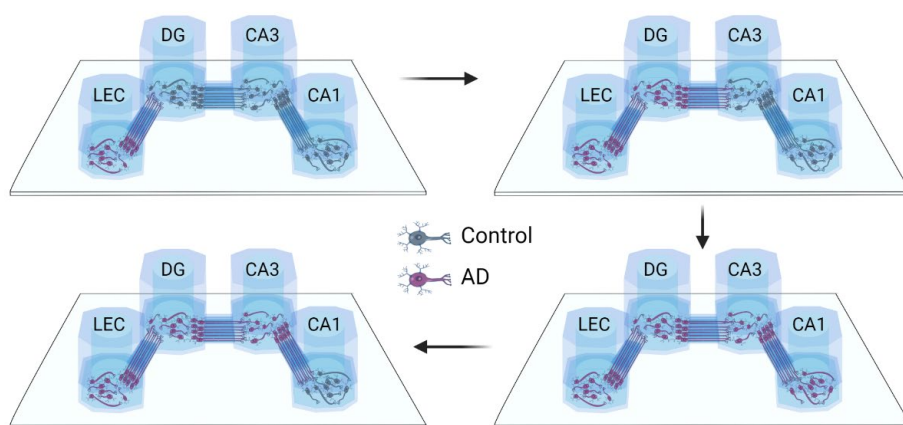

Figure 16. Schematic of disease spread in a neural network on a microfluidic device. Schematics created by Nicolai Winter-Hjelm.

Assessment of structural and functional network dynamics to capture critical time points

Assessing the pathological load at the structural level and understanding its relationship with alterations in network activity at the functional level is crucial for gaining insights into the mechanisms of AD. By understanding the time points when such structural and functional alterations occur in relation to each other, identify potential targets for intervention aimed at delaying or preventing the onset of functional impairments. Work from others on transgenic AD model animals has investigated network dysfunctions in AD and shown that hyperactivity occurs in neurons surrounded by Aβ plaques (Busche et al., 2008; Busche et al., 2015), soluble Aβ (Busche et al., 2012). On the other hand, accumulation of tau has been shown to suppress network activity leading to a hypoactive state (Busche, 2019), even before the formation of NFTs occurs. Furthermore, epileptiform activity and seizures have been shown in animals and are also observed in human patients, suggesting deposition of Aβ to be particularly likely to be associated with seizures (as reviewed in (Friedman et al., 2012)). The risk of epileptic seizures is particularly high in AD patients during early disease stages (Amatniek et al., 2006).

In Paper III, we sought to investigate ongoing structural and functional network responses after perturbation by transducing cells with viral vectors containing a human tau mutation (P301-L) in a two-nodal microfluidic device. The viral vector was added in the presynaptic node at 28 DIV, a time point when primary neural networks are considered mature (Chiappalone et al., 2006; Winter-Hjelm N, 2023). Four days after perturbation, we observed axonal retraction starting in the presynaptic node

(site of transduction) (**Fig. 13A**), which progressed drastically up to 52 DIV. At 52 DIV, axonal retraction was also evident in the postsynaptic node. Axonal retraction was not observed in the control networks **(Fig. 13A)**. This structural reorganization observed in the perturbed networks can be associated with the transduction with human mutated tau likely causing destabilization of labile microtubule domains (Qiang et al., 2018), loss of structural integrity of axonal projections (Strain et al., 2018), further leading to a reduction in axonal elongation (Biswas et al., 2018). The fact that we did not have a culture containing control GFP-virus should be taken into consideration for assessment of the viral load potentially affecting structural and functional network dynamics. However, we observed an increased fluorescent intensity of AT8 and Phospho-Tau in the cytosol of the cells in perturbed conditions compared to unperturbed controls, indicating increased phosphorylation of pathological tau (Rajbanshi et al., 2023; Vale et al., 2010). Furthermore, after several rounds of testing the titration of the viral load we did not observe any neuronal death over time in culture. As such, the structural alterations of our perturbed networks, by axonal retraction is suggestive to be caused by an increased load of pathological tau.

Functionally, our perturbed networks displayed a decrease in both the mean firing rate and mean burst rate in the presynaptic node ($p < 0.001$) **(Fig. 13B)**. This observed increase in synchrony of the network activity can indicate the network reaching a hyperactive state. A number of studies have reported synchronized network activity early in AD disease stages. In an AD-mouse model (APP23xPS45), a decrease in neuronal activity was seen in 29% of layer 2/3 cortical neurons, however, 21% of neurons displayed an unexpected increase in the frequency of spontaneous Ca^{2+} transients (Busche et al., 2008). Not only did hyperactive neurons fire more frequently, but they also did this in a correlated manner, thus increasing the risk for seizure-like activity. To enhance our understanding of pathogenesis in relation to altered network activity and vice versa, it is crucial to implement long-term monitoring of networks.

Interacting mechanisms involved in structural and functional network connectivity

As several neurodegenerative diseases may affect the mature brain, it is important to take into consideration the differences in development of both structural and functional network behavior of both embryonic and adult neurons when moved to culture. These differences in network dynamics of embryonic and adult neurons, as well as the variations in epigenetic profile, should be carefully considered when studying neurodegenerative diseases. During maturation of a network, there are several interacting mechanisms that help determine the structural organization, functional connectivity, and network dynamics (Chiappalone et al., 2007). Based on electrophysiological and

molecular characteristics, neural networks established from embryonic neurons are thought to mature between 21-28 DIV (Chiappalone et al., 2006; Weir et al., 2023; Winter-Hjelm N, 2023). The determining mechanisms operate at both the subcellular and network level in an ongoing manner, influencing development of the network over time. Despite the fact that the exact same methods and handling techniques may be employed, each cultured network ultimately acquires unique characteristics. The formation of the networks will be influenced by a combination of factors, including neuronal type, the *in vitro* microenvironment, and the precise timing of different developmental events. For example, there will always be a slight variance in the formation of the astrocytic monolayer, the plating density of neurons and how the neurons self-organize into networks. As a result, the unique re-formation of structural connections will further influence the development of functional connectivity, which involves changes in the strength and number of connections between neurons. Such mechanisms and factors work together to shape the development of a network, ultimately giving rise to unique structural and functional characteristics that are specific to each individual network.

In my work, neurons derived from both adult AD transgenic mice- (Paper I and II) and rats (Paper II) attached to the culture surface within two hours and re-formed structural connections within a week in culture, in line with previous studies culturing adult primary neuronal networks (Eide et al., 2005) (Brewer, 1997). Furthermore, the adult networks exhibited electrophysiological activity in the form of spikes from 15 DIV until cultures were terminated at 69 DIV (Paper I) and 47 DIV (Paper II). Typical for both adult entorhinal and hippocampal cultures were an overall low firing rate and an absence of bursting behavior. This activity pattern may be a generic feature of adult neurons when moved to culture. In patch-clamp experiments of adult cultured neurons, other groups have reported the neurons to exhibit activity as single-spike events (Evans et al., 1998) (Varghese et al., 2009) rather than synchronized activity. In a recent study, it was also shown that adult hippocampal and cortical neurons elicited few bursts (<1 per minute) throughout a 10-minute recordings session (van Niekerk et al., 2022). In comparison, the electrophysiological behaviour of cultured embryonic cortical and hippocampal neurons typically develops as patterns of rhythmic activity, with increased bursting behaviour throughout the first 21 DIV (Chiappalone et al., 2006; Weir et al., 2023; Winter-Hjelm N, 2023).

The developmental disparities between adult and embryonic neurons can influence the formation and organization of neural networks, which in turn affect the manifestation and progression of AD pathology. By considering the distinct characteristics of these cell types, researchers can accurately model disease progression, explore the impact on different stages of neural development, and gain

insights into the molecular and genetic factors involved. Studying adult neurons derived from AD transgenic models provides relevant context and helps understand how the disease manifests in the mature brain. Additionally, comparing the network dynamics and epigenetic profiles of adult and embryonic neurons reveals vulnerabilities and resilience to Alzheimer's-related processes. Acknowledging these developmental disparities enables the interpretation of experimental results and the development of targeted therapeutic approaches. Ultimately, a comprehensive understanding of both cell types will contribute to improved diagnostics and tailored treatments for different stages of Alzheimer's disease. However, it is important to emphasize that more work is needed since the body of literature on adult neuronal cultures is sparse, which should, at present, temper conclusions regarding their normal or typical behaviour.

Future perspectives

The work conducted in this thesis illustrates the robustness and potential of advanced *in vitro* model systems as a tool to recapitulate complex network dynamics in AD. As AD constitutes a highly complex disease with several progressing intertwined mechanisms, dissecting the complexities by engineered neural networks represent an excellent tool to capture ongoing structural and functional alterations in an isolated environment. Thus, contributing to our understanding of fundamental disease mechanisms, *when* they occur, and importantly *how* we can stop these disease mechanisms. As we showed in Paper III, by transduction of human mutant tau in engineered feedforward neural networks, we can capture ongoing structural and functional network alterations. These model systems serve to complement *in vivo* models by adding insights and perspectives that are hard, or not even feasible to obtain in living animals. The use of cell cultures has proven to be an efficient model system for drug screening (Kumar et al., 2022; Trinchese et al., 2004), and engineered neural networks as we present through the work in this thesis further add novelty by enabling drug application in separate nodes with the ability to monitor effects in feedforward interconnected subpopulations of neurons. In the recent years, the implementation of human cell lines and induced pluripotent stem cells (IPSCs) has showed promising results as preclinical model systems to mimic the disease cascades in human specific neurons (T. Li et al., 2016; Sahlgren Bendtsen et al., 2023; Yagi et al., 2011). By combining such human specific cells with the tools presented in my work, like neuroengineering, microfluidic technology, electrophysiology, and computational analytic tools, this introduces a state-of-the-art model system for preclinical disease modelling in AD. Reverse engineering of vulnerable neural networks as a model system is not only relevant for AD research, but applicable to other neurodegenerative diseases as well.

Concluding remarks

The main objectives of the work for this thesis were to: (i) dissect and culture layer and subregion specific neurons from the entorhinal cortex and hippocampus of adult AD model mice and rats, (ii) implement anatomically relevant neural networks on engineered microfluidic devices with a feedforward connectivity, and iii) study structural and functional changes in network dynamics after perturbation of mature neural networks by transduction by human mutated tau. In accordance with these objectives, the method for extraction and culturing of lLEC-LII neurons (Paper I), and the dissections and culturing of LEC LII in addition to hippocampal DG-gl, CA3-pyr and CA1-pyr from AD model mice and rats (Paper II), show the ability to culture adult neurons from AD model animals long-term. Additionally, the findings from Paper II and III show that anatomically relevant neural networks self-organize and enable the study of subcellular and network level network dynamics.

Based on the results from the included papers, we can conclude that:

i) Adult layer specific entorhinal and subregion specific hippocampal neurons from AD model mice and rats can be cultured long-term, enabling the study of pathogenesis and disease modelling in AD.

ii) Engineered neural networks on microfluidic devices enables the study of ongoing structure-function network dynamics. Interconnection of the multinodal networks contributed to emergence of complex structure-function dynamics both within and across nodes containing subregion specific neuronal populations.

iii) Perturbation of mature healthy neural networks by transduction with human mutant tau result in altered structural organization by axonal retraction. Furthermore, the functional connectivity was affected by decreased firing rate and networks bursts with a concomitant increase in synchrony of the remaining activity.

Combined, these results present a valuable reductionist approach for modelling anatomically relevant neural networks in AD research, further enabling the study of function and dysfunction of subcellular and network level dynamics. I believe that the work presented in this thesis makes a valuable contribution to the research field with the potential for studying pathogenesis and aid in drug development in anatomically relevant neural networks for AD. By continuing to innovate and improve our models, we may eventually be able to elucidate fundamental disease mechanisms, develop more effective treatments, and ultimately find a cure for this devastating disease.

References

2023 Alzheimer's disease facts and figures. (2023). *Alzheimers Dement, 19*(4), 1598-1695. doi:10.1002/alz.13016

Adams, J. N., Maass, A., Harrison, T. M., Baker, S. L., & Jagust, W. J. (2019). Cortical tau deposition follows patterns of entorhinal functional connectivity in aging. *Elife, 8*. doi:10.7554/eLife.49132

Allison, S. L., Fagan, A. M., Morris, J. C., & Head, D. (2016). Spatial Navigation in Preclinical Alzheimer's Disease. *J Alzheimers Dis, 52*(1), 77-90. doi:10.3233/jad-150855

Alzheimer, A., Stelzmann, R. A., Schnitzlein, H. N., & Murtagh, F. R. (1995). An English translation of Alzheimer's 1907 paper, "Uber eine eigenartige Erkankung der Hirnrinde". *Clin Anat, 8*(6), 429-431. doi:10.1002/ca.980080612

Amaral, D. G., Dolorfo, C., & Alvarez-Royo, P. (1991). Organization of CA1 projections to the subiculum: a PHA-L analysis in the rat. *Hippocampus, 1*(4), 415-435. doi:10.1002/hipo.450010410

Amatniek, J. C., Hauser, W. A., DelCastillo-Castaneda, C., Jacobs, D. M., Marder, K., Bell, K., . . . Stern, Y. (2006). Incidence and predictors of seizures in patients with Alzheimer's disease. *Epilepsia, 47*(5), 867-872. doi:10.1111/j.1528-1167.2006.00554.x

Ambrose, C. T. (2019). An amended history of tissue culture: Concerning Harrison, Burrows, Mall, and Carrel. *J Med Biogr, 27*(2), 95-102. doi:10.1177/0967772016685033

Apostolova, L. G., Green, A. E., Babakchanian, S., Hwang, K. S., Chou, Y. Y., Toga, A. W., & Thompson, P. M. (2012). Hippocampal atrophy and ventricular enlargement in normal aging, mild cognitive impairment (MCI), and Alzheimer Disease. *Alzheimer Dis Assoc Disord, 26*(1), 17-27. doi:10.1097/WAD.0b013e3182163b62

Bauer, U. S., Fiskum, V., Nair, R. R., van de Wijdeven, R., Kentros, C., Sandvig, I., & Sandvig, A. (2022). Validation of Functional Connectivity of Engineered Neuromuscular Junction With Recombinant Monosynaptic Pseudotyped ΔG-Rabies Virus Tracing. *Front Integr Neurosci, 16*, 855071. doi:10.3389/fnint.2022.855071

Bayer, T. A., & Wirths, O. (2010). Intracellular accumulation of amyloid-Beta - a predictor for synaptic dysfunction and neuron loss in Alzheimer's disease. *Front Aging Neurosci, 2*, 8. doi:10.3389/fnagi.2010.00008

Beffert, U., Morfini, G., Bock, H. H., Reyna, H., Brady, S. T., & Herz, J. (2002). Reelin-mediated signaling locally regulates protein kinase B/Akt and glycogen synthase kinase 3beta. *J Biol Chem, 277*(51), 49958-49964. doi:10.1074/jbc.M209205200

Bejanin, A., Schonhaut, D. R., La Joie, R., Kramer, J. H., Baker, S. L., Sosa, N., . . . Rabinovici, G. D. (2017). Tau pathology and neurodegeneration contribute to cognitive impairment in Alzheimer's disease. *Brain, 140*(12), 3286-3300. doi:10.1093/brain/awx243

Bekris, L. M., Yu, C. E., Bird, T. D., & Tsuang, D. W. (2010). Genetics of Alzheimer disease. *J Geriatr Psychiatry Neurol, 23*(4), 213-227. doi:10.1177/0891988710383571

Benedikz, E., Kloskowska, E., & Winblad, B. (2009). The rat as an animal model of Alzheimer's disease. *J Cell Mol Med, 13*(6), 1034-1042. doi:10.1111/j.1582-4934.2009.00781.x

Bierer, L. M., Hof, P. R., Purohit, D. P., Carlin, L., Schmeidler, J., Davis, K. L., & Perl, D. P. (1995). Neocortical neurofibrillary tangles correlate with dementia severity in Alzheimer's disease. *Arch Neurol, 52*(1), 81-88. doi:10.1001/archneur.1995.00540250089017

Biswas, S., & Kalil, K. (2018). The Microtubule-Associated Protein Tau Mediates the Organization of Microtubules and Their Dynamic Exploration of Actin-Rich Lamellipodia and Filopodia of Cortical Growth Cones. *J Neurosci, 38*(2), 291-307. doi:10.1523/jneurosci.2281-17.2017

Bjorkli, C. (2022). *The inside-out of Alzheimer's disease* (Ph.d.). Norwegian University of Science and Technology Doctoral theses at NTNU;2022:222.

Boehler, M. D., Wheeler, B. C., & Brewer, G. J. (2007). Added astroglia promote greater synapse density and higher activity in neuronal networks. *Neuron Glia Biol, 3*(2), 127-140. doi:10.1017/s1740925x07000440

Botella-López, A., Cuchillo-Ibáñez, I., Cotrufo, T., Mok, S. S., Li, Q. X., Barquero, M. S., . . . Sáez-Valero, J. (2010). Beta-amyloid controls altered Reelin expression and processing in Alzheimer's disease. *Neurobiol Dis, 37*(3), 682-691. doi:10.1016/j.nbd.2009.12.006

Brewer, G. J. (1997). Isolation and culture of adult rat hippocampal neurons. *J Neurosci Methods, 71*(2), 143-155. doi:10.1016/s0165-0270(96)00136-7

Brewer, G. J., Boehler, M. D., Ide, A. N., & Wheeler, B. C. (2009). Chronic electrical stimulation of cultured hippocampal networks increases spontaneous spike rates. *J Neurosci Methods, 184*(1), 104-109. doi:10.1016/j.jneumeth.2009.07.031

Brewer, G. J., Boehler, M. D., Leondopulos, S., Pan, L., Alagapan, S., DeMarse, T. B., & Wheeler, B. C. (2013). Toward a self-wired active reconstruction of the hippocampal trisynaptic loop: DG-CA3. *Front Neural Circuits, 7*, 165. doi:10.3389/fncir.2013.00165

Brewer, G. J., & Torricelli, J. R. (2007). Isolation and culture of adult neurons and neurospheres. *Nat Protoc, 2*(6), 1490-1498. doi:10.1038/nprot.2007.207

Brewer, G. J., Torricelli, J. R., Evege, E. K., & Price, P. J. (1993). Optimized survival of hippocampal neurons in B27-supplemented Neurobasal, a new serum-free medium combination. *J Neurosci Res, 35*(5), 567-576. doi:10.1002/jnr.490350513

Braak, H., & Braak, E. (1991). Neuropathological stageing of Alzheimer-related changes. *Acta Neuropathol, 82*(4), 239-259. doi:10.1007/bf00308809

Braak, H., & Del Tredici, K. (2011). The pathological process underlying Alzheimer's disease in individuals under thirty. *Acta Neuropathol, 121*(2), 171-181. doi:10.1007/s00401-010-0789-4

Buée, L., Bussière, T., Buée-Scherrer, V., Delacourte, A., & Hof, P. R. (2000). Tau protein isoforms, phosphorylation and role in neurodegenerative disorders. *Brain Res Brain Res Rev, 33*(1), 95-130. doi:10.1016/s0165-0173(00)00019-9

Burwell, R. D., & Amaral, D. G. (1998). Cortical afferents of the perirhinal, postrhinal, and entorhinal cortices of the rat. *J Comp Neurol, 398*(2), 179-205. doi:10.1002/(sici)1096-9861(19980824)398:2<179::aid-cne3>3.0.co;2-y

Busche, M. A. (2019). Tau suppresses neuronal activity in vivo, even before tangles form. *Brain, 142*(4), 843-846. doi:10.1093/brain/awz060

Busche, M. A., Chen, X., Henning, H. A., Reichwald, J., Staufenbiel, M., Sakmann, B., & Konnerth, A. (2012). Critical role of soluble amyloid-β for early hippocampal hyperactivity in a mouse model of Alzheimer's disease. *Proc Natl Acad Sci U S A, 109*(22), 8740-8745. doi:10.1073/pnas.1206171109

Busche, M. A., Eichhoff, G., Adelsberger, H., Abramowski, D., Wiederhold, K. H., Haass, C., . . . Garaschuk, O. (2008). Clusters of hyperactive neurons near amyloid plaques in a mouse model of Alzheimer's disease. *Science, 321*(5896), 1686-1689. doi:10.1126/science.1162844

Busche, M. A., & Konnerth, A. (2015). Neuronal hyperactivity--A key defect in Alzheimer's disease? *Bioessays, 37*(6), 624-632. doi:10.1002/bies.201500004

Busche, M. A., & Konnerth, A. (2016). Impairments of neural circuit function in Alzheimer's disease. *Philos Trans R Soc Lond B Biol Sci, 371*(1700). doi:10.1098/rstb.2015.0429

Butterworth, S. (1930). On the Theory of Filter Amplifiers *Experimental Wireless and the Wireless Engineer, 7*, 536-541.

Baas, P. W., & Qiang, L. (2019). Tau: It's Not What You Think. *Trends Cell Biol, 29*(6), 452-461. doi:10.1016/j.tcb.2019.02.007

Cajal, R. Y. (1902). Sobre un ganglio especial de la corteza esfeno-occipital. *Trab. del Lab. de Invest. Biol. Univ. Madrid, 1*, 189.

Canto, C. B., & Witter, M. P. (2012a). Cellular properties of principal neurons in the rat entorhinal cortex. I. The lateral entorhinal cortex. *Hippocampus, 22*(6), 1256-1276. doi:10.1002/hipo.20997

Canto, C. B., & Witter, M. P. (2012b). Cellular properties of principal neurons in the rat entorhinal cortex. II. The medial entorhinal cortex. *Hippocampus, 22*(6), 1277-1299. doi:10.1002/hipo.20993

Chakrabarti, S., Khemka, V. K., Banerjee, A., Chatterjee, G., Ganguly, A., & Biswas, A. (2015). Metabolic Risk Factors of Sporadic Alzheimer's Disease: Implications in the Pathology, Pathogenesis and Treatment. *Aging Dis, 6*(4), 282-299. doi:10.14336/ad.2014.002

Chen, Y., Beffert, U., Ertunc, M., Tang, T. S., Kavalali, E. T., Bezprozvanny, I., & Herz, J. (2005). Reelin modulates NMDA receptor activity in cortical neurons. *J Neurosci, 25*(36), 8209-8216. doi:10.1523/jneurosci.1951-05.2005

Chiappalone, M., Bove, M., Vato, A., Tedesco, M., & Martinoia, S. (2006). Dissociated cortical networks show spontaneously correlated activity patterns during in vitro development. *Brain Res, 1093*(1), 41-53. doi:10.1016/j.brainres.2006.03.049

Chiappalone, M., Vato, A., Berdondini, L., Koudelka-Hep, M., & Martinoia, S. (2007). Network dynamics and synchronous activity in cultured cortical neurons. *Int J Neural Syst, 17*(2), 87-103. doi:10.1142/s0129065707000968

Chin, J., Massaro, C. M., Palop, J. J., Thwin, M. T., Yu, G. Q., Bien-Ly, N., . . . Mucke, L. (2007). Reelin depletion in the entorhinal cortex of human amyloid precursor protein transgenic mice and humans with Alzheimer's disease. *J Neurosci, 27*(11), 2727-2733. doi:10.1523/jneurosci.3758-06.2007

Cuchillo-Ibañez, I., Mata-Balaguer, T., Balmaceda, V., Arranz, J. J., Nimpf, J., & Sáez-Valero, J. (2016). The β-amyloid peptide compromises Reelin signaling in Alzheimer's disease. *Sci Rep, 6*, 31646. doi:10.1038/srep31646

Cullen, D. K., Gilroy, M. E., Irons, H. R., & Laplaca, M. C. (2010). Synapse-to-neuron ratio is inversely related to neuronal density in mature neuronal cultures. *Brain Res, 1359*, 44-55. doi:10.1016/j.brainres.2010.08.058

D'Andrea, M. R., Nagele, R. G., Wang, H. Y., Peterson, P. A., & Lee, D. H. (2001). Evidence that neurones accumulating amyloid can undergo lysis to form amyloid plaques in Alzheimer's disease. *Histopathology, 38*(2), 120-134. doi:10.1046/j.1365-2559.2001.01082.x

D'Arcangelo, G., Homayouni, R., Keshvara, L., Rice, D. S., Sheldon, M., & Curran, T. (1999). Reelin is a ligand for lipoprotein receptors. *Neuron, 24*(2), 471-479. doi:10.1016/s0896-6273(00)80860-0

Davis, K. A., Wu, P. J., Cahall, C. F., Li, C., Gottipati, A., & Berron, B. J. (2019). Coatings on mammalian cells: interfacing cells with their environment. *J Biol Eng, 13*, 5. doi:10.1186/s13036-018-0131-6

de Cheveigné, A., & Nelken, I. (2019). Filters: When, Why, and How (Not) to Use Them. *Neuron, 102*(2), 280-293. doi:10.1016/j.neuron.2019.02.039

De Strooper, B. (2007). Loss-of-function presenilin mutations in Alzheimer disease. Talking Point on the role of presenilin mutations in Alzheimer disease. *EMBO Rep, 8*(2), 141-146. doi:10.1038/sj.embor.7400897

DeMarse, T. B., Pan, L., Alagapan, S., Brewer, G. J., & Wheeler, B. C. (2016). Feed-Forward Propagation of Temporal and Rate Information between Cortical Populations during Coherent Activation in Engineered In Vitro Networks. *Front Neural Circuits, 10*, 32. doi:10.3389/fncir.2016.00032

Deutsch, S. I., Rosse, R. B., & Deutsch, L. H. (2006). Faulty regulation of tau phosphorylation by the reelin signal transduction pathway is a potential mechanism of pathogenesis and therapeutic target in Alzheimer's disease. *Eur Neuropsychopharmacol, 16*(8), 547-551. doi:10.1016/j.euroneuro.2006.01.006

Djemil, S., Chen, X., Zhang, Z., Lee, J., Rauf, M., Pak, D. T. S., & Dzakpasu, R. (2020). Activation of nicotinic acetylcholine receptors induces potentiation and synchronization within in vitro hippocampal networks. *J Neurochem, 153*(4), 468-484. doi:10.1111/jnc.14938

Doan, T. P., Lagartos-Donate, M. J., Nilssen, E. S., Ohara, S., & Witter, M. P. (2019). Convergent Projections from Perirhinal and Postrhinal Cortices Suggest a Multisensory Nature of Lateral,

but Not Medial, Entorhinal Cortex. *Cell Rep, 29*(3), 617-627.e617. doi:10.1016/j.celrep.2019.09.005

Doehner, J., & Knuesel, I. (2010). Reelin-mediated Signaling during Normal and Pathological Forms of Aging. *Aging Dis, 1*(1), 12-29.

Dong, L., Liu, C., Sha, L., Mao, C., Li, J., Huang, X., . . . Gao, J. (2022). PSEN2 Mutation Spectrum and Novel Functionally Validated Mutations in Alzheimer's Disease: Data from PUMCH Dementia Cohort. *J Alzheimers Dis, 87*(4), 1549-1556. doi:10.3233/jad-220194

Dong, Y., Digman, M. A., & Brewer, G. J. (2019). Age- and AD-related redox state of NADH in subcellular compartments by fluorescence lifetime imaging microscopy. *Geroscience, 41*(1), 51-67. doi:10.1007/s11357-019-00052-8

Dong, Y., Sameni, S., Digman, M. A., & Brewer, G. J. (2019). Reversibility of Age-related Oxidized Free NADH Redox States in Alzheimer's Disease Neurons by Imposed External Cys/CySS Redox Shifts. *Sci Rep, 9*(1), 11274. doi:10.1038/s41598-019-47582-x

Dorostkar, M. M., Zou, C., Blazquez-Llorca, L., & Herms, J. (2015). Analyzing dendritic spine pathology in Alzheimer's disease: problems and opportunities. *Acta Neuropathol, 130*(1), 1-19. doi:10.1007/s00401-015-1449-5

Drummond, E., & Wisniewski, T. (2017). Alzheimer's disease: experimental models and reality. *Acta Neuropathol, 133*(2), 155-175. doi:10.1007/s00401-016-1662-x

Dworak, B. J., & Wheeler, B. C. (2009). Novel MEA platform with PDMS microtunnels enables the detection of action potential propagation from isolated axons in culture. *Lab Chip, 9*(3), 404-410. doi:10.1039/b806689b

Eide, L., & McMurray, C. T. (2005). Culture of adult mouse neurons. *Biotechniques, 38*(1), 99-104. doi:10.2144/05381rr02

El-Agnaf, O. M., Mahil, D. S., Patel, B. P., & Austen, B. M. (2000). Oligomerization and toxicity of beta-amyloid-42 implicated in Alzheimer's disease. *Biochem Biophys Res Commun, 273*(3), 1003-1007. doi:10.1006/bbrc.2000.3051

Esquerda-Canals, G., Montoliu-Gaya, L., Güell-Bosch, J., & Villegas, S. (2017). Mouse Models of Alzheimer's Disease. *J Alzheimers Dis, 57*(4), 1171-1183. doi:10.3233/jad-170045

Evans, M. S., Collings, M. A., & Brewer, G. J. (1998). Electrophysiology of embryonic, adult and aged rat hippocampal neurons in serum-free culture. *J Neurosci Methods, 79*(1), 37-46. doi:10.1016/s0165-0270(97)00159-3

Fellin, T. (2009). Communication between neurons and astrocytes: relevance to the modulation of synaptic and network activity. *J Neurochem, 108*(3), 533-544. doi:10.1111/j.1471-4159.2008.05830.x

Fiskum, V., Sandvig, A., & Sandvig, I. (2021). Silencing of Activity During Hypoxia Improves Functional Outcomes in Motor Neuron Networks in vitro. *Front Integr Neurosci, 15*, 792863. doi:10.3389/fnint.2021.792863

Forró, C., Thompson-Steckel, G., Weaver, S., Weydert, S., Ihle, S., Dermutz, H., . . . Vörös, J. (2018). Modular microstructure design to build neuronal networks of defined functional connectivity. *Biosens Bioelectron, 122*, 75-87. doi:10.1016/j.bios.2018.08.075

Frega, M., Pasquale, V., Tedesco, M., Marcoli, M., Contestabile, A., Nanni, M., . . . Chiappalone, M. (2012). Cortical cultures coupled to micro-electrode arrays: a novel approach to perform in vitro excitotoxicity testing. *Neurotoxicol Teratol, 34*(1), 116-127. doi:10.1016/j.ntt.2011.08.001

Friedman, D., Honig, L. S., & Scarmeas, N. (2012). Seizures and epilepsy in Alzheimer's disease. *CNS Neurosci Ther, 18*(4), 285-294. doi:10.1111/j.1755-5949.2011.00251.x

Fyhn, M., Hafting, T., Witter, M. P., Moser, E. I., & Moser, M. B. (2008). Grid cells in mice. *Hippocampus, 18*(12), 1230-1238. doi:10.1002/hipo.20472

Games, D., Adams, D., Alessandrini, R., Barbour, R., Berthelette, P., Blackwell, C., . . . et al. (1995). Alzheimer-type neuropathology in transgenic mice overexpressing V717F beta-amyloid precursor protein. *Nature, 373*(6514), 523-527. doi:10.1038/373523a0

Gold, C., Henze, D. A., Koch, C., & Buzsáki, G. (2006). On the origin of the extracellular action potential waveform: A modeling study. *J Neurophysiol, 95*(5), 3113-3128. doi:10.1152/jn.00979.2005

Goldberg, T. E., Huey, E. D., & Devanand, D. P. (2020). Association of APOE e2 genotype with Alzheimer's and non-Alzheimer's neurodegenerative pathologies. *Nat Commun, 11*(1), 4727. doi:10.1038/s41467-020-18198-x

Gomez-Isla, T., Price, J. L., McKeel, D. W., Jr., Morris, J. C., Growdon, J. H., & Hyman, B. T. (1996). Profound loss of layer II entorhinal cortex neurons occurs in very mild Alzheimer's disease. *J Neurosci, 16*(14), 4491-4500.

Gong, C. X., & Iqbal, K. (2008). Hyperphosphorylation of microtubule-associated protein tau: a promising therapeutic target for Alzheimer disease. *Curr Med Chem, 15*(23), 2321-2328. doi:10.2174/092986708785909111

González-Billault, C., Engelke, M., Jiménez-Mateos, E. M., Wandosell, F., Cáceres, A., & Avila, J. (2002). Participation of structural microtubule-associated proteins (MAPs) in the development of neuronal polarity. *J Neurosci Res, 67*(6), 713-719. doi:10.1002/jnr.10161

Gonzalez-Sulser, A., Wang, J., Queenan, B. N., Avoli, M., Vicini, S., & Dzakpasu, R. (2012). Hippocampal neuron firing and local field potentials in the in vitro 4-aminopyridine epilepsy model. *J Neurophysiol, 108*(9), 2568-2580. doi:10.1152/jn.00363.2012

Gouras, G. K., Tsai, J., Naslund, J., Vincent, B., Edgar, M., Checler, F., . . . Relkin, N. R. (2000). Intraneuronal Abeta42 accumulation in human brain. *Am J Pathol, 156*(1), 15-20. doi:10.1016/s0002-9440(10)64700-1

Habibey, R., Rojo Arias, J. E., Striebel, J., & Busskamp, V. (2022). Microfluidics for Neuronal Cell and Circuit Engineering. *Chem Rev, 122*(18), 14842-14880. doi:10.1021/acs.chemrev.2c00212

Haile, Y., Berski, S., Dräger, G., Nobre, A., Stummeyer, K., Gerardy-Schahn, R., & Grothe, C. (2008). The effect of modified polysialic acid based hydrogels on the adhesion and viability of primary neurons and glial cells. *Biomaterials, 29*(12), 1880-1891. doi:10.1016/j.biomaterials.2007.12.030

Hanssen, K. S., Witter, M. P., Sandvig, A., Sandvig, I., & Kobro-Flatmoen, A. (2023). Dissection and culturing of adult lateral entorhinal cortex layer II neurons from APP/PS1 Alzheimer model mice. *J Neurosci Methods, 390*, 109840. doi:10.1016/j.jneumeth.2023.109840

Heggland, I., Storkaas, I. S., Soligard, H. T., Kobro-Flatmoen, A., & Witter, M. P. (2015). Stereological estimation of neuron number and plaque load in the hippocampal region of a transgenic rat model of Alzheimer's disease. *Eur J Neurosci, 41*(9), 1245-1262. doi:10.1111/ejn.12876

Hsia, A. Y., Masliah, E., McConlogue, L., Yu, G. Q., Tatsuno, G., Hu, K., . . . Mucke, L. (1999). Plaque-independent disruption of neural circuits in Alzheimer's disease mouse models. *Proc Natl Acad Sci U S A, 96*(6), 3228-3233. doi:10.1073/pnas.96.6.3228

Hyman, B. T. (1997). The neuropathological diagnosis of Alzheimer's disease: clinical-pathological studies. *Neurobiol Aging, 18*(4 Suppl), S27-32. doi:10.1016/s0197-4580(97)00066-3

Hyman, B. T., Van Hoesen, G. W., Kromer, L. J., & Damasio, A. R. (1986). Perforant pathway changes and the memory impairment of Alzheimer's disease. *Ann Neurol, 20*(4), 472-481. doi:10.1002/ana.410200406

Insausti, R., Herrero, M. T., & Witter, M. P. (1997). Entorhinal cortex of the rat: cytoarchitectonic subdivisions and the origin and distribution of cortical efferents. *Hippocampus, 7*(2), 146-183. doi:10.1002/(sici)1098-1063(1997)7:2<146::Aid-hipo4>3.0.Co;2-l

Iwatsubo, T., Odaka, A., Suzuki, N., Mizusawa, H., Nukina, N., & Ihara, Y. (1994). Visualization of A beta 42(43) and A beta 40 in senile plaques with end-specific A beta monoclonals: evidence that an initially deposited species is A beta 42(43). *Neuron, 13*(1), 45-53. doi:10.1016/0896-6273(94)90458-8

Jawhar, S., Trawicka, A., Jenneckens, C., Bayer, T. A., & Wirths, O. (2012). Motor deficits, neuron loss, and reduced anxiety coinciding with axonal degeneration and intraneuronal Aβ aggregation in the 5XFAD mouse model of Alzheimer's disease. *Neurobiol Aging, 33*(1), 196.e129-140. doi:10.1016/j.neurobiolaging.2010.05.027

Kaufman, S. K., Del Tredici, K., Thomas, T. L., Braak, H., & Diamond, M. I. (2018). Tau seeding activity begins in the transentorhinal/entorhinal regions and anticipates phospho-tau pathology in Alzheimer's disease and PART. *Acta Neuropathol, 136*(1), 57-67. doi:10.1007/s00401-018-1855-6

Kenessey, A., & Yen, S. H. (1993). The extent of phosphorylation of fetal tau is comparable to that of PHF-tau from Alzheimer paired helical filaments. *Brain Res, 629*(1), 40-46. doi:10.1016/0006-8993(93)90478-6

Kerr, K. M., Agster, K. L., Furtak, S. C., & Burwell, R. D. (2007). Functional neuroanatomy of the parahippocampal region: the lateral and medial entorhinal areas. *Hippocampus, 17*(9), 697-708. doi:10.1002/hipo.20315

Kim, C. K., Lee, Y. R., Ong, L., Gold, M., Kalali, A., & Sarkar, J. (2022). Alzheimer's Disease: Key Insights from Two Decades of Clinical Trial Failures. *J Alzheimers Dis, 87*(1), 83-100. doi:10.3233/jad-215699

Kim, H., Devanand, D. P., Carlson, S., & Goldberg, T. E. (2022). Apolipoprotein E Genotype e2: Neuroprotection and Its Limits. *Front Aging Neurosci, 14*, 919712. doi:10.3389/fnagi.2022.919712

Knierim, J. J. (2015). The hippocampus. *Curr Biol, 25*(23), R1116-1121. doi:10.1016/j.cub.2015.10.049

Kobro-Flatmoen, A., Battistin, C., Nair, R. R., Bjorkli, C., Skender, B., Kentros, C., . . . Witter, M. P. (2023). Lowering levels of reelin in entorhinal cortex layer II-neurons results in lowered levels of intracellular amyloid-β. *Brain Commun, 5*(2), fcad115. doi:10.1093/braincomms/fcad115

Kobro-Flatmoen, A., Lagartos-Donate, M. J., Aman, Y., Edison, P., Witter, M. P., & Fang, E. F. (2021). Re-emphasizing early Alzheimer's disease pathology starting in select entorhinal neurons, with a special focus on mitophagy. *Ageing Res Rev, 67*, 101307. doi:10.1016/j.arr.2021.101307

Kobro-Flatmoen, A., Nagelhus, A., & Witter, M. P. (2016). Reelin-immunoreactive neurons in entorhinal cortex layer II selectively express intracellular amyloid in early Alzheimer's disease. *Neurobiol Dis, 93*, 172-183. doi:10.1016/j.nbd.2016.05.012

Kobro-Flatmoen, A., & Witter, M. P. (2019). Neuronal chemo-architecture of the entorhinal cortex: A comparative review. *Eur J Neurosci, 50*(10), 3627-3662. doi:10.1111/ejn.14511

Koganezawa, N., Roppongi, R. T., Sekino, Y., Tsutsui, I., Higa, A., & Shirao, T. (2023). Easy and Reproducible Low-Density Primary Culture using Frozen Stock of Embryonic Hippocampal Neurons. *J Vis Exp*(191). doi:10.3791/64872

Kordower, J. H., Chu, Y., Stebbins, G. T., DeKosky, S. T., Cochran, E. J., Bennett, D., & Mufson, E. J. (2001). Loss and atrophy of layer II entorhinal cortex neurons in elderly people with mild cognitive impairment. *Ann Neurol, 49*(2), 202-213.

Kramer, P. L., Xu, H., Woltjer, R. L., Westaway, S. K., Clark, D., Erten-Lyons, D., . . . Ott, J. (2011). Alzheimer disease pathology in cognitively healthy elderly: a genome-wide study. *Neurobiol Aging, 32*(12), 2113-2122. doi:10.1016/j.neurobiolaging.2010.01.010

Krstic, D., Pfister, S., Notter, T., & Knuesel, I. (2013). Decisive role of Reelin signaling during early stages of Alzheimer's disease. *Neuroscience, 246*, 108-116. doi:10.1016/j.neuroscience.2013.04.042

Kuchibhotla, K. V., Goldman, S. T., Lattarulo, C. R., Wu, H. Y., Hyman, B. T., & Bacskai, B. J. (2008). Abeta plaques lead to aberrant regulation of calcium homeostasis in vivo resulting in structural and functional disruption of neuronal networks. *Neuron, 59*(2), 214-225. doi:10.1016/j.neuron.2008.06.008

Kumar, N., Gahlawat, A., Kumar, R. N., Singh, Y. P., Modi, G., & Garg, P. (2022). Drug repurposing for Alzheimer's disease: in silico and in vitro investigation of FDA-approved drugs as acetylcholinesterase inhibitors. *J Biomol Struct Dyn, 40*(7), 2878-2892. doi:10.1080/07391102.2020.1844054

Kundu, A., Micholt, L., Friedrich, S., Rand, D. R., Bartic, C., Braeken, D., & Levchenko, A. (2013). Superimposed topographic and chemical cues synergistically guide neurite outgrowth. *Lab Chip, 13*(15), 3070-3081. doi:10.1039/c3lc50174d

Leon, W. C., Canneva, F., Partridge, V., Allard, S., Ferretti, M. T., DeWilde, A., . . . Cuello, A. C. (2010). A novel transgenic rat model with a full Alzheimer's-like amyloid pathology displays pre-plaque intracellular amyloid-beta-associated cognitive impairment. *J Alzheimers Dis, 20*(1), 113-126. doi:10.3233/jad-2010-1349

Lewis, D. I. (2019). Animal experimentation: implementation and application of the 3Rs. *Emerg Top Life Sci, 3*(6), 675-679. doi:10.1042/etls20190061

Li, N. M., Liu, K. F., Qiu, Y. J., Zhang, H. H., Nakanishi, H., & Qing, H. (2019). Mutations of beta-amyloid precursor protein alter the consequence of Alzheimer's disease pathogenesis. *Neural Regen Res, 14*(4), 658-665. doi:10.4103/1673-5374.247469

Li, T., Pires, C., Nielsen, T. T., Waldemar, G., Hjermind, L. E., Nielsen, J. E., . . . Freude, K. K. (2016). Generation of induced pluripotent stem cells (iPSCs) from an Alzheimer's disease patient carrying an A79V mutation in PSEN1. *Stem Cell Res, 16*(2), 229-232. doi:10.1016/j.scr.2016.01.002

Li, Z., Shue, F., Zhao, N., Shinohara, M., & Bu, G. (2020). APOE2: protective mechanism and therapeutic implications for Alzheimer's disease. *Mol Neurodegener, 15*(1), 63. doi:10.1186/s13024-020-00413-4

Liang, S., & Crutcher, K. A. (1992). Neuronal migration on laminin in vitro. *Brain Res Dev Brain Res, 66*(1), 127-132. doi:10.1016/0165-3806(92)90148-p

Liu, C., Tan, F. C., Xiao, Z. C., & Dawe, G. S. (2015). Amyloid precursor protein enhances Nav1.6 sodium channel cell surface expression. *J Biol Chem, 290*(19), 12048-12057. doi:10.1074/jbc.M114.617092

Lopera, F., Marino, C., Chandrahas, A. S., O'Hare, M., Villalba-Moreno, N. D., Aguillon, D., . . . Quiroz, Y. T. (2023). Resilience to autosomal dominant Alzheimer's disease in a Reelin-COLBOS heterozygous man. *Nat Med, 29*(5), 1243-1252. doi:10.1038/s41591-023-02318-3

Lublin, A. L., & Gandy, S. (2010). Amyloid-beta oligomers: possible roles as key neurotoxins in Alzheimer's Disease. *Mt Sinai J Med, 77*(1), 43-49. doi:10.1002/msj.20160

Maccione, A., Gandolfo, M., Massobrio, P., Novellino, A., Martinoia, S., & Chiappalone, M. (2009). A novel algorithm for precise identification of spikes in extracellularly recorded neuronal signals. *J Neurosci Methods, 177*(1), 241-249. doi:10.1016/j.jneumeth.2008.09.026

Mahoney, M. J., Chen, R. R., Tan, J., & Saltzman, W. M. (2005). The influence of microchannels on neurite growth and architecture. *Biomaterials, 26*(7), 771-778. doi:10.1016/j.biomaterials.2004.03.015

Malpetti, M., Kievit, R. A., Passamonti, L., Jones, P. S., Tsvetanov, K. A., Rittman, T., . . . Rowe, J. B. (2020). Microglial activation and tau burden predict cognitive decline in Alzheimer's disease. *Brain, 143*(5), 1588-1602. doi:10.1093/brain/awaa088

Manthorpe, M., Engvall, E., Ruoslahti, E., Longo, F. M., Davis, G. E., & Varon, S. (1983). Laminin promotes neuritic regeneration from cultured peripheral and central neurons. *J Cell Biol, 97*(6), 1882-1890. doi:10.1083/jcb.97.6.1882

Marcantoni, A., Raymond, E. F., Carbone, E., & Marie, H. (2014). Firing properties of entorhinal cortex neurons and early alterations in an Alzheimer's disease transgenic model. *Pflugers Arch, 466*(7), 1437-1450. doi:10.1007/s00424-013-1368-z

Medeiros, R., Baglietto-Vargas, D., & LaFerla, F. M. (2011). The role of tau in Alzheimer's disease and related disorders. *CNS Neurosci Ther, 17*(5), 514-524. doi:10.1111/j.1755-5949.2010.00177.x

Minkeviciene, R., Rheims, S., Dobszay, M. B., Zilberter, M., Hartikainen, J., Fülöp, L., . . . Tanila, H. (2009). Amyloid beta-induced neuronal hyperexcitability triggers progressive epilepsy. *J Neurosci, 29*(11), 3453-3462. doi:10.1523/jneurosci.5215-08.2009

Moehlmann, T., Winkler, E., Xia, X., Edbauer, D., Murrell, J., Capell, A., . . . Steiner, H. (2002). Presenilin-1 mutations of leucine 166 equally affect the generation of the Notch and APP

intracellular domains independent of their effect on Abeta 42 production. *Proc Natl Acad Sci U S A, 99*(12), 8025-8030. doi:10.1073/pnas.112686799

Mori, C., Spooner, E. T., Wisniewsk, K. E., Wisniewski, T. M., Yamaguch, H., Saido, T. C., . . . Lemere, C. A. (2002). Intraneuronal Abeta42 accumulation in Down syndrome brain. *Amyloid, 9*(2), 88-102.

Mullan, M., Crawford, F., Axelman, K., Houlden, H., Lilius, L., Winblad, B., & Lannfelt, L. (1992). A pathogenic mutation for probable Alzheimer's disease in the APP gene at the N-terminus of beta-amyloid. *Nat Genet, 1*(5), 345-347. doi:10.1038/ng0892-345

Mullen, R. J., Buck, C. R., & Smith, A. M. (1992). NeuN, a neuronal specific nuclear protein in vertebrates. *Development, 116*(1), 201-211. doi:10.1242/dev.116.1.201

Maass, A., Berron, D., Libby, L. A., Ranganath, C., & Düzel, E. (2015). Functional subregions of the human entorhinal cortex. *Elife, 4*. doi:10.7554/eLife.06426

Naber, P. A., Lopes da Silva, F. H., & Witter, M. P. (2001). Reciprocal connections between the entorhinal cortex and hippocampal fields CA1 and the subiculum are in register with the projections from CA1 to the subiculum. *Hippocampus, 11*(2), 99-104. doi:10.1002/hipo.1028

Nagy, Z., Esiri, M. M., Jobst, K. A., Johnston, C., Litchfield, S., Sim, E., & Smith, A. D. (1995). Influence of the apolipoprotein E genotype on amyloid deposition and neurofibrillary tangle formation in Alzheimer's disease. *Neuroscience, 69*(3), 757-761. doi:10.1016/0306-4522(95)00331-c

Napoli, A., & Obeid, I. (2016). Comparative Analysis of Human and Rodent Brain Primary Neuronal Culture Spontaneous Activity Using Micro-Electrode Array Technology. *J Cell Biochem, 117*(3), 559-565. doi:10.1002/jcb.25312

Navarro Schröder, T., Haak, K. V., Zaragoza Jimenez, N. I., Beckmann, C. F., & Doeller, C. F. (2015). Functional topography of the human entorhinal cortex. *Elife, 4*. doi:10.7554/eLife.06738

Oddo, S., Caccamo, A., Shepherd, J. D., Murphy, M. P., Golde, T. E., Kayed, R., . . . LaFerla, F. M. (2003). Triple-transgenic model of Alzheimer's disease with plaques and tangles: intracellular Abeta and synaptic dysfunction. *Neuron, 39*(3), 409-421. doi:10.1016/s0896-6273(03)00434-3

Oddo, S., Caccamo, A., Smith, I. F., Green, K. N., & LaFerla, F. M. (2006). A dynamic relationship between intracellular and extracellular pools of Abeta. *Am J Pathol, 168*(1), 184-194. doi:10.2353/ajpath.2006.050593

Olsen, R. K., Yeung, L. K., Noly-Gandon, A., D'Angelo, M. C., Kacollja, A., Smith, V. M., . . . Barense, M. D. (2017). Human anterolateral entorhinal cortex volumes are associated with cognitive decline in aging prior to clinical diagnosis. *Neurobiol Aging, 57*, 195-205. doi:10.1016/j.neurobiolaging.2017.04.025

Palmqvist, S., Janelidze, S., Quiroz, Y. T., Zetterberg, H., Lopera, F., Stomrud, E., . . . Hansson, O. (2020). Discriminative Accuracy of Plasma Phospho-tau217 for Alzheimer Disease vs Other Neurodegenerative Disorders. *Jama, 324*(8), 772-781. doi:10.1001/jama.2020.12134

Palop, J. J., Chin, J., Roberson, E. D., Wang, J., Thwin, M. T., Bien-Ly, N., . . . Mucke, L. (2007). Aberrant excitatory neuronal activity and compensatory remodeling of inhibitory hippocampal circuits in mouse models of Alzheimer's disease. *Neuron, 55*(5), 697-711. doi:10.1016/j.neuron.2007.07.025

Palop, J. J., & Mucke, L. (2009). Epilepsy and cognitive impairments in Alzheimer disease. *Arch Neurol, 66*(4), 435-440. doi:10.1001/archneurol.2009.15

Palop, J. J., & Mucke, L. (2010). Amyloid-beta-induced neuronal dysfunction in Alzheimer's disease: from synapses toward neural networks. *Nat Neurosci, 13*(7), 812-818. doi:10.1038/nn.2583

Pan, L., Alagapan, S., Franca, E., Leondopulos, S. S., DeMarse, T. B., Brewer, G. J., & Wheeler, B. C. (2015). An in vitro method to manipulate the direction and functional strength between neural populations. *Front Neural Circuits, 9*, 32. doi:10.3389/fncir.2015.00032

Pasquale, V., Martinoia, S., & Chiappalone, M. (2010). A self-adapting approach for the detection of bursts and network bursts in neuronal cultures. *J Comput Neurosci, 29*(1-2), 213-229. doi:10.1007/s10827-009-0175-1

Patterson, C. (2018). *World Alzheimer Report 2018*. Retrieved from Alzheimer's Disease International: https://www.alz.co.uk/research/WorldAlzheimerReport2018.pdf

Peyrin, J. M., Deleglise, B., Saias, L., Vignes, M., Gougis, P., Magnifico, S., . . . Brugg, B. (2011). Axon diodes for the reconstruction of oriented neuronal networks in microfluidic chambers. *Lab Chip, 11*(21), 3663-3673. doi:10.1039/c1lc20014c

Poli, D., Wheeler, B. C., DeMarse, T. B., & Brewer, G. J. (2018). Pattern separation and completion of distinct axonal inputs transmitted via micro-tunnels between co-cultured hippocampal dentate, CA3, CA1 and entorhinal cortex networks. *J Neural Eng, 15*(4), 046009. doi:10.1088/1741-2552/aabc20

Price, J. L., Ko, A. I., Wade, M. J., Tsou, S. K., McKeel, D. W., & Morris, J. C. (2001). Neuron number in the entorhinal cortex and CA1 in preclinical Alzheimer disease. *Arch Neurol, 58*(9), 1395-1402. doi:10.1001/archneur.58.9.1395

Prince, M., Bryce, R., Albanese, E., Wimo, A., Ribeiro, W., & Ferri, C. P. (2013). The global prevalence of dementia: a systematic review and metaanalysis. *Alzheimers Dement, 9*(1), 63-75.e62. doi:10.1016/j.jalz.2012.11.007

Qiang, L., Sun, X., Austin, T. O., Muralidharan, H., Jean, D. C., Liu, M., . . . Baas, P. W. (2018). Tau Does Not Stabilize Axonal Microtubules but Rather Enables Them to Have Long Labile Domains. *Curr Biol, 28*(13), 2181-2189.e2184. doi:10.1016/j.cub.2018.05.045

Radde, R., Bolmont, T., Kaeser, S. A., Coomaraswamy, J., Lindau, D., Stoltze, L., . . . Jucker, M. (2006). Abeta42-driven cerebral amyloidosis in transgenic mice reveals early and robust pathology. *EMBO Rep, 7*(9), 940-946. doi:10.1038/sj.embor.7400784

Rajbanshi, B., Guruacharya, A., Mandell, J. W., & Bloom, G. S. (2023). Localization, induction, and cellular effects of tau phosphorylated at threonine 217. *Alzheimers Dement*. doi:10.1002/alz.12892

Reitz, C., & Mayeux, R. (2014). Alzheimer disease: epidemiology, diagnostic criteria, risk factors and biomarkers. *Biochem Pharmacol, 88*(4), 640-651. doi:10.1016/j.bcp.2013.12.024

Rischel, E. B., Gejl, M., Brock, B., Rungby, J., & Gjedde, A. (2022). In Alzheimer's disease, amyloid beta accumulation is a protective mechanism that ultimately fails. *Alzheimers Dement*. doi:10.1002/alz.12701

Roos, T. T., Garcia, M. G., Martinsson, I., Mabrouk, R., Israelsson, B., Deierborg, T., . . . Gouras, G. K. (2021). Neuronal spreading and plaque induction of intracellular Aβ and its disruption of Aβ homeostasis. *Acta Neuropathol, 142*(4), 669-687. doi:10.1007/s00401-021-02345-9

Roses, A. D. (1996). Apolipoprotein E alleles as risk factors in Alzheimer's disease. *Annu Rev Med, 47*, 387-400. doi:10.1146/annurev.med.47.1.387

Sáez-Valero, J., Costell, M., Sjögren, M., Andreasen, N., Blennow, K., & Luque, J. M. (2003). Altered levels of cerebrospinal fluid reelin in frontotemporal dementia and Alzheimer's disease. *J Neurosci Res, 72*(1), 132-136. doi:10.1002/jnr.10554

Sahlgren Bendtsen, K. M., & Hall, V. J. (2023). The Breakthroughs and Caveats of Using Human Pluripotent Stem Cells in Modeling Alzheimer's Disease. *Cells, 12*(3). doi:10.3390/cells12030420

Sanchez, P. E., Zhu, L., Verret, L., Vossel, K. A., Orr, A. G., Cirrito, J. R., . . . Mucke, L. (2012). Levetiracetam suppresses neuronal network dysfunction and reverses synaptic and cognitive deficits in an Alzheimer's disease model. *Proc Natl Acad Sci U S A, 109*(42), E2895-2903. doi:10.1073/pnas.1121081109

Scarmeas, N., Luchsinger, J. A., Schupf, N., Brickman, A. M., Cosentino, S., Tang, M. X., & Stern, Y. (2009). Physical activity, diet, and risk of Alzheimer disease. *Jama, 302*(6), 627-637. doi:10.1001/jama.2009.1144

Scheff, S. W., Price, D. A., Schmitt, F. A., & Mufson, E. J. (2006). Hippocampal synaptic loss in early Alzheimer's disease and mild cognitive impairment. *Neurobiol Aging, 27*(10), 1372-1384. doi:10.1016/j.neurobiolaging.2005.09.012

Scheyer, O., Rahman, A., Hristov, H., Berkowitz, C., Isaacson, R. S., Diaz Brinton, R., & Mosconi, L. (2018). Female Sex and Alzheimer's Risk: The Menopause Connection. *J Prev Alzheimers Dis, 5*(4), 225-230. doi:10.14283/jpad.2018.34

Sciarretta, C., & Minichiello, L. (2010). The preparation of primary cortical neuron cultures and a practical application using immunofluorescent cytochemistry. *Methods Mol Biol, 633*, 221-231. doi:10.1007/978-1-59745-019-5_16

Scoville, W. B., & Milner, B. (1957). Loss of recent memory after bilateral hippocampal lesions. *J Neurol Neurosurg Psychiatry, 20*(1), 11-21. doi:10.1136/jnnp.20.1.11

Seripa, D., Matera, M. G., Franceschi, M., Daniele, A., Bizzarro, A., Rinaldi, M., . . . Pilotto, A. (2008). The RELN locus in Alzheimer's disease. *J Alzheimers Dis, 14*(3), 335-344. doi:10.3233/jad-2008-14308

Serrano-Pozo, A., Frosch, M. P., Masliah, E., & Hyman, B. T. (2011). Neuropathological alterations in Alzheimer disease. *Cold Spring Harb Perspect Med, 1*(1), a006189. doi:10.1101/cshperspect.a006189

Šišková, Z., Justus, D., Kaneko, H., Friedrichs, D., Henneberg, N., Beutel, T., . . . Remy, S. (2014). Dendritic structural degeneration is functionally linked to cellular hyperexcitability in a mouse model of Alzheimer's disease. *Neuron, 84*(5), 1023-1033. doi:10.1016/j.neuron.2014.10.024

Slanzi, A., Iannoto, G., Rossi, B., Zenaro, E., & Constantin, G. (2020). In vitro Models of Neurodegenerative Diseases. *Front Cell Dev Biol, 8*, 328. doi:10.3389/fcell.2020.00328

Squire, L. R. (1992). Memory and the hippocampus: a synthesis from findings with rats, monkeys, and humans. *Psychol Rev, 99*(2), 195-231. doi:10.1037/0033-295x.99.2.195

Stacey, G. N. (2011). Cell culture contamination. *Methods Mol Biol, 731*, 79-91. doi:10.1007/978-1-61779-080-5_7

Strain, J. F., Smith, R. X., Beaumont, H., Roe, C. M., Gordon, B. A., Mishra, S., . . . Ances, B. M. (2018). Loss of white matter integrity reflects tau accumulation in Alzheimer disease defined regions. *Neurology, 91*(4), e313-e318. doi:10.1212/wnl.0000000000005864

Syversen, I. F., Witter, M. P., Kobro-Flatmoen, A., Goa, P. E., Navarro Schröder, T., & Doeller, C. F. (2021). Structural connectivity-based segmentation of the human entorhinal cortex. *Neuroimage, 245*, 118723. doi:10.1016/j.neuroimage.2021.118723

Takada, L. T., Aláez-Verson, C., Burgute, B. D., Nitrini, R., Sosa, A. L., Castilhos, R. M., . . . Llibre-Guerra, J. J. (2022). Discovery and validation of dominantly inherited Alzheimer's disease mutations in populations from Latin America. *Alzheimers Res Ther, 14*(1), 108. doi:10.1186/s13195-022-01052-1

Takahashi, R. H., Milner, T. A., Li, F., Nam, E. E., Edgar, M. A., Yamaguchi, H., . . . Gouras, G. K. (2002). Intraneuronal Alzheimer abeta42 accumulates in multivesicular bodies and is associated with synaptic pathology. *Am J Pathol, 161*(5), 1869-1879. doi:10.1016/s0002-9440(10)64463-x

Taylor, A. M., Blurton-Jones, M., Rhee, S. W., Cribbs, D. H., Cotman, C. W., & Jeon, N. L. (2005). A microfluidic culture platform for CNS axonal injury, regeneration and transport. *Nat Methods, 2*(8), 599-605. doi:10.1038/nmeth777

Taylor, A. M., Rhee, S. W., Tu, C. H., Cribbs, D. H., Cotman, C. W., & Jeon, N. L. (2003). Microfluidic Multicompartment Device for Neuroscience Research. *Langmuir, 19*(5), 1551-1556. doi:10.1021/la026417v

Thal, D. R., Rüb, U., Orantes, M., & Braak, H. (2002). Phases of A beta-deposition in the human brain and its relevance for the development of AD. *Neurology, 58*(12), 1791-1800. doi:10.1212/wnl.58.12.1791

Thomas, C. A., Jr., Springer, P. A., Loeb, G. E., Berwald-Netter, Y., & Okun, L. M. (1972). A miniature microelectrode array to monitor the bioelectric activity of cultured cells. *Exp Cell Res, 74*(1), 61-66. doi:10.1016/0014-4827(72)90481-8

Tissir, F., & Goffinet, A. M. (2003). Reelin and brain development. *Nat Rev Neurosci, 4*(6), 496-505. doi:10.1038/nrn1113

Tissir, F., Lambert de Rouvroit, C., & Goffinet, A. M. (2002). The role of reelin in the development and evolution of the cerebral cortex. *Braz J Med Biol Res, 35*(12), 1473-1484. doi:10.1590/s0100-879x2002001200007

Trinchese, F., Liu, S., Ninan, I., Puzzo, D., Jacob, J. P., & Arancio, O. (2004). Cell cultures from animal models of Alzheimer's disease as a tool for faster screening and testing of drug efficacy. *J Mol Neurosci, 24*(1), 15-21. doi:10.1385/jmn:24:1:015

Tsao, A., Sugar, J., Lu, L., Wang, C., Knierim, J. J., Moser, M. B., & Moser, E. I. (2018). Integrating time from experience in the lateral entorhinal cortex. *Nature, 561*(7721), 57-62. doi:10.1038/s41586-018-0459-6

Vakilna, Y. S., Tang, W. C., Wheeler, B. C., & Brewer, G. J. (2021). The Flow of Axonal Information Among Hippocampal Subregions: 1. Feed-Forward and Feedback Network Spatial Dynamics Underpinning Emergent Information Processing. *Front Neural Circuits, 15*, 660837. doi:10.3389/fncir.2021.660837

Valderhaug, V. D., Heiney, K., Ramstad, O. H., Bråthen, G., Kuan, W. L., Nichele, S., . . . Sandvig, I. (2021). Early functional changes associated with alpha-synuclein proteinopathy in engineered human neural networks. *Am J Physiol Cell Physiol, 320*(6), C1141-c1152. doi:10.1152/ajpcell.00413.2020

Vale, C., Alonso, E., Rubiolo, J. A., Vieytes, M. R., LaFerla, F. M., Giménez-Llort, L., & Botana, L. M. (2010). Profile for amyloid-beta and tau expression in primary cortical cultures from 3xTg-AD mice. *Cell Mol Neurobiol, 30*(4), 577-590. doi:10.1007/s10571-009-9482-3

van den Pol, A. N., Robek, M. D., Ghosh, P. K., Ozduman, K., Bandi, P., Whim, M. D., & Wollmann, G. (2007). Cytomegalovirus induces interferon-stimulated gene expression and is attenuated by interferon in the developing brain. *J Virol, 81*(1), 332-348. doi:10.1128/jvi.01592-06

van Niekerk, E. A., Kawaguchi, R., Marques de Freria, C., Groeniger, K., Marchetto, M. C., Dupraz, S., . . . Tuszynski, M. H. (2022). Methods for culturing adult CNS neurons reveal a CNS conditioning effect. *Cell Rep Methods, 2*(7), 100255. doi:10.1016/j.crmeth.2022.100255

van Strien, N. M., Cappaert, N. L., & Witter, M. P. (2009). The anatomy of memory: an interactive overview of the parahippocampal-hippocampal network. *Nat Rev Neurosci, 10*(4), 272-282. doi:10.1038/nrn2614

Varghese, K., Das, M., Bhargava, N., Stancescu, M., Molnar, P., Kindy, M. S., & Hickman, J. J. (2009). Regeneration and characterization of adult mouse hippocampal neurons in a defined in vitro system. *J Neurosci Methods, 177*(1), 51-59. doi:10.1016/j.jneumeth.2008.09.022

Verret, L., Mann, E. O., Hang, G. B., Barth, A. M., Cobos, I., Ho, K., . . . Palop, J. J. (2012). Inhibitory interneuron deficit links altered network activity and cognitive dysfunction in Alzheimer model. *Cell, 149*(3), 708-721. doi:10.1016/j.cell.2012.02.046

Viola, K. L., & Klein, W. L. (2015). Amyloid β oligomers in Alzheimer's disease pathogenesis, treatment, and diagnosis. *Acta Neuropathol, 129*(2), 183-206. doi:10.1007/s00401-015-1386-3

Vossel, K. A., Beagle, A. J., Rabinovici, G. D., Shu, H., Lee, S. E., Naasan, G., . . . Mucke, L. (2013). Seizures and epileptiform activity in the early stages of Alzheimer disease. *JAMA Neurol, 70*(9), 1158-1166. doi:10.1001/jamaneurol.2013.136

Walker, L. C. (2018). Prion-like mechanisms in Alzheimer disease. *Handb Clin Neurol, 153*, 303-319. doi:10.1016/b978-0-444-63945-5.00016-7

Wang, X., Zhang, X. G., Zhou, T. T., Li, N., Jang, C. Y., Xiao, Z. C., . . . Li, S. (2016). Elevated Neuronal Excitability Due to Modulation of the Voltage-Gated Sodium Channel Nav1.6 by Aβ1-42. *Front Neurosci, 10*, 94. doi:10.3389/fnins.2016.00094

Wegmann, S., Bennett, R. E., Delorme, L., Robbins, A. B., Hu, M., McKenzie, D., . . . Hyman, B. T. (2019). Experimental evidence for the age dependence of tau protein spread in the brain. *Sci Adv, 5*(6), eaaw6404. doi:10.1126/sciadv.aaw6404

Weir, J. S., Christiansen, N., Sandvig, A., & Sandvig, I. (2023). Selective inhibition of excitatory synaptic transmission alters the emergent bursting dynamics of in vitro neural networks. *Front Neural Circuits, 17*, 1020487. doi:10.3389/fncir.2023.1020487

West, M. J., Kawas, C. H., Stewart, W. F., Rudow, G. L., & Troncoso, J. C. (2004). Hippocampal neurons in pre-clinical Alzheimer's disease. *Neurobiol Aging, 25*(9), 1205-1212. doi:10.1016/j.neurobiolaging.2003.12.005

Westhaus, A., Cabanes-Creus, M., Rybicki, A., Baltazar, G., Navarro, R. G., Zhu, E., . . . Lisowski, L. (2020). High-Throughput In Vitro, Ex Vivo, and In Vivo Screen of Adeno-Associated Virus Vectors Based on Physical and Functional Transduction. *Hum Gene Ther, 31*(9-10), 575-589. doi:10.1089/hum.2019.264

Winter-Hjelm N, T. Å. B., Sikoriski P, Sandvig A, Sandvig I. (2023). Structure-Function Dynamics of Engineered, Modular Neuronal Networks with Controllable Afferent-Efferent Connectivity. *Journal of Neural Engineering* doi:DOI 10.1088/1741-2552/ace37f

Witter, M. P., Groenewegen, H. J., Lopes da Silva, F. H., & Lohman, A. H. (1989). Functional organization of the extrinsic and intrinsic circuitry of the parahippocampal region. *Prog Neurobiol, 33*(3), 161-253. doi:10.1016/0301-0082(89)90009-9

Wu, L., Rosa-Neto, P., Hsiung, G. Y., Sadovnick, A. D., Masellis, M., Black, S. E., . . . Gauthier, S. (2012). Early-onset familial Alzheimer's disease (EOFAD). *Can J Neurol Sci, 39*(4), 436-445. doi:10.1017/s0317167100013949

Xu, W., Fitzgerald, S., Nixon, R. A., Levy, E., & Wilson, D. A. (2015). Early hyperactivity in lateral entorhinal cortex is associated with elevated levels of AbetaPP metabolites in the Tg2576 mouse model of Alzheimer's disease. *Exp Neurol, 264*, 82-91. doi:10.1016/j.expneurol.2014.12.008

Yagi, T., Ito, D., Okada, Y., Akamatsu, W., Nihei, Y., Yoshizaki, T., . . . Suzuki, N. (2011). Modeling familial Alzheimer's disease with induced pluripotent stem cells. *Hum Mol Genet, 20*(23), 4530-4539. doi:10.1093/hmg/ddr394

Yan, Y., & Wang, C. (2006). Abeta42 is more rigid than Abeta40 at the C terminus: implications for Abeta aggregation and toxicity. *J Mol Biol, 364*(5), 853-862. doi:10.1016/j.jmb.2006.09.046

Yu, N. N., Tan, M. S., Yu, J. T., Xie, A. M., & Tan, L. (2016). The Role of Reelin Signaling in Alzheimer's Disease. *Mol Neurobiol, 53*(8), 5692-5700. doi:10.1007/s12035-015-9459-9

Zhang, X. Y., Li, J., Li, C. J., Lin, Y. Q., Huang, C. H., Zheng, X., . . . Yan, S. (2021). Differential development and electrophysiological activity in cultured cortical neurons from the mouse and cynomolgus monkey. *Neural Regen Res, 16*(12), 2446-2452. doi:10.4103/1673-5374.313056

Zheng, H., & Koo, E. H. (2006). The amyloid precursor protein: beyond amyloid. *Mol Neurodegener, 1*, 5. doi:10.1186/1750-1326-1-5

Zhu, S., Wang, J., Zhang, Y., He, J., Kong, J., Wang, J. F., & Li, X. M. (2017). The role of neuroinflammation and amyloid in cognitive impairment in an APP/PS1 transgenic mouse model of Alzheimer's disease. *CNS Neurosci Ther, 23*(4), 310-320. doi:10.1111/cns.12677

Zott, B., Simon, M. M., Hong, W., Unger, F., Chen-Engerer, H. J., Frosch, M. P., . . . Konnerth, A. (2019). A vicious cycle of β amyloid-dependent neuronal hyperactivation. *Science, 365*(6453), 559-565. doi:10.1126/science.aay0198

Supplementary material
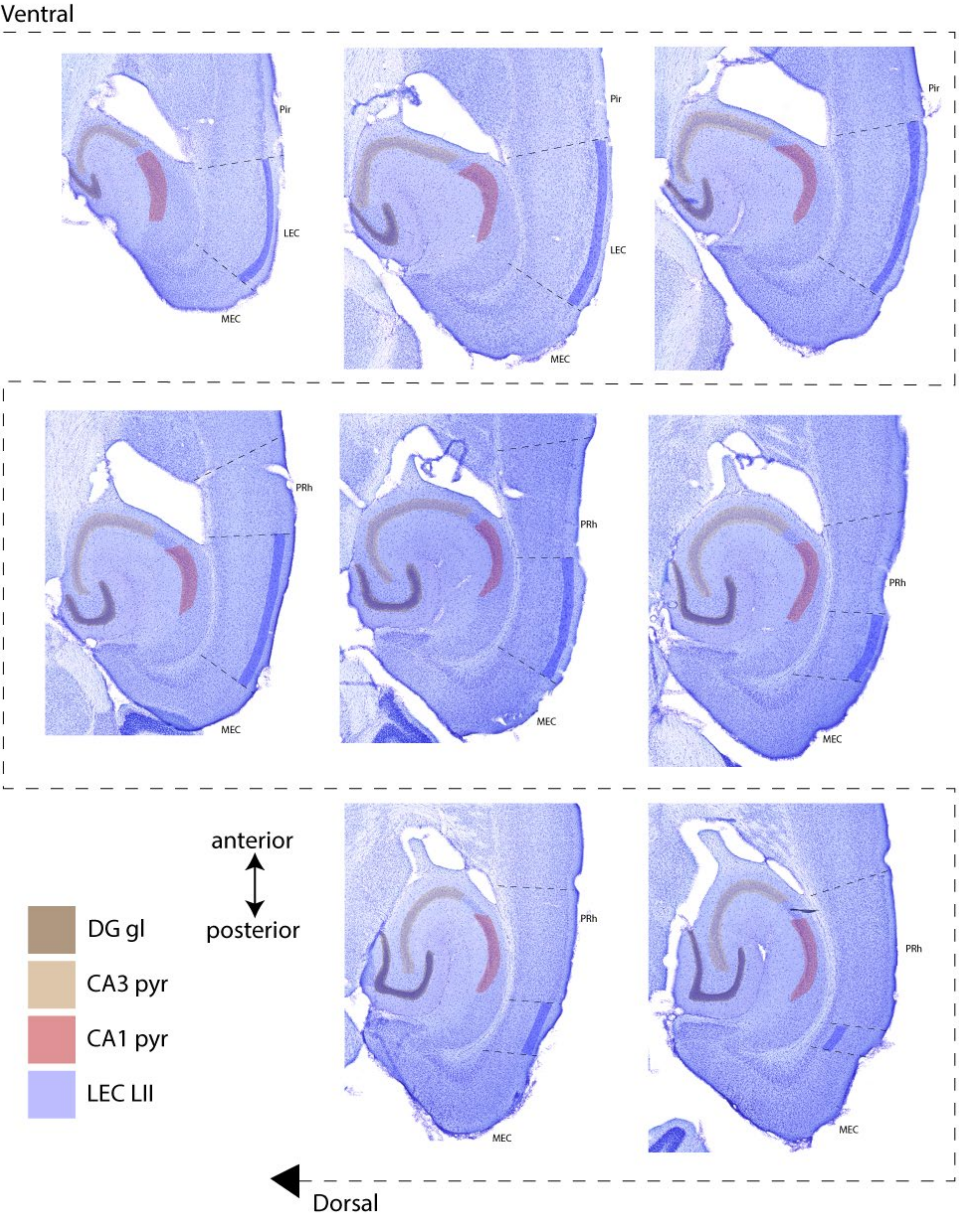
Supplementary figure 1. Delineation of LEC and hippocampal DG-gl and CA3/CA1-pyr layers from the ventral to dorsal plane.

Supplementary table 1. Animals included in Paper I and II.

Paper I			
Animal model	Sex	Age	Genotype
APP/PS1	M	P48 (n =2)	+/-
APP/PS1	M	P48 - P54 (n =3)	-/-
APP/PS1	F	P60 (n = 4)	+/-
Paper II			
Animal model	Sex	Age and number	Genotype
APP/PS1	F	P79 - P80 (n= 2)	+/-
McGill-R-Thy1-APP	M	P46 - P53 (n =4)	-/-
McGill-R-Thy1-APP	M	P38 - P89 (n =5)	+/-
McGill-R-Thy1-APP	M	P43 - P78 (n =4)	+/+
McGill-R-Thy1-APP	F	P53 (n =1)	-/-
McGill-R-Thy1-APP	F	P39 - P81 (n= 14)	+/-
McGill-R-Thy1-APP	F	P37 - P72 (n =7)	+/+

Supplementary Table 2. Primary and secondary antibodies included in Paper I-III.

Primary and secondary antibodies	Concentration	Producer
Paper I		
Ms Anti Reelin Antibody	1:1000	Abcam, ab78540
Rb Anti NeuN Antibody	1:1000	Sigma-Aldrich, ABN90P
Gp Oligomeric A11 Antibody	1:1000	Invitrogen, AHB0052
Alexa Fluor™ 488 Goat-anti-Ms IgG	1:1000	Invitrogen, Cat A-11001
Alexa Fluor™ 546 Goat-anti-Gp IgG	1:1000	Invitrogen, A-11074
Alexa Fluor™ 647 Goat-anti-Rb IgG	1:1000	Invitrogen, A32733
Paper II		
Chk Anti β3-Tubulin Antibody	1:1000	Abcam, ab78078
Rb Anti GAP-43 Antibody	1:500	Sigma-Aldrich, 9264
Ms Anti GFAP Antibody	1:1000	Abcam, ab7260
Chk Anti MAP2 Antibody	1:5000	Abcam, ab5392
Ms Anti Reelin Antibody	1:1000	Abcam, ab78540
Chk Anti Neurofilament Heavy Antibody	1:1000	Abcam, ab4680
Rb Anti NeuN Antibody	1:1000	Abcam, ab 279295
Alexa Fluor™ 647 Goat-anti-Ms IgG	1:1000	Invitrogen, A21236
Alexa Fluor™ 488 Goat-anti-Rb IgG	1:1000	Invitrogen, A21244
Alexa Fluor™ 546 Goat-anti-Chk IgG	1:1000	Abcam, ab175477
Paper III		
Chk Anti Map2 Antibody	1:1000	Abcam, ab5392
Rb Anti GAD65/67 Antibody	1:1000	Abcam, ab183999
Ms Anti Calmodulin (CaMKIIa) Antibody	1:200	Invitrogen, MA3-918
Chk Anti Neurofilament Heavy Antibody	1:1000	Abcam, ab4680
Ms Anti AT8 (Ser202) Antibody	1:1000	Invitrogen, MN1020
Alexa Fluor™ 647 Goat-anti-Ms IgG	1:1000	Invitrogen, A21236
Alexa Fluor™ 488 Goat-anti-Rb IgG	1:1000	Invitrogen, A21244
Alexa Fluor™ 546 Goat-anti-Chk IgG	1:1000	Abcam, ab175477

Ms; mouse, Rb; rabbit, Gp; guinea pig, Chk; chicken.

Papers I-III

Paper I

Dissection and culturing of adult lateral entorhinal cortex layer II neurons from APP/PS1 Alzheimer model mice

Katrine Sjaastad Hanssen [a,b], Menno P. Witter [a,c], Axel Sandvig [b,d,e,f], Ioanna Sandvig [b], Asgeir Kobro-Flatmoen [a,c,*]

[a] *Kavli Institute for Systems Neuroscience, Centre for Neural Computation, Egil and Pauline Braathen and Fred Kavli Centre for Cortical Microcircuits, Norwegian University of Science and Technology (NTNU), Trondheim, Norway*
[b] *Department of Neuromedicine and Movement Science, Faculty of Medicine and Health Sciences, NTNU, Trondheim, Norway*
[c] *K.G. Jebsen Centre for Alzheimer's Disease, Faculty of Medicine and Health Sciences, NTNU, Trondheim, Norway*
[d] *Umeå University Hospital, Division of Neuro, Head and Neck, Umeå, Sweden*
[e] *Department of Community Medicine and Rehabilitation, Umeå University, Umeå, Sweden*
[f] *Department of Neurology and Clinical Neurophysiology, St Olav's Hospital, Trondheim, Norway*

ABSTRACT

Background: Primary neuronal cultures enable cell-biological studies of Alzheimer's disease (AD), albeit typically non-neuron-specific. The first cortical neurons affected in AD reside in layer II of the lateralmost part of the entorhinal cortex, and they undergo early accumulation of intracellular amyloid-β, form subsequent tau pathology, and start degenerating pre-symptomatically. These vulnerable entorhinal neurons uniquely express the glycoprotein reelin and provide selective inputs to the hippocampal memory system. Gaining a more direct access to study these neurons is therefore highly relevant. *New method:* We demonstrate a methodological approach for dissection and long-term culturing of adult lateral entorhinal layer II-neurons from AD-model mice. *Results:* We maintain adult dissected lateralmost entorhinal layer II-neurons beyond two months in culture. We show that they express neuronal markers, and that they are electrophysiologically active by 15 days in vitro and continuing beyond 2 months. *Comparison with existing methods:* Primary neurons are typically harvested from embryonic or early postnatal brains because such neurons are easier to culture compared to adult neurons. Methods to culture adult primary neurons have been reported, however, to our knowledge, culturing of adult entorhinal neuron-type specific primary neurons from AD-model animals have not been reported. *Conclusions:* Our methodological approach offers a window to study initial pathological changes in the AD disease-cascade. This includes the study of proteinopathy, single-neuron changes, and network-level dysfunction.

1. Introduction

For more than two decades, cultured cells have been widely used to model aspects of the neurodegenerative cascade inherent to Alzheimer's disease (AD) (Trinchese et al., 2004), and constitute an indispensable tool to complement in vivo models (Belle et al., 2018). Cellular culture models typically make use of established cell lines of rodent or human origin, or they rely on harvesting primary neurons. The latter are typically obtained from embryonic or early postnatal cortical tissue from rats or mice (Calvo-Rodríguez et al., 2017; Kaech et al., 2006; Konings et al., 2021; Roos et al., 2021; Sahu et al., 2019). However, AD affects subsets of mature neurons, and we may therefore gain insights also by

studying cultures of fully developed neurons, for example by harvesting these from *adult* AD-model animals. This approach not only avoids possible confounds from developmental factors operating in embryonic and early postnatal neurons but may also offer a better representation of how neurons respond to AD-relevant pathologies in the actual disease. Methods to extract and culture adult primary neurons from mice (Brewer et al., 2007; Eide et al., 2005; Varghese et al., 2009) and rats (Brewer, 1997; Brewer et al., 2007), including subregional entorhinal cortex (EC) and hippocampal neurons from AD-model animals (Brewer et al., 2020; Dong and Brewer, 2019; Dong, Digman et al., 2019; Dong, Sameni et al., 2019) have previously been reported, however, work on cultures of neuron-type specific EC neurons from adult AD-model
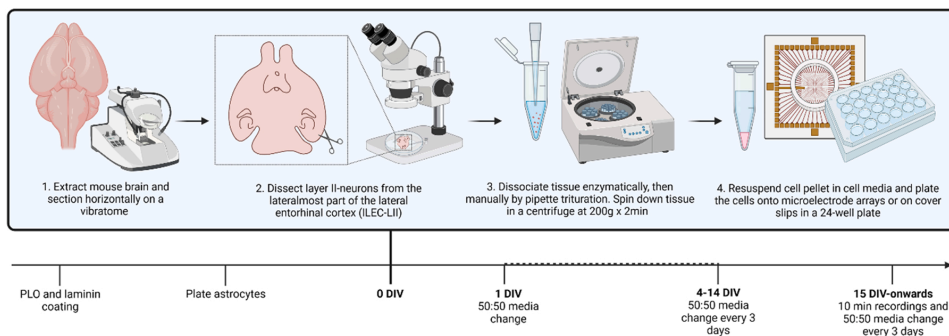
Fig. 1. Overview of experimental setup. Before plating of the lateralmost lateral entorhinal cortex layer II (lLEC-LII-neurons), we coated the culture wells with Poly-L-Ornithine (PLO) and laminin. On day 0, we extracted and horizontally sectioned APP/PS1 mouse brains, and then dissected strips of lLEC-LII-neurons under a stereoscope. The strips were dissociated enzymatically and then manually triturated with a 100 μL pipette, and then spun down in a centrifuge at 200 g x 2 min. The cell pellet was resuspended in 100 μL cell media before plating. At 1 DIV half the media was changed; this was subsequently repeated every 3 days. From 15 DIV we started recording spontaneous activity. DIV; days in vitro. Created with BioRender.com.

animals is lacking.

Immunohistochemical studies (Braak et al., 1991; Gomez-Isla et al., 1996; Kordower et al., 2001) as well as sophisticated live human imaging methods (Holbrook et al., 2020; Kulason et al., 2019; Olsen et al., 2017; Tran et al., 2022; Tward et al., 2017) show that cortical AD-related pathological changes predominantly start in layer II (LII) neurons located in the lateralmost part of the entorhinal cortex (EC), i.e., close to the collateral sulcus. In rodents, equivalent neurons are situated in the cytoarchitectonically defined lateral entorhinal cortex (LEC), and, even though exact borders for a corresponding cytoarchitectonic subdivision of human EC have not yet been decisively established, the same LII neuron-types are present in the lateralmost EC of rodents as those in the lateralmost EC of humans (reviewed in (Kobro-Flatmoen et al., 2019)). Such ECLII-neurons exhibit early AD-related alterations in firing properties (Marcantoni et al., 2014), tend to form tangle pathology prior to other cortical areas (Berron et al., 2021; Braak et al., 1991), and start to die already at preclinical stages of AD (Gomez-Isla et al., 1996; Kordower et al., 2001).

In humans as well as rodents, AD vulnerable ECLII-neurons are unique in expressing reelin (Re+) (Kobro-Flatmoen et al., 2019), which is a large glycoprotein that promotes synaptic plasticity and, of particular relevance to AD, inhibits glycogen synthase kinase 3β-mediated phosphorylation of tau. Work on rodents has established that levels of reelin in such Re+ ECLII-neurons align along a gradient where the lateralmost neurons express high levels of reelin, while those located increasingly further medially express successively lower levels of reelin (Kobro-Flatmoen et al., 2016). Intriguingly, such Re+ ECLII-neurons are highly prone to accumulating intracellular amyloid-β42 (Aβ42), and this accumulation of Aβ42 takes the form of a pattern which aligns along the same gradient as that for reelin (Kobro-Flatmoen et al., 2016). Recent experimental work established that in Re+ ECLII-neurons, Aβ42 directly interacts with reelin. Furthermore, levels of Aβ42 are dependent on levels of reelin, and selectively lowering levels of reelin in these neurons results in a concomitant lowering of Aβ42-levels (Kobro-Flatmoen et al., 2022).

Using adult APP/PS1 mice (Radde et al., 2006), we here present a methodological approach to dissect and culture neurons from the lateralmost part of LEC layer II (lLEC-LII). As we dissect out our population of choice directly, this approach is simpler than the cited gradient purification method for isolation of adult neurons (Brewer et al., 2007). Fig. 1 shows an overview of our experimental setup. Our work is based on mice at ages ranging from postnatal day (P) 48 to P60, thus representing the brain with a fully developed EC (Donato et al., 2017; Semple et al., 2013). We find that cultured adult lLEC-LII-neurons form connections within the two first weeks and remain viable beyond two months. We confirm the lLEC-LII-specific nature of our cultured neurons by showing that they co-express NeuN and reelin. We also find that reelin expression colocalizes with that of Aβ, indicating that the tendency of such neurons to express Aβ (Kobro-Flatmoen et al., 2022, 2016) is retained when they are cultured. The lLEC-LII-networks show spontaneous neuronal activity by two weeks post-seeding and remain active beyond two months. Our approach may thus represent a valuable tool for studying very early proteinopathy, and offers neuron- and network specific modelling of AD pathology in vitro.

2. Materials and methods

2.1. Animals

To develop the cell culture method, we used a total of 48 adult mice, including APP/PS1 model mice and littermate controls, ranging in age from postnatal day 28 (P28) to P115, including 25 males and 23 females. Of these, we collected data from 9 animals (7 males, 2 females; Supplementary Table A.1). All our work complies with the ARRIVE guidelines (Percie du Sert et al., 2020) and the protocol was approved by The Norwegian Food Safety Authority (FOTS ID 8433 and ID 22321), according to the EU Directive 2010/63/EU for animal experiments. Animals were bred at the Comparative Medicine Core Facility (CoMed) at the Norwegian University of Science and Technology (NTNU) and were held in standard lab cages (up to 5 animals per cage), in temperatures of $22 \pm 2\ ^\circ$C, and kept at a light/dark cycle of 12:12 h, with access to food and water ad libitum. Minimum one week before experiments, animals were transferred to the animal facility at the Kavli Institute for Systems Neuroscience, Centre for Neural Computation, NTNU, where brain extractions and dissections were performed. Subsequent processing and experiments were carried out at the Department of Neuromedicine and Movement Science, NTNU. Embryonic primary rat cortical astrocytes were purchased (Gibco™, Cat# N7745–100), stored at − 80 degrees and thawed and plated as recommended by the manufacturer (Invitrogen, Cat #MAN0001679). Astrocytes at passage 2 or 3 was used in our experiments.

2.1.1. APP/PS1 mouse model and genotyping

The APP/PS1 mouse model is a transgenic familial AD-model, with a C57BL/6 J genetic background, co-expressing mutated human amyloid precursor protein (KM670/671NL) and mutated human presenilin 1 (L166). In the model, both mutated proteins are driven by expression cassettes under the Thy1 promoter, which causes accumulation of Aβ with extracellular cortical deposits appearing from around 6 weeks of age (Radde et al., 2006) and cognitive deficits with suppressed spatial

Table 1
Composition of solutions.

Dissection medium (HABG)a	Cell medium (growth medium)	Laminin solution
Hibernate™-A Medium2% B27™ Plus Supplement 0.5 mM GlutaMAX™ Supplement (2 mL/L) 1% Penicillin-Streptomycin	Neurobasal Plus Medium 2% B27™ Plus Supplement 0.5 mM GlutaMAX™ Supplement (2 mL/L) 10% Fetal Bovine Serum 1% Penicillin-Streptomycin 1:1000 RHO/ROCK pathway inhibitor 1:1000 BDNF Human Recombinant	L15 medium 2.5% Sodium Bicarbonate1,66% Mouse laminin **Astrocyte medium** * * 85% DMEM (high glucose) 15% Fetal Bovine Serum 1% Penicillin-Streptomycin

^a Same media used for dissection and centrifugation of neurons. * *Media recommended by the manufacturer of rat primary cortical astrocytes (Gibco™, #N7745–100). Source and catalogue number of all supplements can be found in Table 2.

learning and memory are observed by 7 months (Serneels et al., 2009). The animals used in our experiments were genotyped for expression of the transgene by quantitative PCR (qPCR) using the KAPA Mouse genotyping kit (Merck, Cat# MGKITKB-KK7301), with primer sequence (5'−3') APP-F (GATTCCGACATGACTCAGG) and APP-R (CTTCTGCTGCATCTTGGACA).

2.2. Preparation of culture plates, coating, and seeding of astrocytic monolayer

Table 1 lists all compositions of solutions and Table 2 lists all media components used for the dissection and culture. For electrophysiological recordings we used microelectrode arrays (MEAs; 60EcoMEA-Glass-gr, Multichannel Systems, MCS, Reutlingen, Germany), while for immunocytochemistry (ICC) we used 13 mm round coverslips (WVR, Cat #630–2118) in a 24-well plate (VWR, Cat #10062–896). Additionally, ICC was done on one MEA. Cleaning, sterilization, and impedance measurement of the MEAs was done as recommended by the manufacturer (Microelectrode Array (MEA) Manual). The culture surfaces (MEAs and glass coverslips) were first coated with 400 µL Poly-L-Ornithine (PLO; Sigma-Aldrich, Cat# P3655–50 mg) in an incubator at 37 °C with 5% CO_2 for 2 h. Subsequently, all PLO was discarded, and the surface was rinsed gently three times with sterile Milli-Q-water before we added 400 µL laminin solution (See Table 1). We then incubated the culture vessels at 37 °C with 5% CO_2 for 2 h. The laminin solution was then discarded, and 200 µL fresh pre-warmed astrocyte media (see Table 1) was incubated in the culture plates at 37 °C with 5% CO_2 for ~10 min, before plating ~1.500 embryonic Rat Primary Cortical Astrocytes (Gibco™, Cat# N7745–100) per culture well. The astrocytes were plated 24–48 h prior to plating lLEC-LII neurons. Through extensive pilot experimentation, we concluded that a monolayer of astrocytes is crucial for the attachment and viability of adult lLEC-LII-neurons, and a complete lack of neuronal attachment resulted when astrocytes were plated either simultaneously or following that of the neurons.

2.3. Dissection of brain tissue

Table 2 lists all media components used for the dissection and culture. All tools were sterilized by autoclaving before use. Mice were deeply anesthetized using isoflurane gas (Abbott Lab, Cat# 05260–05) and then decapitated using surgical scissors (FST, Cat# 14007–14). Subsequently, the head was quickly immersed in 70% ethanol followed by sterile phosphate buffered saline (Thermo Fischer Scientific, Cat# 14040–117), before being submersed in ice cold Hanks Balanced Salt Solution (HBSS; Thermo Fischer Scientific, Cat# 88284) in a sterilized glass dish resting on ice. While fully submerged, we cut and peeled away the scalp, and then used fine scissors (FST, Cat# 14568–09) to open the

Table 2
Reagents, equipment, materials, and antibodies.

Reagents	
Accutase Cell Dissociation Medium	(Thermo Fischer Scientific, Cat# A1110501)
AGAR	(VWR; Cat# 20767.298)
Anti-Fade Fluorescence Mounting Medium – Aqueous,	(Abcam, Cat# ab104135)
B-27™ Plus Supplement	(Gibco™, Cat# A3582801)
Brain derived neurotrophic factor [BDNF Human Recombinant]	(Neurotrophins, Cat# 450-02)
Dulbecco's Phosphate Buffered Saline	(Thermo Fischer Scientific, Cat# 14040-117)
DMEM (high glucose)	(Gibco™, Cat# 11995065)
Fetal Bovine Serum (FBS)	(Sigma-Aldrich, Cat# 12106C-100ML)
GlutaMAX™ Supplement	(Gibco™, Cat# 35050061)
Goat Serum	(Sigma-Aldrich, Cat# G9023)
Hanks Balanced Salt Solution (HBSS)	(Thermo Fischer Scientific, Cat# 88284)
Hibernate™-A Medium	(Thermo Fischer Scientific, Cat# A1247501)
Hoechst 33342 Trihydrochloride	(Sigma-Aldrich, Cat# 14533)
Isoflurane	(Abbott Lab, Cat# 05260-05)
Laminin Mouse Protein, Natural	(Thermo Fischer Scientific, Cat# 23017015)
L15 Medium	(Sigma-Aldrich, Cat# L5520)
Neurobasal Plus Medium	(Gibco™, Cat# A3582901)
Neuronal isolation enzyme Papain	(Thermo Fischer Scientific, Cat# 88285)
Paraformaldehyde	(Sigma-Aldrich, Cat# P6148)
Penicillin Streptomycin (PS)	(Gibco™, Cat# 15070063)
Poly-L-Ornithine (PLO)	(Sigma-Aldrich, Cat# P3655-50mg)
Rat Primary Cortical Astrocytes	(Gibco™, Cat# N7745-100)
Sodium Bicarbonate	(Sigma Aldrich, Cat# S5761)
StemPro™ Accutase™ Cell Dissociation Enzyme	(Gibco™, Cat #A1110501)
Trypan Blue Stain	(Sigma-Aldrich, Cat# T10282)
Y-27632 (Dihydrochloride) RHO/ROCK pathway inhibitor (RI)	(STEMCELL™ Technologies, Cat# 72302)

Equipment and materials	
BrandTech Accu-jet pro Pipette Controller	(BrandTech Scientific, Cat# 26330)
Corning 24 well plates	(VWR, Cat #10062-896)
Countess II Automated cell counter	(Thermo Fischer, Cat #AMQAX1000)
Round Glass Coverslips	(VWR, Cat #630-2118)
EVOS M5000 Imaging System	(Thermo Fischer Scientific, Cat #AMF5000)
Falcon tube (15 mL)	(Merck, Cat #CLS430791)
Surgical Scissors	(FST, Cat# 14007-14)
Fine Scissors	(FST, Cat# 14568-09)
RSG Solingen Spatulae	(VWR, Cat# 231-2262)
S&T Forceps	(FST, Cat# 00108-11)
Stereoscope	(SteREO Discovery V8; Zeiss)
Vannas Spring Scissors	(FST, Cat# 15018-10)
Vibrating blade microtome	(Leica Biosystems, Cat# 14047235613)

Primary and secondary antibodies	
Anti-Reelin Antibody (1:1000)	(Abcam, Cat #ab78540)
Anti-NeuN Antibody (1:1000)	(Sigma-Aldrich, Cat# ABN90P)
Oligomer A11 Polyclonal Antibody (1:1000)	(Invitrogen, Cat# AHB0052)
Alexa Fluor™ 488 Goat-anti-Mouse IgG	(Thermo Fischer Scientific, Cat #A-11001)
Alexa Fluor™ 546 Goat-anti-Guinea Pig IgG	(Thermo Fischer Scientific, Cat #A-11074)
Alexa Fluor™ 647 Goat-anti-Rabbit IgG	(Thermo Fischer Scientific, Cat #A32733)

skull along the midline, before prying each resulting half of the skull aside using the same scissors along with a pair of S&T forceps (FST, Cat# 00108–11), thus exposing the brain. A spatula (RSG Solingen, Cat# 231-2262) served to sever the cranial nerves, allowing us to gently lift out the brain and transfer it to a sterile cup containing ice cold HBSS.
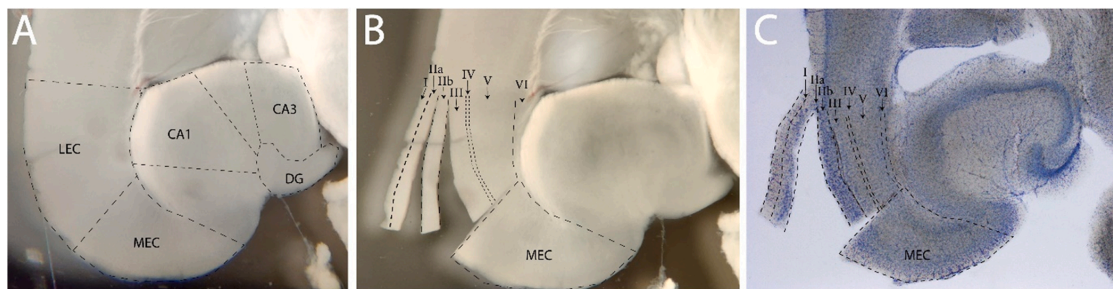
Fig. 2. Dissecting lLEC-LII-neurons. **(A)** Horizontal brain section cut at 300 μm. Salient neuroanatomical features are recognizable when viewed in a stereoscope under cross-polarized light, using optic lamps. **(B)** Same brain section as in (A) with tissue delineated (dashed lines) and LEC layers IIa and IIb cut and slightly spread apart. **(C)** Same brain section as in (A-B) stained with Cresyl Violet. Note that layer IIb has now been pushed against LIII, such that only LIIa points out towards the left side. Furthermore, due to drying and coverslipping, the section is shrunk and flattened, and the delineations are adjusted accordingly. Abbreviations: LEC, lateral entorhinal cortex; MEC, medial entorhinal cortex; DG, dentate gyrus; CA3, cornu ammonis 3; CA1, cornu ammonis 1.

Immediately before mounting the brain, we took it out of the HBSS in order to slice off the cerebellum plus ~300 μm of the brains' dorsal surface, which gave us a flat surface for better attachment. Subsequently, that (dorsal) surface of the brain was glued to the specimen disc using Loctite 401 superglue (Henkel-Adhesives). Abutting the caudal end of the brain we glued on a supportive barrier of freshly made AGAR 0.02 g/mL (VWR; Cat# 20767.298) for structural support vis a vis the direction traversed by the blade. The specimen disc containing the brain and the supportive AGAR was then submerged into the vibratome container (Leica Biosystems, Cat# 14047235613) containing ice cold HBSS. We sectioned in the rostral-to-caudal direction at a thickness of 300 μm, setting the blade at a frequency of 5.3 Hz with a speed of 8 mm/s. By using sterilized plastic pipettes cut to shape, each section was transferred to separate wells in a sterile 24-well plate resting on ice, containing a solution of Hibernate-A medium, 2% B27 Plus Supplement, and 2.5 mM/mL GlutaMAX Supplement (HABG; (Brewer et al., 2007)), in addition to 1% penicillin streptomycin (Gibco™, Cat# 15070063). A sterile glass petri dish, placed up-side-down on top of a pool of ice at the stage of a stereoscope (SteREO Discovery V8; Zeiss), served as our dissection platform. One-by-one we then transferred each section from the 24-well plate onto the surface of the petri dish, which viewed under the stereoscope using cross polarized optic fibre lights, allows for sufficient contrast to recognize anatomical landmarks. We then dissected lLEC-LII as detailed in the subsequent section.

2.3.1. Dissecting entorhinal cortex layer II-neurons from the lateral domain

EC is a six-layered periallocortex. Rodent EC contains two major cytoarchitectonic subdivisions that are anchored to specific connectivity patterns, known as the medial entorhinal cortex (MEC) and the lateral entorhinal cortex (LEC) (Insausti et al., 1997). For reasons explained in the introduction, we specifically targeted the *lateralmost part of LEC layer II* (lLEC-LII), i.e., the part close to the rhinal fissure, by taking advantage of a set of characteristics that are recognizable on fresh sections when viewed under a stereoscope and illuminated by cross polarized light. Thus, we separated LEC from MEC by identifying and tracing the characteristic layer V neurons of MEC, which align to give the appearance of radial columns, a feature that abruptly disappears to mark the medial border of LEC. We then deliberately placed our initial cut a distance away from this border to ensure targeting of lLEC-LII. On the other side, literally, as one moves into the most lateral domain of LEC, big fan and pyramidal neurons locate superficially in LII (sometimes referred to as layer IIa; these neurons stain positive for reelin). These LII-neurons are separated from a more deeply situated layer of pyramidal neurons (IIb, calbindin-positive) by a cell-free zone that is only present towards the lateral extreme. This feature, together with the notably smaller superficial neurons residing in the perirhinal- and postrhinal cortices, which

form the anterior and dorsal borders of LEC, is sufficient to reliably delineate and dissect lLEC-LII-neurons (Kobro-Flatmoen et al., 2019). We cut strips of lLEC-LII-tissue using Vannas Spring scissors (FST, Cat #15018–10), immediately transferred the strips to 15 mL polypropylene Falcon tubes (Merck, Cat #CLS430791) containing HABG (Table 1), and immersed these tubes in crushed ice. To safeguard our ability to target the region of interest, we used sections from one mouse and mounted and stained these sections using cresyl violet (Fig. 2). This, along with immunocytochemistry (ICC; see Section 2.5), confirmed our ability to consistently target and extract lLEC-LII-neurons.

2.4. Processing and culturing of lLEC-LII-neurons

To remove potential debris from the dissection, we discarded HABG from the 15 mL Falcon tubes and rinsed the tissue strips by adding and removing 3 mL cold Hibernate-A medium three times, letting the tube rest in ice for 20 s in between each rinse. We then transferred the tissue into a sterile 1.5 mL Eppendorf tube containing 250 μL Neuronal Isolation Enzyme Papain (Thermo Fischer Scientific, Cat# 88285; reconstituted as described by manufacturer (Thermo Fischer Scientific, #MAN0011896)) and incubated the tissue in a standard humified incubator (37 °C, 5% CO_2, 20% O^2) for 15 min. Subsequently, we discarded the isolation enzyme papain and added 100 μL pre-warmed HABG and manually triturated the tissue by running it through a 100 μL pipette ten times for a total duration of about 45 s. The resulting cell suspension was transferred to a 15 mL Falcon tube containing 2.9 mL pre-warmed (37 °C) HABG, to give a total of 3 mL, and then centrifuged at 200x g for 2 min at 21 °C (room temperature). Subsequently, we discarded all HABG, added 100 μL cell media (see Table 1), and completed the dissociation by again triturating the tissue by running it through a 100 μL pipette ten times, while taking care to ensure no air bubbles reached the pipette. A cell count was performed using a Countess™ Automated cell counter (Thermo Fischer, Cat #AMQAX1000). For each separate culture (MEAs or 24-well plates) we used neurons from two animals, which gave between 140,000 and 170,000 cells/1.9 cm^2. The neurons (cell suspension) were plated in 100 μL cell media and incubated for 2 h, then 800 μL of fresh pre-warmed (37 °C) cell media was added to give a total of 1 mL cell media. The cultures were incubated for 24 h at 37 °C (5% CO_2, 20% O^2). Then, 50% of the cell media was replaced with fresh pre-warmed (37 °C) cell media. In cases of excess debris in the cultures 24 h after plating, we carried out extra rinses by aspirating 90% of the media, and then tilted the cultures slightly while slowly adding 500 μL cell media such that the culture was gently flushed, before we added new media.

We supplemented the cultures every third day by aspirating half the cell media and replenishing it with fresh, pre-warmed media (37 °C);
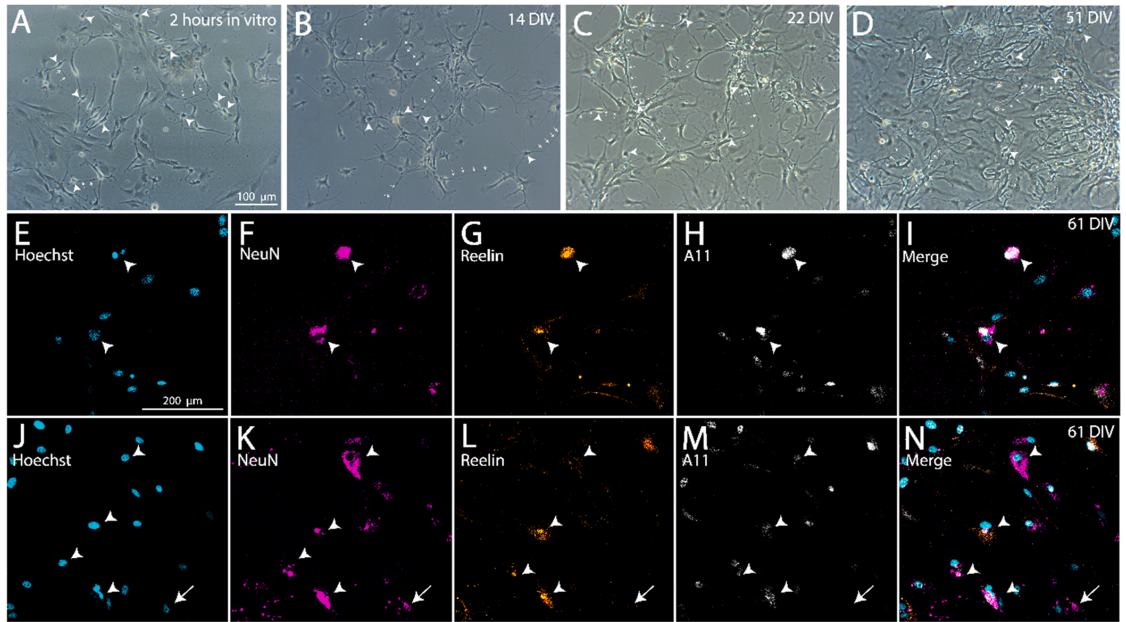
Fig. 3. Adult dissected lLEC-LII-neurons self-organize in culture and express selective markers. **(A-D)** Phase-contrast images of lLEC-LII-neurons from the same culture at 2 h (A), 14 days (B), 22 days (C), 51 days (D) in vitro. Arrowheads indicate neuronal somata, based on their round morphological shape and their situation on top of an astrocytic monolayer. Smaller arrows indicate neurites. Scalebar in A applies for A-D. **(E-N)** Immunocytochemical labeling of the same culture at 61 days in vitro. Immunolabels include DNA-marker Hoechst (E, J; cyan), neuronal marker NeuN (F, K; magenta), reelin (G, L; orange) and oligomeric Aβ A11 (H, M; grey). Overlay of (E-H and J-M) is shown in (I and N), respectively; arrowheads indicate reelin-expressing neurons that co-expresses oligomeric Aβ. Arrow in J-N indicating a neuron expressing NeuN, but negative for reelin and A11. Scale bar in E applies for E-N.

this frequency of media changes was determined to be optimal by extensive experimentation (Supplementary fig. A.1). Degenerating and dying neurons were readily identifiable by observing their retracting neurites and detaching cell bodies. On the days of electrophysiological recordings, media changes were made after the recording was completed. Imaging and media changes were done within a time window of < 3 min, as longer time periods outside the incubator will affect the cultures' pH levels and induce cytotoxicity.

2.5. Immunocytochemistry (ICC) and imaging

ICC was carried out as follows. We aspirated all media from the cultures before adding 500 µL Dulbecco's Phosphate Buffered Saline (DPBS; Thermo Fischer Scientific, Cat# 14040–117) to clear away debris. Then we fixed the cultures for 15 min by applying a solution of purified and deionized water containing 0.4 Molar phosphate buffer and 4% freshly depolymerized paraformaldehyde (PFA; Sigma-Aldrich, Cat# P6148) followed by 10 × 3 min rinses in DPBS. To block unspecific antigens, we incubated the cultures in a solution of DPBS containing 3% goat serum and 0.1% Triton-X, for 1 h at room temperature. The cultures were then incubated overnight with primary antibodies (see Table 2) in a solution of DPBS containing 1% goat serum, on a shaker at 4 °C. Then the cultures were rinsed three times in DPBS, immediately before incubation in DPBS containing secondary antibodies at room temperature for 2 h (see Table 2). Hoechst dye (1:10.000; Sigma-Aldrich, Cat# 14533) was added for the last 10 min of the secondary antibody incubation time. To identify Re+ lLEC-LII-neurons in vitro, we chose antibodies against neuronal somata marker and reelin. As the APP/PS1 animals express Aβ accumulation by 6 weeks (Radde et al., 2006) we also stained for Aβ prefibrils (Kayed et al., 2003) to determine whether the Re+ lLEC-LII-neurons express Aβ prefibrils in

vitro, as is known to be the case in vivo (Kobro-Flatmoen et al., 2022). Primary antibody exclusion was done for all three antibodies (Re+, NeuN and A11), resulting in a complete absence of signal. Images were acquired with an EVOS M5000 microscope connected to a LED light source and using an Olympus 20x/0.75 NA objective (N1480500), with the following filter sets/channels: DAPI (AMEP4650), CY5 (AMEP4656), GFP (AMEP4651) and TxRed (AMEP4655). For image processing we used Zen 2.6 (blue edition), along with contrast adjustments in Adobe Photoshop 2020. To quantify overlap between A11, NeuN and reelin, we took images of each immunolabel/each channel, from five different regions in one culture. We then applied a threshold to identify neuronal somata using Fiji (version 1.53i), and then overlaid the channels in order to count the degree of overlap.

2.6. Electrophysiological recordings

We recorded electrophysiological activity from two cultures on MEAs using a Multichannel MEA2100 recording system (Multichannel Systems, MCS, Reutlingen, Germany). The stage temperature was set to 37 °C, which minimizes thermal stress, and we used EcoMEAs covered with a MEA-MEM-Ring (Multichannel Systems, MCS, Reutlingen, Germany) to avoid contaminants and media evaporation. After removal from the incubator, the cultures were left to rest for ~3 min on the stage before spontaneous electrophysiological activity was recorded for 10-minute epochs. This recording time was chosen as our system does not maintain stable CO2-levels, such that time out of the incubator will affect pH levels and thus cell-viability (Lloyd & Williams, 2015). Data sampling was collected at a rate of 10 kHz/channel. We converted raw data to an .h5 Hierarchical Data Format file using the Multichannel DataManager (V.1.14.4.22018) system and imported it to MatLAB2020a for analyses. Spontaneous neuronal network activity was thus recorded
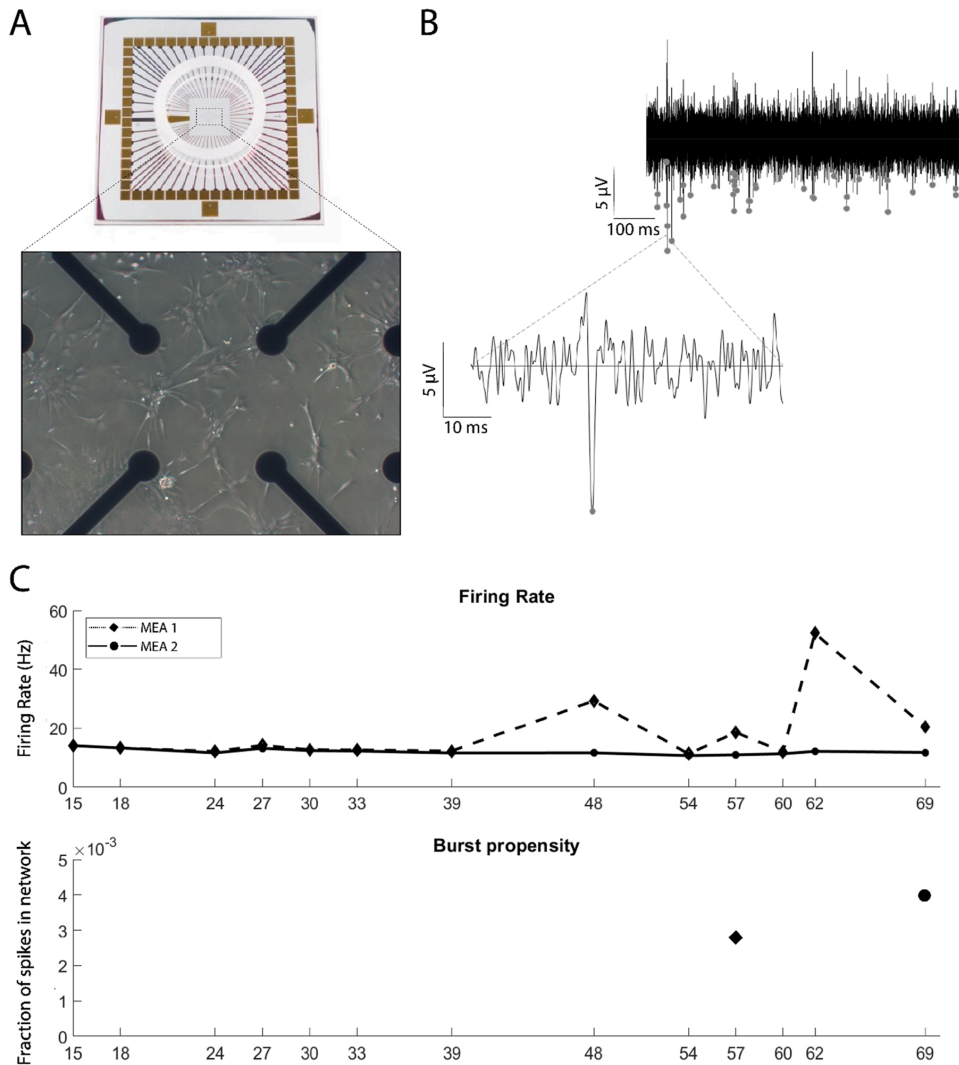
Fig. 4. Cultured adult lLEC-LII-neurons develop sustained electrophysiological activity. **(A)** lLEC-LII-neuronal network at 24 DIV on an MEA. **(B)** Spike train (top) from one electrode with detected spikes indicated as grey dots. Inset (bottom) shows the waveform of an example spike. From recording at 33 DIV. **(C)** Firing rate (Hz) and burst propensity of the network from 15 DIV to 69 DIV. A single burst was detected for each culture as indicated (for MEA1 at 57 DIV; for MEA2 at 69 DIV). Abbreviations: lLEC-LII, lateralmost lateral entorhinal cortex layer II; DIV, days in vitro.

at the following timepoints (DIV): 15, 18, 24, 27, 30, 33, 39, 48, 54, 57, 60, 62 and 69 (n = 2; MEA 1 and MEA 2).

2.7. Data analysis

For spike detection we used the Precise Timing Spike Detection (PTSD) algorithm developed by (Maccione et al., 2009). To reduce artifacts from the raw data we used a fourth order Butterworth-filter with a high pass cutoff frequency at 300 Hz and a low pass cutoff frequency at 3000 Hz. We additionally used a Notch filter to exclude electrical noise at 50 Hz from the mains hum. A signal was defined and recorded as a spike when reaching beyond a differential threshold of 7.5 times the standard deviation of the background activity. Firing rate and burst propensity (a measure of fraction of spikes in networks bursts) were

analysed using an in-house made MATLAB script, reported previously (Fiskum et al., 2021). A network burst was identified when a binned spike distribution of 50 ms bins exceeded a threshold of firing rate of 7.5 standard deviations and more than 20% of all active electrodes in the recording fired.

3. Results

3.1. Dissection and culturing of lLEC-LII-neurons

Our procedure to dissect and culture adult lLEC-LII-neurons is outlined in Fig. 1. Each culture consisted of cells from two animals, and, at the time of plating, contained from 140,000 to 170,000 cells as estimated by a Countess II Automated cell counter (Thermo Fischer, Cat

#AMQAX1000). Putative neurons attached and began extending neurites already by 2 h in vitro (Fig. 3A; Supplementary Fig. A.3A). By 14 DIV, we observed a pronounced growth of neurites, and many of these had already formed structural networks (Fig. 3 B-D). Highly branched neurites were still present by 51 DIV (Supplementary Fig. A.3B). Such networks remained viable beyond two months, at which point we terminated the cultures to establish cell-identities by way of ICC (Fig. 3E-N). We found our cultures to be rich in cells that stained double-positive for NeuN and reelin, providing strong support that we in fact successfully acquired Re+ lLEC-LII-neurons (Fig. 3; Supplementary Fig. A.2). We furthermore found that the Re+ neurons co-expressed oligomeric Aβ (Fig. 3E-N), in line with the known strong intracellular expression of Aβ in such neurons (Kobro-Flatmoen et al., 2016). By quantifying the immunolabeling in five different regions of one culture, we found that out of 88 neurons (NeuN-positive), 84 were positive for reelin and A11, while two were negative for reelin and A11, and two were negative for reelin but positive for A11.

3.2. Cultured lLEC-LII-neurons demonstrate spontaneous, sustained electrophysiological activity

An example of an MEA and its recording electrodes is shown in Fig. 4A. Both lLEC-LII-neuron networks (MEA1 and MEA2) displayed spontaneous neuronal activity by 15 DIV, lasting until we terminated the cultures at 69 DIV (Fig. 4B). Their firing rate remained low throughout the whole recording period, and burst propensity was absent until about two months, when both networks showed a single burst (Fig. 4C).

4. Discussion

To enable culturing of neurons and networks more relevant for the initiating stages of AD, we used adult APP/PS1 mice and dissected tissue from the lateralmost domain of LEC, aiming for the Re+ lLEC-LII-neurons. Once dissociated and plated, neurons self-organized into networks within two weeks and remained viable beyond two months (Fig. 3; Supplementary Fig. A.2). We confirmed our ability to obtain the superficially situated Re+ lLEC-LII-neurons by double-immunolabeling against NeuN and reelin, from which we observed several double-positive neurons (Fig. 3; Supplementary Fig. A.2). A further observation was that reelin expression co-localizes with that of Aβ, indicating that the tendency of such neurons to express Aβ (Kobro-Flatmoen et al., 2022, 2016) is retained when they are cultured (Fig. 3). In line with previous findings, an astrocytic feeder layer was crucial for survival and optimal growth of our cultured Re+ lLEC-LII-neurons. More specifically, the presence of glial cells supports long term survival of adult primary neuronal cultures (Ray et al., 2009), promote synaptogenesis (Hama et al., 2004), and modulate neuronal excitability (reviewed in (Araque et al., 2004).

By two weeks in culture, our neurons self-organized into networks and began exhibiting spontaneous spiking activity (Fig. 4). The network complexity continued to increase over time, and the spontaneous spiking activity persisted for the entire culture period, consisting exclusively of very low burst propensity. This activity type may be a generic feature of adult cultured neurons, as previous studies reported that, in contrast to embryonic neuron cultures, adult neuron cultures tend to have non-repetitive firing patterns, rather exhibiting single-spike events (Evans et al., 1998; Varghese et al., 2009). Another possibility is that the low burst propensity we observe in our cultured lLEC-LII-neurons is, at least in part, a result of the inherent biology of these neurons. Whole-cell current clamp experiments of lLEC-LII-neurons revealed that they tend to fire late and with few spikes upon small depolarizing current-steps, and that a large depolarizing current-step is required to elicit a burst (Nilssen et al., 2018). The timing of media change relative to the time of recording is also likely to affect network activity. For example, human motor neurons were found to have a higher firing frequency 24 h after media change compared to

48 h after media change (Fiskum et al., 2021). The fact that we recorded activity 72 h after media change may thus contribute to the very low burst propensity exhibited in our networks. An additional consideration is the fact that our lLEC-LII-neurons express increased amounts of amyloid-β. Whether and how this affects lLEC-LII-neurons was beyond the scope of this study and should be addressed in future work.

Aside from the relevance of Re+ lLEC-LII-neurons in the onset of AD, it is likely that culturing of *adult* neurons offers a more relevant model for the disease, because it removes potential confounds owing to developmental factors operating in embryonic or early postnatal neurons. The ability to extract and move Re+ lLEC-LII-neurons into an in vitro setting furthermore enables direct monitoring of their network properties and offers ease of access with respect to chemogenetic (Bauer et al., 2022; Westhaus et al., 2020), molecular, (Valderhaug et al., 2021) and pharmacological tools (Han et al., 2017). Our approach may thus represent a valuable tool for studying very early proteinopathy and offers neuron- and network specific modelling of initiating AD pathology in vitro.

CRediT authorship contribution statement

Katrine Sjaastad Hanssen: Methodology, Investigation, Formal analysis, Writing – original draft. **Axel Sandvig:** Resources, Writing – review & editing. **Menno P. Witter:** Resources, Writing – review & editing, Funding acquisition. **Ioanna Sandvig:** Resources, Conceptualization, Methodology, Data curation, Supervision, Funding acquisition, Writing – review & editing. **Asgeir Kobro-Flatmoen:** Conceptualization, Funding acquisition, Project administration, Supervision, Resources, Methodology, Data curation, Writing – review & editing.

Data Availability

Data will be made available on request.

Appendix A. Supporting information

Supplementary data associated with this article can be found in the online version at doi:10.1016/j.jneumeth.2023.109840.

References

Araque, A., Perea, G., 2004. Glial modulation of synaptic transmission in culture. Glia 47 (3), 241–248. https://doi.org/10.1002/glia.20026.

Bauer, U.S., Fiskum, V., Nair, R.R., van de Wijdeven, R., Kentros, C., Sandvig, I., Sandvig, A., 2022. Validation of functional connectivity of engineered neuromuscular junction with recombinant monosynaptic pseudotyped ΔG-Rabies Virus Tracing. Front Integr. Neurosci. 16, 855071 https://doi.org/10.3389/fnint.2022.855071.

Belle, A.M., Enright, H.A., Sales, A.P., Kulp, K., Osburn, J., Kuhn, E.A., Wheeler, E.K., 2018. Evaluation of in vitro neuronal platforms as surrogates for in vivo whole brain systems. Sci. Rep. 8 (1), 10820. https://doi.org/10.1038/s41598-018-28950-5.

Berron, D., Vogel, J.W., Insel, P.S., Pereira, J.B., Xie, L., Wisse, L.E.M., Hansson, O., 2021. Early stages of tau pathology and its associations with functional connectivity, atrophy and memory. Brain 144 (9), 2771–2783. https://doi.org/10.1093/brain/awab114.

Braak, H., Braak, E., 1991. Neuropathological stageing of Alzheimer-related changes. Acta Neuropathol. 82 (4), 239–259. https://doi.org/10.1007/bf00308809.

Brewer, G.J., 1997. Isolation and culture of adult rat hippocampal neurons. J. Neurosci. Methods 71 (2), 143–155. https://doi.org/10.1016/s0165-0270(96)00136-7.

Brewer, G.J., Torricelli, J.R., 2007. Isolation and culture of adult neurons and neurospheres. Nat. Protoc. 2 (6), 1490–1498. https://doi.org/10.1038/nprot.2007.207.

Brewer, G.J., Herrera, R.A., Philipp, S., Sosna, J., Reyes-Ruiz, J.M., Glabe, C.G., 2020. Age-related intraneuronal aggregation of amyloid-β in endosomes, mitochondria, autophagosomes, and lysosomes. J. Alzheimers Dis. 73 (1), 229–246. https://doi.org/10.3233/jad-190835.

Calvo-Rodríguez, M., de la Fuente, C., García-Durillo, M., García-Rodríguez, C., Villalobos, C., Núñez, L., 2017. Aging and amyloid β oligomers enhance TLR4 expression, LPS-induced Ca(2+) responses, and neuron cell death in cultured rat hippocampal neurons. J. Neuroinflamm. 14 (1), 24. https://doi.org/10.1186/s12974-017-0802-0.

Donato, F., Jacobsen, R.I., Moser, M.B., Moser, E.I., 2017. Stellate cells drive maturation of the entorhinal-hippocampal circuit. Science 355 (6330). https://doi.org/10.1126/science.aai8178.

Dong, Y., Brewer, G.J., 2019. Global Metabolic Shifts in Age and Alzheimer's Disease Mouse Brains Pivot at NAD+/NADH Redox Sites. J. Alzheimers Dis. 71 (1), 119–140. https://doi.org/10.3233/jad-190408.

Dong, Y., Digman, M.A., Brewer, G.J., 2019. Age- and AD-related redox state of NADH in subcellular compartments by fluorescence lifetime imaging microscopy. Geroscience 41 (1), 51–67. https://doi.org/10.1007/s11357-019-00052-8.

Dong, Y., Sameni, S., Digman, M.A., Brewer, G.J., 2019. Reversibility of age-related oxidized free NADH redox states in Alzheimer's Disease neurons by imposed external Cys/CysS redox shifts. Sci. Rep. 9 (1), 11274. https://doi.org/10.1038/s41598-019-47582-x.

Eide, L., McMurray, C.T., 2005. Culture of adult mouse neurons. Biotechniques 38 (1), 99–104. https://doi.org/10.2144/05381rr02.

Evans, M.S., Collings, M.A., Brewer, G.J., 1998. Electrophysiology of embryonic, adult and aged rat hippocampal neurons in serum-free culture. J. Neurosci. Methods 79 (1), 37–46. https://doi.org/10.1016/s0165-0270(97)00159-3.

Fiskum, V., Sandvig, A., Sandvig, I., 2021. Silencing of activity during hypoxia improves functional outcomes in motor neuron networks in vitro. Front Integr. Neurosci. 15, 792863 https://doi.org/10.3389/fnint.2021.792863.

Gomez-Isla, T., Price, J.L., McKeel Jr., D.W., Morris, J.C., Growdon, J.H., Hyman, B.T., 1996. Profound loss of layer II entorhinal cortex neurons occurs in very mild Alzheimer's disease. J. Neurosci. 16 (14), 4491–4500.

Hama, H., Hara, C., Yamaguchi, K., Miyawaki, A., 2004. PKC signaling mediates global enhancement of excitatory synaptogenesis in neurons triggered by local contact with astrocytes. Neuron 41 (3), 405–415. https://doi.org/10.1016/s0896-6273(04)00007-8.

Han, Y., Li, H., Lang, Y., Zhao, Y., Sun, H., Zhang, P., Wang, C., 2017. The effects of acute GABA treatment on the functional connectivity and network topology of cortical cultures. Neurochem Res 42 (5), 1394–1402. https://doi.org/10.1007/s11064-017-2190-3.

Holbrook, A.J., Tustison, N.J., Marquez, F., Roberts, J., Yassa, M.A., Gillen, D.L., 2020. Anterolateral entorhinal cortex thickness as a new biomarker for early detection of Alzheimer's disease. Alzheimers Dement. 12 (1), e12068 https://doi.org/10.1002/dad2.12068.

Insausti, R., Herrero, M.T., Witter, M.P., 1997. Entorhinal cortex of the rat: cytoarchitectonic subdivisions and the origin and distribution of cortical efferents. Hippocampus 7 (2), 146–183. https://doi.org/10.1002/(sici)1098-1063(1997)7:2<146::Aid-hipo4>3.0.Co;2-l.

Kaech, S., Banker, G., 2006. Culturing hippocampal neurons. Nat. Protoc. 1 (5), 2406–2415. https://doi.org/10.1038/nprot.2006.356.

Kayed, R., Head, E., Thompson, J.L., McIntire, T.M., Milton, S.C., Cotman, C.W., Glabe, C.G., 2003. Common structure of soluble amyloid oligomers implies common mechanism of pathogenesis. Science 300 (5618), 486–489. https://doi.org/10.1126/science.1079469.

Kobro-Flatmoen, A., Witter, M.P., 2019. Neuronal chemo-architecture of the entorhinal cortex: a comparative review. Eur. J. Neurosci. 50 (10), 3627–3662. https://doi.org/10.1111/ejn.14511.

Kobro-Flatmoen, A., Nagelhus, A., Witter, M.P., 2016. Reelin-immunoreactive neurons in entorhinal cortex layer II selectively express intracellular amyloid in early Alzheimer's disease. Neurobiol. Dis. 93, 172–183. https://doi.org/10.1016/j.nbd.2016.05.012.

Kobro-Flatmoen, A., Battistin, C., Raveendran, R.N., Bjorkli, C., Skender, B., Kentros, C., Witter, M.P., 2022. Lowering levels of reelin in entorhinal cortex layer II-neurons results in lowered levels of intracellular amyloid-β. bioRxiv 1–34. https://doi.org/10.1101/2022.01.28.478143.

Konings, S.C., Torres-Garcia, L., Martinsson, I., Gouras, G.K., 2021. Astrocytic and neuronal apolipoprotein E isoforms differentially affect neuronal excitability. Front Neurosci. 15, 734001 https://doi.org/10.3389/fnins.2021.734001.

Kordower, J.H., Chu, Y., Stebbins, G.T., DeKosky, S.T., Cochran, E.J., Bennett, D., Mufson, E.J., 2001. Loss and atrophy of layer II entorhinal cortex neurons in elderly people with mild cognitive impairment. Ann. Neurol. 49 (2), 202–213.

Kulason, S., Tward, D.J., Brown, T., Sicat, C.S., Liu, C.F., Ratnanather, J.T., Miller, M.I., 2019. Cortical thickness atrophy in the transentorhinal cortex in mild cognitive impairment. Neuroimage Clin. 21, 101617 https://doi.org/10.1016/j.nicl.2018.101617.

Lloyd, D., Williams, C.F., 2015. Avoid excessive oxygen levels in experiments with organisms, tissues and cells. Adv. Micro Physiol. 67, 293–314. https://doi.org/10.1016/bs.ampbs.2015.09.001.

Maccione, A., Gandolfo, M., Massobrio, P., Novellino, A., Martinoia, S., Chiappalone, M., 2009. A novel algorithm for precise identification of spikes in extracellularly recorded neuronal signals. J. Neurosci. Methods 177 (1), 241–249. https://doi.org/10.1016/j.jneumeth.2008.09.026.

Marcantoni, A., Raymond, E.F., Carbone, E., Marie, H., 2014. Firing properties of entorhinal cortex neurons and early alterations in an Alzheimer's disease transgenic model. Pflug. Arch. 466 (7), 1437–1450. https://doi.org/10.1007/s00424-013-1368-z.

Nilssen, E.S., Jacobsen, B., Fjeld, G., Nair, R.R., Blankvoort, S., Kentros, C., Witter, M.P., 2018. Inhibitory connectivity dominates the fan cell network in layer II of lateral entorhinal cortex. J. Neurosci. 38 (45), 9712–9727. https://doi.org/10.1523/jneurosci.1290-18.2018.

Olsen, R.K., Yeung, L.K., Noly-Gandon, A., D'Angelo, M.C., Kacollja, A., Smith, V.M., Barense, M.D., 2017. Human anterolateral entorhinal cortex volumes are associated with cognitive decline in aging prior to clinical diagnosis. Neurobiol. Aging 57, 195–205. https://doi.org/10.1016/j.neurobiolaging.2017.04.025.

Percie du Sert, N., Hurst, V., Ahluwalia, A., Alam, S., Avey, M.T., Baker, M., Würbel, H., 2020. The ARRIVE guidelines 2.0: updated guidelines for reporting animal research. PLoS Biol. 18 (7), e3000410 https://doi.org/10.1371/journal.pbio.3000410.

Radde, R., Bolmont, T., Kaeser, S.A., Coomaraswamy, J., Lindau, D., Stoltze, L., Jucker, M., 2006. Abeta42-driven cerebral amyloidosis in transgenic mice reveals early and robust pathology. EMBO Rep. 7 (9), 940–946. https://doi.org/10.1038/sj.embor.7400784.

Ray, B., Bailey, J.A., Sarkar, S., Lahiri, D.K., 2009. Molecular and immunocytochemical characterization of primary neuronal cultures from adult rat brain: Differential expression of neuronal and glial protein markers. J. Neurosci. Methods 184 (2), 294–302. https://doi.org/10.1016/j.jneumeth.2009.08.018.

Roos, T.T., Garcia, M.G., Martinsson, I., Mabrouk, R., Israelsson, B., Deierborg, T., Gouras, G.K., 2021. Neuronal spreading and plaque induction of intracellular Aβ and its disruption of Aβ homeostasis. Acta Neuropathol. 142 (4), 669–687. https://doi.org/10.1007/s00401-021-02345-9.

Sahu, M.P., Nikkilä, O., Lågas, S., Kolehmainen, S., Castrén, E., 2019. Culturing primary neurons from rat hippocampus and cortex. Neuron Signal 3 (2), Ns20180207. https://doi.org/10.1042/ns20180207.

Semple, B.D., Blomgren, K., Gimlin, K., Ferriero, D.M., Noble-Haeusslein, L.J., 2013. Brain development in rodents and humans: identifying benchmarks of maturation and vulnerability to injury across species. Prog. Neurobiol. 106–107, 1–16. https://doi.org/10.1016/j.pneurobio.2013.04.001.

Serneels, L., Van Biervliet, J., Craessaerts, K., Dejaegere, T., Horré, K., Van Houtvin, T., De Strooper, B., 2009. gamma-Secretase heterogeneity in the Aph1 subunit: relevance for Alzheimer's disease. Science 324 (5927), 639–642. https://doi.org/10.1126/science.1171176.

Tran, T.T., Speck, C.L., Gallagher, M., Bakker, A., 2022. Lateral entorhinal cortex dysfunction in amnestic mild cognitive impairment. Neurobiol. Aging 112, 151–160. https://doi.org/10.1016/j.neurobiolaging.2021.12.008.

Trinchese, F., Liu, S., Ninan, I., Puzzo, D., Jacob, J.P., Arancio, O., 2004. Cell cultures from animal models of Alzheimer's disease as a tool for faster screening and testing of drug efficacy. J. Mol. Neurosci. 24 (1), 15–21. https://doi.org/10.1385/jmn:24:1:015.

Tward, D.J., Sicat, C.S., Brown, T., Bakker, A., Gallagher, M., Albert, M., Miller, M., 2017. Entorhinal and transentorhinal atrophy in mild cognitive impairment using longitudinal diffeomorphometry. Alzheimers Dement (Amst.) 9, 41–50. https://doi.org/10.1016/j.dadm.2017.07.005.

Valderhaug, V.D., Heiney, K., Ramstad, O.H., Bråthen, G., Kuan, W.L., Nichele, S., Sandvig, I., 2021. Early functional changes associated with alpha-synuclein proteinopathy in engineered human neural networks. C1141-c1152 Am. J. Physiol. Cell Physiol. 320 (6). https://doi.org/10.1152/ajpcell.00413.2020.

Varghese, K., Das, M., Bhargava, N., Stancescu, M., Molnar, P., Kindy, M.S., Hickman, J. J., 2009. Regeneration and characterization of adult mouse hippocampal neurons in a defined in vitro system. J. Neurosci. Methods 177 (1), 51–59. https://doi.org/10.1016/j.jneumeth.2008.09.022.

Westhaus, A., Cabanes-Creus, M., Rybicki, A., Baltazar, G., Navarro, R.G., Zhu, E., Lisowski, L., 2020. High-throughput in vitro, ex vivo, and in vivo screen of adeno-associated virus vectors based on physical and functional transduction. Hum. Gene Ther. 31 (9–10), 575–589. https://doi.org/10.1089/hum.2019.264.

Paper II

Reverse Engineering of Feedforward Cortical-Hippocampal Neural Networks Relevant for Preclinical Disease Modelling

Katrine Sjaastad Hanssen*[1,2,✉], Nicolai Winter-Hjelm*[1,✉], Salome Nora Niethammer[1,2], Asgeir Kobro-Flatmoen[2,3], Menno P. Witter[2,3], Axel Sandvig[1,4], and Ioanna Sandvig*[1,✉]

[1]Department of Neuromedicine and Movement Science, Faculty of Medicine and Health Sciences, Norwegian University of Science and Technology (NTNU), Norway
[2]Kavli Institute for Systems Neuroscience, Centre for Neural Computation, Egil and Pauline Braathen and Fred Kavli Centre for Cortical Microcircuits, NTNU, Norway
[3]K.G. Jebsen Centre for Alzheimer's Disease, Faculty of Medicine and Health Sciences, NTNU, Norway
[4]Department of Neurology and Clinical Neurophysiology, St Olav´s University Hospital, Trondheim, Norway

Engineered biological neural networks are indispensable tools for investigating neural function in both healthy and diseased states from the subcellular to the network level. Neurons *in vitro* self-organize over time into networks of increasing structural and functional complexity, thus maintaining emergent dynamics of neurons in the brain. While *in vitro* neural network model systems have advanced significantly over the past decade, there is still a need for models able to recapitulate topological and functional organization of brain networks. Especially relevant in this context are interfaces which can support the establishment of multinodal interconnected networks of different neural populations, which at the same time enable control of the direction of connectivity between the nodes. An added required feature of such interfaces is compatibility with electrophysiological techniques and optical imaging tools to facilitate studies of neural network structure-function dynamics. In this study, we applied a custom-designed microfluidic device with Tesla-valve inspired microchannels for structuring multinodal neural networks with controllable feedforward connectivity between rat primary cortical and hippocampal neurons. By interfacing these devices with nanoporous microelectrode arrays, we demonstrate how both spontaneously evoked and stimulation induced activity propagates, as intended, in a feedforward pattern between the different interconnected neural nodes. Moreover, we show that these multinodal networks exhibit functional dynamics suggestive of capacity for both segregated and integrated activity. To advocate the broader applicability of this model system, we also provide proof of concept of long-term culturing of subregion- and layer specific neurons extracted from the entorhinal cortex and hippocampus of adult Alzheimer´s-model mice and rats. We show that these neurons re-form structural connections and develop spontaneous spiking activity after 15 days *in vitro*. Our results thus highlight the suitability and potential of our approach for reverse engineering of biologically and anatomically relevant multinodal neural networks supporting the study of dynamic structure-function relationships in both healthy and pathological conditions.

Advanced modelling | Self-organization | In vitro | Microfluidic Device | Electrophysiology | Cortex | Entorhinal cortex | Hippocampus | Adult neural networks | Alzheimer's model animals |
Correspondence: *katrine.s.hanssen@ntnu.no | nicolai.winter-hjelm@ntnu.no | ioanna.sandvig@ntnu.no*
***These authors share first authorship**

Introduction

Engineered biological neural networks facilitate the study of dynamic properties of network structure and function at the micro- and mesoscale in highly controllable experimental conditions. There is compelling evidence that neurons *in vitro* maintain their inherent self-organizing properties and over time form neural networks with complex structure and function, thus recapitulating fundamental behaviour of brain networks (1–3). As such, engineered neural networks offer an complementary approach to *in vivo* studies for investigations of neural structure and function from the subcellular to the network level. In recent years, several methodological and technological developments have enabled advanced neural network modelling *in vitro* using microfluidic devices to engineer multinodal neural networks (4, 5). However, most studies to date are typically limited to using two-nodal microfluidic devices (6, 7). Thus, the potential of such neuroengineering approaches to recapitulate anatomically relevant network configurations Reis still underutilised. Additionally, the models tend to be limited in terms of their reproducibility, scalability, and adaptability especially in terms of being able to support multi-nodal, directional topological configurations resembling *in vivo* neural assemblies.

A key determinant for establishing anatomically relevant neural network configurations *in vitro* is facilitation and control of multi-nodality. Neural assemblies in the brain are structured into highly specialized functional regions connected through precise afferent-efferent axonal pathways, aiding feedforward and/or feedback signal propagation between pre- and postsynaptic nodes (8). During neural development in the brain, such directional projection sequences are established by finely tuned spatiotemporally regulated molecular and chemical guidance cues regulating axon growth and guidance (9–11). Such gradients are absent in an *in vitro* microenvironment, and alternative approaches are required to facilitate establishment of directional projections between the neural nodes. Several recent studies, including studies from our group, have demonstrated that directional axonal outgrowth between interconnected nodes can be achieved and controlled by embedding geometrical constraints within the microchannel architecture in microfluidic interfaces (12–20). Such models support control of connectivity between multiple neural subpopulations with high precision, rendering them especially interesting in the context of recapitulating anatomically relevant neural networks (21–24). By interfacing such microfluidic devices with microelectrode arrays (MEAs), emerging structure-function dynamics can also be studied electrophysiologically (25). Previous studies suggest that containment of neural networks into modular configurations can promote the development of a broader repertoire of activity dynamics compared to unstructured networks, akin

to complex information processing seen *in vivo* (22). For instance, we and others have shown that structurally coupled neural networks exhibit functional asymmetry, with independently regulated information processing within the interconnected nodes, as well as controlled information flow between them (20, 21, 26, 27).

A relevant neural network configuration to study using such interfaces is the highly interconnected entorhinal-hippocampal network, a brain area important for processing and storage of memories (28). This entorhinal-hippocampal network consists of multiple subregion specific cell types connected through axonal projections. Multinodal microfluidic devices offer an opportunity to reconstruct this network, and to study ongoing structural and functional dynamics in a highly controlled microenvironment. Furthermore, the entorhinal-hippocampal network is particularly vulnerable to Alzheimer's disease (AD), evidenced by early accumulation of tau pathology (29), amyloid-beta plaque load (30), altered neuronal activity in form of seizure-like hyperactivity (31), and major neuronal (32, 33) and synaptic loss (34, 35). Thus, this network is of high interest to study at preclinical stages of AD. We and others have demonstrated that adult entorhinal and hippocampal subregion specific cells from AD model mice are able to reconnect in culture (36–38). We also recently reported a method for long-term (>2 months) culturing and recording of lateral entorhinal cortex layer II (LEC LII) neurons from AD model animals *in vitro* (39). To our knowledge, culturing layer and subregion specific entorhinal-hippocampal neurons from AD model animals in multinodal microfluidics has however not been demonstrated.

In this study, we demonstrate reverse engineering of anatomically relevant biological neural networks, including layer specific neurons derived from adult AD model animals, using custom-designed microfluidic MEA interfaces. By incorporating Tesla-valve inspired microchannels, we can structure multi-nodal neural networks with controllable feedforward connectivity, and record spontaneously evoked and stimulation induced signal propagation in a feedforward pattern between the nodes. This engineering approach supports longitudinal study of dynamic structure-function relationships in both healthy and diseased neural networks with high temporal and spatial precision. Moreover, we demonstrate long-term culturing of region and layer specific neurons extracted from adult AD-model mice and rats on the platforms, in an anatomically relevant configuration. We show that these adult neurons re-form structural connections, and develop spontaneous electrophysiological spiking activity after 15 days *in vitro*. As such, we provide proof of concept for future applications of this model system for advanced preclinical disease modelling.

Materials and Methods

Experimental Design. An experimental timeline including a schematic of the microfluidic MEA design can be seen in **Figure 1**. Our neural cultures comprised either commercially available rat embryonic cortical and hippocampal neurons (hereafter referred to as cortical-hippocampal net-

works), or lateral entorhinal cortex layer II neurons (LEC-LII), Dentate Gyrus granular neurons (DG-gl), CA3 pyramidal neurons (CA3-pyr) and CA1 pyramidal neurons (CA1-pyr) freshly dissected from adult McGill-R-Thy1-APP AD-model rats or APP/PS1 AD-model mice (hereafter referred to as adult entorhinal-hippocampal AD networks). The method for the dissection and culturing of adult hippocampal neurons was refined from our previously reported protocol for adult lateralmost LEC LII (lLEC-LII) neurons from APP/PS1 model mice (39). For all cultures, coating and establishment of an astrocytic feeder layer was conducted using the same protocol.

Design & Fabrication of Microdevices. The four-nodal microdevices were designed using Clewin 4 (WieWeb Software, Enschede). Each node was 5 mm in diameter and 60 μm high. Furthermore, the nodes were connected by 20 microchannels. To induce unidirectional axonal outgrowth between the nodes, a geometrical design inspired by the Tesla-valve was implemented within the microchannel architecture (20). All channels were 350 μm long, 10 μm wide and 5 μm high. The design also had spine structures on the postsynaptic side to misguide axons trying to enter the microchannels. 49 nanoporous platinum electrodes of 50 μm diameter were positioned evenly spread across the four nodes. Additionally, 9 electrodes were positioned within the microfluidic channels to confirm active connections between the nodes. A reference electrode was split between all four chambers for enhanced signal-to-noise ratio. The design, as well as an image of a fabricated microdevice can be seen in **Figure S1**. Fabrication of all microdevices was conducted according to our recently reported protocol (20).

Animals Models and Genotyping. All animal experiments comply with the ARRIVE guidelines (40), were approved by the Norwegian Food Safety Authority and carried out in accordance with the EU (European Union) Directive 2010/63/EU for animal experiments. The animals were held in standard lab cages (up to 5 animals per cage), with temperatures of 22 ± 2 °C, and kept at a light/dark cycle of 12:12 hours, with access to food and water *ad libitum*. We used a total of 43 adult McGill-R-Thy1-APP rats, including female (n=22) and male (n=21), and a total of 2 female, adult APP/PS1 mice. See **Supplementary Table S2** for a total overview of sex, age and genotype of all animals.

The APP/PS1 mouse model is a transgenic familial AD-model, with a C57BL/6J genetic background, co-expressing mutated human amyloid precursor protein (hAPP) (KM670/671NL) and mutated human presenilin 1 (L166). Both mutated proteins are driven by expression cassettes under the Thy1 promoter. This causes increased levels of Aβ leading to formation of extracellular cortical Aβ-deposits starting already from around 6 weeks of age (41). The APP/PS1 mice were genotyped using a KAPA-kit as described in Hanssen *et al.* (39). The McGill-R-Thy1-APP rat model is a transgenic familial AD model with a Wistar (Hsd-Brl:WH) genetic background, co-expressing mutated hAPP (APP K670M671delinsNL) and (APP V717F) (42). The
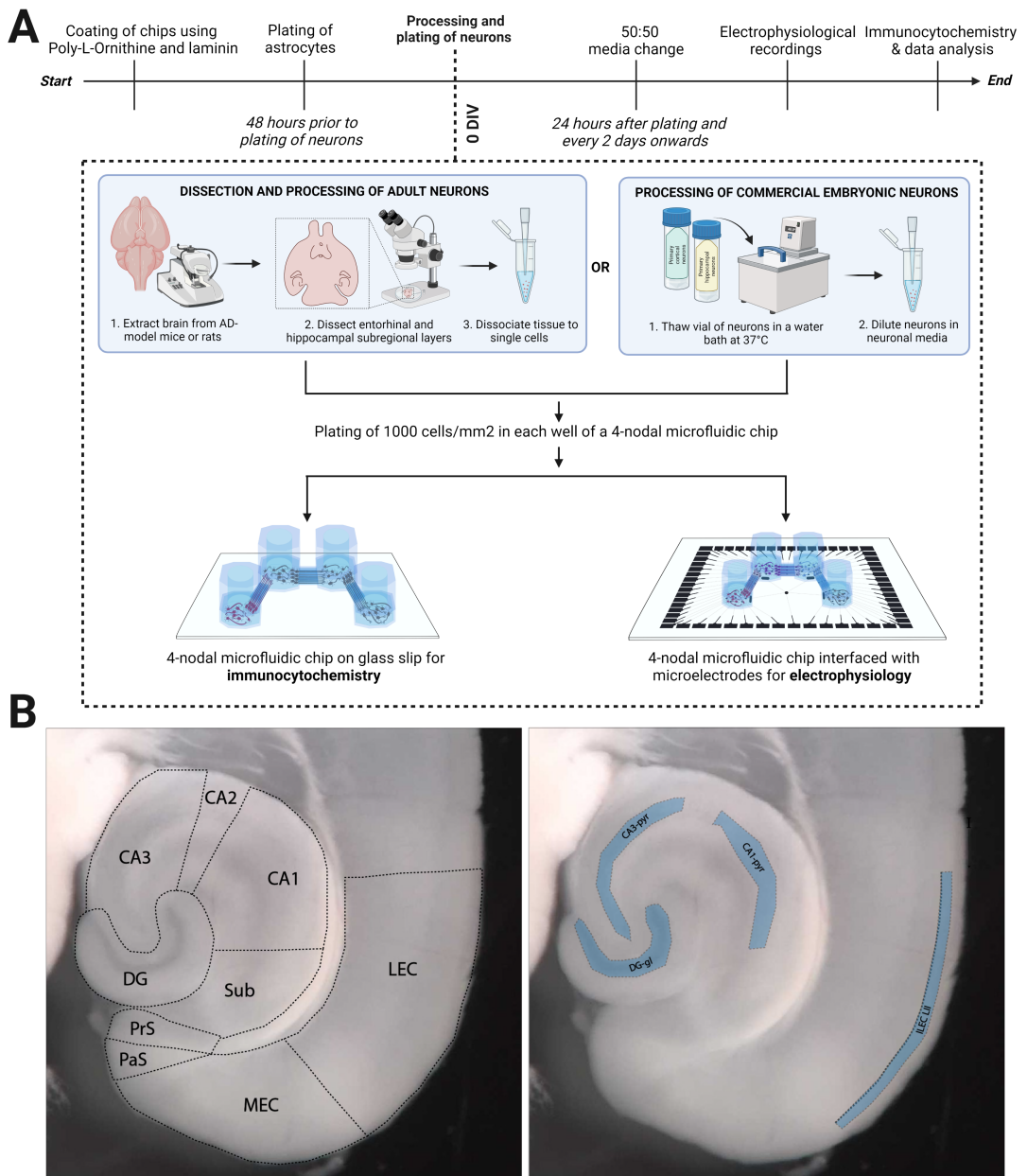
Hanssen & Winter-Hjelm *et al.* | June 26th, 2023

Figure 1 | Experimental timeline. (A.) Microfluidic chips were coated with Poly-L-Ornithine and laminin prior to plating of rat cortical astrocytes. On day 0, brains of adult mice and rats were extracted and horizontally sectioned before dissection of the lateral entorhinal cortex layer II, and hippocampal subregional layers (dentate gyrus granular layer, and CA3- and CA1 pyramidal layers). Dissected entorhinal and hippocampal tissue were furthermore dissociated into single cells enzymatically and manually by trituration. Commercial embryonic rat cortical and hippocampal primary neurons were collected from a nitrogen tank and immediately thawed in a water bath at $37\,^\circ\mathrm{C}$. The cortical-hippocampal and adult entorhinal-hippocampal neurons were plated at a density of 750 and $1000\,\mathrm{cells/mm^2}$ in each well of a four-nodal microfluidic chip, respectively. For the adult cultures, LEC LII, DG-gl, CA3-pyr and CA1-pyr were plated in nodes 1-4, respectively. For the embryonic cultures, cortical neurons were plated in node 1, and hippocampal neurons in nodes 2-4. These devices were interfaced with glass coverslips or microelectrode arrays. **(B.)** A horizontally cut brain section viewed under a stereoscope using fiber optic lamps for contrast with delineation of entorhinal and hippocampal subregions (left). Lateral entorhinal cortex layer II (LEC LII) and hippocampal dentate gyrus granular layer (DG-gl), CA3 pyramidal layer (CA3-pyr) and CA1 pyramidal layer (CA1-pyr) highlighted in blue. Figure created in BioRender.com.

McGill-R-Thy1-APP rats were genotyped using quantitative PCR (qPCR) and genomic DNA isolated from ear tissue as described in previous studies (43, 44).

Cell Experiments and Models.

Coating of Culturing Platforms. Prior to coating, all microdevices were sterilized in UV light over night in a biosafety cabinet. Consecutively, the distilled (DI) water in the devices was replaced by Poly-L-Ornithine solution (PLO) (Sigma-Aldrich, A-004-C) at a concentration of $0.1 \, \text{mg/mL}$ and incubated at $37\,^{\circ}\text{C}$, $5\,\%$ CO_2 for $2\,\text{h}$ *or* overnight at $4\,^{\circ}\text{C}$. Subsequently, all PLO was discarded and the microdevices rinsed three times for $10\,\text{min}$ with milli-Q (MQ) water. After the last rinse, laminin solution consisting of $16\,\mu\text{g/mL}$ natural mouse laminin (Gibco™, 23017015) in phosphate-buffered saline (PBS, Sigma-Aldrich, D8537) was added and the microdevices incubated at $37\,^{\circ}\text{C}$, $5\,\%$ CO_2 for $2\,\text{h}$. A hydrostatic pressure gradient was established during all coating to ensure flow of the coating solution through the microchannels. This was achieved by filling the chambers with an unequal amount of coating solution.

Seeding of Astrocyte Feeder Layer. For the astrocytic feeder layer, a solution consisting of DMEM, low glucose (Gibco™, 11885084) supplemented with $15\,\%$ Fetal Bovine Serum (Sigma-Aldrich, F9665) and $2\,\%$ Penicillin-Streptomycin (Sigma-Aldrich, P4333) was prepared. Next, the coating solution was replaced by the astrocyte media, and rat cortical astrocytes (Gibco™, N7745100) were seeded at a density of $100 \, \text{cells/mm}^2$, i.e., 2000 cells per microchamber. The astrocytes were allowed to expand for $48\,\text{h}$, before seeding of either embryonic cortical and hippocampal neurons or adult entorhinal and hippocampal neurons.

Embryonic Neurons: Plating and Maintenance. Neural media consisting of Neurobasal Plus Medium (Gibco™, A3582801) supplemented with $2\,\%$ B27+ (Gibco™, A358201), $1\,\%$ GlutaMax (Gibco™, 35050038) and $2\,\%$ Penicillin-Streptomycin (Sigma-Aldrich, P4333) was prepared. Rock Inhibitor (Y-27632 dihydrochloride, Y0503, Sigma-Aldrich) was additionally added to the media during the first two days of neural growth at a concentration of $0.1\,\%$ to increase neural survival. Rat cortical neurons from Sprague Dawley rats (Gibco, A36511) were plated at a density of $1000 \, \text{cells/mm}^2$, equalling 20 000 cells in the first node. The cortical neurons were thereafter allowed to settle in an incubator for $3\,\text{h}$ before plating the hippocampal neurons. Next, rat hippocampal neurons from Sprague Dawley rats (Gibco, A36513) were plated at a density of $1000 \, \text{cells/mm}^2$ in the three remaining nodes. Half the neural media was replaced with fresh neural media 4 hours after plating, and again after $24\,\text{h}$. From here on, half the neural media was replaced every second day throughout the experimental period.

Adult Neurons: Dissection. All tools were sterilized by autoclaving before use. Both mice and rats were deeply anesthetized using $5\,\%$ isoflurane gas (Abbott Lab, 05260–05)

and checked for absence of reflexes before the head was decapitated with a guillotine for rats or surgical scissors (FST, 14007–14) for mice. Subsequently, dissection and sectioning of the brain were conducted as described previously for both mice and rats (39) where a full detailed description of the procedure can be found. Brains were extracted in a petri dish filled with Hanks Balanced Salt Solution (Thermo Fischer Scientific, 88284) kept on ice. Extracted brains were sectioned horizontally on a vibratome (thickness of $300\,\mu\text{m}$, frequency of $5.3\,\text{Hz}$ and speed of $8\,\text{mm/s}$) with $0.2\,\%$ AGAR (VWR, 20767.298) supporting the caudal end of the brain. Sectioned brain slices were immediately transferred to wells of a sterile 24-well plate held on ice. Sections were further transferred to a petri dish held on ice and viewed under a stereoscope with fiber optic lamps, allowing for sufficient contrast of the cytoarchitechtonic landmarks. Dissection of the lateral entorhinal cortex layer II (LEC-LII) was conducted as described in our recent study for both mice and rats (39). Additionally, the dentate gurys granular layer (DG-gl), CA3 pyramidal (pyr) and CA1-pyr layers were dissected (see **Figure 1B**). The DG-gl can be separated from the molecular layer and hilus with its densely packed layer of granular neurons (45). Similarly, the pyramidal layer in CA3 and CA1 consists of densely packed pyramidal neurons (46) that can be distinguished from deeper layers lucidum, radiatum and stratum locus molecular and superficial layer oriens (28). All dissected strips of tissue were placed by region in four separate sterile $15\,\text{mL}$ tubes filled with dissection media (HABG-P) consisting of Hibernate-A (Thermo Fischer Scientific, A1247501) supplemented with $2\,\%$ B27+ (Gibco™, A3582801), $2.5\,\%$ GlutaMAX (Gibco™, 35050061) and $1\,\%$ Penicillin-streptomycin (Sigma-Aldrich, P4333), placed on ice.

Adult Neurons: Plating and Maintenance. All dissected tissue was rinsed for debris three times by adding and removing $3\,\text{mL}$ of HABG-P. Following this, all media was discarded and the tissue was dissociated for $15\,\text{min}$ at $37\,^{\circ}\text{C}$, $5\,\%$ CO_2, $20\,\%$ O_2 in Neural Isolation Enzyme Papain (Thermo Fischer Scientific, 88285) reconstituted in Hank's Balanced Salt solution (Thermo Fischer Scientific, 88284) as described by the manufacturer (Thermo Fischer Scientific, MAN0011896). Subsequently, all dissociation enzyme was discarded, $100\,\mu\text{L}$ HABG-P was added and the tissue was manually triturated 10 times by using a $100\,\mu\text{L}$ pipette tip. Further, all HABG-P was topped up to a total of $3\,\text{mL}$ and the vials of tissue were centrifuged at x200 g for $2\,\text{min}$ in room temperature. After centrifugation, all HABG-P was discarded and $100\,\mu\text{L}$ neural media was added before manual trituration 10 times using a $100\,\mu\text{L}$ pipette tip. Neural media consisting of Neurobasal Plus Medium (Gibco™, A3582801) supplemented with $2\,\%$ B27+ (Gibco™, A358201), $1\,\%$ GlutaMax (Gibco™, 35050038), $2\,\%$ Penicillin-Streptomycin (Sigma-Aldrich, P4333), $0.1\,\%$ Rock Inhibitor (Y-27632 dihydrochloride, Y0503, Sigma-Aldrich) and $10\,\%$ Fetal Bovine Serum (Sigma Aldrich, 12106C). For adult neurons derived from mice, $0.1\,\%$ BDNF (Neurotrophins, 450-02) was added to the neural media. For adult neurons derived

from rats, 0.1% FGF2 (Thermo Fisher Scientific, 13256-029) was added to the neural media. We plated the neurons at a total density of $750\,\text{cells}/\text{mm}^2$, equalling 15 000 cells in each node of the microfluidic chip. Half the neural media was replaced every second day throughout the experimental period.

Immunocytochemistry. For immunocytochemistry, both cortical-hippocampal and adult entorhinal-hippocampal neurons were plated in microfluidic platforms bonded to glass coverslips (VWR International, 24x24 mm No. 1 Menzel-Gläser). Fixation of cortical-hippocampal cultures was conducted using glyoxal solution based on the protocol by Richter *et al.* (47). This fixative consisted of 71% MQ water, 20% ethanol absolute (Kemetyl, 100%), 8.0% Glyoxal solution (Sigma-Aldrich, 128465) and 1% acetic acid (Sigma-Aldrich, 1.00063). Fixation of adult entorhinal-hippocampal cultures was conducted using PBS (Sigma-Aldrich, D8537) containing $0.4\,\text{M}$ phosphate buffer and 4% freshly depolymerized paraformaldehyde (PFA; Sigma-Aldrich, P6148). The cultures were washed with PBS to remove debris, before the fixative was applied for $15\,\text{min}$ at RT. Subsequently, all chambers were washed with PBS 3 times for $15\,\text{min}$ each. Next, 0.5% Triton-X (Sigma-Aldrich, 1086431000) diluted in PBS was applied to permeabilize the cells. All chambers were again washed twice with PBS before a blocking solution consisting of 5% goat serum (Abcam, ab7481) diluted in PBS was added to the cultures, and the cultures incubated at room temperature on a shaking table at $30\,\text{rpm}$ for $1\,\text{h}$. Primary antibody solutions were prepared in PBS with 5% goat serum, and antibody concentrations according to the ones listed in **Table 1**. Cultures were placed on a shaker table at $30\,\text{rpm}$ at $4\,^\circ\text{C}$ overnight. Following, the primary antibody solution was removed, and the cell cultures were rinsed three times with PBS for $15\,\text{min}$ each. Next, a secondary antibody solution consisting of 0.2% secondaries and 5% goat serum diluted in PBS was added to the cultures. The cultures were left to rest on a shaker table at $30\,\text{rpm}$ for $3\,\text{h}$ at RT. Prior to applying the secondary antibody solution, the prepared solutions were centrifuged at $6000\,\text{rpm}$ for at least $15\,\text{min}$ to remove precipitates. Subsequently, the secondary antibody solution was replaced by Hoechst (Abcam, ab228550) at a concentration of 0.1% diluted in PBS, and the cultures left on a shaker table for another $30\,\text{min}$. Eventually, all cultures were washed three more times in PBS, then twice in MQ water prior to imaging.

Table 1 | Antibodies and concentrations used for Immunocytochemistry.

Marker	Catalogue Number	Concentration
β3-Tubulin	Ab78078	1/1000
GAP-43	9264 (Sigma-Aldrich)	1/500
GFAP	Ab7260	1/1000
MAP2	Ab5392	1/5000
NeuN	Ab279295	1/500
Neurofilament Heavy	Ab4680	1/5000
Reelin	Ab78540	1/10000

All antibodies were purchased from Abcam unless otherwise stated.

All images were acquired using an EVOS M5000 microscope (Invitrogen). The microscope was equipped with DAPI (AMEP4650), CY5 (AMEP4656), GFP (AMEP4651) and TxRed (AMEP4655) LED light cubes and Olympus UP-LSAP0 4X/0.16 NA and 20x/0.75 NA objectives. Postprocessing of images was conducted in ImageJ/Fiji or Adobe Photoshop 2020.

Imaging and Quantification of Neurite Length. For quantification of neurite length, phase contrast images acquired using a Zeiss Axio Vert V.1 brightfield 20x/53 WD/0.4 NA objective with an Axiocam 202 mono were used. For analysis, Neurolucida was used to quantify neurite length of the adult neurons.

Electrophysiology and Data Analysis.

Electrophysiological Recordings. A MEA2100 workstation (Multichannel Systems) was utilized for all recordings with a sampling rate of $25\,000\,\text{Hz}$. An external temperature controller (TC01, Multichannel Systems) was used to maintain the temperature at $37\,^\circ\text{C}$. All cultures were allowed to equilibrate at the workstation for $5\,\text{min}$ prior to recordings, and recordings lasted for $15\,\text{min}$ for cortical-hippocampal cultures and $10\,\text{min}$ for adult entorhinal-hippocampal neural networks. A 3D-printed plastic cover with a gas-permeable membrane was used to keep cultures in a sterile environment during the recordings.

Electrical Stimulations. Stimulations were performed for the cortical-hippocampal neurons following the recordings at 28 and 32 DIV using a train of 60 spikes at $\pm\,800\,\text{mV}$ (positive phase first) of $200\,\mu\text{s}$ duration with an inter-spike interval of $5\,\text{s}$. The most active electrode measured in spikes per second in the cortical cell population was chosen for stimulations. This was done to assure that the electrode chosen for stimulation had sufficient coupling with a neuron to induce activity.

Data Analysis. All data preprocessing and analysis was conducted in Matlab R2021b, and graphs were plotted using the matlab function linspecer (48), based on the color palette colorBrewer (49). A 4th order Butterworth bandpass filter was used to remove noise below $300\,\text{Hz}$ and above $3000\,\text{Hz}$, and a notch filter to remove noise at $50\,\text{Hz}$ from the power supply mains. All filters were run using zero-phase digital filtering. For spike detection, the Precise Timing Spike Detection (PTSD) algorithm developed by Maccione *et al.* (50) was utilized. A threshold of 9 times the standard deviation was chosen for the cortical-hippocampal cultures, with a maximum peak duration of $1\,\text{ms}$ and a refractory periode of $1.6\,\text{ms}$. For the adult entorhinal-hippocampal cultures, a standard deviation of 7.5 was chosen due to the lower signal-to-noise ratio of the activity in these cultures overall. The SpikeRasterPlot function developed by Kraus (51) was adapted and used for creating raster plots.

Burst detection was conducted using the logISI algorithm developed by Pasquale *et al.* (1). A minimum of four consecutive spikes was set as a hard threshold for a burst to be detected, and the maximum inter-spike interval to $100\,\text{ms}$. Net-

work bursts were detected using the logIBEI approach (52), with a minimum of 10% of all active electrodes required to exhibit bursting activity for a network burst to be classified. After binning the data into $50\,\text{ms}$ time bins, functional connectivity was analysed using Pearson correlation. Intranodal correlation was evaluated by taking the average correlation of all active connections within each node. Internodal correlation was evaluated by taking the correlation between the summed activity of all four nodes in the four-nodal network. To visualize key network features, graphs were plotted using the functional connectivity as edges between the individual nodes (herein representing the individual electrodes). Firing rate (Hz) was furthermore used to represent the node color, betweenness centrality the node size and node edge color the community belonging. Graph theoretical measures were calculated using the Brain Connectivity Toolbox developed by Rubinov & Sporns (53), from which the Louvain algorithm was used to perform community detection (54).

To remove stimulation artifacts, stimulation data was run through the SALPA filter developed by Wagenaar *et al.* (55). Additionally, $15\,\text{ms}$ of the filtered data was blanked following each stimulation time point. Subsequently, the data was binned into $20\,\text{ms}$ time bins, and peristimulus time histograms of the average response of the stimulations in each node plotted.

Results

Establishment of Feedforward Cortical-Hippocampal Networks.
In this study, we reverse engineered multi-nodal rodent cortical-hippocampal neural networks with controllable afferent-efferent connectivity using custom-designed microfluidic devices interfaced with microelectrode arrays. We found that neurites from presynaptic nodes started entering the microchannels within the first week after plating, while axonal bundles could be observed crossing the microchannels between all nodes as early as 14 DIV (**Figure 2A**). At this timepoint, electrophysiological recordings indicated that spontaneous neural activity had already started transitioning from immature tonic firing to synchronous bursting within the nodes, consistent with previous findings (1, 2, 20, 56, 57). Representative graphs of both bursting activity and individual spikes within the cortical and hippocampal nodes can be seen in **Figure 2B**.

Both spontaneously evoked and stimulation induced network bursts were used to assess the capacity of the networks for feedforward activity propagation between the four unidirectionally connected nodes. All four nodes exhibited bursting activity already at 12 DIV, and the burst rate increased steadily with time (**Figure 2C**). Until 20 DIV, bursts were mainly contained within the individual nodes, or spread between only a subset of the nodes. As the networks continued to mature, more bursts initiated in the cortical node could be seen spreading sequentially through all three hippocampal nodes. A $200\,\text{s}$ representative raster plot of a multinodal cortical-hippocampal network at 28 DIV can be seen in **Figure 2D**, with the different nodes marked with different shades of blue. Observation of a typical network burst clearly shows

how activity originating from the cortical node is spreading in a feedforward manner between all four interconnected nodes. Furthermore, electrical stimulation delivered to the cortical node initiated activity propagating sequentially between the four nodes, as seen in the peristimulus time histogram in **Figure 2E**. **Figure 2F** shows the percentage of all network bursts that were initiated within the cortical node and where either contained in the specific node, or spread to the next two or three nodes. The total number of network bursts detected during a typical recording is seen along the secondary y-axis. At 28 DIV, as much as 24.2% of the network bursts propagated through all four nodes, compared to less than 2% at 12 DIV. For comparison (at 28 DIV) 4.5%, 13.4% and 4.4% of the network bursts that were initiated in the cortical node propagated and stopped after the first, second and third node, respectively. This indicated establishment of more mature directional projection sequences between the nodes. The remaining percentages of network bursts were initiated within the second, third or fourth node. Similar trends were found for the other five networks (see **Figure S2**).

Functional Integration Increases, While Functional Segregation is Maintained Over Time in Reverse Engineered Multinodal Neural Networks.
The functional connectivity of the networks was evaluated using Pearson correlation. Both intranodal and internodal correlation increased over time. Correlation matrices showing the temporal development in functional connectivity for one representative network can be seen in **Figure 3A**. While some internodal correlation could be observed between nodes already at 12 DIV, integration of all neighboring nodes was not established until 20 DIV. At 28 DIV, a higher correlation was also seen between non-neighboring nodes, indicative of a higher network-wide synchronization at this point (20, 26, 27). The graph representation of the network seen in **Figure 3B** furthermore highlights this network-wide functional integration. It additionally shows how the internodal correlation is clearly strongest between neighboring nodes, while the intranodal correlation on average is higher than the internodal correlation.

Furthermore, the entire reverse-engineeered cortical-hippocampal network could be mathematically delineated into four distinct modules using the Louvain algorithm, represented as the node edge color in **Figure 3B**. The median modularity value stayed close to 0.6 for all networks throughout the experimental period, indicating that the networks retained functional segregation of the four nodes (**Figure 3C**).

Structural Maturation of Cortical-Hippocampal Networks.
As we saw a high level of functional integration between the nodes beyond 20 DIV, we also evaluated the networks' structural maturation using immunocytochemistry. To do so, we stained cells in each of the four nodes for both developmental and mature cytoskeletal and nucleic markers at 27 DIV. High levels of Growth-Associated Protein 43 (GAP43) were expressed for both the cortical and hippocampal nodes at 27 DIV (**Figure 4A**). This marker was used
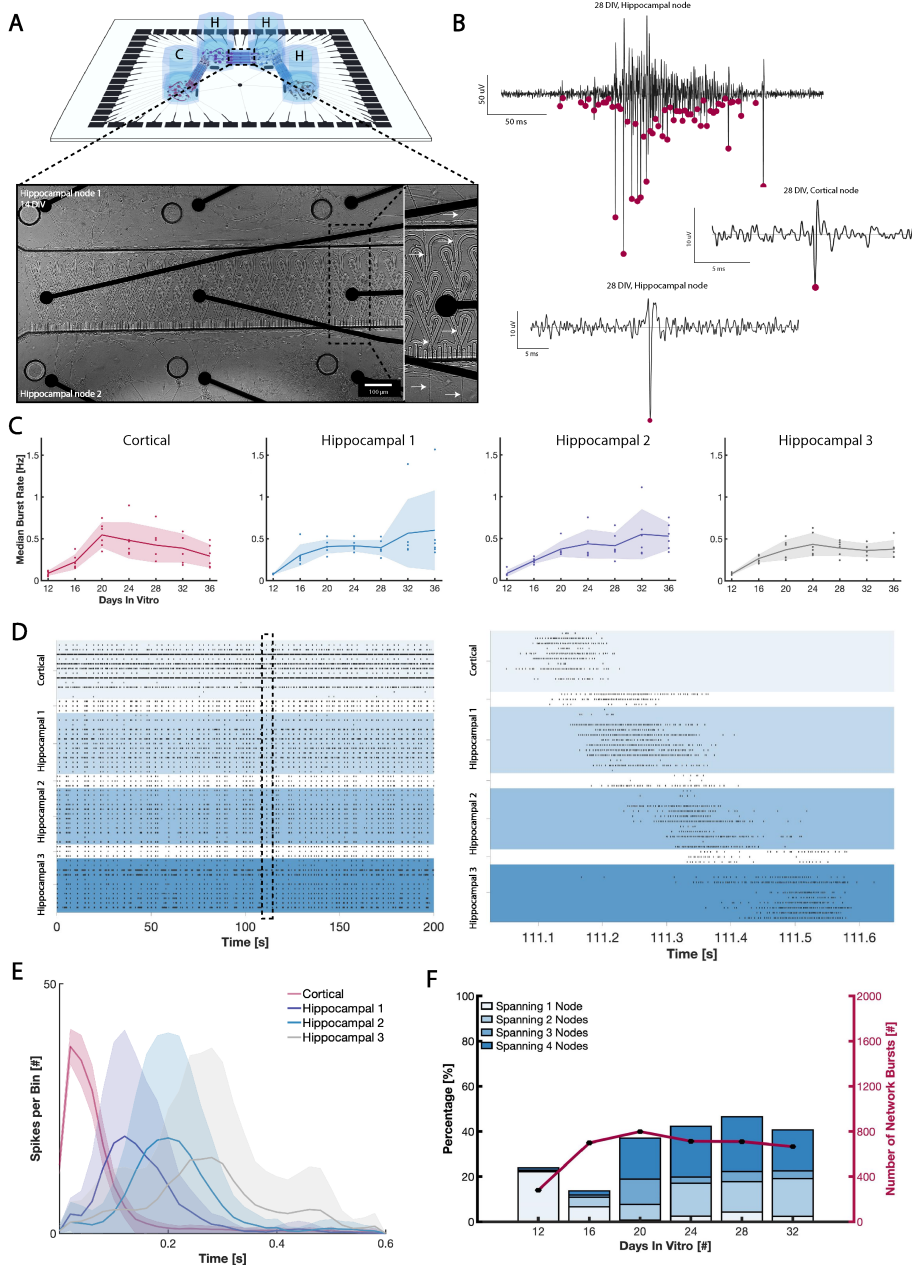
Figure 2 | Feedforward activity propagation in the four-nodal cortical-hippocampal networks. (A.) Representative micrograph of axons within the microchannels connecting two hippocampal nodes at 14 DIV. Examples of axonal bundles passing through microchannels (both with and without embedded microelectrodes) are highlighted with white arrows. **(B.)** Voltage traces showing a burst detected within one of the hippocampal nodes at 28 DIV, as well as representative examples of spikes detected within the cortical and hippocampal nodes. Pink specks represent spikes detected by the PTSD algorithm. **(C.)** Plots of the median burst rate for the four individual nodes. All nodes displayed an increasing burst rate until 20 DIV, at which point the rate started to flatten out. **(D.)** Representative raster plot showing the complex network dynamics emerging in the four-nodal cultures. A fraction of the network bursts were also clearly spreading from the cortical node throughout all four nodes, as represented in the zoomed-in graph. **(E.)** Peristimulus time histogram displaying the average response of each of the four nodes following repeated (n=60) stimulations of the cortical node for one network at 28 DIV. The stimulations clearly induced feedforward activity propagating throughout all four nodes. **(F.)** Histogram showing the percentage of spontaneously evoked network bursts initiated within the cortical population, and the number of nodes they spanned. The total number of network bursts initiated at each DIV is shown along the secondary y-axis.
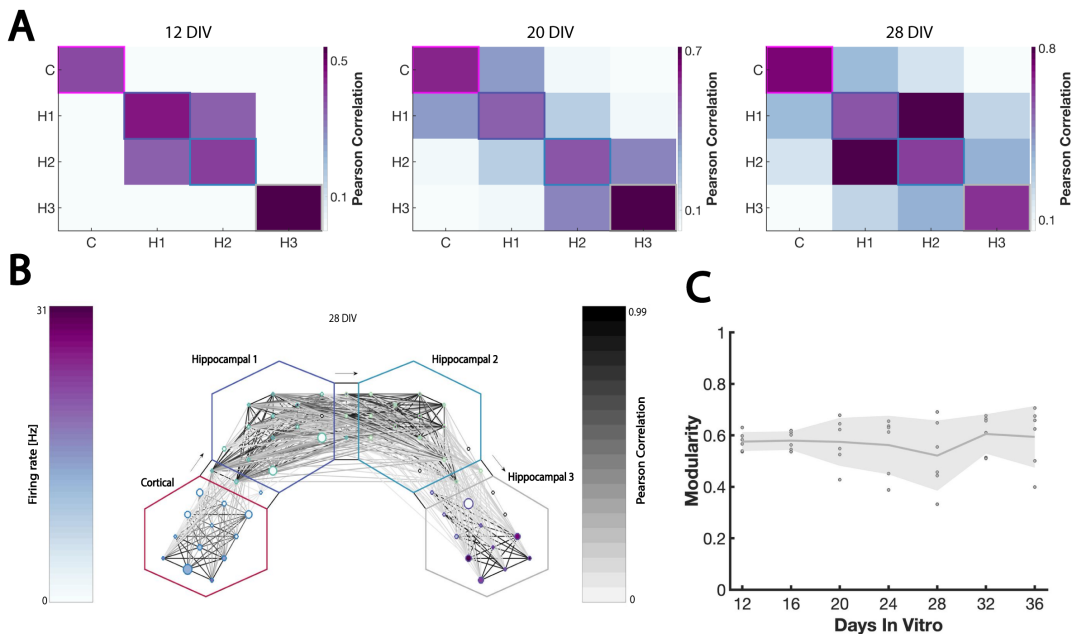
Figure 3 | Functional connectivity of the cortical-hippocampal networks. (A.) Correlation matrices showing the temporal increase in functional connectivity of one representative network over time from 12 DIV to 28 DIV. **(B.)** Representative graph of a single network at 28 DIV displaying individual electrodes as nodes and their correlation as edges. Node color represents firing rate, node size betweenness centrality and node edge color community belonging. As illustrated, the network can be clearly delineated into distinct communities, with higher intranodal than internodal functional connectivity. **(C.)** Modularity for the four-nodal networks, indicating a retained functional segregation over time.

in combination with the cytoskeletal proteins Microtubule-Associated Protein 2 (MAP2) and β3-Tubulin, which are expressed from early axiogenesis and onwards (58–62). As GAP43 is critical for neurodevelopment and growth cone migration, these expression levels indicate that structural changes were still evolving beyond three weeks *in vitro* (63). Furthermore, both Neural Nuclear Protein (NeuN) and Neurofilament Heavy (NFH) have been found to be specific for mature neurons, and were used here to assess the maturity of the engineered networks (**Figure 4B**) (64, 65). These markers were used in combination with the glial marker GFAP (66). We found all these proteins to be prominently expressed at 27 DIV, indicating that the networks were reaching structural maturity. This is also consistent with the findings from the electrophysiology, showing highly integrated dynamics between the nodes (**Figure 3**).

Adult Entorhinal and Hippocampal AD Neurons Reform Structural Networks and Exhibit Electrophysiological Activity. To further demonstrate the wider applicability of our model system for reverse engineering anatomically relevant networks for preclinical disease modelling, we used this system to culture neurons extracted from brain regions of interest from adult AD model animals. Our procedure to dissect and culture adult LEC LII neurons along with hippocampal DG-gr, CA3-pyr and CA1-pyr neurons from AD-model mice and rats is outlined in **Figure 1**. This method

for the dissection and culturing of layer specific entorhinal and hippocampal neurons from AD model rats and mice builds upon our recently published method for extraction and culturing of LEC LII neurons from adult AD model APP/PS1 mice (39). We found that adult neurons from both AD model rats- (**Figure 5**) and mice (**Figure S4**) were able to re-form structural connections *in vitro*. Furthermore, we found that an astrocytic feeder layer was crucial for attachment of adult entorhinal and hippocampal AD neurons (**Figure S3A**), in line with our previous findings (39). Various combinations of neural media supplements were tested (**Table S1**), and neurites of adult rat neurons were found to significantly enhance their outgrowth when adding the growth factor FGF2 (10ng/mL) after 5 DIV (**Figure S3B & S3C**, all p-values for P3 < 0.01). Immunocytochemistry of our cultured adult neurons showed co-expression of neural marker NeuN and reelin in the LEC LII neurons, thus confirming regional identity, and co-expression of NeuN and Neurofilament Heavy for hippocampal DG-gr, CA3-pyr and CA1-pyr. This confirmed that the engineered network consisted of the neurons of interest (**Figure 6**). From 15 DIV, the networks started exhibiting spontaneous spiking activity (**Figure 7B** for rats, **Figure S5A** for mice). A raster plot showing that the neurons expressed sparse, desynchronized spiking activity with no bursts is seen in **Figure 7C**. Calculations of the median firing rate over time showed that the networks remained active up to at least 47 days *in vitro* (**Figure 7D**).
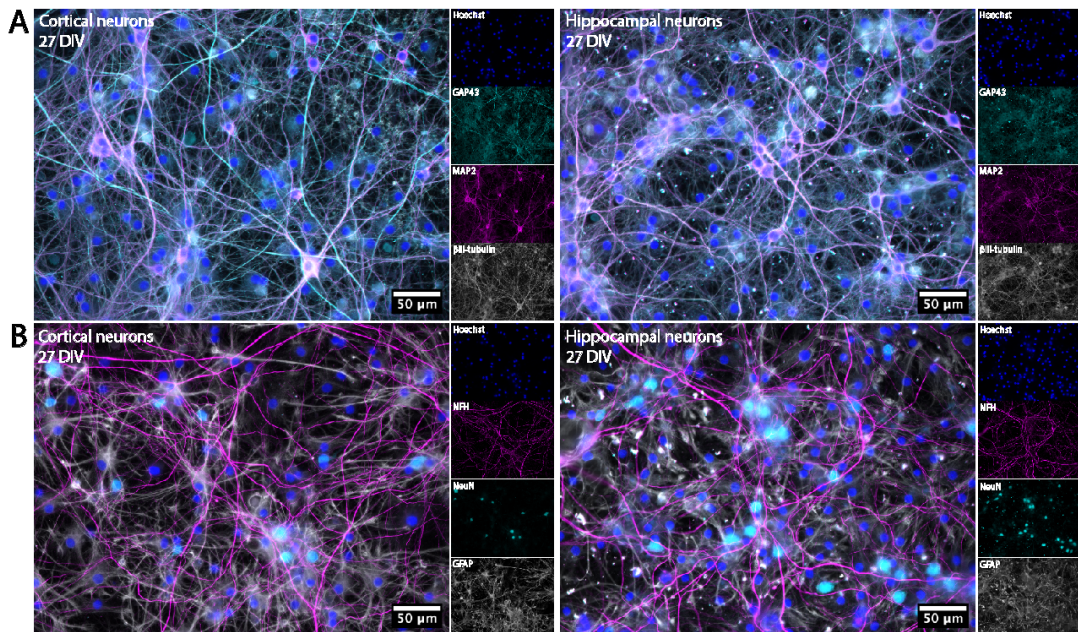
Figure 4 | Immunocytochemistry of cortical-hippocampal networks. (A.) Both cortical and hippocampal cultures self-organized into complex networks, as indicated by the cytoskeletal marker proteins β3-Tubulin and MAP2. The networks still underwent some level of self-organization and maturation at 27 DIV, as indicated by GAP43, a protein critical for neurodevelopment and growth cone migration. **(B.)** The networks had reached a high level of structural maturity at 27 DIV, indicated by the mature markers Neurofilament Heavy (NFH) and NeuN.

Discussion

In this study we have demonstrated reverse engineering of complex multi-nodal cortical-hippocampal neural networks with controllable afferent-efferent connectivity. We have furthermore illustrated the potential of this approach for advanced modelling of neural network function and dysfunction, by providing proof of concept of long-term culture of layer specific entorhinal-hippocampal networks from adult AD transgenic rats and mice.

Our engineered embryonic cortical-hippocampal networks recapitulated fundamental neural design principles by exhibiting spontaneous, complex structure-function dynamics over time. Specifically, these networks exhibited both segregated and integrated bursting activity across the four nodes (**Figure 2F**). Furthermore, electrical stimulations of the presynaptic, cortical node within these networks readily induced bursting activity that propagated sequentially, in a feedforward pattern, through the rest of the interconnected nodes (**Figure 2E**). The differences in number of nodes that network bursts spanned can be indicative of the networks' capacity for gating information, i.e. selectively transmitting only a subset of the information to other nodes (20, 21, 26, 27). Our results furthermore showed that the network modularity remained close to 0.6 for all networks throughout the experimental period. In comparison, in our previous study, we found the median modularity value to be 0.39 and 0.03 for two-nodal and one-nodal networks (20).

As such, the four-nodal configuration of the present model system promoted efficient network organization, exhibited both integrated and segregated functional dynamics resembling those seen in neural networks *in vivo* (67–69).

The adult neural networks derived from AD model mice and rats exhibited electrophysiological spiking activity from 15 DIV (**Figure 7**). Spontaneously evoked neural activity was recorded, and a desynchronized firing pattern with no apparent bursting was observed (**Figure 7C**), in line with our recently reported findings from adult mouse LEC-LII neuron cultures (39). Additionally, previous studies performing patch-clamp recordings on cultured adult mouse hippocampal neurons have reported the neurons to exhibit activity as single spike events, rather than repetitive firing patterns (70, 71). A recent study also showed that both cortical and hippocampal neurons derived from adult wild-type mice expressed sparse bursting (<1 bursts per minute) (72). Furthermore, *ex vivo* whole-cell patch-clamp recordings from LEC LII neurons have shown that large depolarizing current-steps are necessary to elicit a burst in these neurons (73).

Advanced engineered interfaces as the ones demonstrated in this study can be particularly useful for modelling disease development and progression. The increasing body of literature on healthy development and maturation of neural networks *in vitro* aids in establishing baseline conditions for such studies. As previously described, healthy networks show a gradual transitioning from tonic, desynchronized intranodal fir-
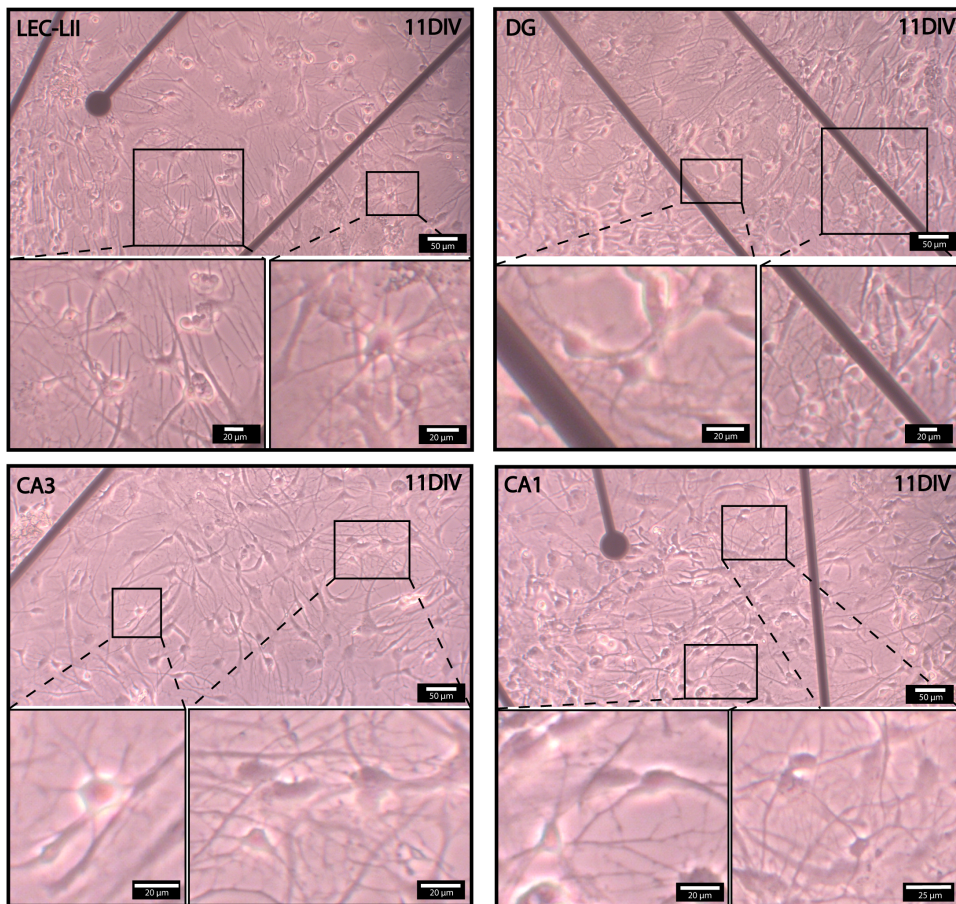
Figure 5 | Adult entorhinal and hippocampal AD neurons re-form structural connections *in vitro*. Phase-contrast images of adult neurons from LEC LII, DG, CA3 and CA1 at 11 DIV. Enlarged insets from all regions showing neural bodies with extruding neurites. Scalebars as indicated. LEC LII; lateral entorhinal cortex layer II. DG; denate gyrus. CA3/CA1; Cornu ammonis 3 and 1. DIV; days *in vitro*.

ing to network wide internodal integration of function during development (1, 2, 20, 57). Furthermore, they establish mature synaptic connections and an excitation-inhibition balance (20, 56). By comparing healthy networks to networks exhibiting pathological traits, such as the neurons from AD model animals used in this study, intra- and internodal changes in response to developing pathology can be modelled and studied. Such changes could for instance be hyperactivity in neurons surrounded by amyloid-β plaques (74) or changes in firing characteristics in form of decreased firing frequency (75). A critical risk factor for several neurodegenerative diseases and disorders, including AD, is also age. To accurately model disease development and progression, using cells from adult animals can as such have an impact on structural and functional dynamics due to the variations in epigenetic profile between embryonic and adult cells. The division of the distinct neural subpopulations into separate nodes can addi-

tionally support studies of propagation of pathological processes from pre- to postsynaptic nodes, further expanding on previous findings from our group (76). The ability to model such processes is highly relevant for elucidation of disease mechanisms, as well as identification of potential time windows and modes of therapeutic intervention.

Neural microcircuits in the brain, such as the entorhinal-hippocampal network, are profoundly complex systems with an intricate microarchitecture involving distinct subpopulations of neurons and other cells. Capturing the full complexity of such microarchitectures *in vitro* is per definition beyond the scope of reverse engineering approaches. Nonetheless, the present study clearly illustrates the robustness and potential of advanced neuroengineering in recapitulating complex network dynamics *in vitro*, and as such, it builds upon and expands on previous work (20, 21, 57, 76–79).
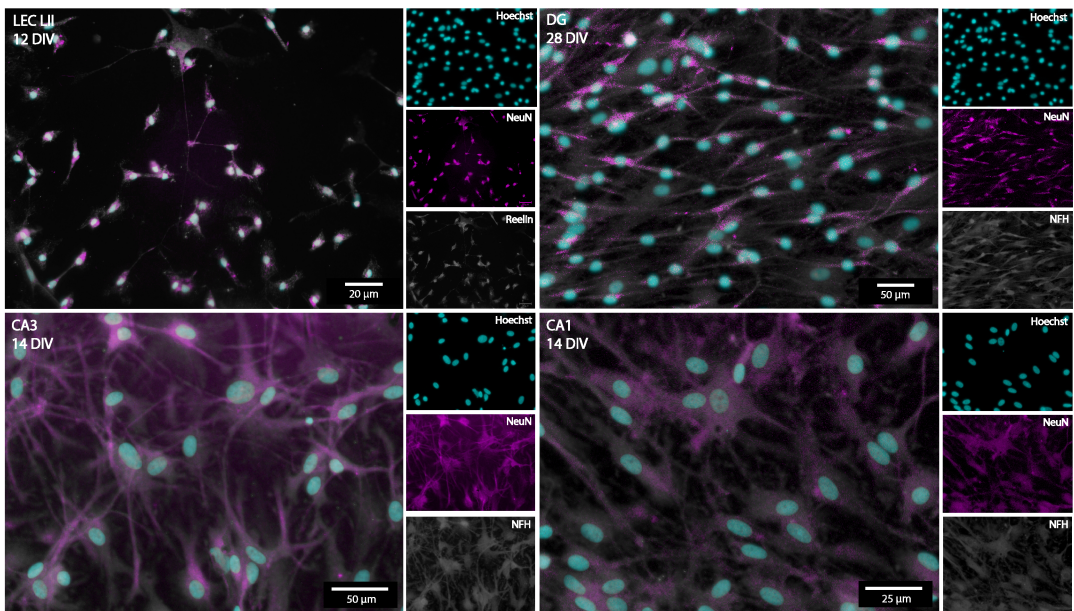
Figure 6 | **Immunocytochemistry of entorhinal-hippocampal AD networks.** Co-expression of the neural marker NeuN and reelin in the LEC LII neurons, and co-expression of NeuN and Neurofilament Heavy for hippocampal DG-gr, CA3-pyr and CA1-pyr confirmed the presence of the neurons of interest.
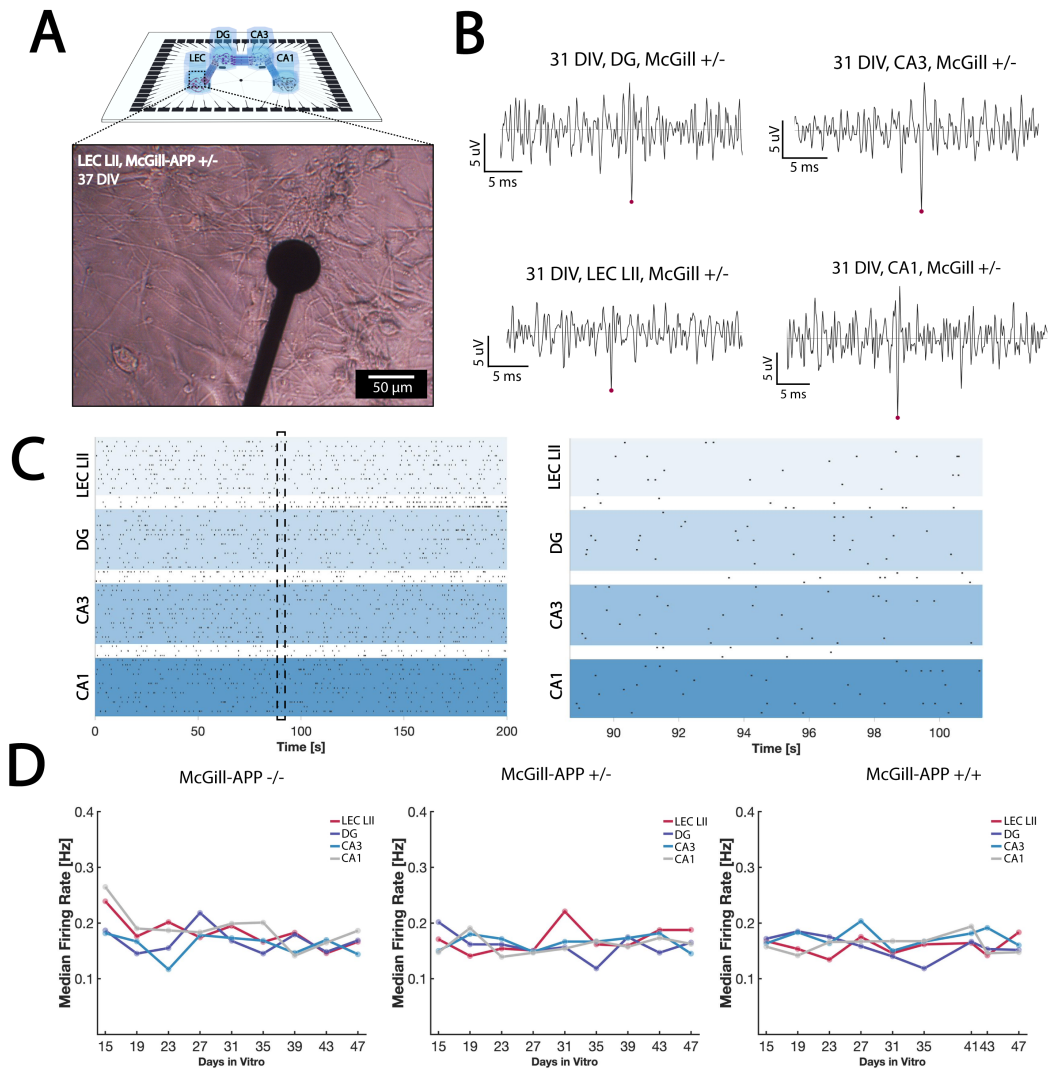
Figure 7 | Adult entorhinal and hippocampal neural networks from AD-model rats develop sustained electrophysiological activity. (A.) Illustration of a four-nodal microfluidic chip on a microelectrode array with an inset of a phase contrast image of a lateral entorhinal cortex layer II (LEC LII) neural network derived from a McGill-APP rat +/- (heterozygote genotype). **(B.)** Spike traces showing one representative spike from each subregion, LEC LII (bottom left), DG (top left), CA3 (top right) and CA1 (bottom right) at 31 DIV. **(C.)** Representative raster plots showing spontaneous network activity from all four nodes. One black dot indicates one detected spike. **(D.)** Median firing rate (Hz) over time from 15 DIV up to 47 DIV. LEC LII; Lateral entorhinal cortex layer II. DG; Dentate gyrus. CA3; Cornu ammonis 3. CA1; Cornu ammonis 3. DIV; Days *in vitro*.

Conclusion

In this study, we reverse engineered multinodal cortical-hippocampal neural networks with controllable afferent-efferent connectivity. We validated that both spontaneously evoked and stimulation induced activity propagated in a feed-forward manner between the interconnected nodes in these networks. Interconnection of the multinodal networks contributed to the emergence of complex structure-function dynamics both within and across nodes. This indicates the network´s capacity for both integrated as well as segregated information processing. Furthermore, long-term culturing of adult entorhinal-hippocampal network from AD model animals demonstrate the wide potential of this advanced modelling approach. These neurons self-organize, re-form structural connections and demonstrate spontaneous electrophysiologically activity. Thus, this reverse engineering approach presents a significant step towards modelling anatomically relevant neural networks in different configurations for preclinical disease modelling.

Bibliography

1. V. Pasquale, S. Martinoia, and M. Chiappalone. A self-adapting approach for the detection of bursts and network bursts in neuronal cultures. *J. Comput. Neurosci.*, 29:213–29, 2010. doi: 10.1007/s10827-009-0175-1.

2. D. A. Wagenaar, J. Pine, and S. M. Potter. An extremely rich repertoire of bursting patterns during the development of cortical cultures. *BMC Neurosci.*, 7:11, 2006. doi: 10.1186/1471-2202-7-11.

3. M. Chiappalone, M. Bove, A. Vato, M. Tedesco, and S. Martinoia. Dissociated cortical networks show spontaneously correlated activity patterns during in vitro development. *Brain Res.*, 1093(1):41–53, 2006. doi: 10.1016/j.brainres.2006.03.049.

4. A. M. Taylor, S. W. Rhee, C. H. Tu, D. H. Cribbs, C. W. Cotman, and N. L. Jeon. Microfluidic multicompartment device for neuroscience research. *Langmuir*, 19(5):1551–56, 2003. doi: 10.1021/la026417v.

5. A. M. Taylor, M. Blurton-Jones, S. W. Rhee, D. H. Cribbs, C. W. Cotman, and N. L. Jeon. A microfluidic culture platform for cns axonal injury, regeneration and transport. *Nat. Methods*, 2:599–605, 2005. doi: 10.1038/nmeth777.

6. L. Pan, S. Alagapan, E. Franca, S. S. Leondopulos, T. B. DeMarse, G. J. Brewer, and B. C. Wheeler. An in vitro method to manipulate the direction and functional strength between neural populations. *Front. Neural Circuits*, 9:32, 2015. doi: 10.3389/fncir.2015.00032.

7. T. B. DeMarse, L. Pan, S. Alagapan, G. J. Brewer, and B. C. Wheeler. Feed-forward propagation of temporal and rate information between cortical populations during coherent activation in engineered in vitro networks. *Front. Neural Circuits*, 10, 2016. doi: https://doi.org/10.3389/fncir.2016.00032.

8. V. A. Makarov J. Makarova A. Korovaichuk N. Benito, A. Fernández-Ruiz and O. Herreras. Spatial modules of coherent activity in pathway-specific lfps in the hippocampus reflect

9. G. S. Withers, C. D. James, C. E. Kingman, H. G. Craighead, and G. A. Banker. Effects of substrate geometry on growth cone behavior and axon branching. *J. Neurobiol.*, 66: 1183–94, 2006. doi: 10.1002/neu.20298.

10. E. W. Dent, S. L. Gupton, and F. B. Gertler. The growth cone cytoskeleton in axon outgrowth and guidance. *Cold Spring Harb. Perspect. Biol.*, 3(3), 2011. doi: 10.1101/cshperspect.a001800.

11. G. Gangatharan, S. Schneider-Maunoury, and M. A. Breau. Role of mechanical cues in shaping neuronal morphology and connectivity. *Biology of the Cell*, 110(6):125–36, 2018. doi: 10.1111/boc.201800003.

12. J. M. Peyrin, B. Deleglise, L. Saias, M. Vignes, P. Gougis, S. Magnifico, S. Betuing, M. Pietri, J. Caboche, P. Vanhoutte, J. L. Viovy, and B. Brugg. Axon diodes for the reconstruction of oriented neuronal networks in microfluidic chambers. *Lab Chip*, 11(21):3663–73, 2011. doi: 10.1039/c1lc20014c.

13. E. Malishev, A. Pimashkin, A. Gladkov, Y. Pigareva, A. Bukatin, V. Kazantsev, I. Mukhina, and M. Dubina. Microfluidic device for unidirectional axon growth. *Journal of Physics: Conference Series*, 643, 2015. doi: 10.1088/1742-6596/643/1/012025.

14. J. le Feber, W. Postma, E. de Weerd, M. Weusthof, and W. L. Rutten. Barbed channels enhance unidirectional connectivity between neuronal networks cultured on multi electrode arrays. *Front. Neurosci.*, 9:412, 2015. doi: 10.3389/fnins.2015.00412.

15. A. Gladkov, Y. Pigareva, D. Kutyina, V. Kolpakov, A. Bukatin, I. Mukhina, V. Kazantsev, and A. Pimashkin. Design of cultured neuron networks in vitro with predefined connectivity using asymmetric microfluidic channels. *Sci. Rep.*, 7:15625, 2017. doi: 10.1038/s41598-017-15506-2.

16. Y. Pigareva, A. Gladkov, V. Kolpakov, I. Mukhina, A. Bukatin, V. B. Kazantsev, and A. Pimashkin. Experimental platform to study spiking pattern propagation in modular networks in vitro. *Brain Sci.*, 11(6), 2021. doi: 10.3390/brainsci11060717.

17. S. Na, M. Kang, S. Bang, D. Park, J. Kim, S. J. Sim, S. Chang, and N. L. Jeon. Microfluidic neural axon diode. *Technology*, 4(4):240–8, 2016. doi: https://doi.org/10.1142/S2339547816500102.

18. P. M. Holloway, G. I. Hallinan, M. Hegde, S. I. R. Lane, K. Deinhardt, and J. West. Asymmetric confinement for defining outgrowth directionality. *Lab Chip*, 19(8):1484–89, 2019. doi: 10.1039/c9lc00078j.

19. R. Renault, J. B. Durand, J. L. Viovy, and C. Villard. Asymmetric axonal edge guidance: a new paradigm for building oriented neuronal networks. *Lab Chip*, 16(12):2188–91, 2016. doi: 10.1039/c6lc00479b.

20. N. Winter-Hjelm, Å. B. Tomren, P. Sikorski, A. Sandvig, and I. Sandvig. Structure-function dynamics of engineered, modular neuronal networks with controllable afferent-efferent connectivity. *bioRxiv*, 2022. doi: https://doi.org/10.1101/2022.11.24.517848.

21. Y. S. Vakilna, W. C. Tang, B. C. Wheeler, and G. J. Brewer. The flow of axonal information among hippocampal subregions: 1. feed-forward and feedback network spatial dynamics underpinning emergent information processing. *Front. Neural Circuits*, 15, 2021. doi: https://doi.org/10.3389/fncir.2021.660837.

22. H. Yamamoto, S. Moriya, K. Ide, T. Hayakawa, H. Akima, S. Sato, S. Kubota, T. Tanii, M. Niwano, S. Teller, J. Soriano, and A. Hirano-Iwata. Impact of modular organization on dynamical richness in cortical networks. *Sci. Adv.*, 4(1), 2018. doi: 10.1126/sciadv.aau4914.

23. M. U. Park, Y. Bae, K.-S. Lee, J. H. Song, S. M. Lee, and K.-H. Yoo. Collective dynamics of neuronal activities in various modular networks. *Lab Chip*, 21:951––61, 2021. doi: 10.1039/d0lc01106a.

24. R. van de Wijdeven, O. H. Ramstad, U. S. Bauer, Ø. Halaas, A. Sandvig, and I. Sandvig. Structuring a multi-nodal neural network in vitro within a novel design microfluidic chip. *Biomed. Microdevices*, 20:9, 2018. doi: 10.1007/s10544-017-0254-4.

25. B. J. Dworak and B. C. Wheeler. Novel mea platform with pdms microtunnels enables the detection of action potential propagation from isolated axons in culture. *Lab Chip*, 9(3): 404–10, 2009. doi: 10.1039/b806689b.

26. I. Baruchi, V. Volman, N Raichman, M. Shein, and E. Ben-Jacob. The emergence and properties of mutual synchronizationinin vitrocoupled cortical networks. *Eur. J. Neurosci.*, 28(9):1825–35, 2008. doi: 10.1111/j.1460-9568.2008.06487.x.

27. M. Shein-Idelson, G. Cohen, E. Ben-Jacob, and Y. Hanein. Modularity induced gating and delays in neuronal networks. *PLoS Comput. Biol.*, 12(4):e1004883, 2016. doi: 10.1371/journal.pcbi.1004883.

28. N. M. van Strien, N. L. Cappaert, and M. P. Witter. The anatomy of memory: an interactive overview of the parahippocampal-hippocampal network. *Nat Rev Neurosci*, 10(4):272–82, 2009. ISSN 1471-003x. doi: 10.1038/nrn2614. 1471-0048 van Strien, N M Cappaert, N L M Witter, M P Journal Article Review England 2009/03/21 Cell Adhesion/physiology Cell Communication/*physiology Humans Memory/*physiology Nerve Net/*physiology.

29. H. Braak and E. Braak. Neuropathological stageing of alzheimer-related changes. *Acta Neuropathol*, 82(4):239–259, 1991. doi: 10.1007/bf00308809.

30. D. R. Thal, U. Rüb, M. Orantes, and H. Braak. Phases of a beta-deposition in the human brain and its relevance for the development of ad. *Neurology*, 58(12):1791–800, 2002. doi: https://doi.org/10.1212/wnl.58.12.1791.

31. K.A. Vossel, Beagle A. J., H. Rabinovivi, S. E. Shu, E. Lee, and G. et al. Naasan. Seizures and epileptiform activity in the early stages of alzheimer disease. *JAMA Neurol*, 70(9): 1158–66, 2013. doi: https://doi.org/10.1001/jamaneurol.2013.136.

32. D. W. McKeel Jr. J. C. Morris J. H. Growdon T. Gomez-Isla, J. L. Price and B. T. Hyman. Profound loss of layer ii entorhinal cortex neurons occurs in very mild alzheimer's disease. *J Neurosci*, 16(14):491–500, 1996. doi: PMCID:PMC6578866.

33. G. T. Stebbins S. T. DeKosky E. J. Cochran D. Bennett et al. J. H. Kordower, Y. Chu. Loss and atrophy of layer ii entorhinal cortex neurons in elderly people with mild cognitive impairment. *Ann Neurol*, 49(2):202–213, 2001. doi: PMID:11220740.

34. F. A. Schmitt S. T. DeKosky D. A. Price and E. J. Mufson. Hippocampal synaptic loss in early alzheimer's disease and mild cognitive impairment. *Neurobiol Aging*, 27(6), 2006. doi: 10.1016/j.neurobiolaging.2005.09.012.

35. F. A. Schmitt S. T. DeKosky S. W. Scheff, D. A. Price and E. J. Mufson. Synaptic alterations in ca1 in mild alzheimer disease and mild cognitive impairment. *Neurology*, 68(18):1501–8,

topology and different modes of presynaptic synchronization. *Cereb Cortex*, 24(7):1738–52, 2014. doi: 10.1093/cercor/bht022.

2007. doi: 10.1212/01.wnl.0000260698.46517.8f.

36. Y. Dong and G. J. Brewer. Global metabolic shifts in age and alzheimer's disease mouse brains pivot at nad+/nadh redox sites. *J Alzheimers Dis*, 71(1):119–140, 2019. ISSN 1387-2877 (Print) 1387-2877. doi: 10.3233/jad-190408.

37. Y. Dong, S. Sameni, M. A. Digman, and G. J. Brewer. Reversibility of age-related oxidized free nadh redox states in alzheimer's disease neurons by imposed external cys/cyss redox shifts. *Sci Rep*, 9(1):11274, 2019. ISSN 2045-2322. doi: 10.1038/s41598-019-47582-x.

38. Y. Dong, M. A. Digman, and G. J. Brewer. Age- and ad-related redox state of nadh in subcellular compartments by fluorescence lifetime imaging microscopy. *Geroscience*, 41 (1):51–67, 2019. ISSN 2509-2715 (Print) 2509-2723. doi: 10.1007/s11357-019-00052-8.

39. K. S Hanssen, M. P. Witter, A., I. Sandvig, and A. Kobro-Flatmoen. Dissection and culturing of adult lateral entorhinal cortex layer ii neurons from app/ps1 alzheimer model mice. *J. Neurosci. Methods*, 390, 2023. doi: https://doi.org/10.1016/j.jneumeth.2023.109840.

40. A. Ahluwalia. Alam M. T. Avey M. Baker et al. N. Percie du Sert, V. Hurst. The arrive guidelines 2.0: Updated guidelines for reporting animal research. *PLoS Biol*, 18(7):e3000410, 2020.

41. R. Radde, T. Bolmont, S. A. Kaeser, J. Coomaraswamy, D. Lindau, L. Stoltze, M. E. Calhoun, F. Jäggi, H. Wolburg, S. Gengler, C. Haass, B. Ghetti, C. Czech, C. Hölscher, P. M. Mathews, and M. Jucker. Abeta42-driven cerebral amyloidosis in transgenic mice reveals early and robust pathology. *EMBO Rep*, 7(9):940–6, 2006. ISSN 1469-221X (Print) 1469-221x. doi: 10.1038/sj.embor.7400784.

42. V. Partridge S. Allard M. T. Ferretti A. DeWilde et al. W. C. Leon, F. Canneva. A novel transgenic rat model with a full alzheimer's-like amyloid pathology displays pre-plaque intracellular amyloid-beta-associated cognitive impairment. *J Alzheimers Dis*, 20(1):113–26, 2010. doi: 10.3233/jad-2010-1349.

43. A. Nagelhus A. Kobro-Flatmoen and M. P. Witter. Reelin-immunoreactive neurons in entorhinal cortex layer ii selectively express intracellular amyloid in early alzheimer's disease. *Neurobiol Dis*, 93:172–83, 2016. doi: 10.1016/j.nbd.2016.05.012.

44. P. Kvello I. Heggland and M. P. Witter. Electrophysiological characterization of networks and single cells in the hippocampal region of a transgenic rat model of alzheimer's disease. *eNeuro*, 6(1), 2019. doi: 10.1523/eneuro.0448-17.2019.

45. D. Waters S. E. Counts S. E. Perez S. T. DeKosky et al. E. J. Mufson, L. Mahady. *Neuroscience*, 309:51–67, 2015. doi: 10.1016/j.neuroscience.2015.03.006.

46. G. W. Van Hoesen B. T. Hyman and A. R. Damasio. Alzheimer's disease: glutamate depletion in the hippocampal perforant pathway zone. *Ann Neurol*, 22(1):37–40, 1987. doi: 10.1002/ana.410220110.

47. K. N. Richter, N. H. Revelo, K. J. Seitz, M. S. Helm, D. Sarkar, R. S. Saleeb, E. D'Este, J. Eberle, E. Wagner, C. Vogl, D. F. Lazaro, F. Richter, J. Coy-Vergara, G. Coceano, E. S. Boyden, R. R. Duncan, S. W. Hell, M. A. Lauterbach, S. E. Lehnart, T. Moser, T. F. Outeiro, P. Rehling, B. Schwappach, I. Testa, B. Zapiec, and S. O. Rizzoli. Glyoxal as an alternative fixative to formaldehyde in immunostaining and super-resolution microscopy. *EMBO J.*, 37: 139–59, 2018. doi: 10.15252/embj.201695709.

48. J. C. Lansey. Beautiful and distinguishable line colors + colormap, 2022.

49. C. A. Brewer, G. W. Hatchard, and M. A. Harrower. Colorbrewer in print: A catalog of color schemes for maps. *Cartography and Geographic Information Science*, 30(1):5–32, 2003. doi: https://doi.org/10.1559/152304003100010929.

50. A. Maccione, M. Gandolfo, P. Massobrio, A. Novellino, S. Martinoia, and M. Chiappalone. A novel algorithm for precise identification of spikes in extracellularly recorded neuronal signals. *J. Neurosci. Methods*, 177(1):241–9, 2009. doi: 10.1016/j.jneumeth.2008.09.026.

51. B. Kraus. Spike raster plot, 2022.

52. L. L. Bologna, V. Pasquale, M. Garofalo, M. Gandolfo, P. L. Baljon, A. Maccione, S. Martinoia, and M. Chiappalone. Investigating neuronal activity by spycode multi-channel data analyzer. *Neural Networks*, 23(6):685–97, 2010. doi: 10.1016/j.neunet.2010.05.002.

53. M. Rubinov and O. Sporns. Complex network measures of brain connectivity: uses and interpretations. *NeuroImage*, 52(3):1059–69, 2010. doi: 10.1016/j.neuroimage.2009.10.003.

54. V. D. Blondel, J. L. Guillaume, R. Lambiotte, and E. Lefebvre. Fast unfolding of communities in large networks. *J. Stat. Mech. Theory Exp.*, 2008:P10008, 2008. doi: 10.1088/1742-5468/2008/10/P10008.

55. D. A. Wagenaar and S. M. Potter. Real-time multi-channel stimulus artifact suppression by local curve fitting. *J. Neurosci. Methods*, 120(2):113–20, 2002. doi: 10.1016/s0165-0270(02) 00149-8.

56. J. S. Weir, N. Christiansen, A. Sandvig, and I. Sandvig. Selective inhibition of excitatory synaptic transmission alters the emergent bursting dynamics of in vitro neural networks. *Front. Neural Circuits*, 2023. doi: 10.3389/fncir.2023.1020487.

57. K. Heiney, O. H. Ramstad, V. Fiskum, A. Sandvig, A. Sandvig, and S. Nichele. Neuronal avalanche dynamics and functional connectivity elucidate information propagation in vitro. *Front. Neural Circuits*, 16, 2022. doi: https://doi.org/10.3389/fncir.2022.980631.

58. J. Nunez. Differential expression of microtubule components during brain development. *Dev. Neurosci.*, 8(3):125–41, 1986. doi: https://doi.org/10.1159/000112248.

59. R. P. Tucker. The roles of microtubule-associated proteins in brain morphogenesis: a review. *Brain Res. Rev.*, 15(2):101–20, 1990. doi: https://doi.org/10.1016/0165-0173(90)90013-E.

60. A. Matus. Microtubule-associated proteins and neuronal morphogenesis. *J. Cell Sci.*, 15: 61–7, 1991. doi: https://doi.org/10.1242/jcs.1991.Supplement_15.9.

61. G. V. W. Johnson and R. S. Jope. The role of microtubule-associated protein 2 (map-2) in neuronal growth, plasticity, and degeneration. *J. Neurosci. Res.*, 33(4):505–12, 1992. doi: https://doi.org/10.1002/jnr.490330402.

62. M. A. Tischfield, H. N. Baris, C. Wu, G. Rudolph, L. Van Maldergem, W. He, W.-M. Chan, C. Andrews, J. L. Demer, R. L. Robertson, D. A. Mackey, J. B. Ruddle, T. D. Bird, I. Gottlob, C. Pieh, E. Traboulsi, S. L. Pomeroy, D. G. Hunter, J. S. Soul, A. Newlin, L. J. Sabol, E. J. Doherty, C. E. de Uzcátegui, N. de Uzcátegui, M. L. Z. Collins, E. C. Sener, B. Wabbels, H. Hellebrand, T. Meitinger, T. de Berardinis, A. Magli, C. Schiavi, M. Pastore-Trossello, F. Koc, A. M. Wong, A. V. Levin, M. T. Geraghty, M. Descartes, M. Flaherty, R. V. Jamieson, H. U. Møller, I. Meuthen, D. F. Callen, J. Kerwin, S. Lindsay, A. Meindl, M. L. Gupta, D. Pellman, and E. C. Engle. Human tubb3 mutations perturb microtubule dynamics, kinesin interactions, and axon guidance. *Cell*, 140(1):74–87, 2010. doi: https://doi.org/10.1016/j.cell.2009.12.011.

63. A. B. Oestreicher, P. N. E. De Graan, W. H. Gispen, J. Verhaagen, and L. H. Schrama. B-50, the growth associated protein-43: modulation of cell morphology and communication in the nervous system. *Prog. Neurobiol.*, 53(6):627–86, 1997. doi: https://doi.org/10.1016/S0301-0082(97)00043-9.

64. R. J. Mullen, C. R. Buck, and A. M. Smith. Neun, a neuronal specific nuclear protein in vertebrates. *J. Dev.*, 116(1):201–11, 1992. doi: 10.1242/dev.116.1.201.

65. W. W. Schlaepfer and J. Bruce. Simultaneous up-regulation of neurofilament proteins during the postnatal development of the rat nervous system. *J. Neurosci. Res.*, 25(1):39–49, 1990. doi: https://doi.org/10.1002/jnr.490250106.

66. L. F. Eng, R. S. Ghirnikar, and Y. L. Lee. Glial fibrillary acidic protein: Gfap-thirty-one years (1969–2000). *Neurochem. Res.*, 25:1439–51, 2000. doi: 10.1023/A: 1007677003387.

67. M. Shanahan. Dynamical complexity in small-world networks of spiking neurons. *Phys. Rev. E.*, 78(4), 2008. doi: https://doi.org/10.1103/PhysRevE.78.041924.

68. M. Rubinov, O. Sporns, J.-P. Thivierge, and M. Breakspear. Neurobiologically realistic determinants of self-organized criticality in networks of spiking neurons. *PLoS Comput. Biol.*, 7(6):e1002038, 2011. doi: https://doi.org/10.1371/journal.pcbi.1002038.

69. D. Meunier, R. Lambiotte, and E. T. Bullmore. Modular and hierarchically modular organization of brain networks. *Front. Neurosci.*, 4(200), 2010. doi: https://doi.org/10.3389/fnins.2010.00200.

70. M. A. Collings M. S. Evans and G. J. Brewer. Electrophysiology of embryonic, adult and aged rat hippocampal neurons in serum-free culture. *J Neurosci Methods*, 79(1):37–46, 1998. doi: 10.1016/s0165-0270(97)00159-3.

71. N. Bhargava M. Stancescu P. Molnar M. S. Kindy et al. K. Varghese, M. Das. Regeneration and characterization of adult mouse hippocampal neurons in a defined in vitro system. *J Neurosci Methods*, 177(1):51–9, 2009. doi: 10.1016/j.jneumeth.2008.09.022.

72. C. Marques de Freria K. Groeniger M. C. Marchetto S. Dupraz et al. E. A. van Niekerk, R. Kawaguchi. Methods for culturing adult cns neurons reveal a cns conditioning effect. *Cell Rep Methods*, 2(7):100255, 2022. doi: 10.1016/j.crmeth.2022.100255.

73. E. S. Nilssen, B. Jacobsen, G. Fjeld, R. R. Nair, S. Blankvoort, C. Kentros, and M. P. Witter. Inhibitory connectivity dominates the fan cell network in layer ii of lateral entorhinal cortex. *J Neurosci*, 38(45):9712–9727, 2018. ISSN 0270-6474 (Print) 0270-6474. doi: 10.1523/jneurosci.1290-18.2018.

74. H. A. Henning J. Reichwald M. Staufenbiel B. Sakmann et al. M. A. Busche, X. Chen. Critical role of soluble amyloid-β for early hippocampal hyperactivity in a mouse model of alzheimer's disease. *Proc Natl Acad Sci*, 109(22):8740–5, 2012. doi: 10.1073/pnas.1206171109.

75. E. Carbone A. Marcantoni, E. F. Raymond and H. Marie. Firing properties of entorhinal cortex neurons and early alterations in an alzheimer's disease transgenic model. *Pflugers Arch*, 466(7):1437–50, 2014. doi: 10.1007/s00424-013-1368-z.

76. VD. Valderhaug, OH. Ramstad, R. van de Wijdeven, K. Heiney, S. Nichele, A. Sandvig, and I Sandvig. Structural and functional alterations associated with the lrrk2 g2019s mutation revealed in structured human neural networks. *bioRxiv*, 2021. doi: https://doi.org/10.1101/2020.05.02.073726.

77. A. Bhattacharya, H. Desai, T. B. DeMarse, B. C. Wheeler, and G. J. Brewer. Repeating spatial-temporal motifs of ca3 activity dependent on engineered inputs from dentate gyrus neurons in live hippocampal networks. *Front. Neural Circuits*, 10, 2016. doi: https://doi.org/10.3389/fncir.2016.00045.

78. D. Poli, S. Thiagarajan, T. B. DeMarse, B. C. Wheeler, and G. J. Brewer. Sparse and specific coding during information transmission between co-cultured dentate gyrus and ca3 hippocampal networks. *Front. Neural Circuits*, 11, 2017. doi: https://doi.org/10.3389/fncir.2017.00013.

79. D. Poli, B. C. Wheeler, T. B. DeMarse, and G. J. Brewer. Pattern separation and completion of distinct axonal inputs transmitted via micro-tunnels between co-cultured hippocampal dentate, ca3, ca1 and entorhinal cortex networks. *J. Neural Eng.*, 15, 2018. doi: 10.1088/1741-2552/aabc20.

Hanssen & Winter-Hjelm *et al.* | June 26th, 2023

Supplementary Materials

Table S1 | Overview of media supplement compositions in different protocols used throughout the study.

Protocol 1	Protocol 2	Protocol 3	Protocol 4	Protocol 5	Protocol 6
NPM	NPM	NPM	NPM	NPM	NPM
0.2 % B27+	0.2 % B27+	0.2 % B27+	0.2 % B27+	0.2 % B27+	0.2 % B27+
0.025 GlutaMAX	0.025 GlutaMAX	0.025 GlutaMAX	0.025 GlutaMAX	0.025 GlutaMAX	0.025 GlutaMAX
0.001 % BDNF	5 ng/mL FGF2	10 ng/mL FGF2	10 ng/mL FGF2	0.001 % BDNF	10 ng/mL FGF2
0.01 % Penstrep	0.01 % Penstrep	0.01 % Penstrep	10 ug/mL Gentamycin	0.01 % Penstrep	0.01 % Penstrep
0.001 % RI	0.001 % RI	0.001 % RI	0.00 % RI	0.001 % RI	0.001 % RI
0.1 % FBS	0.1 % FBS	0.1 % FBS	0.0 % FBS	0.1 % FBS	0.1 % FBS

NPM; Neurobasal Plus Medium (Thermo Fischer Scientific. B27+; B27 Plus Supplement (Thermo Fischer Scientidic). BDNF; Brain Derived Neurotrophic Factor (Thermo, Catnr). FGF2; F Growth Factor 2 (Thermo, Catnr). PS; Penicillin-Streptomycin (Catnr, Prod). GlutaMAX Supplement (Prod, Catnr). RI; Rock Inhibitor (Prod, catnr). FBS; Fetal Bovine Serum (Prod, catnr).

Table S2 | Overview of animals in the study.

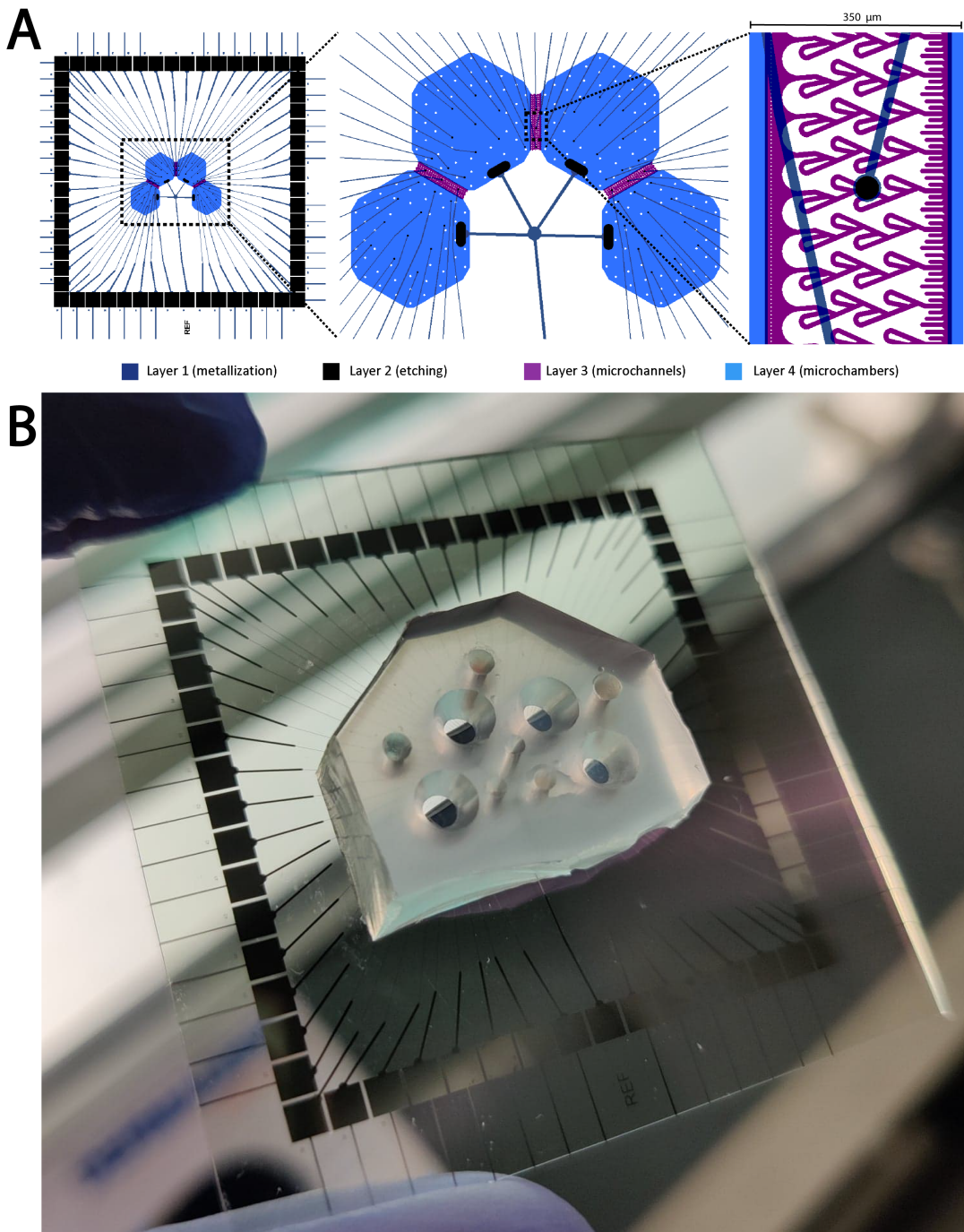| Animal model	Number	Sex	Age	Genotype
McGill-R-Thy1-APP rat	5	M	P38-P89	Heterozygote +/-
McGill-R-Thy1-APP rat	4	M	P46-P53	Homozygote -/-
McGill-R-Thy1-APP rat	12	M	P43-P78	Homozygote +/+
McGill-R-Thy1-APP rat	14	F	P39-P81	Heterozygote +/-
McGill-R-Thy1-APP rat	1	F	P53	Homozygote -/-
McGill-R-Thy1-APP rat	7	F	P37-P72	Homozygote +/+
APP/PS1 mouse	2	F	P79-P80	APP/PS1 +/-

Figure S1 | CAD design of the Microfluidic MEAs. (A.) The microfluidic design with $350\,\mu m$ Tesla-valve channels. Layer 1 represents the design for the metallization (i.e. forming the microelectrodes and corresponding contact pads), layer 2 the etch mask for etching through the passivation layer, layer 3 the mold for the microfluidic channels and layer 4 the mold for the cell compartments. **(B.)** A four-nodal microfluidic chip interfaced with a MEA.
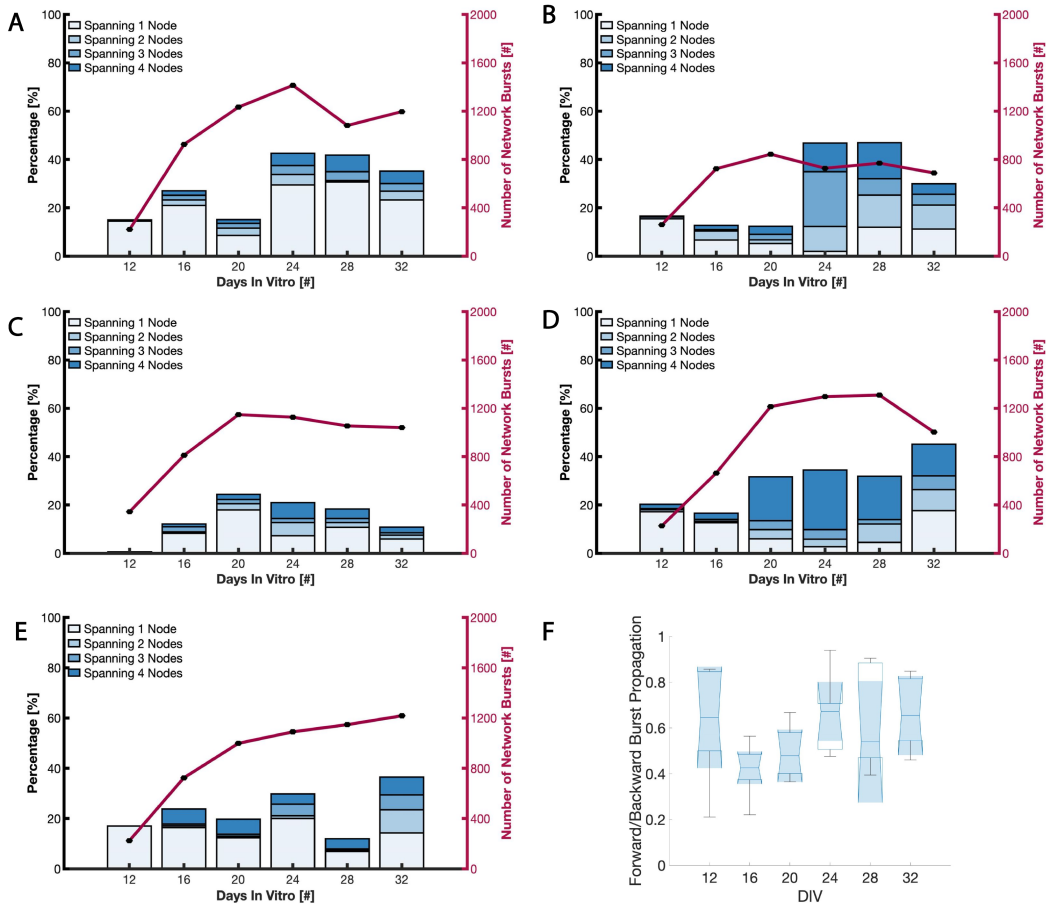
Hanssen & Winter-Hjelm *et al.* | June 26th, 2023

Figure S2 | Network bursts spread through an increasing number of nodes with time. (A.-B.) Histograms showing the percentage of spontaneously evoked network bursts initiated within the cortical population, and the number of nodes they span. Each subfigure represents the activity from a single MEA. The total number of network bursts initiated at each DIV is shown along the secondary y-axis. **(F.)** Box plot showing the fraction of bursts propagating in the forward versus backward direction between the four nodes.
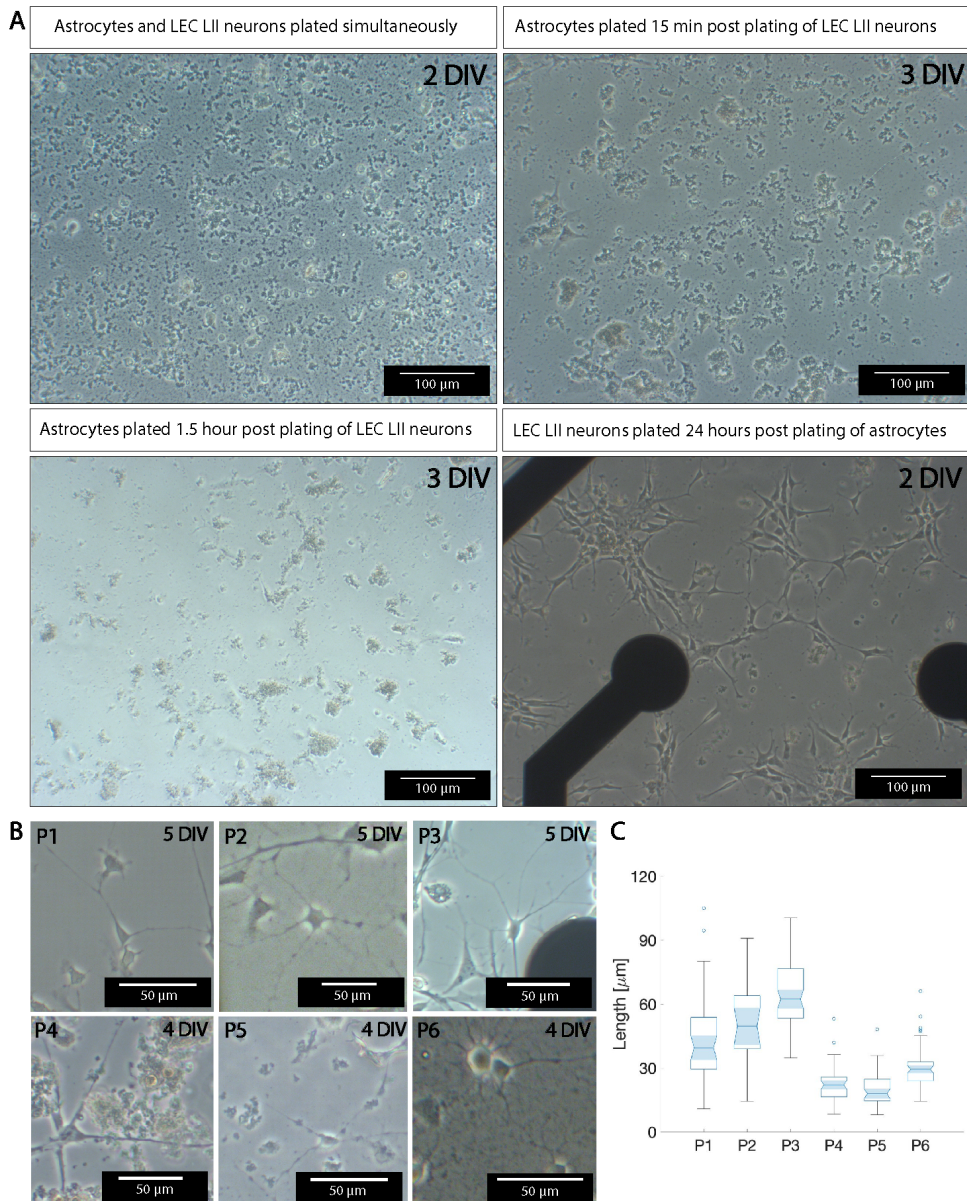
Figure S3 | Importance of an astrocytic monolayer and media supplement combination. (A.) Phase contrast images of astrocytes and LEC LII neurons plated simultaneously (top left), astrocytes plated 15 min post plating of LEC LII neurons (top right), astrocytes plated 1.5 hour post plating of LEC LII neurons (bottom left) and LEC LII neurons plated 24 hours post plating of astrocytes (bottom right). **(B.)** Phase contrast images of cultured neurons on six different media supplement protocols and a bar graph showing the mean neurite length for each culture at 5 or 4 DIV. A total of 285 neurites were measured.

Hanssen & Winter-Hjelm *et al.* | June 26th, 2023
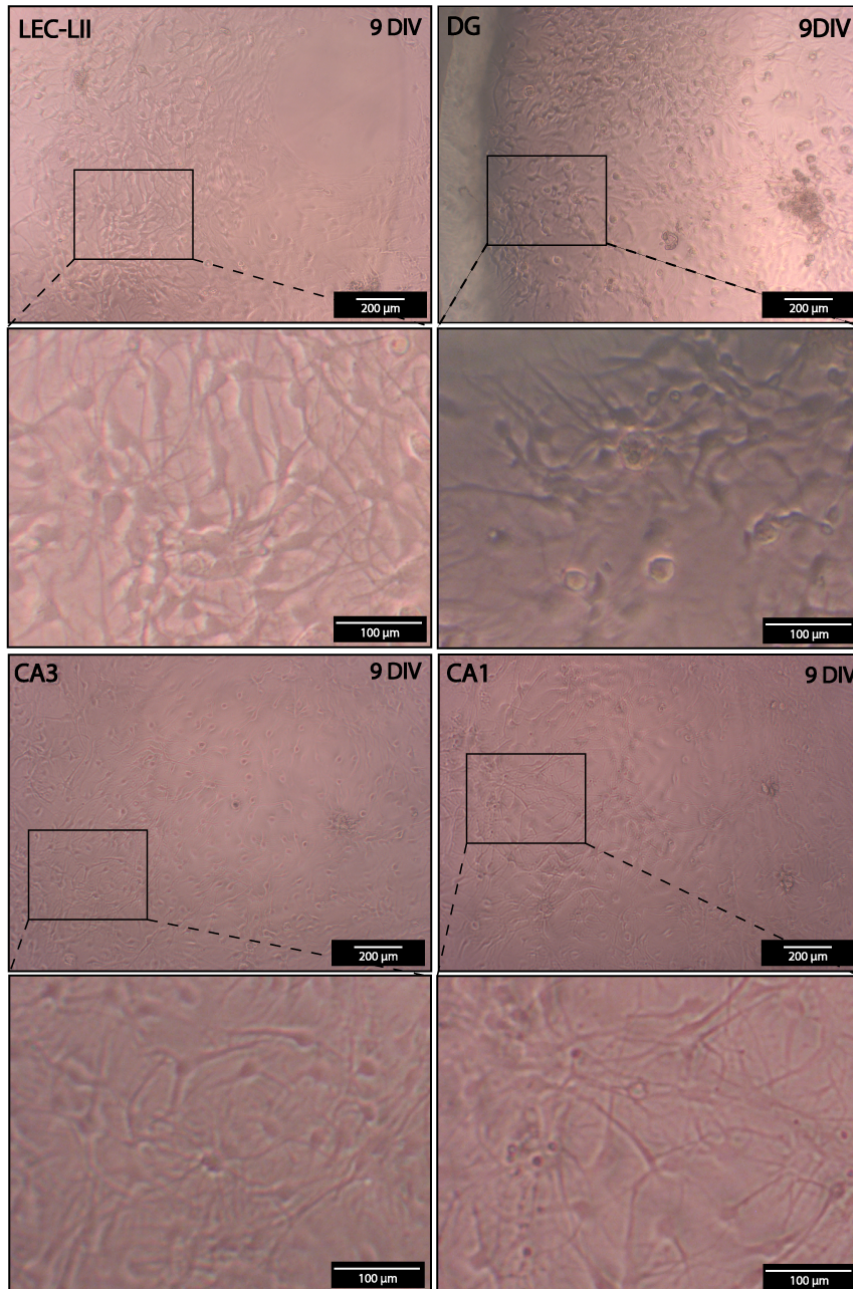
Figure S4 │ Adult mouse neurons reform structural connections in vitro. Phase-contrast images of adult neurons from the APP/PS1 mouse model at 9 DIV. LEC LII; lateral entorhinal cortex layer II. DG; dentage gyrus. CA3/CA1; cornu ammonis 3/1. DIV; days in vitro.
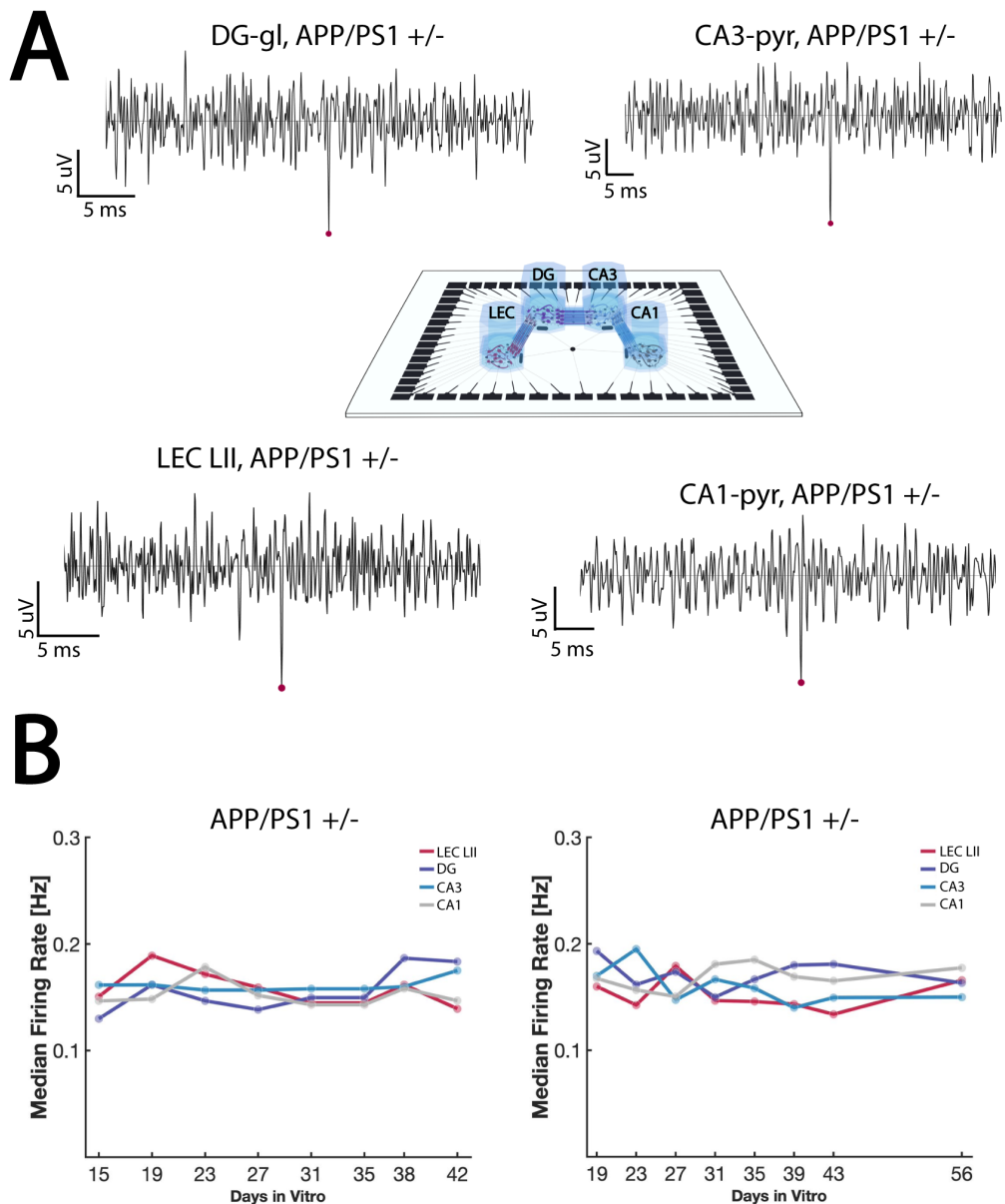
Figure S5 | Adult mouse neurons obtain electrophysiological activity in vitro. (A.) Simplified figure of the 4-nodal mMEA with spike traces showing one detected spike from each region (LEC LII, DG, CA3 and CA1). **(B.)** Graph of median firing rate (Hz) from 15 to 42 DIV (left) and 15 to 56 DIV (right). mMEA; microfluidic microelectrode array. LEC LII; lateral entorhinal cortex layer II. DG-gr; dentate gyrus granular. CA3-pyr/CA1-pyr; Cornu ammonis 1/3 pyramidal).

Paper III

Altered structural organization and functional connectivity in feedforward neural networks after induced perturbation

Janelle S. Weir[1]*, Katrine Sjaastad Hanssen[1,2]*, Nicolai Winter-Hjelm[1], Axel Sandvig[1,3], Ioanna Sandvig[1]

[1]Department of Neuromedicine and Movement Science, Faculty of Medicine and Health Sciences, Norwegian University of Science and Technology (NTNU), Trondheim, Norway
[2] Kavli Institute for Systems Neuroscience, NTNU, Trondheim, Norway
[3] Department of Neurology and Clinical Neurophysiology, St Olav´s University Hospital, Trondheim, Norway

*These authors share first co-authorship
Correspondence: janelle.s.weir@ntnu.no, katrine.s.hanssen@ntnu.no , ioanna.sandvig@ntnu.no

Abstract

Reciprocal structure–function relationships underly both healthy and pathological behaviors in complex neural networks. Neuropathology can have widespread implications on the structural properties of neural networks, and drive changes in the functional interactions among network components at the micro- and mesoscale level. Thus, understanding network dysfunction requires a thorough investigation of the complex interactions between structural and functional network reconfigurations in response to perturbation. However, such network reconfigurations at the micro- and mesoscale level are often difficult to study *in vivo*. For example, subtle, evolving changes in synaptic connectivity, transmission, and electrophysiological shift from healthy to pathological states are difficult to study in the brain. Engineered *in vitro* neural networks are powerful models that enable selective targeting, manipulation, and monitoring of dynamic neural network behavior at the micro- and mesoscale in physiological and pathological conditions. In this study, we first established feedforward cortical neural networks using in-house developed two-nodal microfluidic chips with controllable connectivity interfaced with microelectrode arrays (mMEAs). We subsequently induced perturbations to these networks by adeno-associated virus (AAV) mediated expression of human mutated tau in the presynaptic node and monitored network structure and activity over three weeks. We found that induced perturbation in the presynaptic node resulted in altered structural organization and extensive axonal retraction starting in the perturbed node. Perturbed networks also exhibited functional changes in intranodal activity, which manifested as an overall decline in both firing rate and bursting activity, with a progressive increase in synchrony over time. We also observed impaired spontaneous and evoked internodal signal propagation between pre- and postsynaptic nodes in the perturbed networks. These results provide novel insights into dynamic structural and functional reconfigurations in engineered feedforward neural networks as a result of evolving pathology.

1.   Introduction

An understanding of dynamic structure-function relationships in neural networks in health and disease remains a subject of intense investigation. Such dynamics involve micro- and mesoscale level interactions over different temporal scales. Mechanisms that drive the reciprocal relationship between network structure and function involve Hebbian and homeostatic plasticity working in tandem. These plasticity mechanisms influence pre- and postsynaptic connectivity Henderson and Gong (Henderson et al., 2018), excitatory – inhibitory synaptic transmission (Moore et al., 2018), and hierarchical processing between different areas of the network (Rubinov et al., 2009; Yamamoto et al., 2018). These mechanisms are also inextricably linked both physiologically and pathophysiologically. This means that perturbation within one part of the network can progressively spread and impact other parts through axonal and/or synaptic connections. Furthermore, network impairment may evolve over a long period of time without overt manifestation of dysfunction (Fornito et al., 2015). For example, in neurological diseases which significantly impact the structural and functional integrity of the network, such as Alzheimer's disease (AD), relevant network reconfigurations due to evolving pathology (Katsuno et al., 2018) tend to occur over a long period of time before the emergence of clinical symptoms, by which point, the network has undergone considerable, irreversible damage (reviewed in (Tarawneh et al., 2012).

One of the main structural pathological hallmarks of AD is the accumulation of neurofibrillary tangles in the brain as a result of the hyperphosphorylation of the microtubule associated protein tau (Braak et al., 1991). Tau proteins are mainly found in the axons of neurons and, under physiological conditions, (Götz et al., 2019) they enrich microtubules to promote their assembly in axons (Baas et al., 2019; Qiang et al., 2018). However, under pathological conditions, tau becomes hyperphosphorylated, causing widespread morphological disruption in axons (Jackson et al., 2017; Kopeikina et al., 2013), ultimately affecting synaptic transmission and network function. The high interconnectivity of the brain also implies that neuronal axons and synapses may act as conduits for the spread of such pathology from affected areas, causing progressive, widespread disruption to the structural and functional integrity of the network (Kuhl, 2019). It has also been shown that hyperphosphorylated tau triggers hypoactivity in neurons (Ittner et al., 2011; Menkes-Caspi et al., 2015; Polanco et al., 2018; Wang et al., 2017), thus disturbing excitatory-inhibitory balance, and disrupting synaptic transmission and global integration across the network.

To elucidate how relevant pathological mechanisms gradually affect the structure and function of neural networks, it is imperative to study the underlying processes at the micro- and mesoscale. Such investigations are highly challenging, or de facto not feasible *in vivo* due to the size and complexity of

the brain. This challenge can be overcome with the application of advanced cellular models based on engineered neural networks. Such networks develop with progressively increasing structural and functional complexity over time, essentially recapitulating fundamental aspects of neural network behavior as seen in the brain (Collingridge et al., 2010; Valderhaug et al., 2021; van de Wijdeven et al., 2019; Winter-Hjelm N, 2023). Engineered *in vitro* models thus enable longitudinal studies of dynamic network behavior and allow for selective perturbation and monitoring of network responses at the micro- and mesoscale level (Bauer et al., 2022; Bruno et al., 2020; Fiskum et al., 2021; Gribaudo et al., 2019; Nonaka et al., 2011; Valderhaug et al., 2021; Weir et al., 2023).

In the present study, we longitudinally investigated structural and functional changes in engineered two-nodal feedforward cortical neural networks, following induced expression of human mutated tau in the presynaptic nodes. Our primary aim was to longitudinally monitor and identify dynamic changes in neurite organization and electrophysiological activity of networks with evolving perturbation and compare this with control unperturbed networks. The two-nodal feedforward configuration of the engineered network enabled us to observe structural and functional reconfigurations in response to the perturbation in the affected node, while simultaneously monitoring dynamic changes in the postsynaptic node. Our results demonstrate that prior to perturbation, all neural networks developed increasingly robust firing and bursting activity within the nodes. They had also developed prominent structural connections, and functional internodal connections with spontaneous and evoked feedforward burst propagation from the presynaptic to postsynaptic nodes. However, within four days of inducing perturbation by expression of human mutated tau in the presynaptic node, internodal connectivity was disrupted, manifested as progressive retraction of neurites from the entry zone near microtunnels in the presynaptic node, followed by retraction of neurites from the exit zones near the microtunnels towards the postsynaptic nodes. Neurite retraction persisted over a span of 3 weeks, during which period we observed a concomitant significant reduction in the overall intranodal mean firing rate, mean burst rate, and total number of bursts. Such structural or functional changes were not observed in control unperturbed networks. Furthermore, the neurite retraction and overall decrease in activity in the perturbed networks occurred simultaneously with a significant increase in network synchrony. Increased synchrony over time was not observed in control unperturbed networks. These results provide new insights into dynamic micro- and mesoscale network reconfigurations in response to induced perturbations and illustrate the utility of engineered feedforward neural networks as models of network function and dysfunction.

2.   Methods

2.1.   *In vitro* neural networks

An experimental timeline can be found in **Figure 1**. For this study, we used in-house developed microfluidic chips interfaced with microelectrode arrays (mMEAs; n=7) and 8-well chambered slides (Ibidi, 80841; n=2). Design and fabrication of the mMEAs was conducted as reported previously by our group (Winter-Hjelm N, 2023). Briefly, two compartments (from here on referred to as nodes) (5 mm wide/60 µm high) were connected by 20 microtunnels (700 µm long/10 µm wide/5 µm high) designed to promote unidirectional axonal outgrowth from the presynaptic to the postsynaptic node. Tesla valve microtopographies were included in the microchannels to redirect axons from the postsynaptic node back to their chamber of origin. Furthermore, axon traps were included on the postsynaptic side to misguide outgrowing axons and prevent them from entering the microtunnels. To prevent neuronal somata from entering the microtunnels, 4 µm pillars with 4 µm interspacing were positioned within the presynaptic node. This design promotes formation of feedforward networks by aiding axon outgrowth from the presynaptic node, but not vice versa. Impedance measurements and sterilization of the mMEAs were conducted as reported previously (Winter-Hjelm N, 2023). Prior to seeding, nodes were coated with 0.1 mg/mL Poly-l-Ornithine (PLO; Sigma-Aldrich, #P4957) for 30 min, subsequently replenished with fresh PLO for another 2h at 37°C/5% CO_2. Following this, all PLO was discarded, and the surfaces rinsed three times with distilled Milli-Q-water. Subsequently, the platforms were coated with laminin solution consisting of 16 µg/mL Mouse Natural Laminin (Gibco, #23017015) diluted in PBS (Sigma-Aldrich, D8537) for first 30 min, before being replenished with fresh laminin solution for another 2 h at 37°C/5% CO_2. To ensure proper flow of coating solution through the microtunnels, a hydrostatic pressure gradient was applied during all coating steps. Laminin solution was discarded and replaced by astrocyte media consisting of DMEM (Gibco™, 11885084) supplemented with 15% Fetal Bovine Serum (Sigma-Aldrich, F9665) and 2% Penicillin-Streptomycin (Sigma-Aldrich, #P4333) for 10 min at 37°C/5% CO_2 before rat primary cortical astrocytes (Gibco, #N7745100) were plated at a density of 100 cells/mm² 48 hours prior to plating of neurons Subsequently, rat primary cortical neurons (Gibco, #A1084001) were plated at a density of 1,000 cells/mm² in neuronal media consisting of Neurobasal Plus Medium (Gibco™, A3582801) supplemented with 2% B27 Plus Medium (Gibco™, A358201), 2.5 mL/L Gluta-Max (Gibco™, 35050038) and 1% Penicillin-Streptomycin (Sigma-Aldrich, P4333). 4 and 24 hours after plating the neurons, 90% of the media was replenished. Thereafter, 50% of the media was replenished every 2 days.
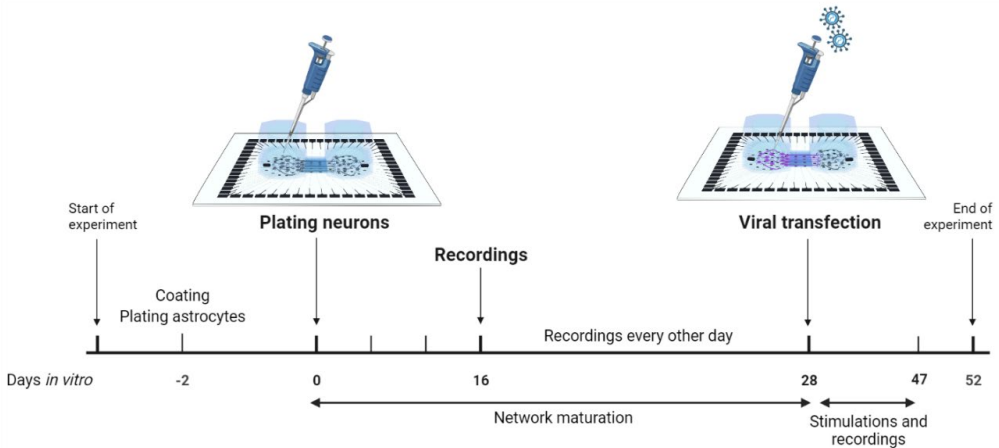
Figure 1. Schematic of the *in vitro* experimental timeline for establishing networks, transduction, and electrophysiological recordings. *Created with BioRender.com.*

2.1.1. AAV8 – GFP – 2A P301L Tau production and *in vitro* transduction

The viral vector was kindly gifted by Dr. Christiana Bjørkli (Department of Neuromedicine and Movement Science, NTNU). Adeno associated virus (AAV) vector production and purification was performed in-house at the Viral Vector Core Facility (Kavli Institute for Systems Neuroscience, NTNU). Tittering of the viral stock was determined as approximately 10^{11} vg/mL. Viral particles encoding experimental AAV8 P301L mutated tau were introduced to healthy networks at 28 DIV to induce perturbation. At 28 DIV, neurons were transduced by removing 70% of the cell media from the presynaptic nodes and directly adding 3×10^2 viral units per neuron diluted in cell media. After addition of the virus, the cultures were gently agitated for 30 s to ensure proper distribution of the viral particles and then incubated for 4 h. The titer of viral particles per neuron was decided after extensive tests of different concentrations. Afterwards, each well was topped up with fresh media without antibiotics and incubated for an additional 20 h at 37°C/5% CO_2. After the incubation period, 50% changes of the media were carried out as scheduled. To ensure comparable conditions with the control networks, an 80% media change was also conducted in the control unperturbed networks at the same time as the addition of AAV P301L to the perturbed networks. The viral vector encoded a GFP fluorescent tag for easy visualization of transduction efficiency.

2.2. Immunocytochemistry

To confirm network maturity including expression of phosphorylated tau (pTau) within the perturbed neural networks, immunocytochemistry (ICC) was performed at 22 DIV, as follows. Prior to immunostaining, cell media were aspirated and discarded from the culture plates, and the cultures were rinsed once with Dulbecco's Phosphate Buffered Saline (DPBS; Thermo Fischer Scientific, Cat

#14040-117). Following this, networks were fixed with 4% Paraformaldehyde (Sigma-Aldrich, #P6148) for 10 min at room temperature followed by 3x10 min washes with DPBS. Further, all DPBS were discarded and replaced by blocking solution consisting of 5% Goat serum (Sigma-Aldrich, Cat# G9023) and 0.3% Triton-X (Thermo Fischer Scientific, Cat# 85111) in DPBS. Next, primary antibodies at the indicated concentration (**Table 1**) were added in a buffer of 0.01% Triton-X and 1% Goat Serum in DPBS overnight at 4°C. The following day, primary antibody solution was discarded, and cultures were rinsed 3x5 min with DBPS before secondary antibodies at the indicated concentration (**Table 1**) were added in a buffer of 0.01% Triton-X and 1% Goat Serum in DPBS for 2 h at room temperature. For staining cellular nuclei, Hoechst dye (bisbenzimide H 33342 trihydrochloride; Sigma-Aldrich, Cat# 14533) was added at 1:10.000 dilution for the last 10 min of the secondary antibody incubation. Samples from the 8-well Ibidi chips were washed with PBS, mounted on glass cover slides with anti-fade fluorescence mounting medium (Abcam, Cat#Ab104135) whereas microfluidic chips were filled with distilled Milli-Q-water before imaging.

Table 1. List of primary and secondary antibodies with concentrations

Primary antibodies	Concentration	Supplier
Ck Map2	1:1000	Abcam, #Ab5392
Rb Phospho-Tau (Thr217) (pTau)	1:1000	Invitrogen, #44-744
Ms AT8 (Ser202/205)	1:1000	Invitrogen, #MN1020
Rb GAD65/67	1:100	Abcam, #Ab183999
Ms Calmodulin (CaMKIIa)	1:200	Invitrogen, #MA3-918
Rb GFAP	1:500	Abcam, #Ab278054
Secondary antibodies	**Concentration**	**Supplier**
Goat-Anti-Mouse Alexa Fluor 674	1:1000	Invitrogen, #A21236
Goat-Anti-Rabbit Alexa Fluor 488	1:1000	Invitrogen, #A21244
Goat-Anti-Chicken Alexa Fluor 568	1:1000	Abcam, #Ab175477

Ms: Mouse, Rb: rabbit, Ck: chicken.

2.2.1 Imaging

All samples from ICC were imaged using an EVOS M5000 microscope (Thermo Fischer Scientific, #AMF5000) connected to a LED light source and using an Olympus 20x/0.75 NA objective (N1480500), with the following filter sets/channels: DAPI (AMEP4650), CY5 (AMEP4656), GFP (AMEP4651) and TxRed (AMEP4655). Phase contrast images were taken using a Zeiss Axio Vert V.1 brightfield 20x/53 WD/0.4 NA objective with an Axiocam 202 mono. Images were processed using Adobe Photoshop 2020. To quantify for fluorescent intensity profile of AT8 and pTau in cell body clusters and axonal bundles in both perturbed and control unperturbed networks, fluorescent signal was measured in Fiji/ImageJ2. A total of six clusters of cell bodies and five axonal bundles were selected as regions of interest. Assessment was done for total fluorescent signal (mean intensity/pixel) measured by mean grayscale.

2.3. Electrophysiological recordings

Electrophysiological activity of neural networks on mMEAs (n=7) was recorded using a MEA2100 recording system (Multichannel Systems, MCS, Reutlingen, Germany) at a sampling rate of 25,000 Hz. A 3D-printed in-house made plastic cap covered by a gas-permeable membrane was used to keep the cultures sterile during recordings. The stage temperature was set to 37°C (TC01, Multichannel Systems) and the cultures were allowed to equalize on the stage for 5 min before spontaneous electrophysiological activity was recorded for 15 min. All networks were recorded 24 h after media changes on the following days *in vitro* (DIV): 16, 20, 24, 26, 28, 31, 33, 35, 37, 39, 41, 43, 45 and 47. From 28 DIV onwards, networks were electrically stimulated and simultaneously recorded for 1 minute (directly following the 15 min recordings of spontaneous electrophysiological activity). Electrical stimulations were applied to one presynaptic electrode with the highest detected mean firing rate [21] during the 15 min recording. Stimulation consisted of a train of 60 spikes at ± 800 mV (positive phase first) of 200 µs duration with an interspike interval of 5s. This was according to previous studies demonstrating that persistent electrical stimulation in *in vitro* networks can increase network activity over time, resulting in enhanced evoked action potentials and an increased frequency of spikes in bursts (Brewer et al., 2009; Ide et al., 2010). Raw data was converted to an .h5 Hierarchical Data Format using Multichannel DataManager (V.1.14.4.22018) system and imported to Matlab R2021b for further analyses using adapted and custom-made scripts.

2.4.   Data analysis

Electrophysiology data analysis was done as previously described (Winter-Hjelm N, 2023). Briefly, raw data was filtered using a 4th order Butterworth bandpass filter removing low frequency fluctuations below 300 Hz and high frequency noise above 3000 Hz. A notch filter was used to remove 50 Hz noise caused by the power supply mains. Stimulation data was filtered using the SALPA filter (Wagenaar et al., 2002), and each stimulation time point was followed by 15 ms blanking. Spike detection was conducted using the Precise Timing Spike Detection (PTSD) algorithm (Maccione et al., 2009) with a threshold of 11 times the standard deviation, a maximum peak duration set to 1 ms and a refractory period of 1.6 ms. Burst detection was conducted using the logISI approach (Pasquale et al., 2010), with a minimum of four consecutive spikes set as a minimum for a burst to be detected, and a hard threshold of 100 ms. Network bursts were detected using the logIBEI approach (Pasquale et al., 2010), with at least 20% of active electrodes required to participate during the span of a network burst. Network synchrony was measured using the coherence index (Timme et al., 2018).

2.5   Statistical analysis

SPSS version 29.0.0.0 was utilized for all statistical analyses. For comparison of the repeated measures, we used Generalized Linear Mixed-Effect Models (GLMMs) with network type (i.e., controls versus perturbed networks) as a fixed effect, and the network characteristics as targets. The network age (DIV) was used as a random effect. Only data from 31 DIV onwards were included in the analysis to specifically compare changes in network characteristics following perturbation to the control unperturbed networks. A gamma probability distribution with a log link function was chosen as the linear model. This selection was based on the Akaike information criterion and initial assessment of distribution fit to the predicted values. For multiple comparisons, we used sequential Bonferroni adjustment.

3.   Results

3.1.   Engineered feedforward cortical networks show intra- and internodal connectivity

Prior to perturbation, we wanted to validate that neurons were structurally connected with each other within the nodes and expressed markers for excitatory and inhibitory synaptic transmission. Our results showed that the engineered neural networks organized into densely interconnected intranodal architectures, with outgrowing neurites in the microtunnels **(Figure 2A and B).** Additionally, immunocytochemistry performed at 22 DIV revealed expression of the microtubule-associated protein 2 marker, MAP2 **(Figure 2C and D)**, the inhibitory neuronal marker glutamic acid decarboxylase 65/67, (GAD65/67) (Fukuda et al., 1997) **(Figure 2C)**, and the excitatory neuronal marker calcium-calmodulin (CaM) – dependent protein kinase II, (CaMKII) (Takao et al., 2005) **(Figure 2D)**. The presence of these markers indicated that the networks consisted of mature neurons with the capacity for excitatory and inhibitory synaptic transmission, a crucial aspect for achieving structural and functional network maturity.

To investigate whether the engineered networks were functionally connected, we monitored and recorded electrophysiological activity commencing at 16 DIV. By 26 DIV, the neural networks displayed a mature electrophysiological profile in line with previous studies [19] (Chiappalone et al., 2006; Winter-Hjelm N, 2023). Specifically, raster plots of spontaneous activity within the network revealed both isolated spikes and synchronized bursts **(Figure 3A)**, while correlation matrices of network connectivity showed strong connectivity within pre- and postsynaptic nodes, as well as functional connectivity between the nodes **(Figure 3B)**. To further validate internodal connectivity, we applied electrical stimulations to the electrode with the highest firing rate within the presynaptic node at 26 DIV. We recorded and assessed the evoked activity in the postsynaptic node, which revealed that electrical stimulations caused a spiking response in the presynaptic node, followed by an on average 40 ms time delay before a subsequent spiking response was observed in the postsynaptic node **(Figure 3C)**. This effectively demonstrated that functional connectivity was established between the- pre and postsynaptic nodes.
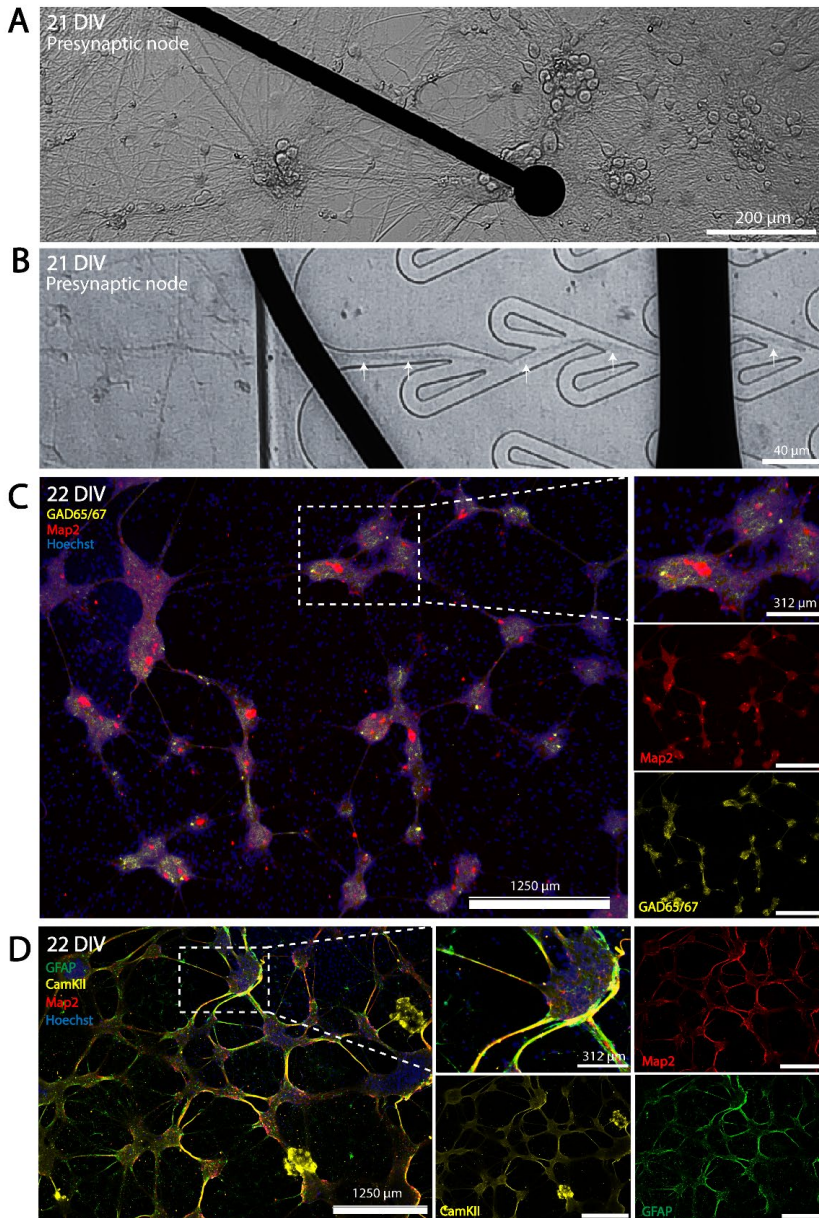
9

Figure 2. Developing structural organization and functional maturity of feedforward engineered neural networks (A-B) Phase contrast images of a neural network in the presynaptic node **(A)** with neurite projections going through the microtunnels **(B)** on a mMEA at 21 DIV. **(C-D)** Networks positively immunolabeled for the neuronal marker MAP2 in addition to the inhibitory marker GAD65/67 **(C)** and the excitatory neuron marker CaMKII **(D).** Glial fibrillary acidic protein (GFAP) antibody labelling of astrocytes in the network. DIV; days in vitro. Scale bar 1250 µm; (magnified area 312 µm).
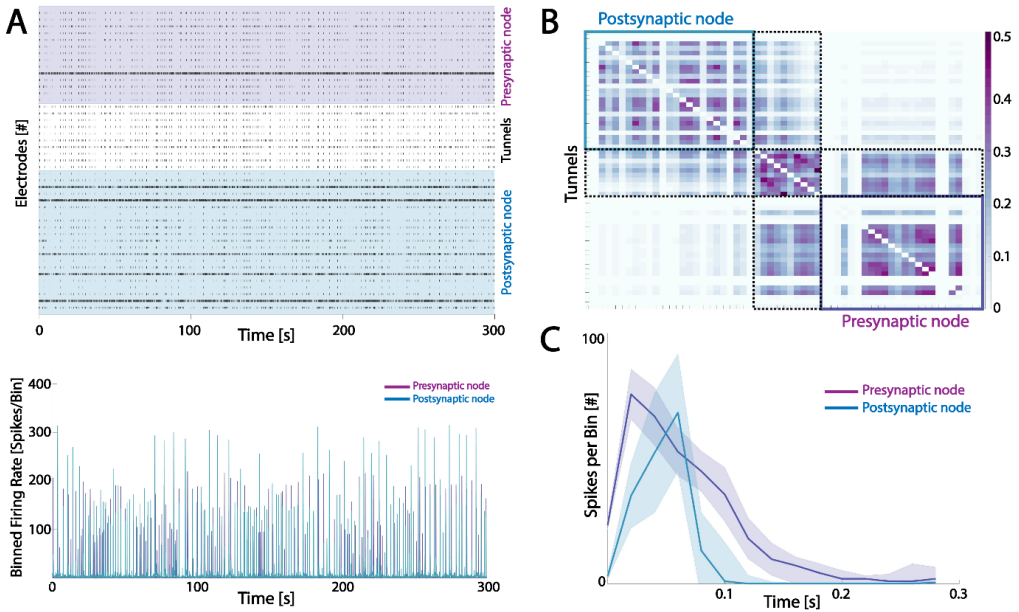
Figure 3. Neural networks displayed intra- and internodal functional connectivity at 26 DIV (A) Raster plots (300 seconds) of the recorded activity (top panel) and binned network activity (bottom panel) of corresponding total firing rate of one representative network. **(B)** Mutual information connectivity matrix showing the correlation in the network activity in nodes and tunnels. **(C)** Peristimulus time histogram of the pre- and postsynaptic response to an electrical stimulation in the presynaptic node. The graphs here show an initial response in the presynaptic node, followed by a delayed response in the postsynaptic node.

3.2. Perturbed networks express human mutated tau

At 28 DIV, we induced expression of human mutated tau protein in the presynaptic nodes of the engineered networks. The AAV construct encodes GFP, which allowed for easy visualization of transduction efficacy. Positive GFP expression was seen in the perturbed networks **(Figure 4B and Figure 5B)** which indicated effective AAV transduction. For additional verification of phosphorylated tau expression, we also labeled the networks for AT8 (Serine 202 and Threonine 205/ tau[202/205]) and Phospho-Tau (Threonine 217/tau[217]) proteins, hereon referred to as tau[202/205] and tau[217], respectively. Both tau[202/205] **(Figure 4B)** and tau[217] **(Figure 5B)** were overexpressed in neuronal cytosols and axons along with GFP in perturbed networks. Healthy networks had higher fluorescent signal for tau[202/205] (Vale et al., 2010) in axonal bundles than perturbed networks, but lower fluorescent signal for tau[217] in axonal bundles **(Figure 6)**. However, perturbed networks had significantly higher expression of both tau[202/205] and tau[217] (Rajbanshi et al., 2023) in the cytosolic compartments compared to controls, while high expression of tau[202/205] was found in axon bundles. Additionally, we conducted primary exclusion immunolabeling for both tau[202/205] and tau[217] to assess the specificity of the binding antigen, and no

expression was found **(Figure 4C and 5C respectively)**. We also performed secondary antibody exclusion to assess the labeling specificity of the primary antibody and found no immunoexpression for either tau$^{202/205}$ or tau^{217} in the networks.
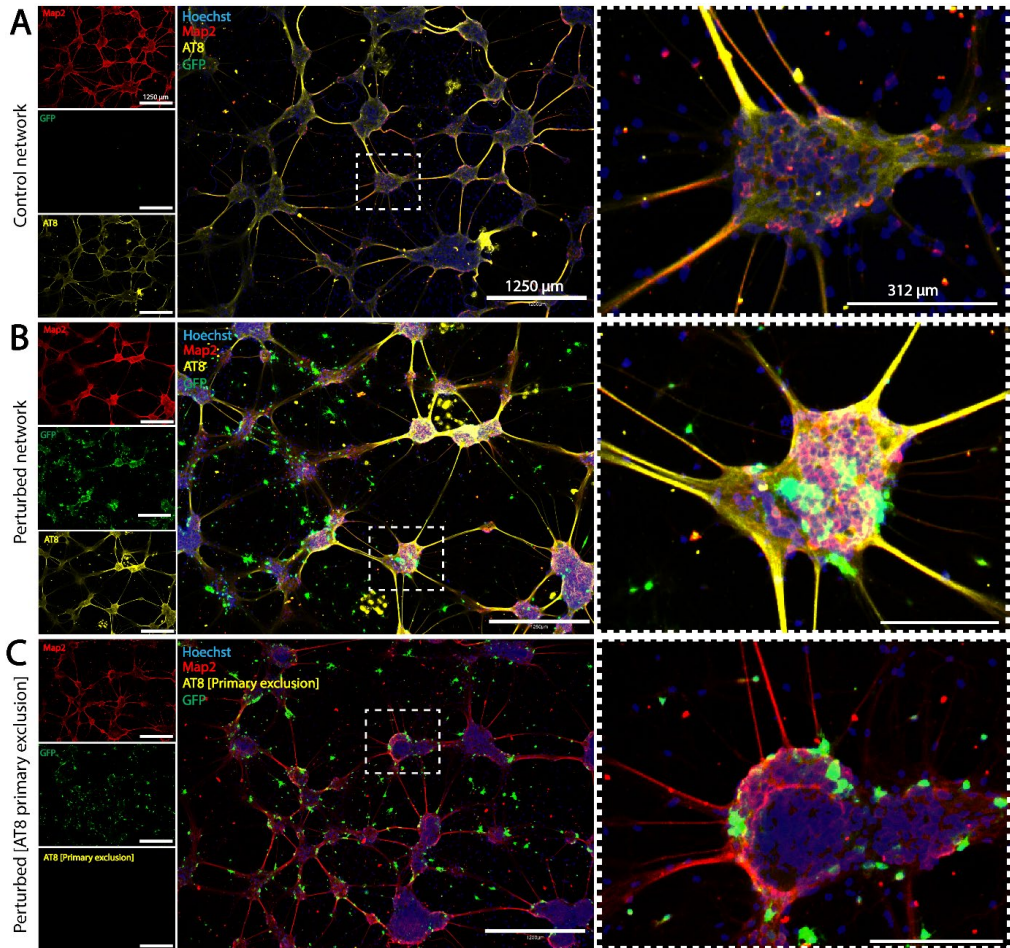

Figure 4. GFP expression exclusively in perturbed networks confirmed efficacy of viral transduction, further validated by AT8 expression. (A) Control unperturbed networks were not transduced with the AAV8-GFP-2A-P301L construct and thus did not express GFP. AT8 labeling was found primarily in axons. **(B)** Perturbed networks were positive for the GFP marker after transduction, with strong axonal and somato-dendritic AT8 expression. **(C)** Exclusion of the primary antibody AT8 to assess the specificity of antigen binding. Scale bar 1250 μm; (magnified area 312 μm).
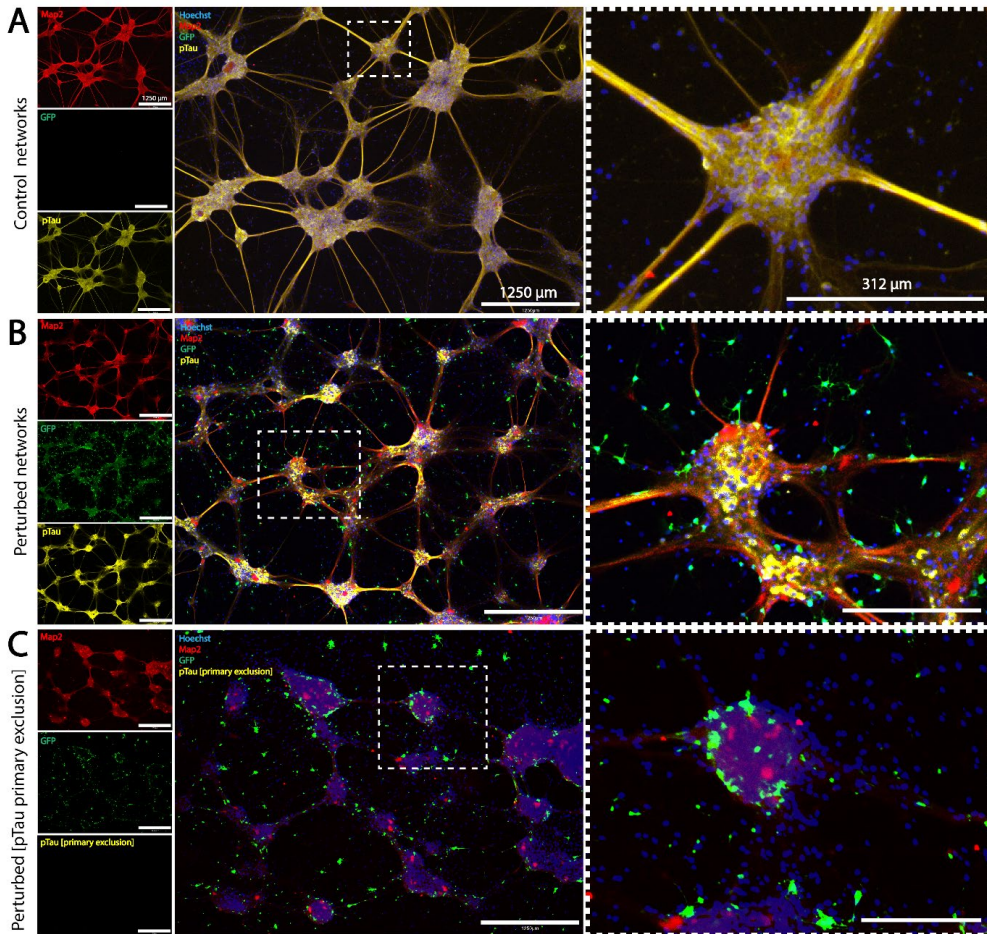
Figure 5. GFP expression exclusively in perturbed networks confirmed efficacy of viral transduction, further validated by pTau expression (A) Control unperturbed networks were not transduced with the AAV8-GFP-2A-P301L construct and thus did not express GFP. pTau labeling found in axons and cytosols. **(B)** Perturbed networks were positive for the GFP marker after transduction, with strong axonal and somato-dendritic pTau expression. **(C)** Primary exclusion of pTau to assess the specificity of antigen binding. Scale bar 1250 μm; (magnified area 312 μm).
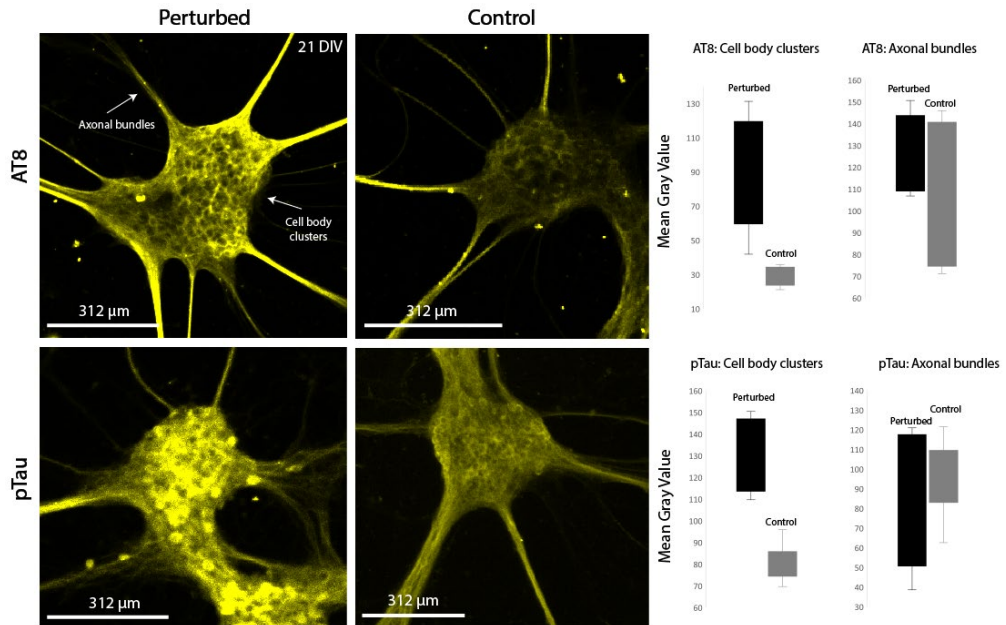
Figure 6. Quantification of fluorescent intensity of AT8 (tau$^{202/205}$) and pTau (tau^{217}) in perturbed and control networks. Representative images from networks with AT8 and pTau labelling showing cell body clusters and axonal bundles. Bar graphs showing the mean gray value of cell body clusters.

3.3.   Progressive internodal axonal retraction observed after perturbation

Prior to induced perturbation, phase contrast imaging of neural networks at 21 DIV confirmed structural connections between the pre- and postsynaptic neural nodes **(Figure 7A).** Interestingly, by four days post perturbation, i.e., at 32 DIV, the neurites within the presynaptic node of the perturbed networks had started retracting from the entry zone near the unidirectional microtunnels, and by 52 DIV all structural connections between the presynaptic and postsynaptic nodes had been lost entirely **(Figure 7A).** Extensive neurite retraction was also observed in the postsynaptic node of the perturbed network by 52 DIV. In contrast, control unperturbed networks maintained robust neurite connections both at the entry zone of the presynaptic node microtunnels and the exit zone in the postsynaptic node **(Figure 7B).**
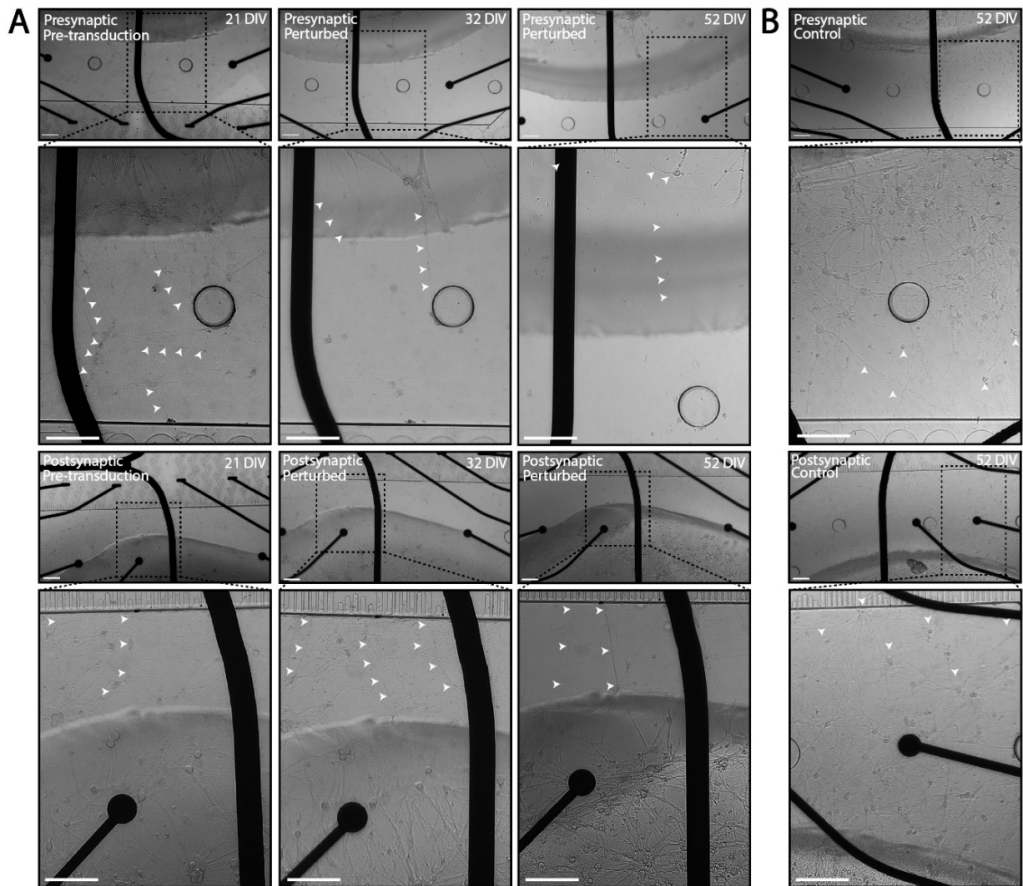
Figure 7. Progressive neurite retraction and active reorganization observed within networks following induced perturbation. (A) The leftmost column shows neurite extensions in the presynaptic node at the entry zone of the unidirectional microtunnels (top) and dense neurites in the postsynaptic node at the exit zone of the unidirectional microtunnels (bottom) at 21 DIV. The middle column is a snapshot of the same region in the network at 32 DIV showing retraction in the presynaptic node (top), but not in the postsynaptic node (bottom). The rightmost column shows extensive retraction in the presynaptic node (top) as well as in the postsynaptic node at 52 DIV (bottom). **(B)** Presynaptic (top) and postsynaptic (bottom) nodes of control unperturbed network depicting dense neurite connections at 52 DIV. Scale bar 100 μm.

3.4. Perturbed networks exhibit a decrease in overall network activity and an increase in network synchrony

Spontaneous network activity was recorded between 16 DIV and 47 DIV for both control unperturbed and perturbed networks. We captured network development from low activity to more mature profiles exhibited as increased mean firing rate **(Figure 8A)** and increased mean burst rate **(Figure 8B)**. Activity recorded from both pre- and postsynaptic nodes revealed the differences between healthy and perturbed networks and their functional evolution. Specifically, the presynaptic nodes of control unperturbed networks exhibited a steady increase in electrical activity between 16 DIV and 31 DIV, consistent with previous studies by us and others capturing developing functional activity in cortical networks (Wagenaar et al., 2006; Weir et al., 2023). Both firing rate and burst rate increased between 33 DIV and 45 DIV in the presynaptic node but not in the postsynaptic node **(Figure 8A and B, respectively)**.
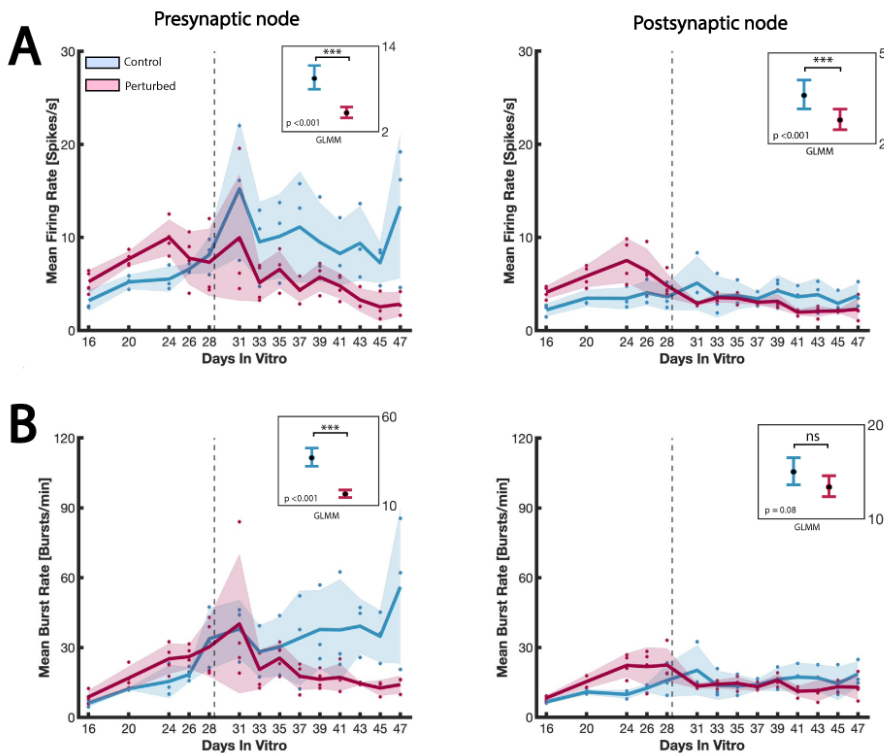

Figure 8. Electrophysiological recordings revealed progressive decrease in firing and burst rate in perturbed networks. (A) Mean firing rate (spikes/second) and **(B)** Mean burst rate (bursts/minute) in the presynaptic and post synaptic nodes for control unperturbed and perturbed networks. The solid lines denote the mean activity for the networks with the solid circles indicating individual data points. The shaded area denotes the standard error of the mean. The stippled line indicates the day of viral transduction in the perturbed networks (28 DIV). Plots showing the GLMM estimated group averages with 95% confidence intervals are depicted in the top right corner of the graphs.

Similarly, prior to induced expression of human mutated tau, the perturbed networks also exhibited a steady increase in both firing rate and burst rate in the presynaptic node between 16 DIV and 28 DIV. However, between 31 DIV and 47 DIV, they exhibited significantly lower firing ($p< 0.001$) and burst ($p< 0.001$) rates compared to healthy controls **(Figure 8A)**. The firing rate in the postsynaptic node of perturbed networks remained significantly lower ($p< 0.001$) than controls for the duration of the study **(Figure 8A)**. There were no significant differences in mean burst rate in the postsynaptic node between healthy controls and perturbed networks **(Figure 8B).**

The postsynaptic node of healthy controls had significantly longer bursts ($p= 0.001$) compared to perturbed networks **(Figure 9B)**, however, there were no significant differences in the mean burst duration in the presynaptic nodes between perturbed and healthy controls between 31 DIV and 47 DIV **(Figure 9A).** Furthermore, the total network activity (pre- and postsynaptic node activity combined) revealed that between 28 DIV and 47 DIV, healthy controls had significantly higher mean network burst duration ($p< 0.001$) compared to perturbed networks **(Figure 9C)**. Specifically, between 28 DIV and 33 DIV, control unperturbed networks exhibited a transient increase in mean network burst duration from 0.23 seconds to 0.26 seconds, however, there was a subsequent decrease between 33 DIV and 47 DIV **(Figure 9C)**. For the perturbed networks, the total network activity for pre- and postsynaptic nodes combined showed that between 33 DIV and 39 DIV there was a transient increase in network burst duration from 0.17 seconds to 0.22 seconds, with a subsequent decrease between 39 DIV and 47 DIV, similar to the healthy controls.

We also found that all networks had a general decrease in mean network burst size (analyzed as the percentage of active electrodes participating in network bursts), between 16 DIV and 28 DIV **(Figure 9D)**. The total bursting activity for pre-and postsynaptic nodes combined showed that control unperturbed networks decreased in burst size from 85% to 45% network participation **(Figure 9D)** between 16 DIV and 28 DIV**.** Similarly, networks before perturbation had a decrease in burst size from 82% to 43% network participation **(Figure 9D)**. Both groups had relatively stable burst size between 28 DIV and 47 DIV, however, perturbed networks had significantly larger network bursts ($p< 0.001$) by 47 DIV (61% of network participation) compared to control unperturbed networks (45% network participation) **(Figure 9D)**. Furthermore, when we examined network synchrony, measured by the coherence index, we observed a general decrease in both pre-and postsynaptic nodes of healthy controls between 16 DIV and 47 DIV **(Figure 9F)**. Both nodes of perturbed networks had progressively increased synchrony that was significantly higher ($p< 0.001$) than in control unperturbed networks between 31 DIV and 47 DIV **(Figure 9F)**.
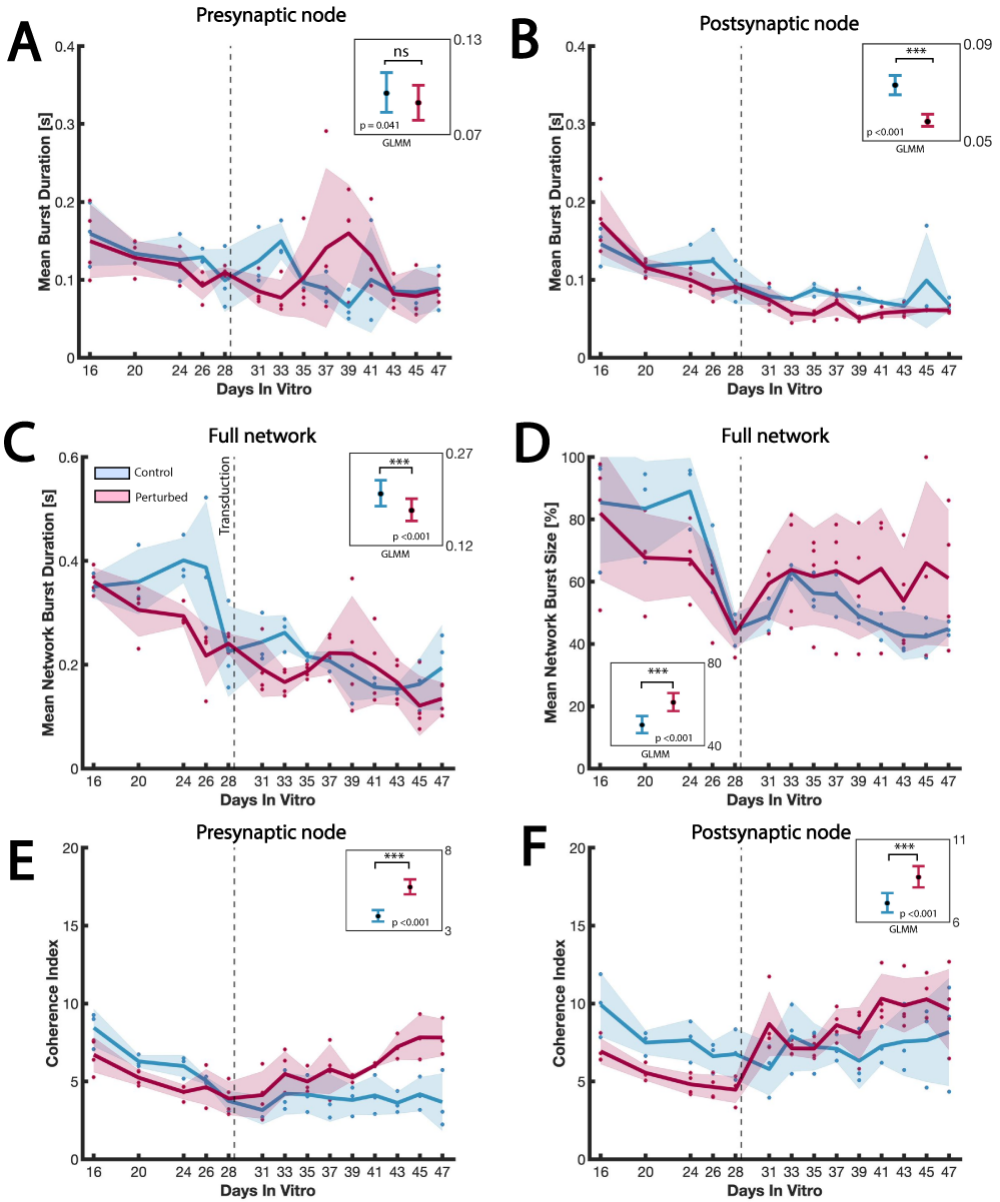
Figure 9. *Electrophysiological recordings revealed a progressive increase in network burst size and synchrony in perturbed networks.* **(A)** *Mean burst duration (seconds) in the pre-and* **(B)** *postsynaptic nodes of control and perturbed networks.* **(C)** *Mean network burst duration in the pre-and postsynaptic nodes combined for control and perturbed networks.* **(D)** *Mean network burst size (percentage) in the pre-and postsynaptic nodes combined for control and perturbed networks.* **(E)** *Coherence Index (measure of network synchrony) in the pre- and* **(F)** *postsynaptic nodes of control and perturbed networks. The solid line denotes the mean activity for the networks with solid circles indicating individual data points. The shaded area denotes the standard error of the mean. The stippled line indicates the day of transduction for the perturbed networks (28 DIV). Plots showing the GLMM estimated group averages with 95% confidence intervals are depicted in the top right corner of the graphs.*

3.5. Induced perturbation results in reduced propagation of spontaneous and evoked activity between nodes

Further analyses were conducted to determine the proportion of bursts propagating between the pre- and postsynaptic nodes in both control unperturbed and perturbed networks. We first evaluated the total number of network bursts exhibited by each network at each recording and identified the percentage of propagating bursts between the pre- and postsynaptic nodes in either direction **(Figure 10)**. Our results showed that between 16 DIV and 28 DIV, both control unperturbed and perturbed networks had a steady increase in the total number of network bursts, with most or all bursts propagating in a feedforward manner from the presynaptic to the postsynaptic node **(Figure 10)**. Additionally, we found that for all subsequent recordings from 28 DIV onwards, burst propagation diminished in the control unperturbed networks to <2% by 47 DIV even though the total number of bursts within the network exceeded 2000 bursts/recording **(Figure 10)**. This implied that bursts were contained primarily within nodes of healthy controls. In contrast, perturbed networks exhibited a steady decline in the total number of network bursts between 33 DIV and 47 DIV (to less than10 bursts/recording by 43 DIV) **(Figure 10)**.
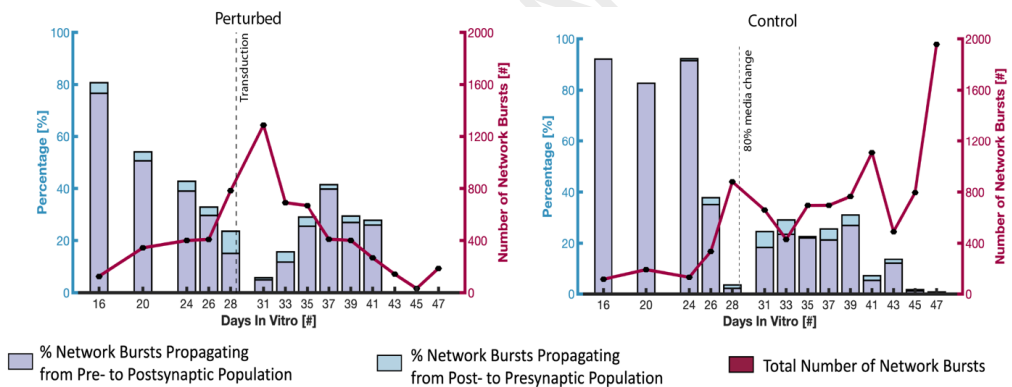

Figure 10. Feedforward burst propagation between pre- and postsynaptic nodes for perturbed (left) and control unperturbed (right) networks. The left y-axis on the graph denotes the percentage of network bursts propagating between the nodes, represented as the bars. The right y-axis denotes the total number of network bursts detected each day represented as the solid line. The x-axis denotes the day in vitro. The stippled line at 28 DIV indicates the day of transduction for the perturbed networks.

We also applied periodical electrical stimulations to the electrode with the highest firing rate in the presynaptic node to assess whether a presynaptic stimulus could evoke a postsynaptic response. The same electrode was stimulated for 1 minute at each recording session between 28 DIV and 47 DIV. We found that electrical stimulation within the presynaptic node of control unperturbed networks produced a spike response followed by a postsynaptic spike response with an average delay time of 20 ms (31 DIV) and 40 ms (35 DIV) **(Figure 11A)**. Control unperturbed networks also produced spike

responses in the presynaptic node at 45 DIV and 47 DIV, although the tuning curves were of lower amplitudes than after previous stimulations. In addition, the spike responses in the postsynaptic node of control unperturbed networks at 45 DIV and 47 DIV were too low to allow for an evaluation of the delay time between the nodes. In contrast, stimulation in the presynaptic node of perturbed networks at 31 and 35 DIV resulted in a presynaptic spike response, with no spike response in the postsynaptic node **(Figure 11B)**. There was no response in presynaptic nor postsynaptic nodes at 45 DIV and 47 DIV in the perturbed networks.
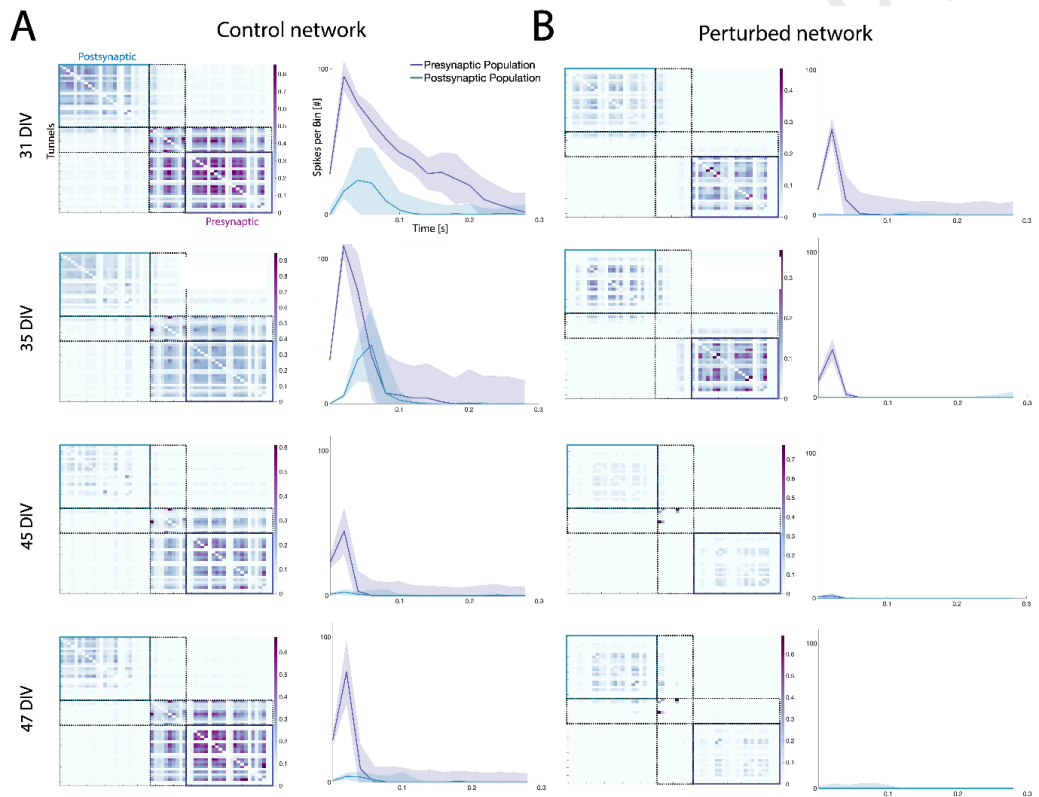

Figure 11. Induced perturbation resulted in progressive decline in presynaptic response to electrical stimulation between the pre-and postsynaptic nodes over time. (A) Mutual information connectivity matrices showing the network activity in chambers and tunnels (left column) and peristimulus time histograms of pre- and postsynaptic responses to electrical stimulations (right column) for control networks at 31, 35, 45 and 47 DIV. (B) Connectivity matrices showing the network activity in chambers and tunnels (left column) and peristimulus time histograms of pre- and postsynaptic responses to electrical stimulations (right column) for perturbed networks at 31, 35, 45 and 47 DIV. The curves show an initial response in the presynaptic network, followed by a delayed response in the postsynaptic network (for control networks) and no postsynaptic response (for perturbed networks). The shaded area denotes the standard error of the mean.

4.   Discussion

Engineered neural networks *in vitro* self-organize into complex topologies and produce a complex profile of activity patterns ranging from individual spikes produced by single neurons to high frequency network bursts generated by neural assemblies (Chiappalone et al., 2006; van de Wijdeven et al., 2018; Weir et al., 2023). The development of complex network activity can be attributed to the structural properties of the network, as function tends to co-evolve with structure (Kapucu et al., 2017). Activity typically evolves with the maturity of neurons, and of excitatory and inhibitory synapses. As shown in **Figure 2**, our engineered neural networks expressed both the excitatory neuronal marker CaMKIIa, and the inhibitory neuronal marker GAD65/67 in conjunction with the neuronal marker MAP2 by 21 DIV, strongly indicating the capacity for excitatory – inhibitory synaptic transmission within the maturing networks. This was further verified through recordings of electrophysiological activity, which showed that in healthy conditions, networks developed highly dynamic and complex age-dependent firing activity and network bursts over time, in line with previous studies by us and others (Chiappalone et al., 2006; Chiappalone et al., 2007; Fiskum et al., 2021; van de Wijdeven et al., 2018; Weir et al., 2023).

The structural organization of neural networks is a crucial determining factor for the emergence of complex network dynamics and information processing. In our engineered feedforward networks, we showed that neurites extended from the presynaptic nodes into the microtunnels towards the postsynaptic nodes, thus establishing structural connections. Furthermore, electrical stimulation at 26 DIV confirmed that these networks were functionally interconnected, as evoked activity in the presynaptic node could propagate and elicit a response in the postsynaptic node (illustrated in **Figure 3**), in line with previous findings (Fair et al., 2009; Ma et al., 2018; Winter-Hjelm N, 2023). These results confirm recapitulation of a feedforward network *in vitro*, where information flows in a unidirectional manner, propagating sequentially from input nodes to output nodes (Barzegaran et al., 2022; Markov et al., 2014). Such feedforward hierarchical organizations are found in many parts of the brain (Markov et al., 2014; Siegle et al., 2021), and facilitate fast, efficient information processing between pre- and postsynaptic neuronal assemblies. We also observed spontaneous feedforward burst propagation in control unperturbed networks occurring from 16 DIV to 43 DIV, and perturbed networks from 16 DIV to 41 DIV **(Figure 10).** The ability of the network to spontaneously transmit information between the nodes is an essential factor in determining its functional capacity since this enables the integration of signals that support coordinated, complex information processing (Fauth et al., 2019; Fukushima et al., 2018; Senden et al., 2018). As such, our results confirmed the intended structural and functional organization of engineered feedforward cortical networks, with the presynaptic node providing input to the postsynaptic node **(Figure 3 and Figure 10)**.

These engineered feedforward networks also enabled us to selectively induce a perturbation, via AVV mediated expression of human mutated tau in the presynaptic node, and to monitor resulting effects within and between nodes. By utilizing this approach, we can effectively recapitulate and monitor a pathological process at the micro- and mesoscale. Such a process not only induces structural and functional changes in the immediately affected node, but also disrupts both structure and function in the postsynaptic node (Kuhl, 2019; Valderhaug et al., 2021). These findings are highly relevant for advanced modelling of evolving pathological processes in neurodegenerative diseases, such as AD, where an association between the progression of tau pathology and altered transsynaptic activity has been demonstrated [36]. Such transsynaptic spread of tau pathology is attributed to the robust connection loops that exist between the putative origin points of tau pathology in the lateral entorhinal cortex layer II (Braak et al., 1991) and feedforward anatomical sites to hippocampal subregions (Liu et al., 2012; Stepan et al., 2015; Witter, 2007; Witter et al., 2017). This feedforward transsynaptic spread of hyperphosphorylated tau may contribute to structural impairments that disrupt the normal functioning of neural networks. In our study, by quantification of fluorescent signaling of tau$^{202/205}$ and tau^{217} expression, we find prominent differences, i.e., increased tau^{217} in the cytosol of neurons in the perturbed networks compared to the control unperturbed ones, signifying detrimental effects of tau phosphorylation. Normal phosphorylation at tau$^{202/205}$ sites is found in maturing brain and is associated with neural development [40], while tau^{217} phosphorylation is found to be associated with the normal development of postsynaptic sites (Rajbanshi et al., 2023). This means that some phosphorylation of tau at these sites is to be expected in control unperturbed networks as shown in **Figure 6**. Furthermore, studies have shown that the phosphorylation of tau at a single site does not preferentially induce neurotoxic effects (Steinhilb et al., 2007). It appears then that the neurotoxic effects of tau depend on a combined high phosphorylation pattern at multiple sites in axons and/or cytosol, which we have demonstrated in our perturbed networks **(Figure 6)**. In addition, recent findings also reported a correlation between high tau^{217} expression and AD pathology progression (Rajbanshi et al., 2023) associated with synaptic decline. Therefore, our finding of increased expression of both tau$^{202/205}$ and tau^{217} in the cytosol of neurons within the perturbed networks suggests that the introduction of human mutated tau, capable of inducing detrimental synaptic effects, has impacted both the structural and functional dynamics of these networks.

This result is further supported by the differences found in the electrophysiological activity of perturbed networks compared to unperturbed controls. Initially, both unperturbed control and perturbed networks had diminished burst propagation between pre- and postsynaptic nodes over time, with very little propagation from 41 DIV in healthy controls, and no propagation after 43 DIV in the perturbed networks, as illustrated in **Figure 10**. The decreased level of spontaneous activity

propagation in healthy networks with age, i.e., DIV, is suggestive of local information processing within nodes, rather than internodal processing. This is further supported by the drastic increase in the total number of bursts detected within nodes of healthy controls (>1800 bursts/recording by 47 DIV), at the same time as the perturbed networks experienced a drastic decline in the total number of bursts within nodes (<10 bursts/recording by 47 DIV) as shown in **Figure 10.** The perturbed networks exhibited differences that can be attributed to increased tau hyperphosphorylation, which, when combined with feedforward propagation between the immediately affected node and the healthy node, precipitated the spread of perturbation effects, leading to disruption in normal synaptic activity across the entire network.

Other studies have found that severity of neuronal loss and atrophy of cortical structures as a result of tau pathology tend to positively correlate with the severity of functional network decline (Adamec et al., 2002; Rascovsky et al., 2005), thus highlighting the complex interrelationship between network structure and function in pathology. The present study revealed such dynamic structural and functional changes in perturbed networks, attributable to the induced expression of human mutated tau at 28 DIV. Between 32 DIV and 52 DIV, we observed progressive neurite retraction from the entry zone near the microtunnels in the presynaptic nodes in the perturbed networks. We also noticed that retraction from the exit zone near the postsynaptic nodes also occurred within weeks of presynaptic retraction as shown in **Figure 7A**. This was not observed in the unperturbed control networks, which maintained a dense neurite network in the zones near the microtunnels in both nodes as seen in **Figure 7B**. The significance of these changes in perturbed networks lies in their potential to adversely affect the network's ability to transmit and integrate information. Prolonged expression of mutant P301L tau exacerbates axonal destabilization (Biswas et al., 2018; Qiang et al., 2018) and impairment of presynaptic terminals (Hunsberger et al., 2021). Furthermore, both maintenance of presynaptic integrity and synaptic plasticity depend on active anterograde and retrograde axonal transport systems (Cai et al., 2011), thus impairment of tau in axons can affect such processes (Lacovich et al., 2017) and severely disrupt synaptic functions between pre- and postsynaptic nodes in perturbed networks. Furthermore, the observed subsequent neurite retraction in the postsynaptic node of the perturbed networks (shown in **Figure 7A**), suggested that the loss of presynaptic input triggered reorganization within postsynaptic nodes. These observations thus indicated a dynamic process of structural and functional reconfiguration across the entire feedforward network in response to presynaptic node perturbation.

The prominent structural changes observed following induced perturbation occurred concomitantly with changes in the electrophysiological profile of the perturbed networks between 28 DIV and 47 DIV. Prior to perturbation and between 16 DIV and 28 DIV, all networks in our study exhibited similar

trends in activity patterns such as firing and burst rate **(Figure 8)**, burst duration and synchrony **(Figure 9)** and burst propagation **(Figure 10)**. In healthy conditions, gradually increasing firing and burst patterns are crucial for the establishment and maintenance of functional synapses, and the elaboration of the network topology into hierarchical processing. Bursts also contribute to the formation and refinement of neural circuits especially during early network formation (between 9 and 21 DIV) [49], where they facilitate the integration of immature neurons into the maturing network. It is therefore expected that all healthy networks would inherently follow this developmental trend of increasing firing and burst rates prior to perturbation. Following the induced expression of human mutated tau, perturbed networks exhibited a steady decline in both firing rate and burst rate in comparison to control unperturbed networks, which continued to display a steady increase over time **(Figure 8)**. Furthermore, these differences in firing rate following perturbation were found to be significant between control unperturbed and perturbed networks in both pre- and postsynaptic nodes. This suggested that perturbed networks became less electrophysiologically active as they underwent structural reorganization, including neurite retraction. The observed decrease in firing and bursting activity also aligned with *in vivo* findings showing that neurons in a mouse model with the Tau-P301 mutation gradually became more hypoactive (Busche et al., 2019). However, Busche et al., (Busche, 2019) also suggested that the disruption in network activity occurred before any prominent structural tau abnormalities were observed in vivo. We have shown however, that the decline in general network activity correlated strongly with the progressive loss of synaptic connectivity and pre- and postsynaptic neurite reorganization. These changes are highly challenging to detect and correlate *in vivo*.

Another interesting result in our study was the significant increase in network burst size and synchrony, as measured by the coherence index, observed in the perturbed networks between 28 DIV and 47 DIV **(Figure 9 E and F)**. Network bursts, which are coordinated patterns of neuronal activity exhibited by multiple interconnected neurons within the network, are ubiquitous for normal network function (Weir et al., 2023). Coordinated neuronal activity also leads to network synchrony (Salinas et al., 2001), and is thus important for information processing, coding, and synaptic integration of distributed signals (Gansel, 2022). Synchrony may also promote activity-dependent establishment of synaptic connections via spike-timing dependent plasticity (STDP) (Anisimova et al., 2022) to support network function. In a recent study by our group, we found that networks that were perturbed by selective silencing of excitatory synaptic transmission also demonstrated increased synchrony during network recovery (Weir et al., 2023). Such behavior may thus be crucial for the network's ability to restore its functional and structural organization within specific time windows after a perturbation.

On the other hand, increased synchrony may also have adverse effects, such as facilitating the spread of perturbations through axons and synapses to affect the entire interconnected network (Uhlhaas et al., 2006), as has been found in AD pathology (Liu et al., 2012; Wang et al., 2017). Furthermore, excessive network bursts and synchrony have been implicated in various neurological disorders, including epilepsy, where they signify a disruption in normal network physiology i.e., impaired excitatory-inhibitory dynamics (Kudela et al., 2003; Wu et al., 2015). Therefore, while a degree of network synchrony is necessary for normal functioning, too much can be problematic. This raises a crucial question regarding whether the observed synchrony in the perturbed networks in our study may represent an adaptive or maladaptive network response to induced perturbation.

Interestingly, synchrony increased concurrently with neurite retraction at 32 DIV, and while firing and burst rate declined. We found that, following perturbation, networks began exhibiting fewer, yet larger synchronized bursts, which can be interpreted as a homeostatic compensatory response to maintain network activity as the overall firing and burst rates declined. In response to low network activity levels, homeostatic scaling, which occurs gradually and over several hours to days, can increase overall input to counteract hypoactivity (Chowdhury et al., 2018; Turrigiano, 2008). This may explain the observation of increasing synchrony between 31 DIV and 47 DIV **(Figure 9 E and F).** However, increased synchrony could also signify pathophysiological changes in the underlying network since it occurred concomitant with the evolution of induced pathology. *In vivo,* induced perturbation caused by hyperphosphorylated tau can disrupt the structural and functional integrity of the affected network, and subsequently result in increased inflammation leading to apoptotic or necrotic cell death (Dong et al., 2022; Thal et al., 2022). Furthermore, it has been suggested that the presence of diverse connections and pathways within a neural network can provide alternative routes for information flow to reduce the reliance on a single synchronized pathway (Kirst et al., 2016), thus acting as a gatekeeping mechanism to prevent excessive synchrony and enhancing overall network robustness. In our study, as induced perturbation led to progressive structural and functional disruption in the network, it is likely that information flow within the network might have been hindered, as there were insufficient alternative routes to effectively distribute activity, ultimately leading to excessive synchrony. This is further supported by observations in control unperturbed during the same time frame between 31 DIV and 47 DIV. During this time, control networks exhibited significantly higher mean firing and burst rates **(Figure 8)** and comparatively more bursts within nodes **(Figure 10)**, without showing excessive synchrony. These networks also maintained the dense neurite architectures between the nodes. This effectively suggests that the unperturbed control networks possessed the ability to maintain their activity within a dynamic range to prevent excessive network wide activation, an ability which the perturbed networks appeared to gradually lose. Based on these

findings, increased network synchrony after induced perturbation might be associated with the deterioration of overall network function in response to the perturbation, rather than serving as an adaptive purpose.

Lastly, to further investigate whether perturbation affected structural and functional connectivity between the nodes, we applied periodic electrical stimulation to one electrode within the presynaptic node and assessed the postsynaptic response. We found that although control unperturbed exhibited a consistent presynaptic spike response to electrical stimulation, there was a gradual decline in the postsynaptic response over time as illustrated in **Figure 11A**. This could be due to activity dependent long-term synaptic changes in the vicinity of the stimulating electrode, such as a reduction in synapse number or downscaling of synaptic receptors on neurons, as previously reported (Collingridge et al., 2010). Such activity dependent structural changes would likely reduce the amplitude of the presynaptic response, thus reducing the strength of the propagating signal (as shown in **Figure 11A**). For perturbed networks, we found that there was no response to presynaptic stimulation in the postsynaptic node by 31 DIV (**Figure 11B)**. This outcome was anticipated as we had already observed extensive neurite retraction in the presynaptic node by the specific time point, indicating the severance of connectivity between nodes. No response to stimulation was observed in the presynaptic node at 45 DIV and 47 DIV, which may be due to possible progressive neuron loss in the network, or structural reorganization of any remaining neurons to areas outside the vicinity of the stimulating electrode. Nevertheless, the differences in response to electrical stimulation between perturbed and control unperturbed networks may reflect the functional capacity of each network, although determination of whether these differences were indeed related to the networks´ functional capacity was beyond the scope of this study.

5. Conclusions and future directions

Using engineered two-nodal feedforward neural networks with controllable afferent-efferent connections, we longitudinally monitored and assessed dynamic structural and functional behaviors in healthy conditions and in response to induced perturbation via expression of human mutated tau. We found that prior to perturbation, both control unperturbed and perturbed networks followed a similar developmental trajectory consistent with relevant literature. The effects of the induced perturbation were evident within one week, with perturbed networks exhibiting significant decreases in firing rate, burst rate and total number of bursts in comparison to the relevant increases observed in control unperturbed networks. These changes align with reported adverse effects of tau hyperphosphorylation. Furthermore, over time, while healthy controls showed a steady decline in burst size and synchrony, perturbed networks showed significant increases in both, suggesting that all the activity was contained within a few, large, synchronized network bursts. Increasing synchrony,

coupled to neurite retraction and the overall decline in firing and burst rates also suggested that the observed synchrony may be a maladaptive, rather than an adaptive, response. Importantly, the relevant changes seen in the perturbed networks were not observed in healthy controls, suggesting that the changes were attributable to the induced perturbation, rather than physiological endogenous tau expression. Taken together, these findings provide significant new insights into dynamic structural and functional reconfigurations at the micro- and mesoscale in engineered feedforward neural networks as a result of evolving tau-associated pathology.

Data availability statement

The raw data that support the findings of this study will be made available by the authors upon request.

Author Contributions

The author contribution follows the CRediT system. JSW, KSH: Conceptualization, Investigation (Cell experiments; Protocol development and optimization; AAV investigations, Immunocytochemistry and Electrophysiological recordings), Writing – Original Draft, Review and Editing, Illustration. NWH: Methodology, Software, Investigation (chip design & manufacturing, electrophysiology, formal analysis), Writing – Review and Editing. AS, IS: Conceptualization, Methodology, Writing – Review & Editing, Funding acquisition, Supervision.

Conflict of Interest

The authors declare that the research was conducted in the absence of any commercial or financial relationships that could be construed as potential conflict of interest.

References

1. Adamec, E., Murrell, J. R., Takao, M., Hobbs, W., Nixon, R. A., Ghetti, B., & Vonsattel, J. P. (2002). P301L tauopathy: confocal immunofluorescence study of perinuclear aggregation of the mutated protein. *J Neurol Sci, 200*(1-2), 85-93. doi:10.1016/s0022-510x(02)00150-8

2. Anisimova, M., van Bommel, B., Wang, R., Mikhaylova, M., Wiegert, J. S., Oertner, T. G., & Gee, C. E. (2022). Spike-timing-dependent plasticity rewards synchrony rather than causality. *Cereb Cortex, 33*(1), 23-34. doi:10.1093/cercor/bhac050

3. Barzegaran, E., & Plomp, G. (2022). Four concurrent feedforward and feedback networks with different roles in the visual cortical hierarchy. *PLoS Biol, 20*(2), e3001534. doi:10.1371/journal.pbio.3001534

4. Bauer, U. S., Fiskum, V., Nair, R. R., van de Wijdeven, R., Kentros, C., Sandvig, I., & Sandvig, A. (2022). Validation of Functional Connectivity of Engineered Neuromuscular Junction With Recombinant Monosynaptic Pseudotyped ΔG-Rabies Virus Tracing. *Front Integr Neurosci, 16*, 855071. doi:10.3389/fnint.2022.855071

5. Biswas, S., & Kalil, K. (2018). The Microtubule-Associated Protein Tau Mediates the Organization of Microtubules and Their Dynamic Exploration of Actin-Rich Lamellipodia and Filopodia of Cortical Growth Cones. *J Neurosci, 38*(2), 291-307. doi:10.1523/jneurosci.2281-17.2017

6. Brewer, G. J., Boehler, M. D., Ide, A. N., & Wheeler, B. C. (2009). Chronic electrical stimulation of cultured hippocampal networks increases spontaneous spike rates. *J Neurosci Methods, 184*(1), 104-109. doi:10.1016/j.jneumeth.2009.07.031

7. Bruno, G., Colistra, N., Melle, G., Cerea, A., Hubarevich, A., Deleye, L., . . . Dipalo, M. (2020). Microfluidic Multielectrode Arrays for Spatially Localized Drug Delivery and Electrical Recordings of Primary Neuronal Cultures. *Front Bioeng Biotechnol, 8*, 626. doi:10.3389/fbioe.2020.00626

8. Braak, H., & Braak, E. (1991). Neuropathological staging of Alzheimer-related changes. *Acta Neuropathol, 82*(4), 239-259. doi:10.1007/bf00308809

9. Busche, M. A. (2019). Tau suppresses neuronal activity in vivo, even before tangles form. *Brain, 142*(4), 843-846. doi:10.1093/brain/awz060

10. Busche, M. A., Wegmann, S., Dujardin, S., Commins, C., Schiantarelli, J., Klickstein, N., . . . Hyman, B. T. (2019). Tau impairs neural circuits, dominating amyloid-β effects, in Alzheimer models in vivo. *Nat Neurosci, 22*(1), 57-64. doi:10.1038/s41593-018-0289-8

11. Baas, P. W., & Qiang, L. (2019). Tau: It's Not What You Think. *Trends Cell Biol, 29*(6), 452-461. doi:10.1016/j.tcb.2019.02.007

12. Cai, Q., Davis, M. L., & Sheng, Z. H. (2011). Regulation of axonal mitochondrial transport and its impact on synaptic transmission. *Neurosci Res, 70*(1), 9-15. doi:10.1016/j.neures.2011.02.005

13. Chiappalone, M., Bove, M., Vato, A., Tedesco, M., & Martinoia, S. (2006). Dissociated cortical networks show spontaneously correlated activity patterns during in vitro development. *Brain Res, 1093*(1), 41-53. doi:10.1016/j.brainres.2006.03.049

14. Chiappalone, M., Vato, A., Berdondini, L., Koudelka-Hep, M., & Martinoia, S. (2007). Network dynamics and synchronous activity in cultured cortical neurons. *Int J Neural Syst, 17*(2), 87-103. doi:10.1142/s0129065707000968

15. Chowdhury, D., & Hell, J. W. (2018). Homeostatic synaptic scaling: molecular regulators of synaptic AMPA-type glutamate receptors. *F1000Res, 7*, 234. doi:10.12688/f1000research.13561.1

16. Collingridge, G. L., Peineau, S., Howland, J. G., & Wang, Y. T. (2010). Long-term depression in the CNS. *Nat Rev Neurosci, 11*(7), 459-473. doi:10.1038/nrn2867

17. Dong, Y., Yu, H., Li, X., Bian, K., Zheng, Y., Dai, M., . . . Kong, W. (2022). Hyperphosphorylated tau mediates neuronal death by inducing necroptosis and inflammation in Alzheimer's disease. *J Neuroinflammation, 19*(1), 205. doi:10.1186/s12974-022-02567-y

18. Fair, D. A., Cohen, A. L., Power, J. D., Dosenbach, N. U., Church, J. A., Miezin, F. M., . . . Petersen, S. E. (2009). Functional brain networks develop from a "local to distributed" organization. *PLoS Comput Biol, 5*(5), e1000381. doi:10.1371/journal.pcbi.1000381

19. Fauth, M. J., & van Rossum, M. C. (2019). Self-organized reactivation maintains and reinforces memories despite synaptic turnover. *Elife, 8*. doi:10.7554/eLife.43717

20. Fiskum, V., Sandvig, A., & Sandvig, I. (2021). Silencing of Activity During Hypoxia Improves Functional Outcomes in Motor Neuron Networks in vitro. *Front Integr Neurosci, 15*, 792863. doi:10.3389/fnint.2021.792863

21. Fornito, A., Zalesky, A., & Breakspear, M. (2015). The connectomics of brain disorders. *Nat Rev Neurosci, 16*(3), 159-172. doi:10.1038/nrn3901

22. Fukuda, T., Heizmann, C. W., & Kosaka, T. (1997). Quantitative analysis of GAD65 and GAD67 immunoreactivities in somata of GABAergic neurons in the mouse hippocampus proper (CA1 and CA3 regions), with special reference to parvalbumin-containing neurons. *Brain Res, 764*(1-2), 237-243. doi:10.1016/s0006-8993(97)00683-5

23. Fukushima, M., Betzel, R. F., He, Y., van den Heuvel, M. P., Zuo, X. N., & Sporns, O. (2018). Structure-function relationships during segregated and integrated network states of human brain functional connectivity. *Brain Struct Funct, 223*(3), 1091-1106. doi:10.1007/s00429-017-1539-3

24. Gansel, K. S. (2022). Neural synchrony in cortical networks: mechanisms and implications for neural information processing and coding. *Front Integr Neurosci, 16*, 900715. doi:10.3389/fnint.2022.900715

25. Gribaudo, S., Tixador, P., Bousset, L., Fenyi, A., Lino, P., Melki, R., . . . Perrier, A. L. (2019). Propagation of α-Synuclein Strains within Human Reconstructed Neuronal Network. *Stem Cell Reports, 12*(2), 230-244. doi:10.1016/j.stemcr.2018.12.007

26. Götz, J., Halliday, G., & Nisbet, R. M. (2019). Molecular Pathogenesis of the Tauopathies. *Annu Rev Pathol, 14*, 239-261. doi:10.1146/annurev-pathmechdis-012418-012936

27. Henderson, J. A., & Gong, P. (2018). Functional mechanisms underlie the emergence of a diverse range of plasticity phenomena. *PLoS Comput Biol, 14*(11), e1006590. doi:10.1371/journal.pcbi.1006590

28. Hunsberger, H. C., Setti, S. E., Rudy, C. C., Weitzner, D. S., Pfitzer, J. C., McDonald, K. L., . . . Reed, M. N. (2021). Differential Effects of Human P301L Tau Expression in Young versus Aged Mice. *Int J Mol Sci, 22*(21). doi:10.3390/ijms222111637

29. Ide, A. N., Andruska, A., Boehler, M., Wheeler, B. C., & Brewer, G. J. (2010). Chronic network stimulation enhances evoked action potentials. *J Neural Eng, 7*(1), 16008. doi:10.1088/1741-2560/7/1/016008

30. Ittner, L. M., & Götz, J. (2011). Amyloid-β and tau--a toxic pas de deux in Alzheimer's disease. *Nat Rev Neurosci, 12*(2), 65-72. doi:10.1038/nrn2967

31. Jackson, J. S., Witton, J., Johnson, J. D., Ahmed, Z., Ward, M., Randall, A. D., . . . Ashby, M. C. (2017). Altered Synapse Stability in the Early Stages of Tauopathy. *Cell Rep, 18*(13), 3063-3068. doi:10.1016/j.celrep.2017.03.013

32. Kapucu, F. E., Valkki, I., Christophe, F., Tanskanen, J. M. A., Johansson, J., Mikkonen, T., & Hyttinen, J. A. K. (2017). On electrophysiological signal complexity during biological neuronal network development and maturation. *Annu Int Conf IEEE Eng Med Biol Soc, 2017*, 3333-3338. doi:10.1109/embc.2017.8037570

33. Katsuno, M., Sahashi, K., Iguchi, Y., & Hashizume, A. (2018). Preclinical progression of neurodegenerative diseases. *Nagoya J Med Sci, 80*(3), 289-298. doi:10.18999/nagjms.80.3.289

34. Kirst, C., Timme, M., & Battaglia, D. (2016). Dynamic information routing in complex networks. *Nat Commun, 7*, 11061. doi:10.1038/ncomms11061

35. Kopeikina, K. J., Polydoro, M., Tai, H. C., Yaeger, E., Carlson, G. A., Pitstick, R., . . . Spires-Jones, T. L. (2013). Synaptic alterations in the rTg4510 mouse model of tauopathy. *J Comp Neurol, 521*(6), 1334-1353. doi:10.1002/cne.23234

36. Kudela, P., Franaszczuk, P. J., & Bergey, G. K. (2003). Changing excitation and inhibition in simulated neural networks: effects on induced bursting behavior. *Biol Cybern, 88*(4), 276-285. doi:10.1007/s00422-002-0381-7

37. Kuhl, E. (2019). Connectomics of neurodegeneration. *Nat Neurosci, 22*(8), 1200-1202. doi:10.1038/s41593-019-0459-3

38. Lacovich, V., Espindola, S. L., Alloatti, M., Pozo Devoto, V., Cromberg, L. E., Čarná, M. E., . . . Falzone, T. L. (2017). Tau Isoforms Imbalance Impairs the Axonal Transport of the Amyloid Precursor Protein in Human Neurons. *J Neurosci, 37*(1), 58-69. doi:10.1523/jneurosci.2305-16.2016

39. Liu, L., Drouet, V., Wu, J. W., Witter, M. P., Small, S. A., Clelland, C., & Duff, K. (2012). Trans-synaptic spread of tau pathology in vivo. *PLoS One, 7*(2), e31302. doi:10.1371/journal.pone.0031302

40. Ma, Z., Ma, Y., & Zhang, N. (2018). Development of brain-wide connectivity architecture in awake rats. *Neuroimage, 176*, 380-389. doi:10.1016/j.neuroimage.2018.05.009

41. Maccione, A., Gandolfo, M., Massobrio, P., Novellino, A., Martinoia, S., & Chiappalone, M. (2009). A novel algorithm for precise identification of spikes in extracellularly recorded neuronal signals. *J Neurosci Methods, 177*(1), 241-249. doi:10.1016/j.jneumeth.2008.09.026

42. Markov, N. T., Vezoli, J., Chameau, P., Falchier, A., Quilodran, R., Huissoud, C., . . . Kennedy, H. (2014). Anatomy of hierarchy: feedforward and feedback pathways in macaque visual cortex. *J Comp Neurol, 522*(1), 225-259. doi:10.1002/cne.23458

43. Menkes-Caspi, N., Yamin, H. G., Kellner, V., Spires-Jones, T. L., Cohen, D., & Stern, E. A. (2015). Pathological tau disrupts ongoing network activity. *Neuron, 85*(5), 959-966. doi:10.1016/j.neuron.2015.01.025

44. Moore, A. K., Weible, A. P., Balmer, T. S., Trussell, L. O., & Wehr, M. (2018). Rapid Rebalancing of Excitation and Inhibition by Cortical Circuitry. *Neuron, 97*(6), 1341-1355.e1346. doi:10.1016/j.neuron.2018.01.045

45. Nonaka, T., & Hasegawa, M. (2011). In vitro recapitulation of aberrant protein inclusions in neurodegenerative diseases: New cellular models of neurodegenerative diseases. *Commun Integr Biol, 4*(4), 501-502. doi:10.4161/cib.4.4.15779

46. Pasquale, V., Martinoia, S., & Chiappalone, M. (2010). A self-adapting approach for the detection of bursts and network bursts in neuronal cultures. *J Comput Neurosci, 29*(1-2), 213-229. doi:10.1007/s10827-009-0175-1

47. Polanco, J. C., Li, C., Durisic, N., Sullivan, R., & Götz, J. (2018). Exosomes taken up by neurons hijack the endosomal pathway to spread to interconnected neurons. *Acta Neuropathol Commun, 6*(1), 10. doi:10.1186/s40478-018-0514-4

48. Qiang, L., Sun, X., Austin, T. O., Muralidharan, H., Jean, D. C., Liu, M., . . . Baas, P. W. (2018). Tau Does Not Stabilize Axonal Microtubules but Rather Enables Them to Have Long Labile Domains. *Curr Biol, 28*(13), 2181-2189.e2184. doi:10.1016/j.cub.2018.05.045

49. Rajbanshi, B., Guruacharya, A., Mandell, J. W., & Bloom, G. S. (2023). Localization, induction, and cellular effects of tau phosphorylated at threonine 217. *Alzheimers Dement*. doi:10.1002/alz.12892

50. Rascovsky, K., Salmon, D. P., Lipton, A. M., Leverenz, J. B., DeCarli, C., Jagust, W. J., . . . Galasko, D. (2005). Rate of progression differs in frontotemporal dementia and Alzheimer disease. *Neurology, 65*(3), 397-403. doi:10.1212/01.wnl.0000171343.43314.6e

51. Rubinov, M., Sporns, O., van Leeuwen, C., & Breakspear, M. (2009). Symbiotic relationship between brain structure and dynamics. *BMC Neurosci, 10*, 55. doi:10.1186/1471-2202-10-55

52. Salinas, E., & Sejnowski, T. J. (2001). Correlated neuronal activity and the flow of neural information. *Nat Rev Neurosci, 2*(8), 539-550. doi:10.1038/35086012

53. Senden, M., Reuter, N., van den Heuvel, M. P., Goebel, R., Deco, G., & Gilson, M. (2018). Task-related effective connectivity reveals that the cortical rich club gates cortex-wide communication. *Hum Brain Mapp, 39*(3), 1246-1262. doi:10.1002/hbm.23913

54. Siegle, J. H., Jia, X., Durand, S., Gale, S., Bennett, C., Graddis, N., . . . Koch, C. (2021). Survey of spiking in the mouse visual system reveals functional hierarchy. *Nature, 592*(7852), 86-92. doi:10.1038/s41586-020-03171-x

55. Steinhilb, M. L., Dias-Santagata, D., Fulga, T. A., Felch, D. L., & Feany, M. B. (2007). Tau phosphorylation sites work in concert to promote neurotoxicity in vivo. *Mol Biol Cell, 18*(12), 5060-5068. doi:10.1091/mbc.e07-04-0327

56. Stepan, J., Dine, J., & Eder, M. (2015). Functional optical probing of the hippocampal trisynaptic circuit in vitro: network dynamics, filter properties, and polysynaptic induction of CA1 LTP. *Front Neurosci, 9*, 160. doi:10.3389/fnins.2015.00160

57. Takao, K., Okamoto, K., Nakagawa, T., Neve, R. L., Nagai, T., Miyawaki, A., . . . Hayashi, Y. (2005). Visualization of synaptic Ca2+ /calmodulin-dependent protein kinase II activity in living neurons. *J Neurosci, 25*(12), 3107-3112. doi:10.1523/jneurosci.0085-05.2005

58. Tarawneh, R., & Holtzman, D. M. (2012). The clinical problem of symptomatic Alzheimer disease and mild cognitive impairment. *Cold Spring Harb Perspect Med, 2*(5), a006148. doi:10.1101/cshperspect.a006148

59. Thal, D. R., & Tomé, S. O. (2022). The central role of tau in Alzheimer's disease: From neurofibrillary tangle maturation to the induction of cell death. *Brain Res Bull, 190*, 204-217. doi:10.1016/j.brainresbull.2022.10.006

60. Timme, N. M., & Lapish, C. (2018). A Tutorial for Information Theory in Neuroscience. *eNeuro, 5*(3). doi:10.1523/eneuro.0052-18.2018

61. Turrigiano, G. G. (2008). The self-tuning neuron: synaptic scaling of excitatory synapses. *Cell, 135*(3), 422-435. doi:10.1016/j.cell.2008.10.008

62. Uhlhaas, P. J., & Singer, W. (2006). Neural synchrony in brain disorders: relevance for cognitive dysfunctions and pathophysiology. *Neuron, 52*(1), 155-168. doi:10.1016/j.neuron.2006.09.020

63. Valderhaug, V. D., Heiney, K., Ramstad, O. H., Bråthen, G., Kuan, W. L., Nichele, S., . . . Sandvig, I. (2021). Early functional changes associated with alpha-synuclein proteinopathy in engineered human neural networks. *Am J Physiol Cell Physiol, 320*(6), C1141-c1152. doi:10.1152/ajpcell.00413.2020

64. Vale, C., Alonso, E., Rubiolo, J. A., Vieytes, M. R., LaFerla, F. M., Giménez-Llort, L., & Botana, L. M. (2010). Profile for amyloid-beta and tau expression in primary cortical cultures from 3xTg-AD mice. *Cell Mol Neurobiol, 30*(4), 577-590. doi:10.1007/s10571-009-9482-3

65. van de Wijdeven, R., Ramstad, O. H., Bauer, U. S., Halaas, Ø., Sandvig, A., & Sandvig, I. (2018). Structuring a multi-nodal neural network in vitro within a novel design microfluidic chip. *Biomed Microdevices, 20*(1), 9. doi:10.1007/s10544-017-0254-4

66. van de Wijdeven, R., Ramstad, O. H., Valderhaug, V. D., Köllensperger, P., Sandvig, A., Sandvig, I., & Halaas, Ø. (2019). A novel lab-on-chip platform enabling axotomy and neuromodulation in a multi-nodal network. *Biosens Bioelectron, 140*, 111329. doi:10.1016/j.bios.2019.111329

67. Wagenaar, D. A., Pine, J., & Potter, S. M. (2006). An extremely rich repertoire of bursting patterns during the development of cortical cultures. *BMC Neurosci, 7*, 11. doi:10.1186/1471-2202-7-11

68. Wagenaar, D. A., & Potter, S. M. (2002). Real-time multi-channel stimulus artifact suppression by local curve fitting. *J Neurosci Methods, 120*(2), 113-120. doi:10.1016/s0165-0270(02)00149-8

69. Wang, Y., Balaji, V., Kaniyappan, S., Krüger, L., Irsen, S., Tepper, K., . . . Mandelkow, E. M. (2017). The release and trans-synaptic transmission of Tau via exosomes. *Mol Neurodegener, 12*(1), 5. doi:10.1186/s13024-016-0143-y

70. Weir, J. S., Christiansen, N., Sandvig, A., & Sandvig, I. (2023). Selective inhibition of excitatory synaptic transmission alters the emergent bursting dynamics of in vitro neural networks. *Front Neural Circuits, 17*, 1020487. doi:10.3389/fncir.2023.1020487

71. Winter-Hjelm N, T. Å. B., Sikoriski P, Sandvig A, Sandvig I. (2023). Structure-Function Dynamics of Engineered, Modular Neuronal Networks with Controllable Afferent-Efferent Connectivity. *Journal of Neural Engineering* doi:DOI 10.1088/1741-2552/ace37f

72. Witter, M. P. (2007). The perforant path: projections from the entorhinal cortex to the dentate gyrus. *Prog Brain Res, 163*, 43-61. doi:10.1016/s0079-6123(07)63003-9

73. Witter, M. P., Doan, T. P., Jacobsen, B., Nilssen, E. S., & Ohara, S. (2017). Architecture of the Entorhinal Cortex A Review of Entorhinal Anatomy in Rodents with Some Comparative Notes. *Front Syst Neurosci, 11*, 46. doi:10.3389/fnsys.2017.00046

74. Wu, Y., Liu, D., & Song, Z. (2015). Neuronal networks and energy bursts in epilepsy. *Neuroscience, 287*, 175-186. doi:10.1016/j.neuroscience.2014.06.046

75. Yamamoto, H., Moriya, S., Ide, K., Hayakawa, T., Akima, H., Sato, S., . . . Hirano-Iwata, A. (2018). Impact of modular organization on dynamical richness in cortical networks. *Sci Adv, 4*(11), eaau4914. doi:10.1126/sciadv.aau4914

NTNU
Norwegian University of
Science and Technology